eman ta zabal zazu

Universidad del País Vasco
Euskal Herriko Unibertsitatea

Merging Metal Catalysis & DFT Studies toward the C–H Functionalization of α-Amino Carbonyl Compounds

Paula Andrade Sampedro

Doctoral Thesis

Supervised by Dr. Arkaitz Correa and Dr. Jon M. Matxain

Química Sintética e Industrial

Departamento de Química Orgánica I

Donostia-San Sebastián, March 2023

List of Publications

1. *Palladium-Catalyzed Site-Selective C(sp^2)−H Acetoxylation of Tyrosine-Containing Peptides.* Urruzuno, I.; Andrade-Sampedro, P.; Correa, A. *Eur. J. Org. Chem.* **2023**, *55*, e202201489.

2. *Ru-Catalyzed C(sp^2)–H Hydroxylation of Tyr-Containing Di- and Tripeptides toward the Assembly of L-DOPA Derivatives.* Andrade-Sampedro, P.; Matxain, J. M.; Correa, A. *Adv. Synth. Catal.* **2022**, *364*, 2072. (Highlighted in *Synfacts* **2022**, *18*, 1047) (Connected to **Chapter 4**)

3. *Late-Stage C−H Acylation of Tyrosine-Containing Oligopeptides with Alcohols.* Urruzuno, I.; Andrade-Sampedro, P.; Correa, A. *Org. Lett.* **2021**, *23*, 7279. (Highlighted in *Synfacts* **2021**, *17*, 1407)

4. *Pd-Catalyzed C(sp^2)−H Alkoxycarbonylation of Phenethyl- and Benzylamines with Chloroformates as CO Surrogates.* Andrade-Sampedro, P.; Matxain, J. M.; Correa, A. *Chem. Eur. J.* **2021**, *27*, 5782. (Connected to **Chapter 3**)

5. *On the Mechanism of Cross-Dehydrogenative Couplings between N-Aryl Glycinates and Indoles: A Computational Study*. Andrade-Sampedro, P.; Matxain, J. M.; Correa, A. *J. Org. Chem*. **2020**, *85*, 13133. (Connected to **Chapter 2**)

Acknowledgements

Paula Andrade kindly acknowledges the financial support from the DIPC and the following research projects:

- Eusko jaurlaritza (IT1033-16)
- Eusko jaurlaritza (IT254-19)
- MINECO (RTI2018-093721-BI00)

I am extremely grateful to my PhD supervisors Dr. Arkaitz Correa and Dr. Jon M. Matxain for their continuous advice and support as well as for sharing with me their deep understanding of organic synthesis and computational chemistry. I appreciate your involvement and I thank you most sincerely for placing your confidence in me to carry out this project. I would also like to thank to Prof. Dr. Syuzanna Harutyunyan for giving me the opportunity to be part of her research group for a three-month period in the University of Groningen. I am also really thankful to Prof. Dr. Iñaki Ganboa for his support and the transmitted knowledge. In general, I am very grateful to my laboratory colleagues and to all the people who have stayed close to me.

Table of contents

Abbreviations and Acronyms

AMLA = Ambiphilic metal ligand activation

AQ = 8-Aminoquinoline

BHT = Butylated hydroxytoluene

BIES = Base Assisted Electrophilic Substitution

bpy = 2,2′-Bipyridyl

BQ = Benzoquinone

CAN = Ceric ammonium nitrate

cap = 2-Carboxyarabinitol-1,5-diphosphate

CDC = Cross-Dehydrogenative Coupling

CMD = Concerted Metalation Deprotonation

Cod = 1,5-Cyclooctadiene

DCE = 1,2-Dichloroethane

DCM = Dichloromethane

DCP = Dicumyl peroxide

DDQ = 2,3-Dichloro-5,6-dicyano-*p*-benzoquinone

DFT = Density Functional Theory

DG = Directing Group

DMA = *N*,*N*-Dimethylacetamide

DMF = *N*,*N*-Dimethylformamide

DMAP = *N*,*N*-Dimethylpyridin-4-amine

DMSO = Dimethyl sulfoxide

dr = Diastereomeric ratio

dppf = 1,1′-Ferrocenediyl-bis(diphenylphosphine)

DTBP = Di-*tert*-Butyl peroxybenzoate

dtbpy = 4,4′-Di-tert-butyl-2,2′-dipyridyl

ee = Enantiomeric excess

ET = Electron Transfer

EWG = Electron With-Drawing Group

Gly = Glycine

GGA = Generalised Gradient Approximation

HF = Hartree-Fock

HOMO = Highest Occupied Molecular Orbital

His = Histidine

Int = Intermediate

KIE = Kinetic Isotope Effect

LC-MS = Liquid chromatography–mass spectrometry

LDA = Local-Density Approximation

L-DOPA = 3,4-Dihydroxyphenilalanine

LUMO = Lowest Occupied Molecular Orbital

Mp = Melting point

NBE = 2-Norbornene

NS = (4-Nitrophenyl)sulfonyl

n.r. = No Reaction

OA = Oxidative Addition

PA = Picolinamide

PCET = Proton Coupled Electron Transfer

PG = Protecting Group

Phe = Phenylalanine

Phth = Phthalimide

PIDA = (Diacetoxyiodo)benzene

PIFA = [Bis(trifluoroacetoxy)iodo]benzene

PMP = *p*-Methoxyphenyl

RE = Reductive Elimination

RPA = Random Phase Approximation

r.t. = Room temperature

Ser = Serine

SET = Single Electron Transfer

TBAI = Tetrabutylammonium Iodide

TBHP = *Tert*-Butyl hydroperoxide

TBS = *Tert*-Butyl silyl

TDG = Transient Directing Group

TEMPO = 2,2,6,6-tetramethyl-1-piperidinyloxy

TFA = Trifluoroacetic acid

THIQ = Tetrahydroisoquinoline

Trp = Tryptophan

TS = Transition State

Tyr = Tyrosine

Abstract

Owing to their improved properties and increased pharmacological activity, the development of new techniques for the synthesis of unnatural amino acids represents a task of prime interest. In this respect, the modification of amino acids via direct C–H functionalization is a powerful approach from step- and atom-economic perspectives because it enables the modification of inert C–H bonds in a site-specific fashion and with retention of the native chirality. For the efficient design of future synthetic methodologies, a deep understanding of the observed reactivities as well as chemical properties is required. The combination of experimental and computational methods offers complementary information and constitutes a tool for going beyond the current knowledge. For these reasons, the general objective of this Thesis relies on the development of new synthetic methodologies for the C–H functionalization of different amino acid derivatives upon a combination of laboratory and computational studies.

CDC-type reactions are one of the most promising synthetic approaches for the α-C(sp^3)–H functionalization of Gly derivatives. This strategy is based on the formation of imine/iminium type intermediates under oxidative reaction conditions. However, for the efficient generation of the electrophilic intermediates an *N*-aryl motif is often required. In this respect, the main objective of *Chapter 1* has been to understand the unique features as well as the current limitations of the existing CDC techniques. For this purpose, we have carried out a deep computational study on the Co-catalyzed α-C(sp^3)–H functionalization of Gly derivatives previously developed by our group (Scheme 1).

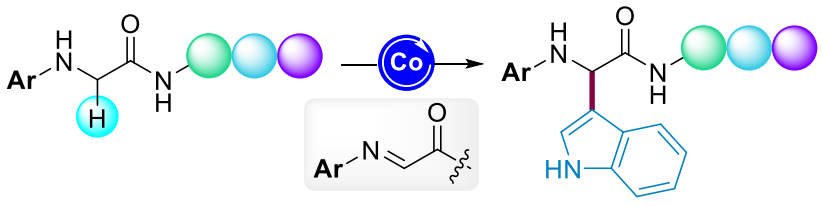

Scheme 1. Co-catalyzed α-C(sp^3)–H functionalization of Gly derivatives.

On *Chapter 2*, we have investigated the δ-C(sp^2)–H diversification of the aromatic side-chain of Phe derivatives. This strategy relied on the use of the picolinamide directing group in a strategic position within the Phe unit, which enabled the Pd-catalyzed site-selective alkoxycarbonylation featuring alkyl chloroformates as versatile coupling partners (Scheme 2).

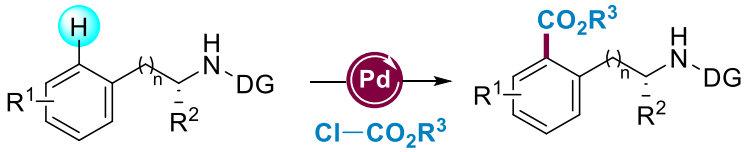

Scheme 2. Pd-catalyzed site-selective δ-C(sp^2)–H alkoxycarbonylation of Phe derivatives.

Finally, *Chapter 3* describes the chelation assisted ε-C(sp^2)–H hydroxylation of Tyr derivatives toward the assembly of L-DOPA derivatives using I^{III} reagents as oxygen source. This strategy features the use of a O-diehtylcarbamate as weak DG in combination with a Ru-based catalyst (Scheme 3).

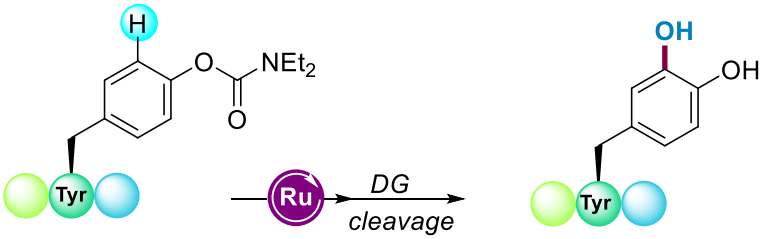

Scheme 3. Ru-catalyzed site-selective ε-C(sp^2)–H hydroxylation of Tyr derivatives.

Resumen

A causa de sus avanzadas propiedades y su mayor actividad farmacológica, el desarrollo de nuevas técnicas para la síntesis de aminoácidos no naturales es de gran interés. En este contexto, la modificación de aminoácidos mediante técnicas de funcionalización C–H es una aproximación sintética muy valiosa debido a que reduce las etapas necesarias en síntesis y favorece la economía atómica del proceso. Además, permite la modificación de enlaces C–H inertes de manera selectiva y, en la mayor parte de los casos, con retención de la quiralidad nativa. Para que el diseño de estrategias sintéticas futuras sea lo más eficiente posible, se requiere un profundo conocimiento tanto de la reactividad como de las propiedades químicas de las moléculas que intervienen en cada proceso. La combinación de métodos computacionales y experimentales ofrece información complementaria y, en consecuencia, es una poderosa herramienta para ir más allá del conocimiento actual. Por estos motivos, el objetivo general de esta Tesis Doctoral ha sido desarrollar nuevas metodologías sintéticas para la funcionalización C–H de diferentes aminoácidos y péptidos combinando estudios experimentales y cálculos computacionales.

En lo que respecta a la funcionalización α-C(sp^3)–H de derivados de glicina, las reacciones de tipo CDC son la aproximación sintética ideal. Esta estrategia se basa en la formación de intermedios electrófilos de tipo imina/iminio bajo condiciones de reacción oxidativas. Desafortunadamente, la presencia de un grupo *N*-arilo es indispensable para que las estructuras electrófilas anteriormente mencionadas se puedan formar de manera adecuada. Debido a esto, el objetivo general del *Capítulo 1* ha sido dilucidar las características y entender las limitaciones de las reacciones de tipo CDC. Para ello, se ha realizado un estudio profundo acerca de la funcionalización α-C(sp^3)–H de derivados de Glicina catalizada por cobalto previamente desarrollada por nuestro grupo (Esquema 1).

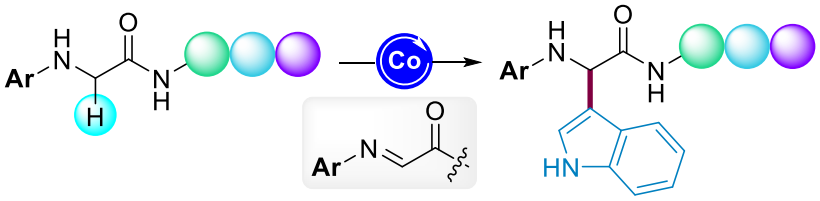

Esquema 1. Funcionalización α-C(sp^3)–H de derivados de glicina catalizada por cobalto.

En el *Capítulo 2* centramos nuestra investigación en la modificación de los enlaces δ-C(sp^2)–H de la cadena lateral de derivados de fenilalanina. Nuestro planteamiento se ha basado en la introducción estratégica de la picolinamida como grupo director, lo que nos ha permitido acoplar selectivamente varios alquil cloroformiatos usando cantidades catalíticas de paladio (Esquema 2).

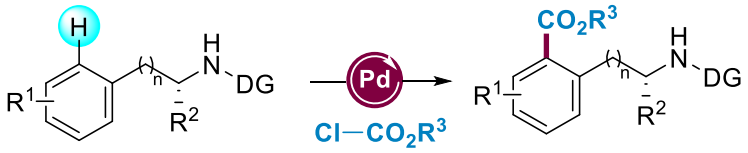

Esquema 2. Alcoxycarbonilación δ-C(sp^2)–H de derivados de fenilalanina catalizada por Pd.

Por último, el *Capítulo 3* describe la síntesis de derivados de L-DOPA mediante una nueva técnica de hidroxilación ε-C(sp^2)–H de derivados de tirosina, utilizando un reactivo de I^{III} como fuente de oxígeno. Esta estrategia se caracteriza por el empleo de un grupo director débil, como el O-dietilcarbamato, en combinación con sales de rutenio (Esquema 3).

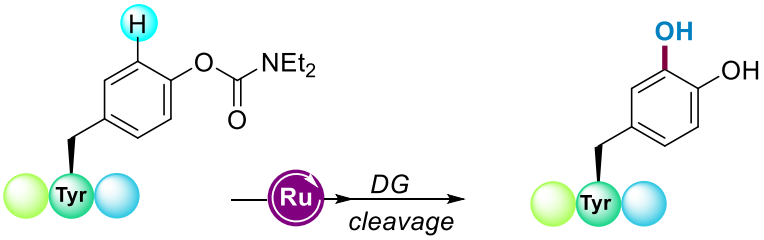

Esquema 3. Hidroxilación ε-C(sp^2)–H selectiva de derivados de tirosina catalizada por rutenio.

Chapter 1.

General Introduction.

ABSTRACT: In this general introduction, a contextual perspective of the tools utilized along this Thesis will be briefly analyzed. Concerning the experimental work, all the chemical processes developed herein involve metal-catalyzed C–H functionalization reactions; hence their importance within the context of organic synthesis will be highlighted. Likewise, the key role of computational studies to elucidate reaction mechanisms will be described.

1.1. Transition Metal-Catalyzed C–H Functionalization

The great social impact of organic chemistry can be understood when we recount its applications in everyday life – food and textile industries, medicine, fuels, polymers, agriculture, new materials and more. The virtually unlimited kingdom of chemicals of different properties is the result of the continuous development of new synthetic methodologies. In particular, transition metal-catalyzed cross-coupling reactions are a very powerful tool for the construction of a wide variety of organic molecules. In the early stages of this research area, different types of coupling reactions were developed such as the Negishi coupling,[1] Suzuki coupling,[2] Sonogashira coupling,[3] Stille coupling,[4] Kumada coupling,[5] Hiyama coupling[6] and Mizoroki Heck reaction (Table 1). Almost 50 years from their discovery, the research in this field still remains very active and significant advances are achieved every year.[7]

Table 1. Transition metal-catalyzed cross-coupling reactions.

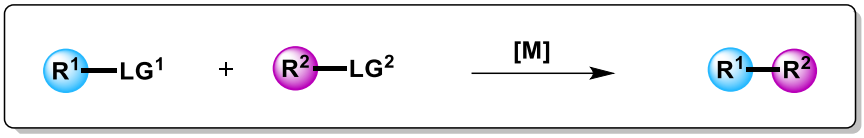

R *or* LG	Negishi	Suzuki	Sonogashira	Stille	Kumada	Hiyama	Heck
R^1	Alkyl, Aryl…	Aryl	Alkynyl	Alkyl, Aryl…	Alkyl, Aryl…	Alkyl, Aryl…	Alkenyl
LG^1	ZnX, AlR^1R^2	BR^1R^2	H	$SnR^1R^2R^3$	MgX, LiX	$SiR^1R^2R^3$	H
R^2	Alkyl, Alkynyl Aryl, Alkenyl	Aryl	Aryl	Alkenyl, Aryl….	Alkyl, Aryl…	Alkyl, Aryl…	Aryl
LG^2	Cl, Br, I, OTf…	Br, I	Br, I, OTf …	Cl, Br, I, OTf …	Cl, Br, I, OTf	Br, I, OTf …	Br, I, OTf…

[1] King, A. O.; Okukado, N.; Negishi, E.-i. *J. Chem. Soc., Chem. Commun.*, **1977**, 683.
[2] Miyaura, N.; Yanagiand, T.; Suzuki, A. *Synth. Commun.* **1981**, *11*, 513.
[3] Sonogashira, K.; Tohda, Y.; Hagihara, N. *Tetrahedron Lett.* **1975**, *16*, 4467.
[4] Stille, J. K. *Angew. Chem. Int. Ed.* **1986**, *25*, 508.
[5] Tamao, K.; Sumitani, K.; Kiso, Y.; Zembayashi, M.; Fujioka, A.; Kodama, S.; Nakajima, I.; Minato A.; Kumada, M. *Bull. Chem. Soc. Jpn.* **1976**, *49*, 1958.
[6] Hatanaka, Y.; Hiyama, T. *J. Org. Chem.* **1988**, *53*, 918.
[7] a) Biffis, A.; Centomo, P.; Del Zotto, A.; Zecca, M. *Chem. Rev*. **2018**, *118*, 2249. b) Magano, J.; Dunetz, J. R. *Chem. Rev*. **2011**, *111*, 2177.

Despite their powerful synthetic utility, they suffer from severe downsides such as the use of prefunctionalized substrates, which results in additional synthetic steps, production of high chemical waste and use of expensive reagents. Accordingly, new alternative and sustainable variants of these classical cross-couplings have been developed along the last decade.

In this context, the direct functionalization of C–H bonds has emerged as a powerful tool for the direct formation of carbon-carbon and carbon-heteroatom bonds (Scheme 4).[8] C–H bonds are ubiquitous in organic molecules and their use as reactive points offers new opportunities on efficient synthesis planning. However, such bonds are relatively inert since their dissociation energy is around 100 kcal·mol^{-1}, mostly because of their low polarity. In addition, differentiate between similar C–H bonds is one of the biggest challenges on this field. One way to address the selectivity problem is by taking advantage of the steric and electronic differences between similar C–H bonds.[9]

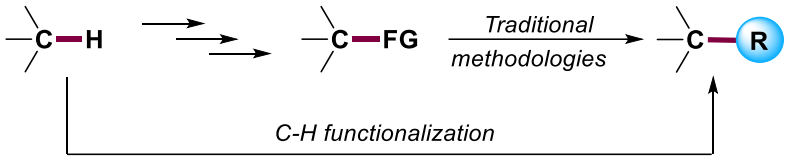

Scheme 4. Traditional cross-coupling technique vs C–H bond functionalization.

For instance, relatively weak C–H bonds can be cleaved in a radical fashion using first-row transition metals, which can easily undergo single electron transfer (SET) or hydrogen atom abstraction (HAT) processes, or even under metal-free reaction conditions (Scheme 5).[10] The rate of these reactions tends to be determined by the inherent strength of the C–H bond. Therefore, the functionalization of benzylic, allylic, tertiary or C–H bonds adjacent to heteroatoms is favored. These *metalloradical* pathways can be classified inside the outer-sphere activation mode, which does not involve the direct interaction between the metal center and the targeted C–H bond. Owing

[8] a) Sinha, S. K.; Guin, S.; Maiti, S.; Biswas, J. P.; Porey, S.; Maiti, D. *Chem. Rev.* **2022**, *122*, 5682. b) Dalton, T.; Faber, T.; Glorius, F. *ACS Cent. Sci.* **2021**, *7*, 245. c) Rej, S.; Ano, Y.; Chatani, N. *Chem. Rev.* **2020**, *120*, 3, 1788. c) Abrams, D. J.; Provencher, P. A.; Sorensen, E. J. *Chem. Soc. Rev.* **2018**, *47*, 8925. d) Gensch, T.; Hopkinson, M. N.; Glorius F.; Wencel-Delord, J. *Chem. Soc. Rev.* **2016**, 45, 2900.
[9] Chen, M. S.; White, M. C. *Science* **2010**, *327*, 566.
[10] Yi, H.; Zhang, G.; Wang, H.; Huang, Z.; Wang, J.; Singh, A. K.; Lei, A. *Chem. Rev.* **2017**, *117*, 9016.

to their less toxicity, natural abundance as well as unique reactivity, in recent years there has been an increase on the development of catalytic methods based on the use of 3*d* metal species.[11]

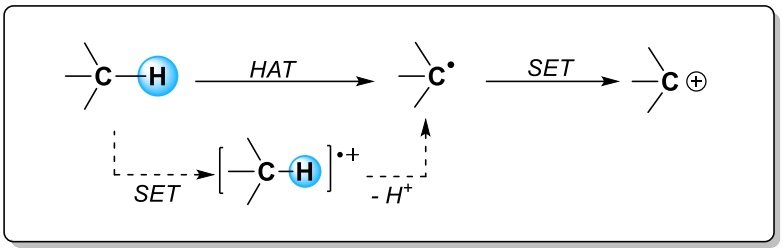

Scheme 5. Outer-sphere C–H functionalization.

Unfortunately, despite its innovative and practical character, in many cases the steric and electronic differences between contiguous C–H bonds are not high enough to develop a reliable and useful site-selective method. In this respect, the organometallic C–H activation represents a general platform for achieving site-selectivities in a variety of substrates. The latter implies the direct interaction between the targeted C–H bond and the metal center upon the formation of reactive C–M species. Based on the first reports regarding inner-sphere C–H activation, the cleavage of the C–H bond has been proposed to occur via four general different reaction pathways: oxidative addition, σ-bond metathesis, 1,2-addition and electrophilic activation.[12]

Inside the most popular variant of the electrophilic activation mechanisms the proton is usually abstracted by an anionic ligand or external anion. These variants are known by different names: AMLA (ambiphilic metal ligand activation) or CMD (concerted metalation-deprotonation). Late-transition metals such as Pd^{II}, Pt^{II}, Rh^{III}, Ir^{III} and Ru^{II} are very versatile tools for this type of transformations.[13] Indeed, their use for catalytic C–H bond activation in organic synthesis can be

[11] a) Gandeepan, P.; Müller, T.; Zell, D.; Cera, G.; Warratz, S.; Ackermann, L. *Chem. Rev.* **2019**, *119*, 2192. b) Gallego, D.; Baquero, E. A. *Open Chem.* **2018**, *16*, 1001. c) Woźniak, L.; Cramer, N. *Trends Chem.* **2019**, *1*, 471.
[12] Altus, K. M.; Love, J. A. *Commun. Chem.* **2021**, *4*, 173.
[13] For selected examples, see: a) Bag, S.; K, S.; Mondal, A.; Jayarajan, R.; Dutta, U.; Porey, S.; Sunoj, R. B.; Maiti, D. *J. Am. Chem. Soc.* **2020**, *142*, 12453. b) He, C.; Whitehurst, W. G.; Gaunt, M. J. *Chem* **2019**, *5*, 1031. c) Yang, K.; Song, M.; Liu, H.; Ge, H. *Chem. Sci.* **2020**, *11*, 12616. d) Choy, P. Y.; Wong, S. M.; Kapdi, A.; Kwong, F. Y. *Org. Chem. Front.* **2018**, *5*, 288. e) Le Bras, J.; Muzart, J. *Eur. J. Org. Chem.* **2018,** 1176. f) Leitch, J. A.; Frost, C. G. *Chem. Soc. Rev.* **2017**, 46, 7145. g) Nareddy, P.; Jordan, F.; Szostak, M. *ACS Catal.* **2017**, *7*, 5721. h) Zha, G.-F.; Qin, H.-L.; Kantchev, E. A. B. *RSC Adv.* **2016**, *6*, 30875. i) Yang, Z.; Yu, J.-T.: Pan, C. *Org. Biomol. Chem.* **2021**, *19*, 8442. j) Rej, S.; Chatani, N. *Angew. Chem. Int. Ed.* **2019**, *58*, 8304. k) Labinger, J. A. *Chem. Rev.* **2017**, 117, 8483. l)

considered as one of the most important breakthroughs. In these cases, DGs are often employed to bring the desired C–H bond closer to the metal center. In this manner, the entropic barrier is reduced and the reaction is favored for the targeted bond (Scheme 6).

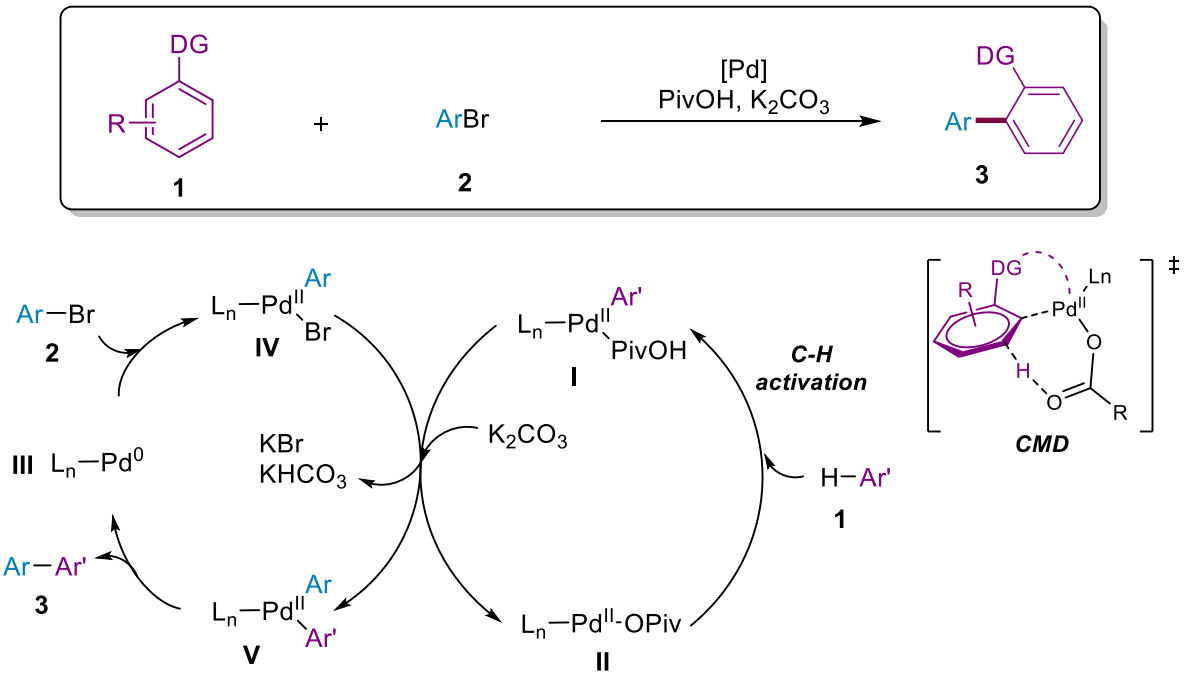

Scheme 6. Representative example of C–H arylation via CMD pathway assisted by a pivaloate anion.

The last years have witnessed an exponential growth on chelation assisted site-selective C–H functionalization methodologies and a variety of functional groups have been reported as DGs.[14] Moreover, the use of TDGs[15] represents a step forward in the field because it avoids the pre-installation and the removal of the selected chelating motif. The understanding of the mechanistic approach towards C–H activation processes has rendered new reactions with improved site-selectivity, augmented efficiency and higher tolerance to different functional groups.

Woźniak, L.; Tan, J.-F.; Nguyen, Q.-H.; Madron du Vigné, A.; Smal, V.; Cao, Y.-X.; Cramer, N. *Chem. Rev.* **2020**, *120*, 10516.

[14] For selected examples, see: a) Das, J.; Mal, D. K.; Maji, S.; Maiti, D. *ACS Catal.* **2021**, 11, 4205. b) Dong, B.; Qian, J.; Li, M.; Wang, Z.-J.; Wang, M.; Wang, D.; Yuan, C.; Han, Y.; Zhao, Y.; Shi, Z. *Sci. Adv.* **2020**, *6*, eabd1378. c) Zhu, R.-Y.; Farmer, M. E.; Chen, Y.-Q.; Yu, J.-Q. *Angew. Chem. Int. Ed.* **2016**, *55*, 10578.

[15] a) Jacob, C.; Maes, B. U. V.; Evano, G. *Chem. Eur. J.* **2021**, *27*, 138. b) Rani, G.; Luxami, V.; Paul, K. *Chem. Commun.* **2020**, *56*, 12479.

1.2. Density Functional Theory

The understanding of the origins of chemical reactivity is a powerful tool for predict and design unprecedented chemical transformations. However, the study of chemical reactions using only experimental techniques is still limited since the transition states and some of the reaction intermediates are proposed to have extremely short lifetimes. Owing to the enormous progress in the development of hardware and software as well as computational methods, computational chemistry can provide complementary information about a great amount of chemical properties in a short time and with high accuracy, complementing the collection of experimental data. The synergistic approach of computational and experimental methods is a tool to elucidate the results and describe the chemical systems in a more accurate way.[16]

In practice, before starting a computational study of a chemical transformation a balance between computational cost and accuracy has to be carried out. In this respect, even for a simple two-electron system, the resolution of the Schrödinger equation is too complex to be solved. As a result, several simplifications and approximations have been introduced along the last decades. Inside the field of organic chemistry, DFT (Density Functional Theory)[17] is the most popular quantum-mechanical atomistic simulation method since it provides accurate results at very low computational cost. In contrast to classical methods based on the multielectronic wavefunction approach (Hartree-Fock derived methods), DFT considers the electron density to determine the ground state energy of the system. Following the Kohn-Sham model, which is based on a virtual reference system of separable and non-interacting electrons, the energy functional can be written as a set of four mathematic terms: Kinetic energy, nuclear-electron attraction, electron-electron repulsion and exchange-correlation terms. Unfortunately, the exchange-correlation term still cannot be fully defined and different approaches have been developed to approximate this energy value. The growth of different functionals have given rise to several DFT methods with different chemical accuracy (Figure 1).[18]

[16] Ghosh, S.; Shilpa, S.; Athira, C.; Sunoj, R. B. *Top. Catal.* **2022**, *65*, 141.
[17] a) Hohenberg, P.; Kohn, W. *Phys. Rev.* **1964,** *136* (3B), B864. b) Kohn, W.; Sham, L. J. *Phys. Rev.* **1965,** *140* (4A), A1133.
[18] Cohen, A. J.; Mori-Sánchez, P.; Yang, W. *Chem. Rev.* **2012**, *112*, 289.

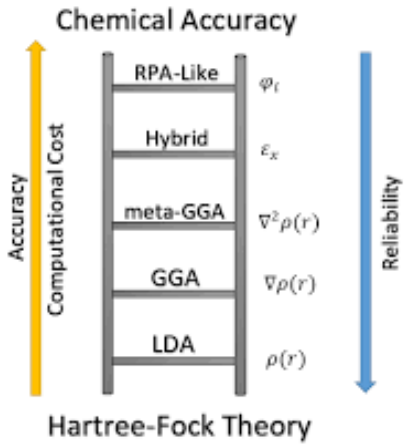

Figure 1. Jacob's Ladder representation. Hierarchy of accuracy for different DFT methods.

The simplest approach, known as the *Local Density Approximation* (LDA), assumes that the density can be treated as a uniform electron gas or as a slightly varying function. However, it underestimates the exchange energy and overestimates the correlation energy. There are more accurate approximations, such as the *Generalised Gradient Approximation* (GGA), which also considers the gradient of the electron density. The *meta-GGA* approximations are more accurate since they include the second derivative of the electron density (Laplacian) and/or the exact kinetic energy term. The *hybrid functionals* have a dependence on HF exact exchange. Finally, the *Random Phase Approximation* (RPA) is fully non-local and includes long-range van der Waals interactions.

Although the character of this Thesis has been mostly experimental, the laboratory work has been complemented with DFT-based computational calculations. For this purpose, the highly parametrized Minnesota functional family, which includes empirical parameters to consider dispersion forces, has been utilized. In particular, we have chosen the M06-2x functional (*meta-GGA*), which contains part of the exchange energy approximated by the HF method and is widely used to calculate thermochemical and kinetic properties as well as non-covalent interactions involving transition metals.

1.3. General Objectives of this Doctoral Thesis

Owing to the importance of C–H functionalization as an innovative tool for the assembly of unprecedented non-proteinogenic amino acids, the fundamental studies of this Doctoral Thesis will be conducted to exploit its synthetic utility within the field of peptide chemistry. Therefore, we established the following objectives:

- To develop new protocols for the C–H functionalization of α-amino carbonyl compounds
- To apply the developed methods to more complex peptide sequences
- To understand the reaction features using DFT studies

1.4. Computational Methodology Applied in This Thesis

All calculations were carried out within the Density Functional Theory (DFT),[17] using the Gaussian16 program package.[19] First, geometry optimizations were performed by using the M06-2X exchange-correlation functional,[20] combined with the 6-31G(d) basis set for the non-metal atoms,[21] and the ECP10MDF Sttutgart-Cologne relavistic core potentials along with the aug-cc-pVDZ-PP basis set for Pd and Ru.[22] After the geometry optimizations, harmonic vibrational frequencies were obtained by analytical differentiation of gradients, at the same level of theory, to identify whether the characterized structures were true minima or Transition States. Such frequencies were then used to evaluate the zero-point vibrational energy (ZPVE) and the thermal (T = 298 K) vibrational corrections to the enthalpy and Gibbs free energy (H^{corr}, G^{corr}). Then, single-point calculations using the 6-311++G(2df,2p) basis set[23] were performed on the optimized structures to refine the electronic energy (E_{elec}), considering the solvent effect by means of the integral equation formalism of the polarized continuum model (IEFPCM).[24] In this vein, the enthalpies (H^{sol}) or Gibbs free energies (G^{sol}) of each species in solution were calculated as follows:

$$H^{sol}=E_{elec}+H^{corr}$$

$$G^{sol}=E_{elec}+G^{corr}$$

These enthalpy values were used to calculate the ΔH or ΔG values of the studied processes

[19] Frisch, M. J.; Trucks, G. W.; Schlegel, H. B.; Scuseria, G. E.; Robb, M. A.; Cheeseman, J. R.; Scalmani, G.; Barone, V.; Petersson, G. A.; Nakatsuji, H.; Li, X.; Caricato, M.; Marenich, A. V.; Bloino, J.; Janesko, B. G.; Gomperts, R.; Mennucci, B.; Hratchian, H. P.; Ortiz, J. V.; Izmaylov, A. F.; Sonnenberg, J. L.; Williams; Ding, F.; Lipparini, F.; Egidi, F.; Goings, J.; Peng, B.; Petrone, A.; Henderson, T.; Ranasinghe, D.; Zakrzewski, V. G.; Gao, J.; Rega, N.; Zheng, G.; Liang, W.; Hada, M.; Ehara, M.; Toyota, K.; Fukuda, R.; Hasegawa, J.; Ishida, M.; Nakajima, T.; Honda, Y.; Kitao, O.; Nakai, H.; Vreven, T.; Throssell, K.; Montgomery Jr., J. A.; Peralta, J. E.; Ogliaro, F.; Bearpark, M. J.; Heyd, J. J.; Brothers, E. N.; Kudin, K. N.; Staroverov, V. N.; Keith, T. A.; Kobayashi, R.; Normand, J.; Raghavachari, K.; Rendell, A. P.; Burant, J. C.; Iyengar, S. S.; Tomasi, J.; Cossi, M.; Millam, J. M.; Klene, M.; Adamo, C.; Cammi, R.; Ochterski, J. W.; Martin, R. L.; Morokuma, K.; Farkas, O.; Foresman, J. B.; Fox, D. J. *Gaussian 16 Rev. B.01*, Wallingford, CT, 2016.

[20] Zhao, Y.; Truhlar, D. G. *Theor. Chem. Acc.* **2008**, *120*, 215.

[21] a) Hariharan, P. C.; Pople, J. A. *Theor. Chem. Acc.* **1973**, *28*, 213. b) Francl, M. M.; Pietro, W. J.; Hehre, W. J.; Binkley, J. S.; DeFrees, D. J.; Pople, J. A.; Gordon, M. S. *J. Chem. Phys.* **1982**, *77*, 3654.

[22] a) Dolg, M.; Wedig, U.; Stoll, H.; Preuss, H. *J. Chem. Phys.* **1987**, *86*, 866. b) Martin, J. M. L.; Sundermann, A. *J. Chem. Phys.* **2001**, *114*, 3408

[23] Krishnan, R.; Binkley, J. S.; Seeger, R.; Pople, J. A. *J. Chem. Phys.* **1980**, *72*, 650.

[24] Scalmani, G.; Frisch, M. J. *J. Chem. Phys.* **2010,** *132*, 114110.

Chapter 2.

On the Mechanism of Cross-Dehydrogenative Couplings between *N*-Aryl Glycinates and Indoles: A Computational Study

ABSTRACT: Despite the widespread use of cross-dehydrogenative couplings in modern organic synthesis, mechanistic studies are still rare in the literature and those applied to *α*-amino carbonyl compounds remain virtually unexplored. Herein, the mechanism of Co-catalyzed cross-dehydrogenative couplings of *N*-aryl glycinates with indoles is described. Density functional theory studies supported the formation of an imine-type intermediate as the more plausible transient electrophilic species. Likewise, key information regarding the role of the *N*-aryl group and free NH motif within the reaction outcome has been gained, which may set the stage for further developments in this field of expertise.

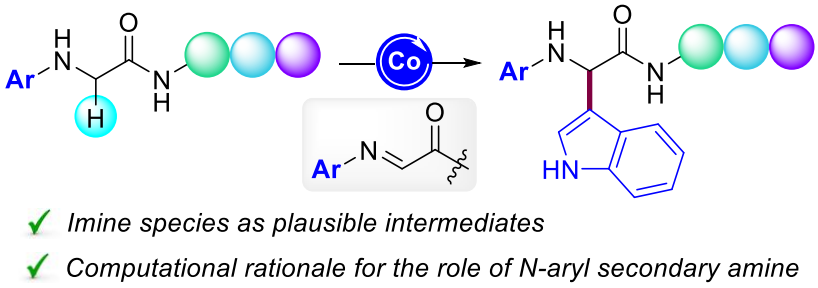

✓ *Imine species as plausible intermediates*

✓ *Computational rationale for the role of N-aryl secondary amine*

2.1. Introduction

2.1.1. C–H Functionalization of α-Amino Carbonyl Compounds

Amino acids and peptides are one of the most important building blocks for the construction of relevant compounds with interesting chemical and biological properties. They have numerous applications in pharmaceutical industry and they are often used as catalysts[25] and chiral ligands[26] in modern organic synthesis. In particular, unnatural amino acids and peptides have gained considerable attention in organic synthesis and drug discovery as they offer innumerable opportunities for the assembly of new compounds with increased activities and improved properties. Some selected examples of commercial drugs incorporating unnatural amino acids in their structure are shown in Figure 2.

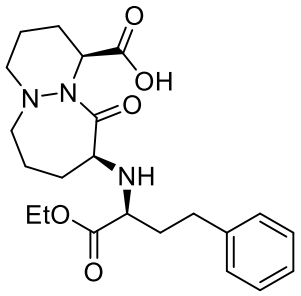

Cilazapril
Treatment of hypertension and heart failure

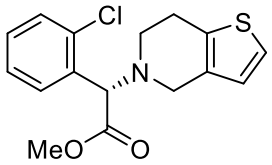

Clopidogrel
Reduce risk of heart disease and stroke

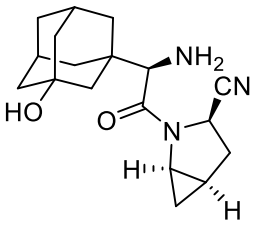

Saxagliptin
Treatement of type 2 diabetes mellitus

Figure 2. Illustrative examples of unnatural amino acids with pharmacological properties.

Due to the increased number of applications of these molecules, the development of new methodologies for the synthesis of α-amino carbonyl derivatives plays a key role in the evolution of synthetic organic chemistry. In contrast to classical methodologies,[27] direct C–H functionalization of amino acids and peptides allows the use of non-functionalized simple starting

[25] Yadav, G.; Deepa Singh, S. *ChemistrySelect* **2019**, *4*, 5591.
[26] Shao, Q.; Wu, K.; Zhuang, Z.; Qian, S.; Yu, J.-Q. *Acc. Chem. Res.* **2020**, *53*, 833.
[27] a) Hashimoto, T.; Maruoka, K. *Chem. Rev.* **2007**, *107*, 5656. b) Shirakawa, S.; Maruoka, K. *Angew. Chem. Int. Ed.* **2013**, *52*, 4312. c) Bondalapati, S.; Jbara, M.; Brik, A. *Nat. Chem.* **2016**, *8*, 407.

materials, being a tool to synthesize a wide range of their unnatural derivatives in an atom-economical manner. Moreover, the mild reaction conditions often employed in combination with the site-selective protocols have enabled the late-stage modification of complex peptides avoiding racemization during the process.

The existing different procedures for the C–H functionalization of amino acids could be classified according to the position of the C–H bond within the structure of the corresponding α-amino carbonyl compound (Figure 3).

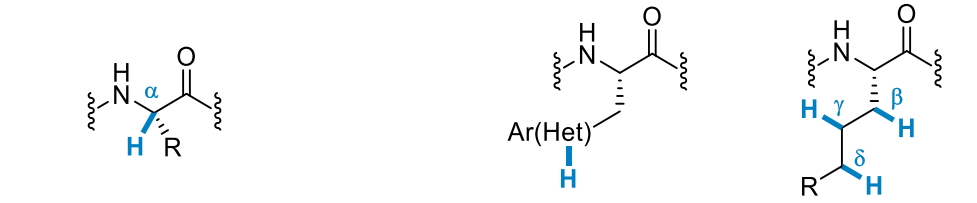

peptide backbone
α-C(sp^3)-H functionalization

peptide side-chain
C(sp^2)-H *vs* C(sp^3)-H functionalization

Figure 3. Different C–H positions in α-amino carbonyl compounds.

Frequently, the α-C(sp^3)–H functionalization at the peptide backbone is proposed to proceed via outer-sphere mechanism, in which a C–metal bond is not formed. Accordingly, these α-C(sp^3)–H bonds are activated by single electron transfer (SET) or hydrogen atom transfer (HAT) events, commonly catalyzed by first-row transition metals. In these cases, cationic or radical electrophilic species are formed, which are prone to react with different nucleophiles. On the other hand, the inner-sphere mechanism involves a direct interaction between the corresponding C–H bond and the metal center, thus forming an organometallic intermediate often with the aid of a DG. Although there are some exceptions, the latter approach is commonly used for the C–H functionalization at the peptide side-chain (Scheme 7).[28]

[28] a) Brandhofer, T.; Mancheño, O. G. *Eur. J. Org. Chem.* **2018**, 6050. b) San Segundo, M.; Correa, A. *Synthesis* **2018**, *50*, 2853.

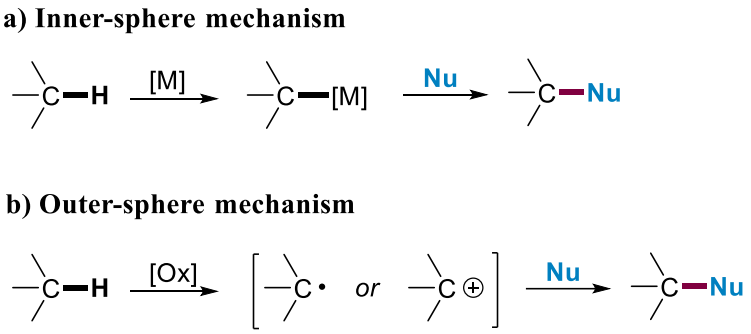

Scheme 7. Inner- and outer-sphere mechanisms.

For the selective functionalization of α-C(sp^3)–H bonds through SET or HAT events, the presence of a heteroatom in α position to the bond to be coupled tends to be essential. Moreover, for *N*-containing compounds the presence of an *N*-aryl motif seems to be of crucial importance.[28,29] Regarding peptide chemistry, *N*-aryl glycine or its derivatives have been widely employed. The *N*-aryl system acts as a DG, turning the C–H bond prone to undergo an easy oxidation step and favoring the formation of α-aldimine or α-aldiminium electrophilic intermediates (Scheme 8).

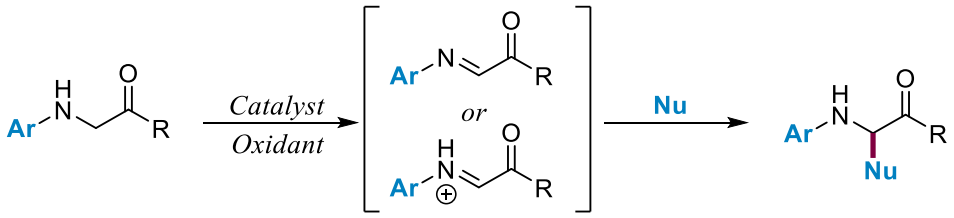

Scheme 8. α-C(sp^3)–H functionalization of glycine derivatives.

[29] a) Tian, T.; Li, Z.; Li, C.-J. *Green Chem.* **2021**, *23*, 6789. b) Huang, C.-Y.; Kang, H.; Li, J.; Li, C.-J. *J. Org. Chem.* **2019**, *84*, 12705. c) Girard, S. A.; Knauber, T.; Li, C.-J. *Angew. Chem. Int. Ed.* **2014**, 53, 74.

2.1.2. Cross-Dehydrogenative Couplings for the C–H Functionalization of Glycine derivatives

Aryl glycines are an important class of non-proteinogenic amino acids present in a large amount of glycopeptides and common intermediates in the synthesis of β-lactam antibiotics.[30] Petasis reaction,[31] Strecker reaction[32] and Ugi reaction[33] are among the traditional methods to prepare this type of compounds. However, the direct α-C(sp^3)–H functionalization through Cross-Dehydrogenative Coupling (CDC) processes could be considered as the most ideal synthetic approach.[29] This CDC strategy involves the direct coupling of two C–H or X–H bonds, being an elegant tool for the diversification of complex peptides in an atom-economical and environmentally friendly manner. Formally, these reactions proceed with the release of H_2 during the process but, nevertheless, it does not occur and the two hydrogen atoms are commonly abstracted by the oxidant (Scheme 9).

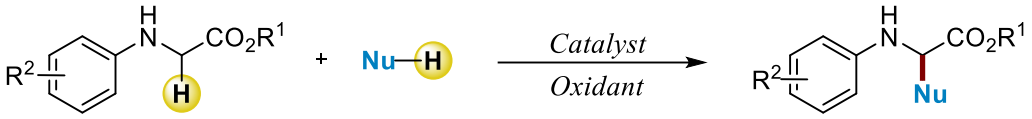

Scheme 9. CDC reactions for the diversification of glycine derivatives.

Inspired by their previous works on the field,[34] in 2008 and 2009 Li and co-workers described the efficient coupling between α-amino carbonyl compounds and different nucleophiles for the first time upon a CDC process (Scheme 10).[35,36] In these pioneering works, by using a catalytic amount of copper bromide in combination with *tert*-butyl hydroperoxide (TBHP) they were able to introduce aromatic alkynes, (hetero)aryl boronic acids and indoles into glycine derivatives and short peptides. Performing a control experiment, they confirmed the generation of an imine within

[30] Elander, R. P. *Appl. Microbiol. Biotechnol.* **2003**, *61*, 385.
[31] Candeias, N. R.; Montalbano, F.; Cal, P. M. S. D.; Gois, P. M. P. *Chem. Rev.* **2010**, *110*, 6169.
[32] Martens, J. *ChemCatChem* **2010**, *2*, 379.
[33] Wessjohann, L. A.; Rhoden, C. R. B.; Rivera, D. G.; Vercillo, O. E. *Top. Heterocycl. Chem.* **2010**, *23*, 199.
[34] For selected examples, see: a) Li, Z.; Bohle, D. S.; Li, C.-J. *Proc. Natl. Acad. Sci. USA* **2006**, *103*, 8928. b) Li, Z.; Li, C.-J. *J. Am. Chem. Soc.* **2004**, *126*, 11810. c) Li, Z.; Li, C.-J. *Org. Lett.* **2004**, *6*, 4997. d) Li, Z.; Li, C.-J. *J. Am. Chem. Soc.* **2005**, *127*, 3672. e) Li, Z.; Li, C.-J. *J. Am. Chem. Soc.* **2005**, 127, 6968.
[35] Zhao, L.; Li, C.-J. *Angew. Chem. Int. Ed.* **2008**, *47*, 7075.
[36] Zhao, L.; Baslé, O.; Li, C.-J. *Proc. Natl. Acad. Sci. USA* **2009**, *106*, 4106.

the catalytic cycle. The mild temperatures for some of these coupling processes could be attributed to the presence of the PMP protecting group within the *N*-terminal unit of the peptide sequence, which apparently lowered the oxidation potential of the corresponding glycine residue, thus enhancing the formation of the proposed imine intermediate.

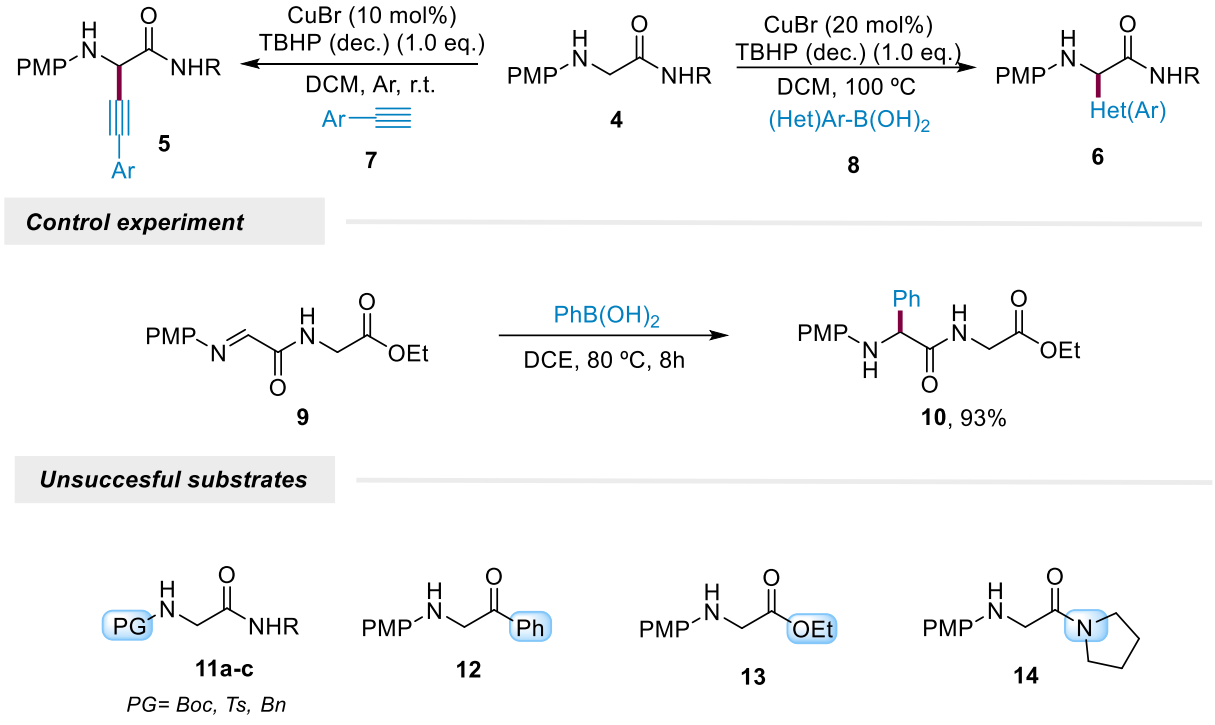

Scheme 10. Seminal work reported by Li and co-workers.

Despite the utility of this method, the synthetic scope was limited to very specific starting materials. On the one hand, when the amide functionality of the *C*-terminal unit was switched to ketone **12** or the ester **13** the reaction did not occur or afforded a complex mixture of unidentified compounds. They hypothesized that the lower oxidation potential of the amide could be the reason for the stabilization of the transient imine intermediate.[36] On the other hand, on the basis that compound **14** was found unreactive when aryl boronic acids were used as coupling partners they suggested that the reaction mechanism could be different depending on the nucleophile employed. Finally, other *N*-protecting groups such as Boc (**11a**), Ts (**11b**) and Bn (**11c**) did not afford the

desired products, which anticipated and reinforced the apparent strong requirement of placing a PMP-group onto the terminal amine for the process to occur.

This seminal work developed by Li and co-workers set de basis on the field. Since then, a high number of methodologies have been developed, which expanded the synthetic scope and overcome some of the drawbacks disclosed above. To date, a wide variety of coupling partners including phenols,[37] ketones,[38] (thio)ethers,[39] alkanes,[40] phosphines,[41] alcohols and thiols have been successfully employed.[42] Moreover, enantioselective CDC reactions of Gly derivatives have been also reported.[43] However, despite the broad scope and high synthetic potential of these reactions for the α-functionalization of amino acid derivatives, they are still limited to the use of *N*-aryl Gly compounds.

2.1.3. Limitations of the CDC Technique

Even though a plethora of strategies have been developed for the synthesis of non-proteinogenic amino acids, their success depends on the presence of an *N*-aryl group at the terminal amine. Although its actual role is not entirely clear, it has been proposed to stabilize the transient radical or cationic intermediates. In fact, there are only two examples in which the CDC methodology was successfully applied for the functionalization of non-aromatic α-amino carbonyl compounds devoid of this *N*-aryl motif. Indeed, although other protecting groups such as Boc, Ts and benzyl were tested, all attempts to obtain the desired products failed.[36,44]

---

[37] Salman, M.; Zhu, Z.-Q.; Huang, Z.-Z. *Org. Lett.* **2016**, *18*, 1526.
[38] a) Xie, J.; Huang, Z.-Z. *Angew. Chem. Int. Ed.* **2010**, *49*, 10181. b) Liu, P.; Wang, Z.; Lin, J.; Hu, X. *Eur. J. Org. Chem.* **2012**, *1583.* c) Gao, X.-W.; Meng, Q.-Y.; Xiang, M.; Chen, B.; Feng, K.; Tung, C.-H.; Wu, L.-Z. *Adv. Synth. Catal.* **2013**, *355*, 2158.
[39] a) Wei, W.-T.; Song, R.-J.; Li, J.-H. *Adv. Synth. Catal.* **2014**, *356*, 1703. b) Peng, H.; Yu, J.-T.; Jiang, Y.; Yang, H.; Cheng, J. *J. Org. Chem.* **2014**, *79*, 9847.
[40] a) Wang, C.; Qi, R.; Xue, H.; Shen, Y.; Chang, M.; Chen, Y.; Wang, R.; Xu, Z. *Angew. Chem Int. Ed.* **2020**, *59*, 7461. b) Tian, H.; Xu, W.; Liu, Y.; Wang, Q. *Org. Lett.* **2020**, *22*, 5005.
[41] a) Yang, B.; Yang, T.-T.; Li, X.-A.; Wang, J.-J.; Yang, S.-D. *Org. Lett.* **2013**, *15*, 5024. b) Zhi, H.; Ung, S. P.-M.; Liu, Y.; Zhao, L.; Li, C.-J. *Adv. Synth. Catal.* **2016**, *358*, 2553. c) Jia, X.; Liu, X.; Yuan, Y.; Yuan, Y.; Zhu, Y.; Hou, W.; Zhang, X. *Adv. Synth. Catal.* **2017**, *359*, 4399.
[42] Liu, X.; Pu, J.; Luo, X.; Cui, X; Wu, Z.; Huang, G. *Org. Chem. Front*. **2018**, *5*, 361.
[43] a) Xie, Z.; Liu, X.; Liu, L. *Org. Lett.* **2016**, *18*, 2982. b) Zhang, G.; Zhang, Y.; Wang, R. *Angew. Chem. Int. Ed.* **2011**, *50*, 10429. c) Tan, Y.; Yuan, W.; Gong, L.; Meggers, E. *Angew. Chem. Int. Ed.* **2015**, *54*, 13045. d) Wei, X.-H.; Wang, G.-W.; Yang, S.-D. *Chem. Commun.* **2015**, *51*, 832.
[44] Zhang, Ni.; Ni, M.; Feng, B. *Org. Biomol. Chem.* **2016**, *14*, 1550.

The first example of a CDC reaction in which the *N*-terminal unit of a Gly moiety is not substituted by an aryl motif was published by the group of Li (Scheme 11).[35] This protocol described the efficient introduction of different malonates into the α-position of *N*-acetylglycine derivatives **15** using copper salts as stoichiometric oxidant in combination with di(2-pyridyl)ketone as ligand. They suggested that the high reactivity of this particular chelating auxiliary could be due to the formation of a six-membered complex. Moreover, its electron withdrawing nature rendered the copper center more electronegative during the transition state and hence, the abstraction of the NH proton could occur more easily.

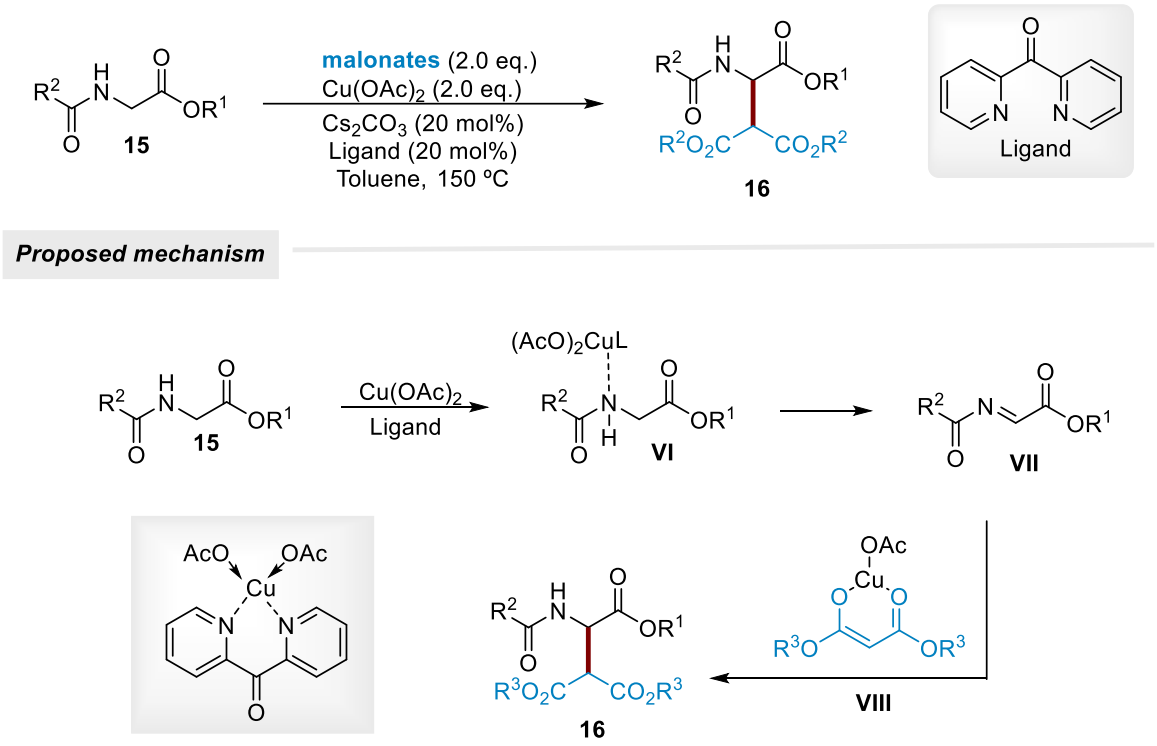

Scheme 11. Functionalization of N-Acyl Gly derivatives using copper salts.

In this specific case, the addition of radical inhibitors did not affect the overall yield, which suggested that the participation of a radical intermediate was unlikely to occur. Consequently, they proposed the formation of the imine species **VII** upon a single-step oxidation with the starting Cu^{II}, followed by a Mannich-type reaction between the electrophilic intermediate and the corresponding malonate to afford the desired product. Notably, Cs_2CO_3 not only acted as a neutralizing agent for the acetic acid released within the process, but also improved the enolization step of the

nucleophile. It is worth mentioning that the required harsh reaction conditions were attributed to the generation of challenging *N*-acetylglycine electrophilic intermediates, which are more unstable than their parent ones derived from *N*-aryl Gly systems.

The second strategy was developed by the group of You between the years 2013 and 2015 (Scheme 12).[45,46] On these works, the authors utilized the PA chelating group to promote the generation of the challenging α-ketimine or α-aldimine intermediates. Upon using first-row transition metals such as $FeCl_3$ or $Ni(acac)_2$ as catalyst, DTBP as oxidant and high temperatures, they were able to synthesize a high amount of tertiary and quaternary amino acid derivatives **18** using different nucleophiles as coupling partners in very good yields. Curiously, when radical nucleophiles were used some mechanistic experiments revealed that the formation of an imine/iminium ion within the catalytic cycle was unlikely to happen. Surprisingly, the use of Gly derivatives required higher temperatures than the α-substituted analogues.

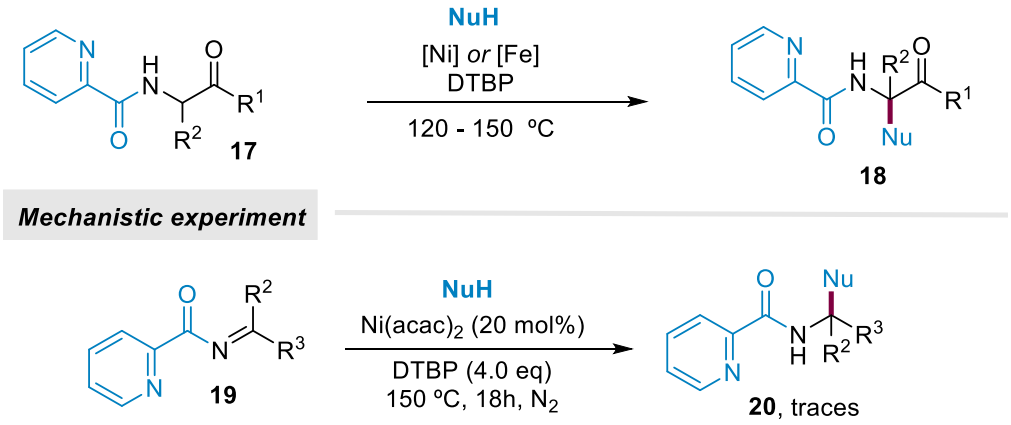

Scheme 12. C–H functionalization of α-amino carbonyl compounds assisted by PA directing group.

On the basis of the mechanistic experiments, they proposed the reaction pathway depicted on Scheme 13. First, Ni^{II} is oxidized by DTBP to produce a Ni^{III} species and *tert*-butoxyl radical. Then, the substrate is coordinated to the metal center and reacts with the previously formed benzylic radical **X** to form the radical cation intermediate **XI**. The latter undergoes an

[45] Li, K.; Wu, Q.; Lan, J.; You, J. *Nat. Commun.* **2015**, *6*, 8404.
[46] Li, K.; Tan, G.; Huang, J.; Song, F.; You, J. *Angew. Chem. Int. Ed.* **2013**, *52*, 12942.

intramolecular SET event catalyzed by the metal center to provide the intermediate **XII**, thereby recycling the catalyst and releasing the product. Nevertheless, this particular mechanistic proposal is not supported by experimental evidences and further studies are required to set the chemical basis of this concrete transformation. Based on previous literature reports, the formation of carbon centered radicals by PCET or HAT events followed by a radical-radical coupling would be a more rationale mechanistic scenario. Although merely speculative, the demand of higher temperatures to functionalize the glycine unit in comparison with the rest of α-substituted amino acids could be in concordance with the lower stability of secondary carbon centered radicals. More recently, Correa and co-workers have expanded the scope of this methodology upon using ethers as coupling partners.[47]

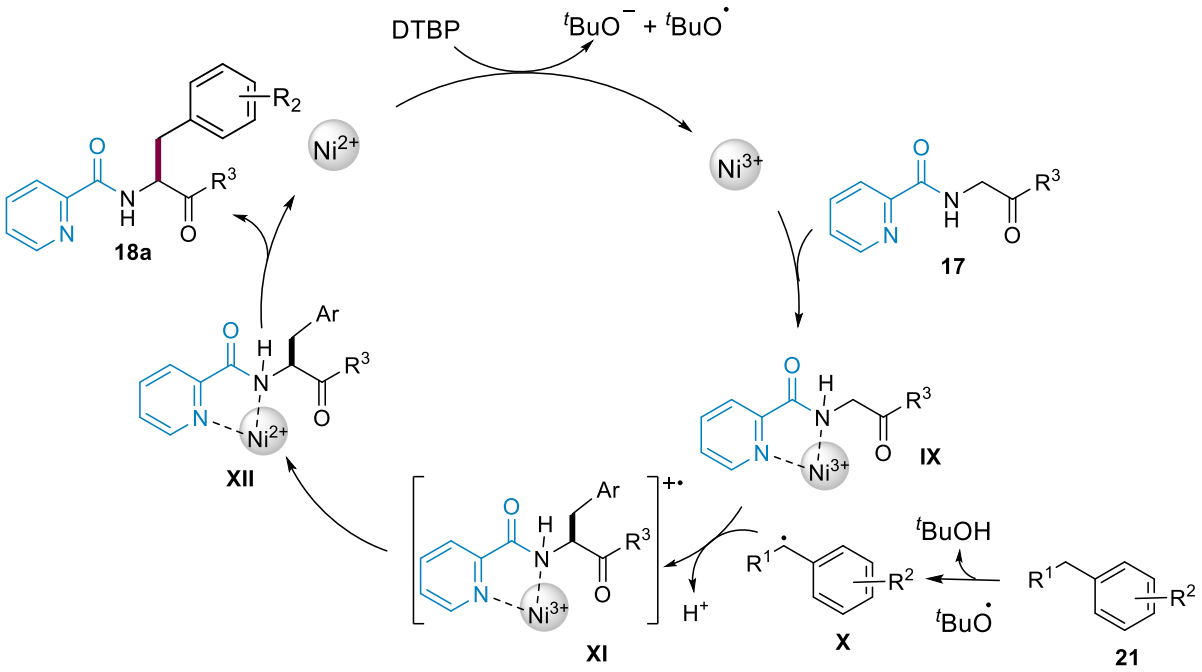

Scheme 13. Proposed mechanism for the Ni-catalyzed functionalization of PA-protected amino acid derivatives.

In general, the functionalization of *N*-aryl Gly derivatives can be carried out under low temperatures, low excess of oxidants and catalytic amounts of first-row transition metals. In

[47] San Segundo, M.; Correa, A. *Adv. Synth. Catal.* **2022**, *364*, 3171.

contrast, the harsh-reaction conditions for the functionalization of *N*-acyl Gly derivatives explained above evidenced the challenging formation of the corresponding transient intermediates. Despite these limitations, CDC reactions have been successfully applied for the synthesis of non-proteinogenic amino acids, which could not be synthesized through traditional Petasis, Strecker and Ugi reactions.

2.1.4. CDC Reactions between Gly Derivatives and Indoles

Indole is a key building block in the field of drug discovery because it is present in many natural and synthetic molecules with high biological activity and relevant applications in medicinal chemistry (Figure 4).[48]

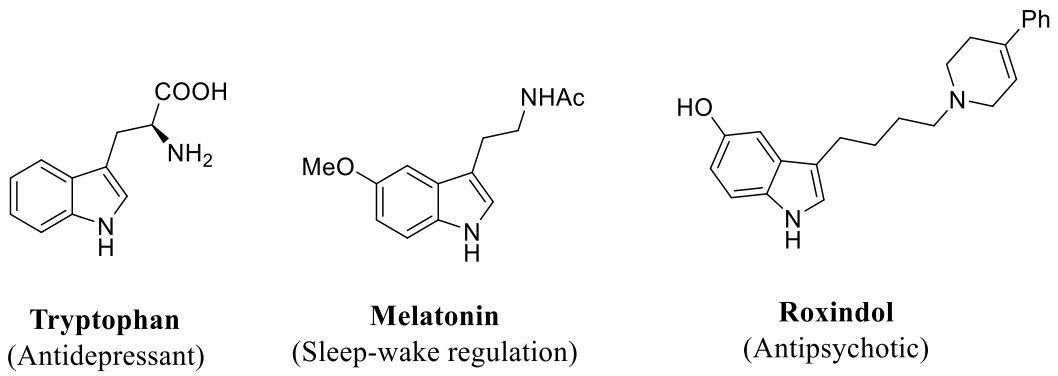

Figure 4. Indole-containing bioactive molecules.

The synthesis of indole-containing Gly derivatives could not be achieved using traditional methods. In contrast, the CDC methodology enables the installation of the indole moiety into the peptide backbone in an operationally simple fashion, under mild reaction conditions and using first-row transition metal catalysis. In this respect, Li and co-workers employed previously developed copper-catalyzed arylation protocol to assemble the first indolylglycine tripeptide **23** with 89% yield (Scheme 14).[36] Since then, great efforts have been made to expand the synthetic

[48] a) Jagtap, R. A.; Punji, B. *Asian J. Org. Chem.* **2020**, *9*, 326. b) Zenkov, R. G.; Ektova, L. V.; Vlasova, O. A.; Belitskiy, G. A.; Yakubovskaya, M. G.; Kirsanov, K. I. *Chem. Heterocycl. Compd.* **2020**, *56*, 644.

scope of this methodology by using different transition metals such as Fe and Co, or even employing photoredox techniques.

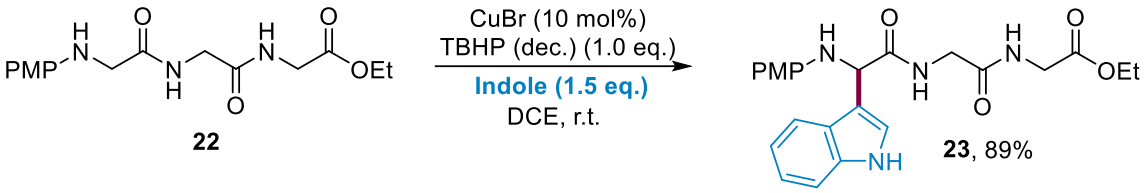

Scheme 14. Synthesis of indolylglycine tripeptide reported by Li.

In 2012, Li and co-workers developed a mild route to the selective synthesis of 2-(1*H*-indol-3-yl)-2-imino-carbonyls **26** and 2-(1*H*-indol-3-yl)-2-oxo-carbonyls **25** by $CuCl_2$-mediated cross-dehydrogenative coupling processes with the aid of *tert*-butyl hydroperoxide (Scheme 15a).[49] Interestingly, when the reaction was carried out under air atmosphere the selectivity of the reaction shifted to 2-ketoesters or 1,2-diones. On the basis of some mechanistic experiments, they proposed the formation of an imine as the transient intermediate through a TBHP-mediated oxidative radical deprotonation. Two years later, Yuan and co-workers reported the first aerobic oxidative α-arylation of glycine esters, glycine amide derivatives and short peptides using CuCl as catalyst (Scheme 15b).[50] In this case, the reaction did not afford the desired product under argon atmosphere. They concluded that molecular oxygen was essential for the initiation of the catalytic cycle. Indeed, they proposed the formation of a C-centered radical catalyzed by the previously oxidized $Cu^{II}OO^{\bullet}$ species, which then could react with a second molecule of Cu^{II} rendering an iminium ion and reducing the Cu^{II} to Cu^{I}.

[49] Wu, J.-C.; Song, R.-J.; Wang, Z.-Q.; Huang, X.-C.; Xie, Y.-X.; Li, J.-H. *Angew. Chem. Int. Ed.* **2012**, *51*, 3453.
[50] Huo, C.; Wang, C.; Wu, M.; Jia, X.; Xie, H.; Yuan, Y. *Adv. Synth. Catal*. **2014**, *356*, 411.

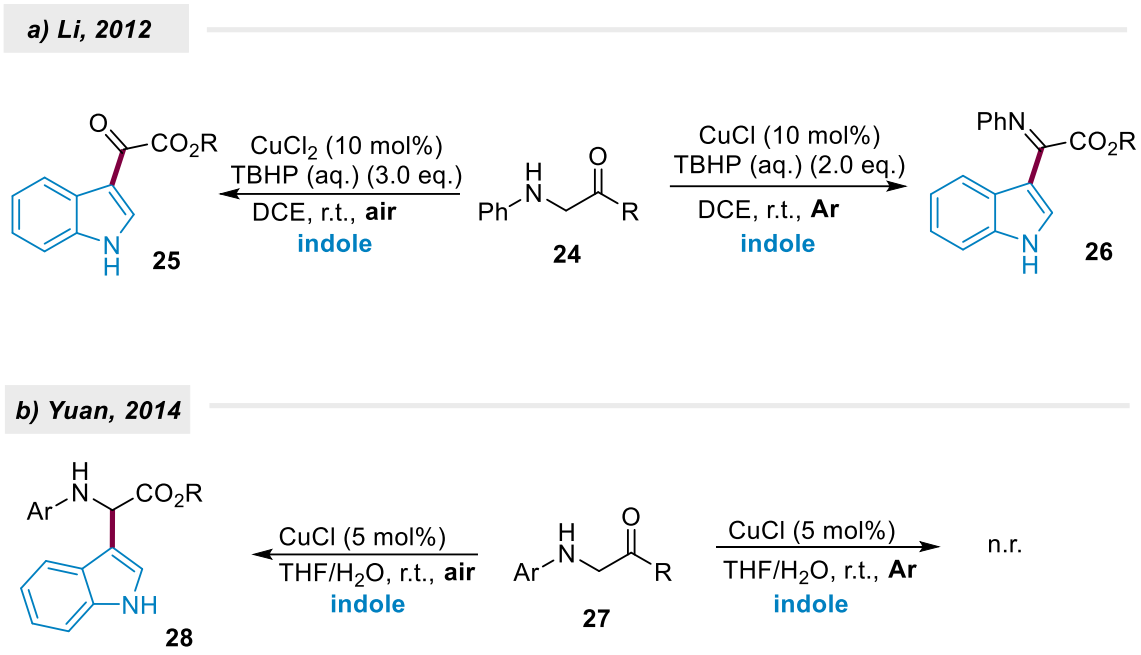

Scheme 15. Complementary strategies developed by Li and Yuan.

More recently, the group of Feng published the first iron-catalyzed α-heteroarylation of glycine esters and derivatives in the presence of aqueous TBHP and under air atmosphere (Scheme 16).[44] In concordance with the previous mechanistic proposals, they confirmed the participation of an imine (**30**) as the transient electrophilic species by *in situ* LC-MS analysis. The optimal conditions were found to be viable for a high number of indoles and *N*-aryl glycines with electron-donating and electron-withdrawing substituents. Curiously, they found that the *N*-methylated Gly derivative **29** did not react under the standard conditions, which evidenced that the hydrogen atom present in the secondary amine could participate within the course of the chemical reaction.

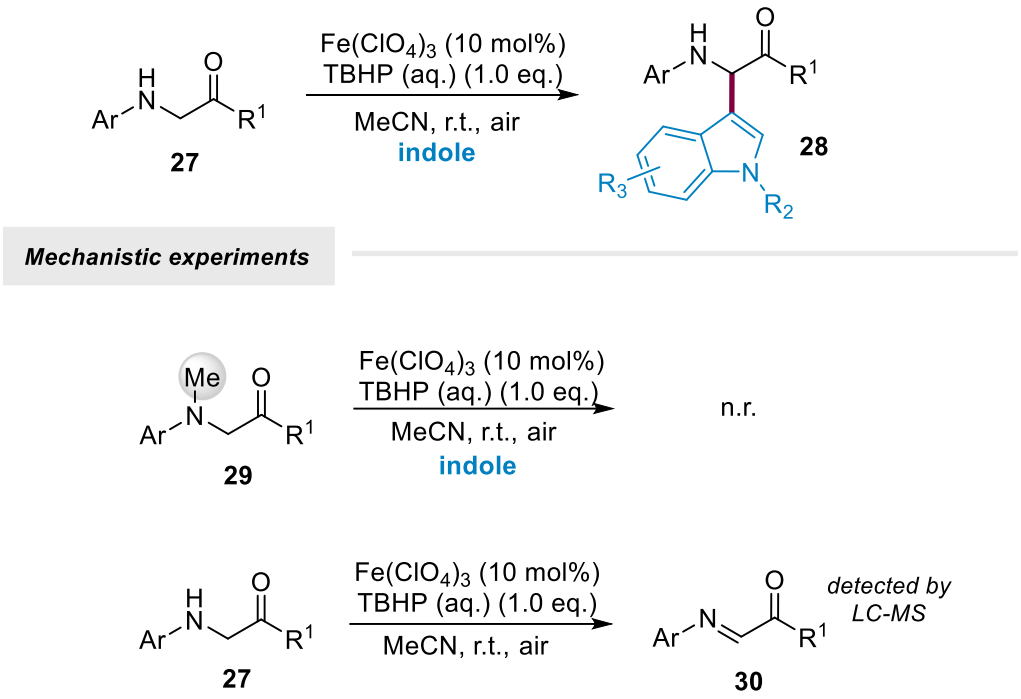

Scheme 16. Mechanistic experiments carried out by Feng.

Regarding photoredox chemistry, Rueping proposed a novel strategy for the C–H functionalization of *N*-aryl glycine derivatives using visible light for the first time,[51] combining a Lewis acid and photoredox catalysis. As depicted on Scheme 17, after the oxidation of the glycinate **31**, the coordination of the Lewis acid during the formation of **XV** with simultaneous activation for nucleophilic attack presumably avoided the undesired side reactions and allowed the formation of the targeted α-arylated products **33** with high selectivity. Although this method was compatible with more complex dipeptides, the scope was limited to *N*-(*p*-tolyl)glycine derivatives **31** and a very expensive and toxic Ir catalyst was needed. It is worth mentioning that Ru-photocatalyzed indolation of glycine derivatives has been reported by Li and co-workers.[52] Nevertheless, this strategy was also limited to *N*-(tolyl)glycine derivatives and required long reaction times.

[51] Zhu, S.; Rueping, M. *Chem. Commun.* **2012**, *48*, 11960
[52] Wang, Z.-Q.; Hu, M.; Huang, X.-C.; Gong, L.-B.; Xie, Y.-X.; Li, J.-H. *J. Org. Chem.* **2012**, *77*, 8705.

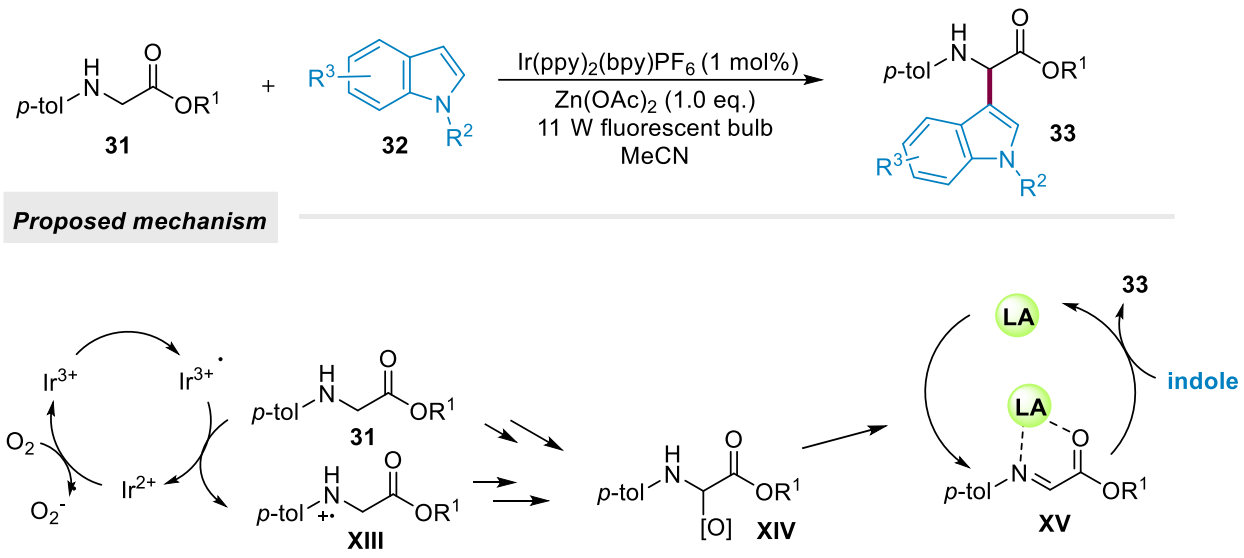

Scheme 17. Visible-light catalyzed C–H functionalization of Gly derivatives.

In 2015, Wu and co-workers described an oxidant-free strategy for the C–H functionalization of PMP-glycine esters **34**, using a combination of visible light, Ru photocatalyst and Co salts (Scheme 18).[53] Interestingly, the only byproduct of this reaction is the gaseous molecular hydrogen. In this strategy, the reaction starts when the photoexcited Ru catalyst reacts with the glycine derivative **34** via a SET process producing *N*-centered radical cation **XVI**, which reacts with the Co^{II} co-catalyst to render the imine/iminum intermediate **XVII**/**XVIII** while the Co^{II} salt is reduced Co^{I}. The cobalt salt plays a key role in the regeneration of the Ru catalyst as well as on the synthesis of gaseous H_2 within the process.

[53] Gao, X.-W.; Meng, Q.-Y.; Li, J.-X.; Zhong, J.-J.; Lei, T.; Li, X.-B.; Tung, C.-H.; Wu, L.-Z. *ACS Catal.* **2015**, *5*, 2391.

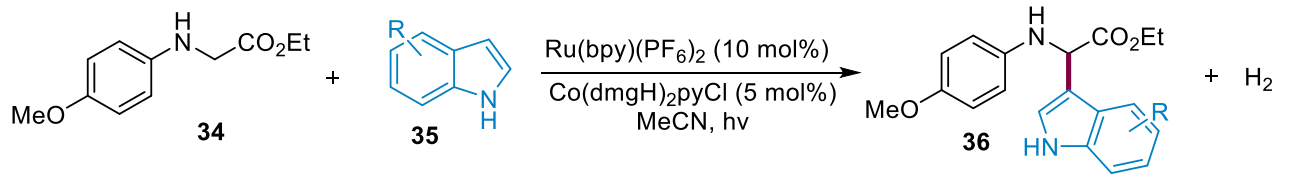

Proposed mechanism

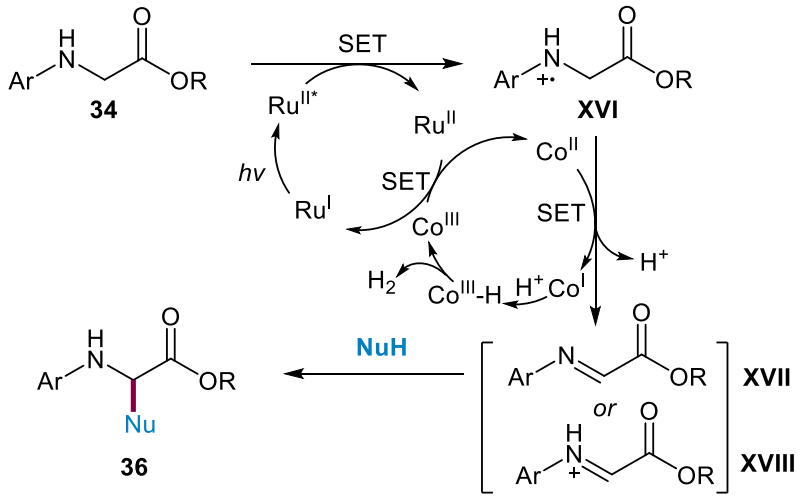

Scheme 18. Visible light mediated functionalization of PMP-Gly-OEt.

In 2017, our group developed a complementary strategy for the CDC reaction between *N*-aryl glycine derivatives **37** and different nucleophiles such as indoles and THF, using $Co(acac)_2$ as catalyst and aqueous TBHP as oxidant (Scheme 19).[54] Under the optimized reaction conditions, a wide variety of electron-rich and electron-poor heteroaryl compounds underwent the coupling reaction with very good yields. Additionally, in contrast with some of the methods previously developed, this protocol was tolerant with a wide range of *N*-aryl moieties and enabled the use of more complex peptide sequences.

[54] Guerrero, I.; San Segundo, M.; Correa, A. *Org. Lett.* **2017**, *19*, 5288.

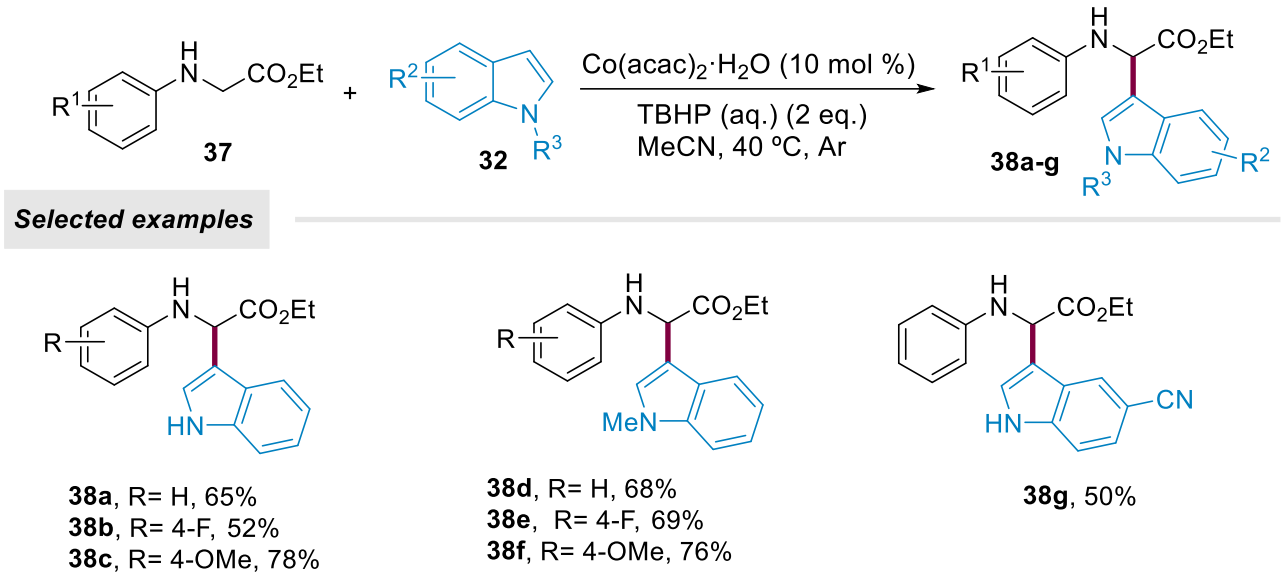

Scheme 19. Co-catalyzed CDC reaction developed by Correa and co-workers.

Based on some mechanistic experiments and previous reports on the field, a preliminary reaction pathway was proposed (Scheme 20). The reaction would start with the Co^{II}-induced decomposition of *t*BuOOH, and subsequent HAT would furnish the alkyl radical intermediate **XIX**. The latter would be likely converted through a SET event assisted by Co^{III} to the electrophilic iminium ion **XXI**, which upon reaction with the corresponding indole would eventually deliver the coupling product.

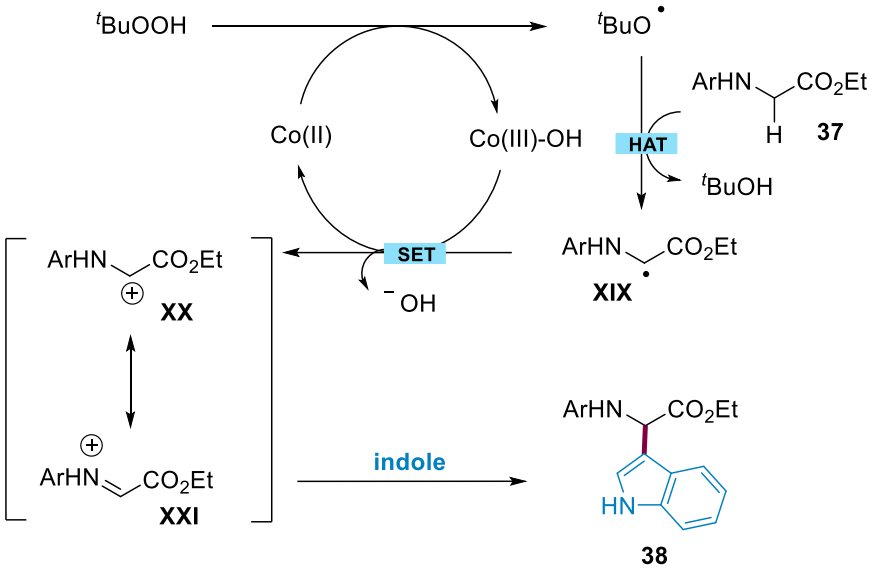

Scheme 20. Proposed mechanism.

As explained in this section, numerous techniques have been developed for the efficient introduction of the indole ring into *N*-aryl Gly derivatives. Although different mechanistic scenarios have been proposed by different research groups, all the studies agree on the formation of an imine/iminium ion through oxidative processes. However, these mechanistic proposals could be considered as speculations and the exact activation mode of the amine is still unclear. In this respect, over the last decade some computational and experimental studies have been made to clarify the mechanistic nuances of CDC reactions involving tertiary amines and different nucleophiles.

2.1.5. DFT Studies on Cross-Dehydrogenative Coupling Reactions Adjacent to a Nitrogen Atom

To date, the existing mechanistic studies and DFT calculations regarding cross-dehydrogenative coupling reactions with amines only involve tertiary amines. Conversely, mechanistic studies featuring secondary amines such as *N*-aryl glycine derivatives are virtually unexplored. Accordingly, the proposed mechanisms are often based on indirect experimental evidences or even mere extensions of the ones proposed for tertiary amines such as *N*,*N*-dimethylanilines and THIQs (Figure 5).

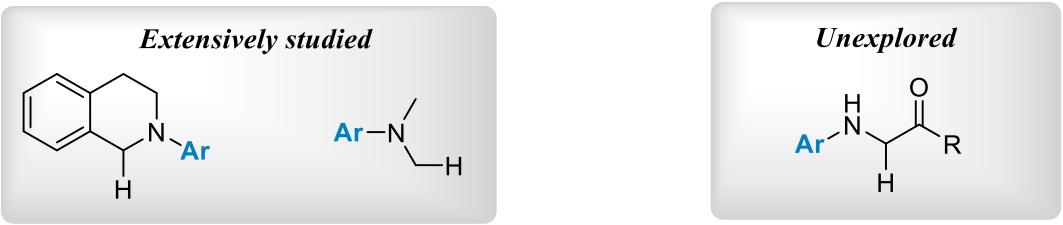

Figure 5. Common substrates used in CDC reactions upon DFT studies.

Since the first reports by Miura[55] and Murahashi[56] on Ru- and Fe-catalyzed oxidative functionalization of tertiary amines, these reactions have been proposed to proceed via the formation of iminium species which subsequently react with different nucleophiles to form the desired products. Although some mechanistic investigations of related reactions have been reported during the last decade, the exact mode of activation of the amine remains unclear. In 2011 Klussmann and co-workers experimentally demonstrated the intermediacy of an iminium ion when using a $CuCl_2/O_2$ system in the oxidative functionalization of *N*-phenyltetrahydroisoquinoline **39** (Scheme 21).[57] They were able to isolate intermediate **XXIII** in 26% yield by crystallization and characterized it by X-ray crystallography, confirming the general nature of the typically proposed reactive copper-iminium species. Moreover, their findings also revealed the existence of solvent-dependent off-cycle intermediates. The latter could act as a stable reservoir for the electrophilic iminium ion, not only upon diminishing undesired side reactions if nucleophilic additions are much slower than the oxidation step, but also releasing the catalyst during the equilibrium process.

[55] Murata, S.; Miura, M.; Nomura, M. *J. Chem. Soc., Chem. Commun.* **1989**, 116.
[56] a) Murahashi, S.-I.; Komiya, N.; Terai, H.; Nakae, T. *J. Am. Chem. Soc.* **2003**, *125*, 15312. b) Murahashi, S.-I.; Komiya, N.; Terai, H.; Nakae, T. *Angew. Chem. Int. Ed.* **2005**, *44*, 6931.
[57] Boess, E.; Sureshkumar, D.; Sud, A.; Wirtz, C.; Farès. C.; Klussmann, M. *J. Am. Chem. Soc.* **2011**, *133*, 8106.

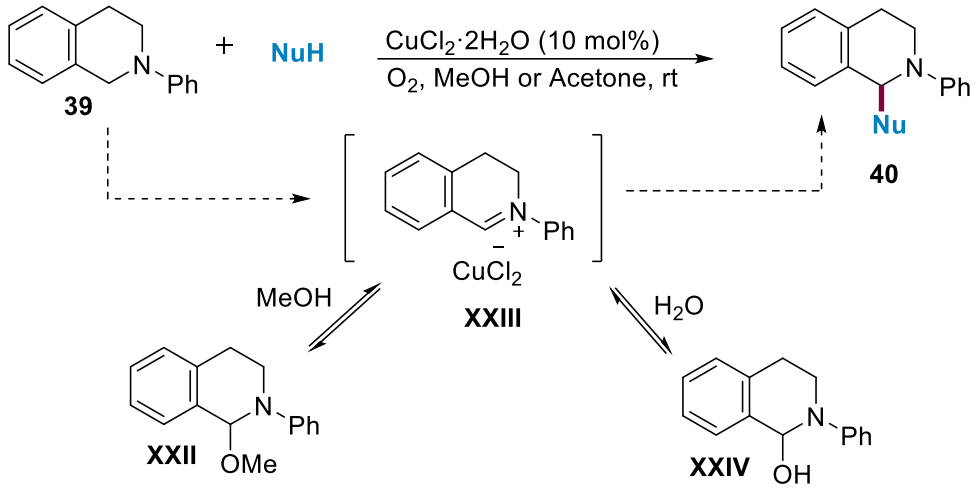

Scheme 21. Preliminary experiments carried out by Klussmann and co-workers.

The next year, they investigated the influence of the nucleophilicity and the concrete role of the oxidant.[58] For this purpose, they compared two different catalytic systems: the $CuCl_2 \cdot H_2O/O_2$ system developed by their own group[59] and the CuBr/TBHP system developed by Li and co-workers (Scheme 10).[34b]

Regarding the $CuCl_2 \cdot H_2O/O_2$ catalytic system, they observed the fast formation of the iminium ion **XXIII** by reacting amine **39** with the catalyst under argon atmosphere. This mechanistic experiment suggested that the copper is the only species involved on the oxidation of the tertiary amine and the role attributed to molecular oxygen was the regeneration of the active catalyst (Scheme 22). On the other hand, they performed a kinetic isotope effect experiment (KIE) and concluded that the oxidation of **39** most likely implied the preliminary formation of an ammoniumyl radical cation through a SET process, which preceded the generation of the iminium salt via HAT or a combination of electron and proton transfer events. This study suggested that the key step could be the oxidative formation of the iminium cation.

[58] Boess, E.; Schmitz, C.; Klussmann, M. *J. Am. Chem. Soc.* **2012**, *134*, 5317.
[59] Sureshkumar, D.; Sud, A.; Klussmann, M. *Synlett* **2009**, 1558.

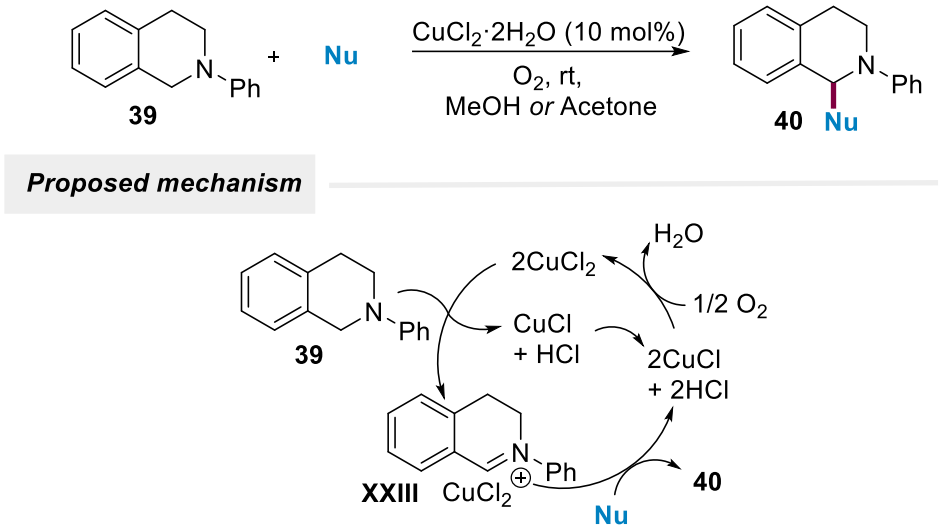

Scheme 22. Reaction pathway for $CuCl_2/O_2$ system.

Curiously, they observed that weak nucleophiles, which did not react under aerobic conditions, could provide the cross-coupling products when O_2 was replaced by TBHP (Scheme 23). By reacting the substrate with 50 mol% of the catalyst in the presence of the oxidant and in the absence of the nucleophile, they did not find any signals of the iminium ion on the NMR analysis. In this case, the only species identifiable was the amino peroxide **XXV**. In contrast to the off-cycle intermediates that were formed under aerobic conditions, they observed the accumulation of the peroxide **XXV** during the initial stages of the reaction and concluded that it should be inside the catalytic cycle. Moreover, the formation of the iminium ion **XXVI** via subsequent SET processes was discarded due to the suppression of the reactivity in the presence of BHT and some KIE experiments. The latter indicated that the break of the C–H bond could be the rate-determining step of the reaction and that a carbon-centered radical was more likely to be involved within the process.

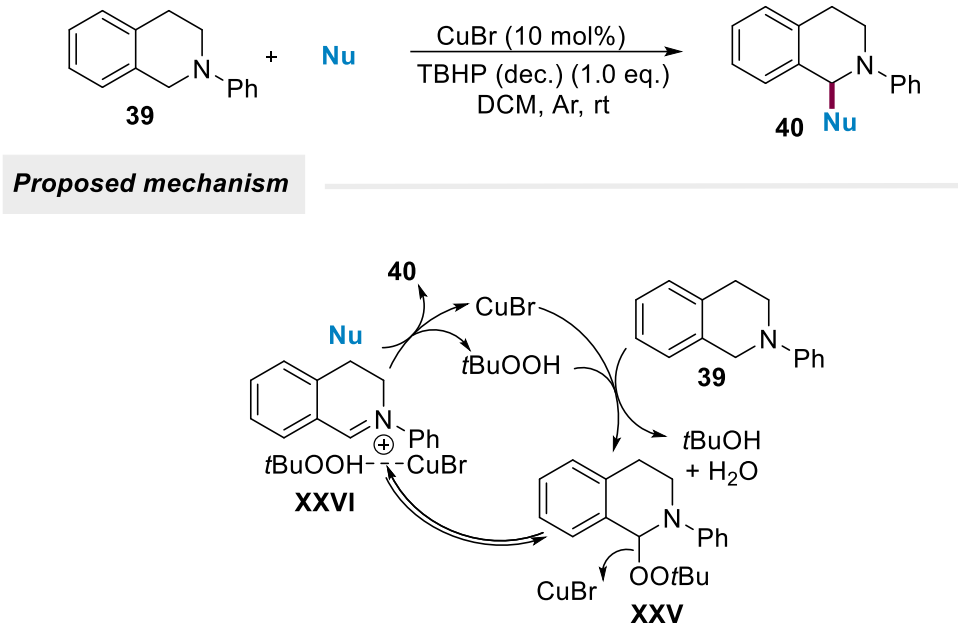

Scheme 23. Reaction pathway for CuBr/tBuOOH system.

Next, they performed experimental and computational studies to confirm whether the HAT or ET was the key step of the oxidation of THIQ catalyzed by Cu/TBHP system (Scheme 24).[60] They showed that the electronic effects caused by different substituents within the *N*-aryl THIQ molecule were minimal, which was in agreement with a HAT mechanism. Moreover, the computed Gibbs free energy values were much higher for the oxidation via ET processes compared with the HAT processes. Furthermore, an alternative PCET was also discarded on the basis that during the oxidation step the majority of the spin density was found to be located within the oxygen atom of the oxidant instead on the nitrogen atom of the THIQ derivative. In addition, kinetic experiments revealed that although the *tert*-butoxyl radical was found to be the major hydrogen acceptor on the reaction, the contribution of the *tert*-butoxylperoxyl radical to the hydrogen abstraction step could be increased by changing either the concentration of the peroxide or the nature of the solvent.

[60] Boess, E.; Wolf, L. M.; Malakar, S.; Salamone, M.; Bietti, M.; Thiel, W.; Klussmann, M. *ACS Catal*. **2016**, *6*, 3253.

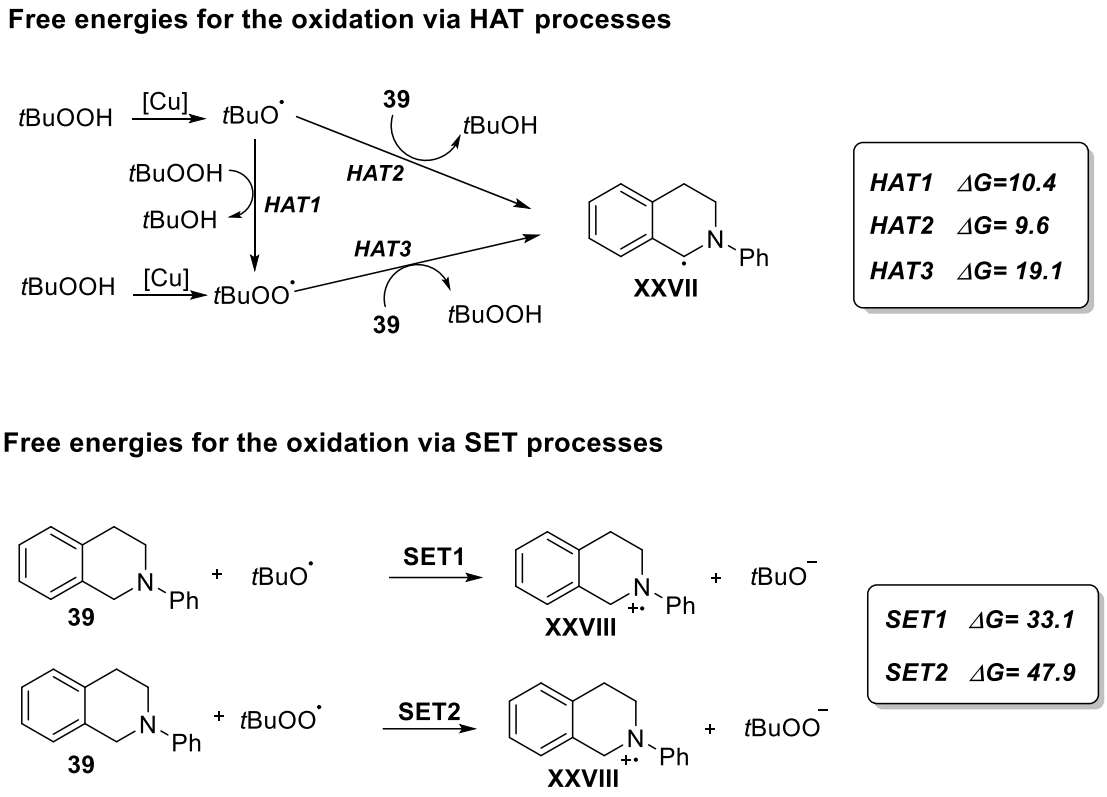

Scheme 24. Gibbs free energies for the functionalization of THIQ derivatives.

Alternatively, Wu and co-workers published the first computational study on the mechanism of Cu-catalyzed CDC reactions of *N*-aryl THIQ, which supported and complemented the hypotheses made by Klussmann and co-workers (Figure 6). For the exploration of the Cu/TBHP system, the DFT calculations were focused on kinetic studies about the formation of the amino peroxide intermediate **XXV** (Scheme 23).[61] As shown in Figure 6, the reaction starts with the oxidation of CuBr by TBHP, forming a CuBr-OH complex **XXX** and releasing a *t*BuO• radical. CuBr–OH reacts then with a second molecule of TBHP, giving CuBr(OO*t*Bu) **XXXIII** and releasing a molecule of H_2O. At this point, the *t*BuO• radical reacts with the *N*-aryl THIQ derivative via hydrogen abstraction process to form the radical **XXXIV** via **TS2**. The latter could react with another molecule of CuBr(OO*t*Bu) to provide the aminoperoxide **XXV** and regenerating the CuBr catalyst in a highly exergonic process. Although these DFT studies showed the radical pathway as

[61] Cheng, G.-J.; Song, L.-J.; Yang, Y.-F.; Zhang, X.; Wiest, O.; Wu, Y.-D. *ChemPlusChem* **2013**, *78*, 943.

the most thermodynamically favored one, the alternative SET mechanism as well as the involvement of high-valent Cu^{III} species could not be entirely discarded.

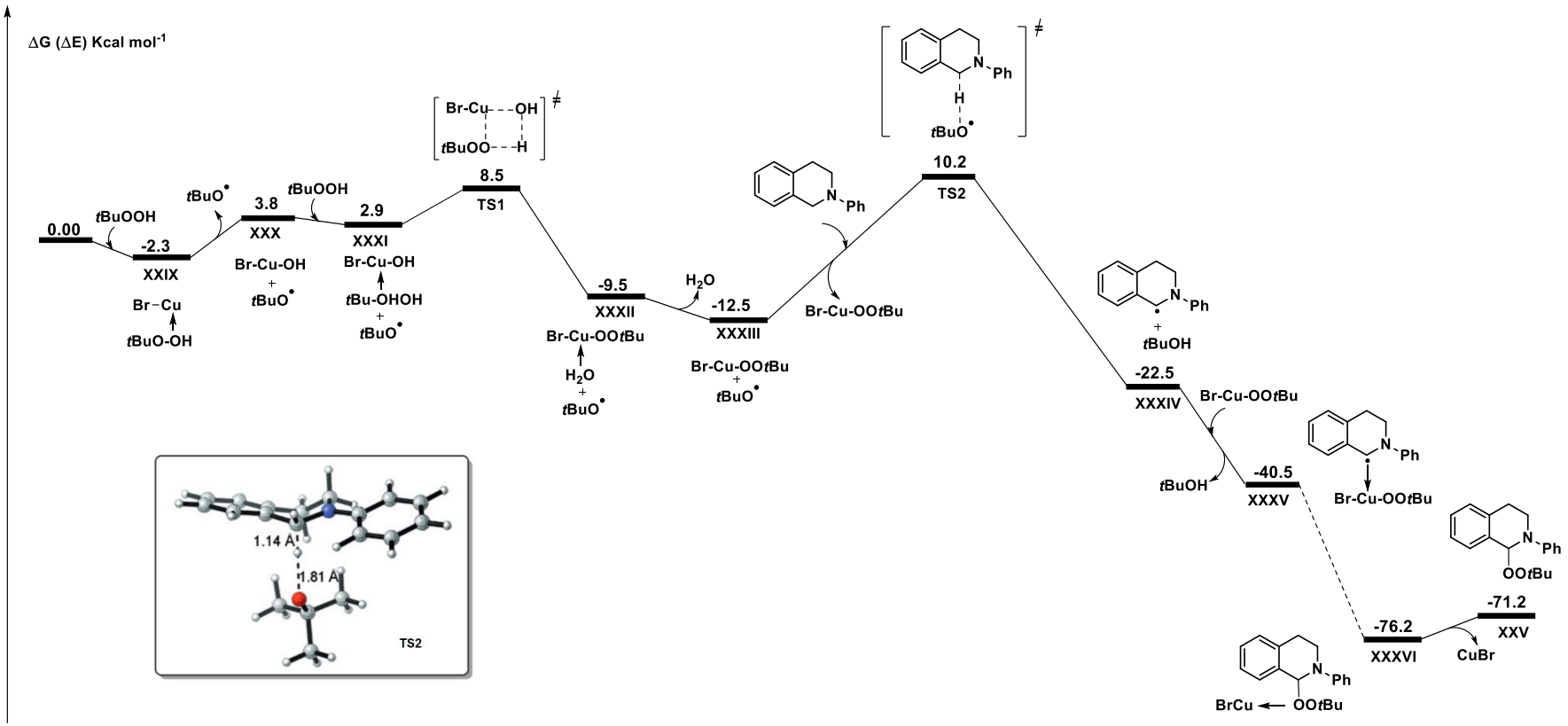

Figure 6. Energy profile of the mechanism of Cu/TBHP mediated functionalization of THIQ derivatives (ref 61).

Previous works suggested that the reactions involving TBHP are often governed by HAT processes. However, the studies explained above were not in agreement with the results reported by Ratnikov and Doyle (Scheme 25).[62] In fact, Ratnikov and Doyle identified the oxidation of *N*,*N*-dimethylanilines mediated by TBHP occurring upon SET events. Through Hammet analysis and investigation of KIE effect, they suggested the initial formation of the *N*-centered radical cation **XXXVII** mediated by the *t*BuO$^{\bullet}$ radical, thereby releasing *tert*-butylperoxyl anion within the process. The latter could react with the intermediate **XXXVII** through an irreversible proton abstraction, to form the *C*-centered radical **XXXVIII**. The irreversible proton transfer could explain the regioselectivity toward the formation of the iminium ion when unsymmetrical substrates are employed. A SET from the radical **XXXVIII** to the *t*BuOO$^{\bullet}$ radical would form the desired iminium intermediate **XXXIX**, which would be in equilibrium with the peroxide **XL**. This species could be prone to react with different nucleophiles, rendering the product **42**. Moreover, they hypothesized that the role of the transition metal was to convert the TBHP into *tert*-butylperoxyl radical.

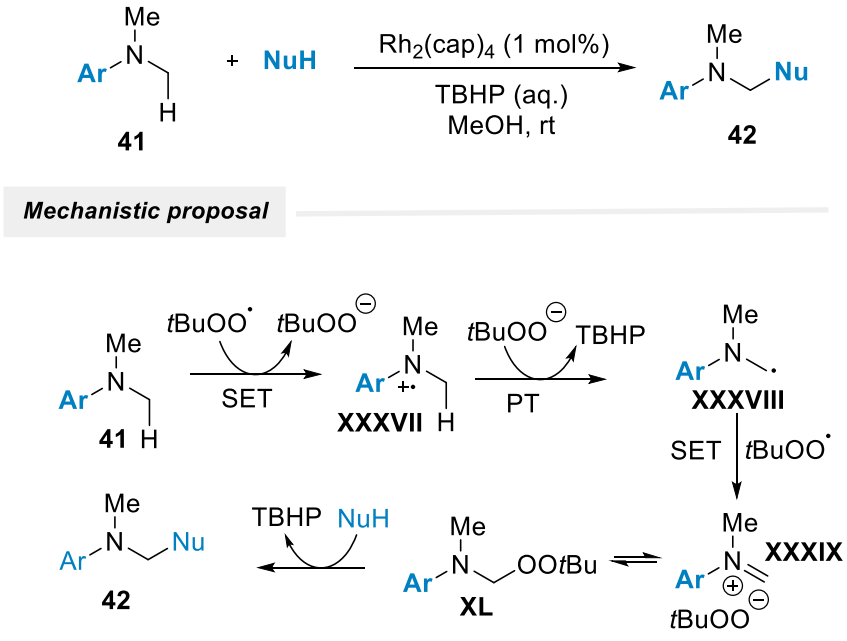

Scheme 25. Mechanistic proposal by Ratnikov and Doyle.

[62] Ratnikov, M. O.; Doyle, M. P. *J. Am. Chem. Soc.* **2013**, *135*, 1549.

All the studies disclosed above only described the functionalization of aromatic amines. However, Ghigo and co-workers investigated a Cu-catalyzed aerobic oxidation of a wide variety of aliphatic and aromatic derivatives (Scheme 26).[63] They proposed the initial formation of a *N*-centered radical cation **XLI** catalyzed by $CuCl_2$, followed by a hydrogen atom transfer to a suitable oxidant to form the iminium cation **XLII**. In this regard, they found that the O_2 seemed to be the main acceptor of the hydrogen atom. With this general study they demonstrated that although the formation of the iminium ion was favored in most of the cases, the generation of the precedent radical cation was limited mostly to aromatic amines. Moreover, they concluded that the steric hindrance of the N atom had an important influence on the reaction outcome: When non-hindered amines were used, the reversible complexation of the substrates to the catalyst made it much less available and hence, the formation of the radical cation intermediates was thermodynamically less favored. Therefore, the authors suggested that the lack of reactivity of alkylamines, such as Et_3N, could be the result of their strong complexation to the catalyst.

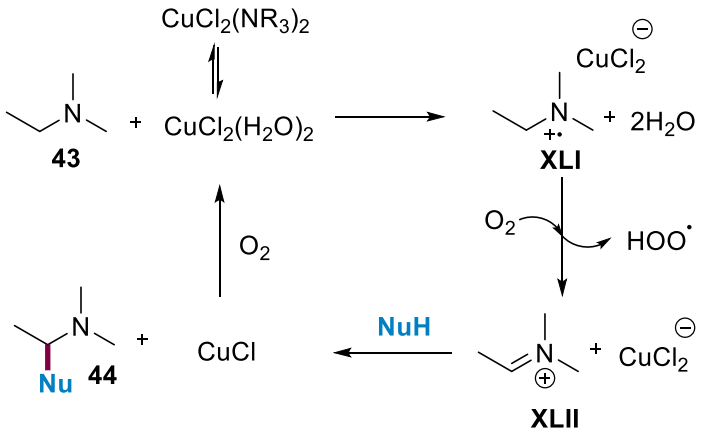

Scheme 26. Mechanistic proposal by Ghigo and co-workers.

In 2017, the group of Todd examined the DDQ-mediated CDC reaction between THIQ derivatives and nitroalkanes (Scheme 27).[64] By using ^{1}H-NMR and UV/VIS analysis they identified the DDQ radical anion at the early stages of the reaction and hence, they suggested the initial formation of

[63] Morgante, P.; Dughera, S.; Ghigo, G. *J. Phys. Chem. A.* **2019**, *123*, 13.
[64] Tsang, A. S.-K.; Hashmi, A. S. K.; Comba, P.; Kerscher, M.; Chan, B.; Todd, M. H. *Chem. Eur. J.* **2017**, *23*, 9313.

a radical cation within the THIQ structure and ruled out a HAT event. Further DFT stability analysis on the closed shell of the TS values supported this hypothesis by revealing a substantial biradical character derived by the proposed radical ions within the transition structure. Based on DFT calculations, they proposed the reaction mechanism depicted on Scheme 27. The reaction starts with a SET from the *N*-aryl THIQ to the DDQ forming the radical cation **XLIII**, which could undergo a hydrogen abstraction to deliver the corresponding iminium ion **XLIV** catalyzed by the previously formed DDQ radical anion. Finally, the reaction between the iminium ion and the nucleophile delivers the targeted product **46**.

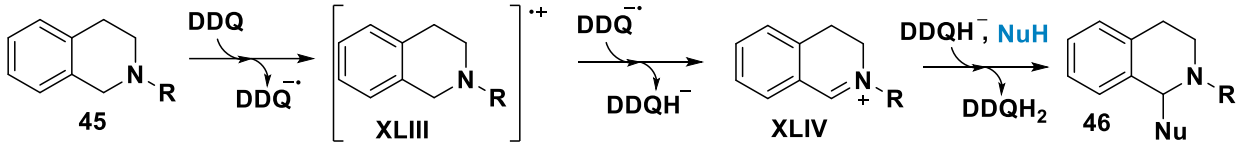

Scheme 27. Proposed mechanism for the DDQ-mediated oxidation of THIQ derivatives.

For *N*-aryl THIQ with different substitution patterns within the aromatic ring, the energetic difference between the reactants and the proposed radical cations **XLIII** is very small (Figure 7, in black). In contrast, for *N*-acetyl or *N*-Boc substituted amines the formation of the same radical cation was much more energetically demanding compared with the *N*-aryl derivatives (Figure 7, in blue). Moreover, UV-VIS spectroscopy experiments revealed that DDQ radical anion was not formed, which suggested that the first SET process was not even taking place for *N*-acetyl or *N*-Boc substituted amines. Although the energy barrier of the hydrogen abstraction (**TS1**) is considerable for **45a**, it was in agreement with the slow decrease of DDQ radical anion observed experimentally. In all cases, the formation of the iminium-DDQ complex **XLIV** is energetically favored and hence, the initial SET process could be considered as the rate-determining step.

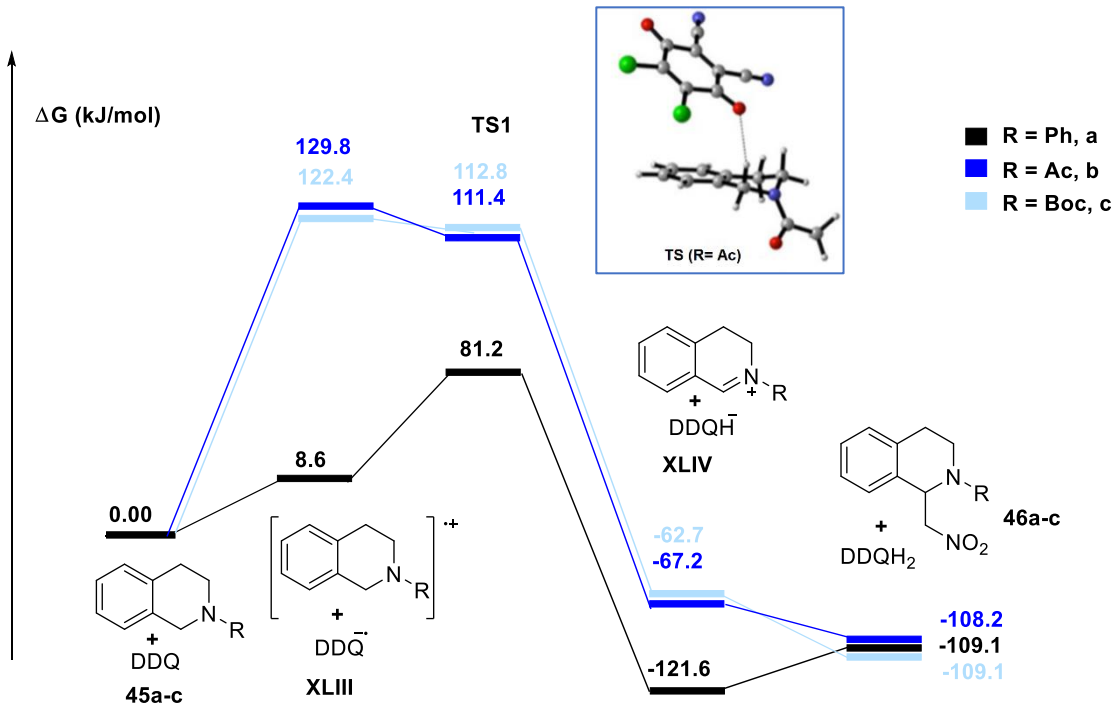

Figure 7. Different energy profiles for N-Ac, N-Boc and N-Ph THIQ derivatives (ref 64).

As explained along this section, the mechanism of CDCs with tertiary amines such as THIQs and *N*,*N*-dimethylanilines still poses a matter of debate. Some studies supported SET events as the key fundamental step and others instead identified HAT as the rate-determining step. Accordingly, a general reaction pathway cannot be stablished and further computational studies must be performed to elucidate the actual mechanism taking place when CDCs occurred in the parent secondary amines such as *N*-aryl glycine derivatives.

2.2. Objective

Owing to the lack of profound studies on transition metal-catalyzed CDC reactions of Gly derivatives, *in-depth* investigations are required to gain some insights into the key steps of the process, thereby understanding the unique features as well as the current limitations of the existing methods. For this purpose, we envisioned that the combination of DFT and experimental investigations could provide a broader perspective and a higher accuracy in order to determine which is the role of the free NH as well as the aryl motif within the chemical oxidation of Gly derivatives.

As previously mentioned in the introduction of this chapter, the intermediacy of an iminium ion was suggested by our group in our initial report.[54] However, the proposed mechanism was merely speculative and limitations of the method remained unrationalized. The main questions to be answered by these theoretical studies are the following:

- Is the iminium ion the key intermediate of the reaction?
- Which is the actual Co redox cycle?
- Why tertiary amines do not react in these processes?
- What is the role of the *N*-aryl group?

2.3. On the Mechanism of Cross-Dehydrogenative Couplings between *N*-Aryl Glycinates and Indoles: A Computational Study

To answer the latter questions, we started considering the intermediacy of other species in addition to the often accepted iminium ion and alternative reaction pathways were advised. It is well-known that the structural diversity of the starting materials as well as the solvent, temperature and catalyst, among others, influence the kinetics and thermodynamics of the overall pathway of a given reaction. In the particular case of CDC reactions adjacent to a nitrogen atom, different mechanistic scenarios could be envisioned depending on the number of substituents which are present on the heteroatom of the molecule to be functionalized. In fact, in the early 1995, while Murahashi's group was investigating the dehydrogenative oxidation of amines with catalysts that simulate monoamine oxidase enzyme, they found that the activation of amines with low-valent transition metals generally rendered two different intermediates: Whereas for a secondary amine the reaction gave an imine metal complex as the key intermediate, the same reaction proceeded through an iminium ion complex for amines without N–H bonds (Scheme 28).[65]

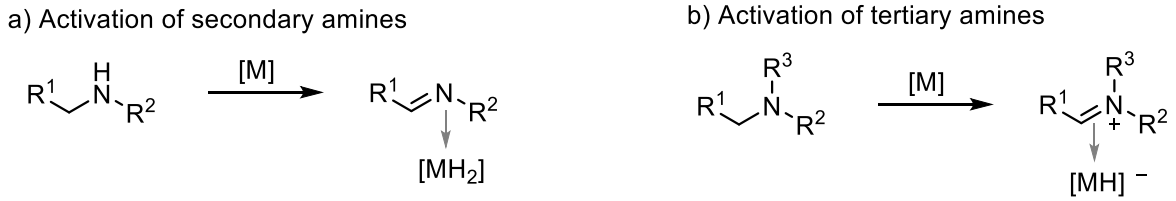

Scheme 28. Simulation of MAO enzyme with low-valent metal complex catalysts.

To date, all the experimental and computational studies on CDC reactions involving *N*-containing molecules only include substrates bearing tertiary amines in their structures. Considering that in our particular case a free NH group is present within the structure of the Gly derivative, we hypothesized that it could actively take part within the process and its role should be carefully studied.

[65] Murahashi, S.-I. *Angew. Chem. Int. Ed. Eng.* **1995**, *34*, 2443.

With these considerations in mind, we proposed the possible reaction pathways that are depicted on Scheme 29. It is often assumed that TBHP can be easily decomposed under thermal conditions and with the aid of either transition metals or iodide salts.[66] Owing to the redox active role of the metal, both *tert*-butoxyl and *tert*-butoxylperoxyl radicals could likely coexist within the reaction conditions. In principle, any of them could be responsible for the first hydrogen abstraction step (**HAT-1**) on the starting material to produce the carbon-centered radical **Int-A** (Scheme 29). However, HAT with *t*BuO· species has been documented to be faster than the formation of *t*BuOO·.[60,67] On the other hand, although the formation of a nitrogen-centered radical cation could not be ruled out, the majority of the previous DFT and experimental studies carried out by Klussmann[58,59,60] suggested that in the presence of TBHP the substrates tend to react with the radical species via HAT processes and hence, we assumed the formation of a carbon-centered radical instead of a *N*-centered radical cation. Moreover, computational studies performed by the group of Wu[61] indicated that whereas for the $CuBr/O_2$ catalytic system the preliminary formation of a *N*-centered radical cation is the most favorable pathway, when CuBr/TBHP system was used the formation of a *C*-centered radical via HAT process is more likely to occur. Once the *C*-centered radical is formed, we envisioned three different reaction pathways. First, a direct radical coupling with the *t*BuOO· would provide **Int-B**, which has been proven to exist in equilibrium with the iminium ion **Int-C** (*route a*). Second is the oxidation to the carbocation **Int-D** upon an electron transfer step (**SET-3**) (*route b*). The latter could also be intercepted by *t*BuOOH or its corresponding anion to yield **Int-B** (*route d*). Third, a direct HAT could furnish a neutral imine intermediate **Int-E** (*route c*).

[66] See, for example: a) Houghton, R. P.; Rice, C. R. *Polyhedron* **1996**, *15*, 1893. b) Minisci, F.; Fontana, F.; Araneo, S.; Recupero, F.; Banfi, S.; Quici, S. *J. Am. Chem. Soc.* **1995**, *117*, 226.
[67] Avila, D. V.; Ingold, K. U.; Lusztyk, J.; Green, W. H.; Procopio, D. R. *J. Am. Chem. Soc.* **1995**, *117*, 2929.

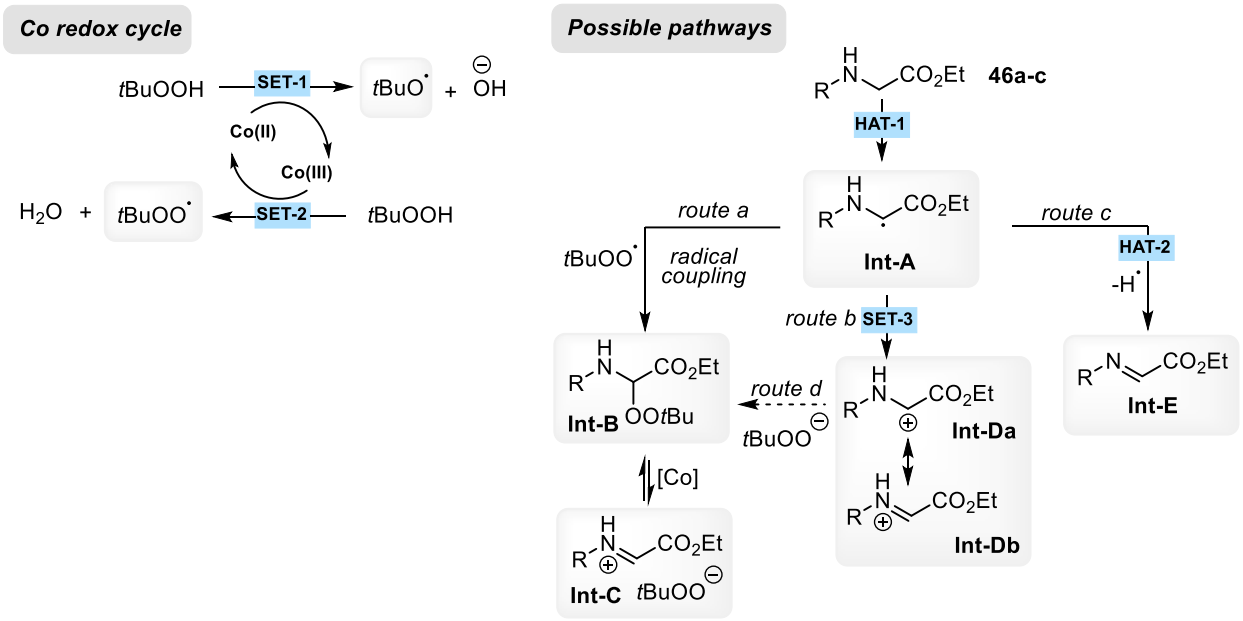

Scheme 29. Co-catalyzed routes toward the formation of electrophilic species.

Before starting with our computational studies, we conducted some control experiments in order to discard or support the intermediacy of some of the possible transient species depicted above. In this regard, we synthesized the highly reactive imine **Int-E-PMP** and the α-*tert*-butyldioxyl intermediate **Int-B-Ph** and submitted to the previously optimized reaction conditions (Scheme 30). The treatment of imine **Int-E-PMP** with indole afforded the CDC product **49b** in 99% yield in the absence of both metal and TBHP even at room temperature, thus discarding any role of the latter components within the nucleophilic attack of the indole. On the other hand, peroxyl derivative **Int-B-Ph** furnished non-functionalized Gly compound **47a** in 41% yield and just traces of the coupling product **49a** were detected under the standard conditions. As a result, experimental evidences would render unlikely the intermediacy of **Int-B** and hence *route a* and *route d* may not represent a feasible mechanistic scenario. Furthermore, in accordance with literature reports,[39a,50,54] tertiary amine **50** remained unreactive under the standard conditions and variations on the nature of the metal source or temperature did not result in the formation of the corresponding product. However, when tertiary amine **50** was submitted to the standard conditions using indole **48b**, the reaction afforded product **49ab** in 18% yield. In light of the spontaneous demethylation undergone by the *N*-methylated glycine derivative **50** to generate the product **49ab**, we could conclude that the presence of the secondary amino moiety was indispensable for the reaction to occur. Additionally,

substrates incorporating non-aromatic protecting groups such as *N*-Ac (**47c**) did not afford the targeted product. It is notheworthy that some mechanistic experiments with radical traps previously carried out by our group suggested the involvement of radical intermediates in the reaction outcome.[54]

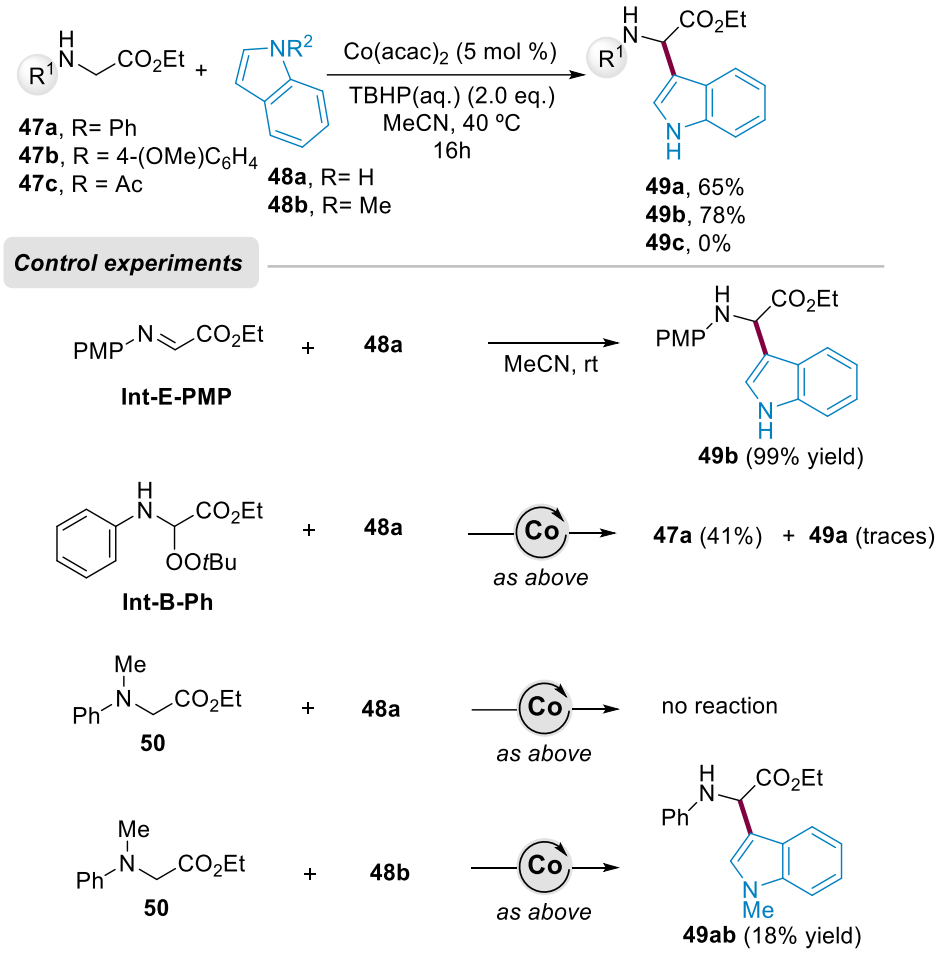

Scheme 30. Control experiments with different Gly derivatives.

Owing to the good performance of Ph-Gly-OEt (**47a**) within the Co-catalyzed CDC with indoles, our initial study commenced with the characterization of its full reaction mechanism including a comparative analysis of previously mentioned routes for the CDC with indoles. The following calculations were carried out using the computational methods described in section 1.4 of Chapter

1. Before going beyond, however, there are two issues that may be fixed: the most favorable spin states of Co^{II} and Co^{III} species as well the Co redox cycle in our reaction pathway.

For the $Co(acac)_2$ complex, there are two conformations to consider: The tetrahedral and the square planar. Additionally, the spin doublet and quadruplet states have to be considered. From the very beginning, the square planar quadruplet and the tetrahedral doublet were discarded for energetical reasons. This is in agreement with the bibliographic reports, which state that from all the possible conformations, the square flat doublet and the tetrahedral quadruplet are the most stable structures.[68] However, there is some controversy when it comes to specifying which is the most favored one between the two mentioned above. The works published to date are not very enlightening, because the results vary depending on the method employed or the nature of the functional used (in DFT calculations) to approximate the correlation and exchange energy. According to our calculations, the most stable structure is the tetrahedral quartet spin state, with 2.96 kcal/mol and 25.83 kcal/mol difference with respect to the quartet and doublet planar structures, respectively. No tetrahedral doublet structure was found. Hence, we have considered the quartet tetrahedral species as the most stable one for the $Co(acac)_2$ catalyst. Based on these results and the electronic characteristics of the metal ($3d^7$) and ligands (π-donor, low field), we assumed that it would be the most likely species in the reaction medium (Figure 8).

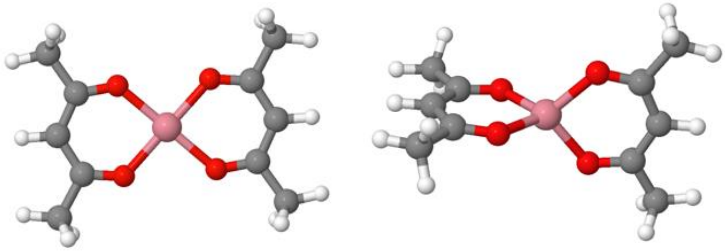

Figure 8. Calculated planar (left) and tetrahedral (right) structures for doublet and quartet spin states of $Co(acac)_2$.

As depicted in Scheme 29, the Co^{II} catalyst would assist the cleavage of the oxidant, thereby providing the *t*BuO$^{\bullet}$ radical and the corresponding hydroxylated Co^{III} complex upon the **SET-1** step. Three possible spin states have been considered for the hydroxylated Co^{III} complex: singlet, triplet, and quintet complexes have been calculated and the most stable species is the quintet, being

[68] Michalak, A.; Sojka, Z.; Radon, M.; Srebro, M.; Pietrzyk, P. *J. Phys. Chem*. *A* **2011**, *115*, 2316.

the triplet and singlet states 22.86 kcal/mol and 29.44 kcal/mol higher in energy, respectively. This peroxidation process leading to quintet $Co(acac)_2OH$ complex, commonly referred to as Haber-Weis cycle, has been studied by UV-VIS spectroscopy[69] and has an energy penalty of 19.31 kcal/mol. Since the Gly counterpart is not involved, this energy value is common to all Gly compounds regardless of their substitution pattern. In principle, the so-formed Co^{III}-OH complex may react with *t*BuOOH, leading to the recovery of the Co^{II} catalyst and the formation of *t*BuOO$^{\bullet}$ through the **SET-2** step. This process is exothermic by -11.82 kcal/mol. Accordingly, this Co-redox cycle upon **SET-1** and **SET-2** would be overall endothermic by 7.49 kcal/mol and hence the formation of *t*BuOO$^{\bullet}$ radical species would be unlikely to happen. Consequently, *route a* could be reasonably discarded. Based on existing precedents and our computational studies, we concluded that *t*BuO$^{\bullet}$ species is much more reactive than *t*BuOO$^{\bullet}$ and that the subsequent HAT event will be more likely to occur with the former radical species. Having all these considerations in mind, Figure 9 collects the proposed reaction mechanism for Gly derivative **47a**.

[69] Turrà, N.; Neuenschwander, U.; Baiker, A.; Peeters, J.; Hermans, I. *Chem. Eur. J.* **2010**, *16*, 13226.

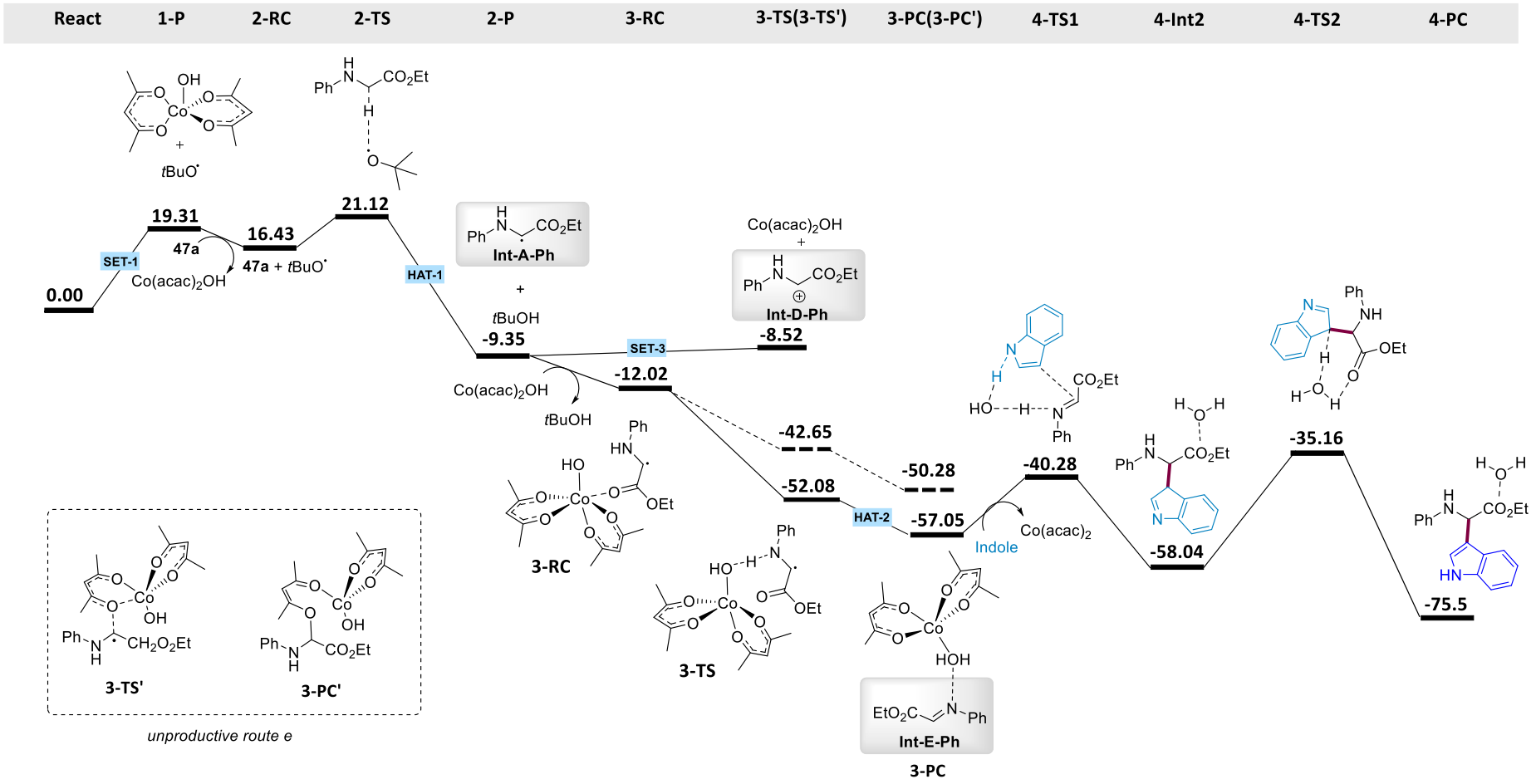

*Figure 9. Full reaction mechanism with compound **47a**. RC, PC and TS stand for reactant complex, product complex and transition state, respectively, and the number in front accounts for the reaction step; energy profile (ΔH) in kcal/mol.*

As described before, the first step would be the catalyst oxidation step through **SET-1** with an energy penalty of 19.31 kcal/mol, leading to the formation of *t*BuO• radical. In this manner, upon initial approach of *t*BuO• species to Gly derivative **47a** a reactant complex slightly stabilized with respect to the separated species would be formed (**2-RC** in Figure 9). The oxygen atom is orientated towards one of the α-hydrogen atoms within Gly **47a**, and the corresponding hydrogen abstraction has a small barrier of around 5 kcal/mol respect to the reactant complex, which would lead to the formation of the carbon-centered radical **Int-A-Ph**. Notice that the latter is stabilized through delocalization within the aromatic group and the π-electron pair of the neighboring nitrogen atom. As a result, intermediate **Int-A-Ph** is planar. The spin density on the α-C atom was calculated to be 0.587 and 0.183 in the adjacent nitrogen atom, which underpinned the existing radical delocalization. The formed intermediate is hence stabilized, and located -26.56 kcal/mol below the reactant complex of this step and -10.16 kcal/mol below the reactants.[70]

Once intermediate **Int-A-Ph** is formed, two plausible reaction pathways could happen: an oxidation toward iminium ion **Int-D-Ph** through **SET-3** (Scheme 29, *route b*) or a hydrogen abstraction through **HAT-2** to deliver imine **Int-E-Ph** (Scheme 29, *route c*). The latter are depicted on Figure 9, wherein it is clearly shown that the formation of the iminium cation intermediate **Int-D** is energetically unfavorable and is located much higher in energy in the potential energy surface. Therefore, the carbon-centered glycine radical **Int-A-Ph** would be prone to undergo a subsequent **HAT-2** step (Scheme 29, *route c*) in order to yield the imine intermediate rather than being oxidized to the ensuing iminium ion **Int-D-Ph** (Scheme 29, *route b*). In this manner, **Int-A-Ph**–Co^{III}-OH reactant complex is formed (**3RC** in Figure 9), which is stabilized by the formation of a hexacoordinated species, where a hydrogen bond is formed between the secondary amine and the OH of the cobalt complex.

As shown in Figure 9, this reaction complex **3RC** is ready to undergo a hydrogen abstraction by the hydroxylate ion leading to the recovery of the Co^{II} catalyst, thereby closing the Co-redox cycle, and the formation of a water molecule. This type of reductions of a Co^{III}-OH complex via hydrogen transfer are known in other catalytic reactions such as decomposition of hydroperoxides.[69] Compared to the initially proposed Co redox cycle where Co^{III}-OH could be reduced to Co^{II} with

[70] For further details, see the supporting information.

an enthalpy difference of -11 kcal/mol upon a **SET-2** step (Scheme 29), the formation of the **Int-E-Ph** and recovery of Co^{II} catalyst via the **HAT-2** step is favored by -45 kcal/mol, thus 34 kcal/mol more favorable.

Interestingly, **Int-A-Ph**–Co^{III}-OH reactant complex **3RC** could undergo an unexpected and unproductive reaction pathway wherein a new C–O bond form is formed between the carbon-centered radical and the oxygen atom within one of the acetylacetonate ligands (*route e*). The latter is competitive in energy with the **HAT-2** process, but the resulting non-reactive adduct lies 7 kcal/mol above, and the calculated TS barrier is 10 kcal/mol higher than the **HAT-2** one. Nevertheless, an intermediate between **3-RC** and both 3-TS is missing. All attempts to locate such intermediate eventually ended on either **Int-E-Ph**–$Co(acac)_2$ complex, or the alternative mentioned adduct. Careful analysis underpinned the crucial importance of the electron density of the carbon atom within the radical species **Int-A** to undergo such an unproductive route and hence the importance of using *N*-aryl groups to minimize the reactivity of the radical intermediate upon effective delocalization (*vide infra*).

As it will be later explained, the released water molecule may play a key role in the final coupling with the corresponding indole. Importantly, this step is crucial in the reaction mechanism and the hydrogen atom transfer could not occur over tertiary amines, which reasonably explains the experimental evidence that *N*-methyl glycine derivative **50** was not reactive under the standard CDC reaction conditions. This concordance between the theoretical and experimental results reinforces the viability of *route c* featuring the formation of an imine intermediate.

Once imine intermediate **Int-E-Ph** is formed, it may undergo further nucleophilic attack by the corresponding indole derivative to furnish the targeted CDC product **49a**. Although straightforward at first sight, this attack was found to occur upon a two-step sequence facilitated by the water molecule released along **HAT-2**. In the first step, indole **48a** would approach to the electrophilic imine **Int-E-Ph**, thus forming a reactant complex by hydrogen bonding with the water molecule. Indeed, the water molecule was found to play a dual role and not only enabled the coordination of the electrophile and the nucleophile but also assisted the nucleophilic attack itself. In this respect, imine **Int-E-Ph** could increase its electrophilicity upon hydrogen bonding with the

water molecule, thus allowing the subsequent attack of the indole to forge the new C–C bond. In the second step (**4-TS2** in Figure 9), rearomatization of the indole motif would deliver the targeted coupling product.

With the aim to clarify the actual role of the phenyl ring in the reaction outcome, the reaction mechanism was also calculated for glycine derivatives **47b** and **47c** bearing a *p*-methoxyphenyl and an acetyl motif at the nitrogen atom, respectively. The first main difference between the *N*-aryl glycinates **47a** and **47b** and the parent *N*-acetyl derivative **47c** is that the carbon-centered radical **Int-A** is much less stabilized for **47c**, which is in accordance with the common trend of utilizing *N*-aryl compounds in these oxidative functionalization reactions. Notice that the products of the formation of the radicals lie around 6-7 kcal/mol higher in energy in comparison to the *N*-aryl substituted radicals. In particular, the stabilization of the aromatic radicals **Int-A-Ph** and **Int-A-PMP** is due to the effective delocalization of the radical. Spin densities for the α-carbon atom show values of 0.587, 0.563 and 0.708 for **Int-A-Ph**, **Int-A-PMP** and **Int-A-Ac**, respectively. Based on these values, it can be concluded that the radical is more delocalized in *N*-aryl derivatives. Recall that the more delocalized the radical is, the higher its stability. This stabilization effect is also observed in the formation of the **Int-A**–Co^{III}-OH complex and the corresponding imine intermediate **Int-E**, which are more stable for *N*-aryl derivatives by roughly 15 kcal/mol. The higher stabilization of the imine derivatives **Int-E-Ph** and **Int-E-PMP** in comparison with **Int-E-Ac** shows that the hydrogen atom transfer occurring in this step is more difficult for **47c** than for the parent aromatic compounds **47a** and **47b**. In fact, owing to the higher electron density of the carbon radical of **Int-A-Ac** derived from the *N*-acetyl glycine derivative **47c**, in this case complex **3RC** would preferentially evolve into the formation of a new adduct (**PC'**) through *route e* instead of the expected **HAT-2** with the concomitant reduction of the Co^{III} catalyst (Scheme 31).

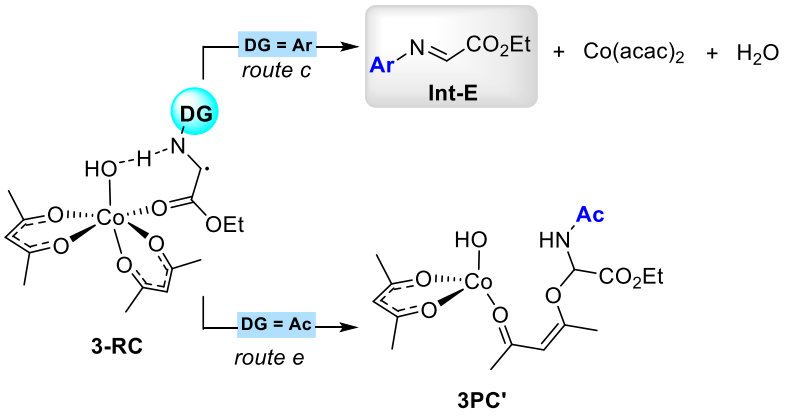

Scheme 31. Distinct reactivity of N-acyl and N-aryl derivatives.

Despite the similar energy values toward the formation of **Int-A**, the presence of an *N*-acetyl group clearly favors the unproductive *route e* (Figure 10). Conversely, in the case of the *N*-aryl compounds, **Int-E-Ph** and **Int-E-PMP** are the preferred products through *route c.* Consequently, the formation of **Int-E-Ac** would be frustrated due to the high spin density concentration in the α-carbon. According to these results, the experimental evidence of the higher reactivity of aromatic amine derivatives versus the lack of reactivity of the acyl analogues may be reasonably explained. *On balance then, we could conclude that the formation of the imine species **Int-E** upon route c is the preferred pathway to obtain the CDC product, which is favored by the presence of aryl groups within the terminal nitrogen atom.*

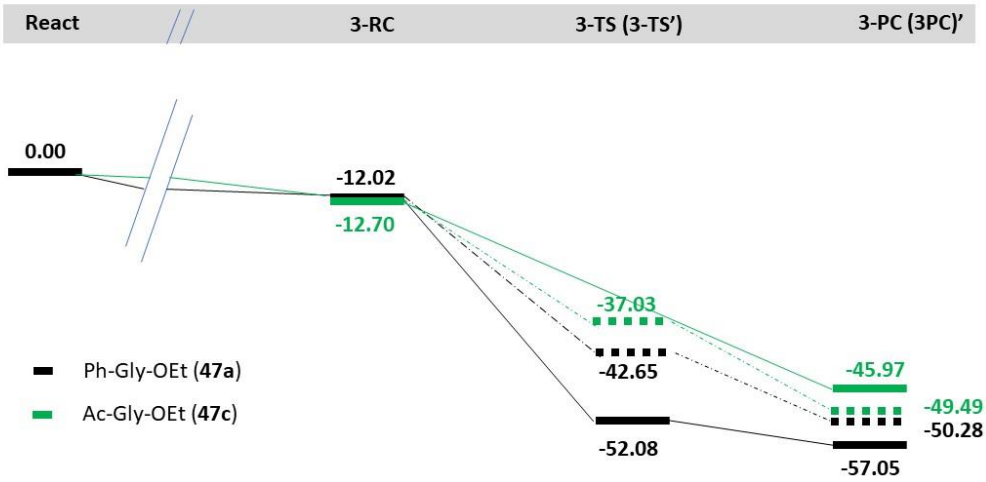

*Figure 10. Comparison of the reaction energetics (in kcal/mol) for **47a** and **47c** within route c (straight line) and route e (dashed line)*

In fact, as explained before, a wide variety of extra experiments were performed with *N*-acyl glycine derivative **47c** but the target CDC product **49c** was never detected, which reinforced the hypothesis that an aromatic moiety within the *N*-terminal position is required for the process to occur. As expected, under the standard reaction conditions *N*-Ac-Gly-OEt (**47c**) did not show reactivity and the starting material remained intact (Table 2, entry 1). To address this issue, a more nucleophilic *N*-methyl indole **48b** was used (Table 2, entry 2). Owing to its higher nucleophilicity, we envisioned that it could act as a driving force to favor the coupling process. Despite the fact that the reaction was carried out at higher temperatures and catalyst loadings (Table 2, entries 3-6), our attempts did not afford the desired products.

Table 2. Screening of indoles and temperature[a]

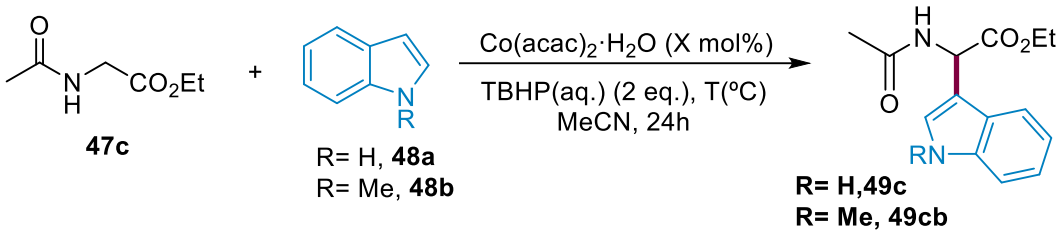

Entry	Indole	$Co(acac)_2 \cdot H_2O$ (x mol%)	T (ºC)	Yield (%)
1	48a	10	40	0
2	48b	10	40	0
3	48b	10	80	0
4[b]	48b	10	80	0
5	48b	10	100	0
6	48b	20	80	0

[a] Reaction conditions: **47c** (1.0 mmol), **48** (0.5 mmol), $Co(acac)_2 \cdot H_2O$ (x mol %), TBHP (aq.) (2.0 eq.), MeCN (1.0 mL) at 40 °C for 24 h under argon. [b] Reaction carried out using 1.0 eq. of *N*-Ac-Gly-OEt.

In view of these preliminary results, we investigated the influence of different cobalt and copper salts. Considering that copper salts often exhibit high catalytic activity on CDC reactions, we assumed that it would be beneficial for the challenging generation of the electrophilic intermediate. Although the coupling product was not obtained, in some cases trace amounts of imine intermediate were detected by ^{1}H-NMR monitoring (Table 3, entries 6,7 and 9). The lack of reactivity of substrate **47c** even at high temperatures and catalyst loadings evidenced the difficulty associated to the formation of the corresponding transient intermediates.

Table 3. Screening of catalysts[a]

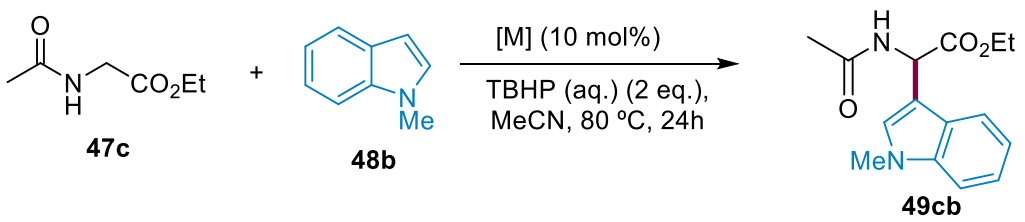

Entry	[M] (10 mol%)	Yield (%)
1	$Cu(OAc)_2$	0
2	Cu(OAc)	0
3	CuBr	0
4	$CuBr_2$	0
5	$Cu(acac)_2$	0
6	$CoBr_2$	0
7	$CoCl_2$	0
8	CoF_2	0
9	$Co(ClO_4)_2$	0

[a] Reaction conditions: **47c** (1.0 mmol), **48b** (0.5 mmol), $Co(acac)_2 \cdot H_2O$ (10 mol %), TBHP(aq.) (2.0 eq.), MeCN (1.0 mL) at 40 °C for 24 h under argon.

2.3.1. Further DFT Studies on the Influence of the Delocalization in the Formation of the Imine Intermediate

The requirement of aryl substituents onto nitrogen atoms could be considered as the main limitation of CDC methodology since they cannot be easily cleaved. In fact, the functionalization of glycine derivatives is limited to the use of peptides in which the glycine unit is located at the *N*-terminal position. Additionally, the cleavage of the *N*-aryl motif could only be carried out for the *N*-PMP protecting group using cerium ammonium nitrate (CAN).[71] This reagent is a strong oxidant and can react with alcohols, phenols, ethers and benzylic C–H bonds. Considering that these functional groups are often present in many of the existing natural amino acids, the deprotection of the aryl motif could be considered as a difficult task.

This aimed us to explore if other functional groups could be suitable to promote the oxidation of the Gly unit in an efficient manner. Based on the previous results, which suggested that a strong delocalization of the radical is required for the process to occur, we decided to perform DFT calculations to obtain the spin density $\rho(C_\alpha)$ values for different functional groups. First, we tried

[71] De Lamo Marin, S.; Martens, T.; Mioskowski, C.; Royer, J. *J. Org. Chem.* **2005**, *70*, 10592.

to determine if the donating- or electron-withdrawing character of the corresponding protecting groups could have a strong influence on the delocalization of the resulting radical. For this purpose, we conducted our studies with a wide variety of different functional groups, even including some groups which could be difficult to install at the nitrogen atom or lack a practical synthetic value (Figure 11).

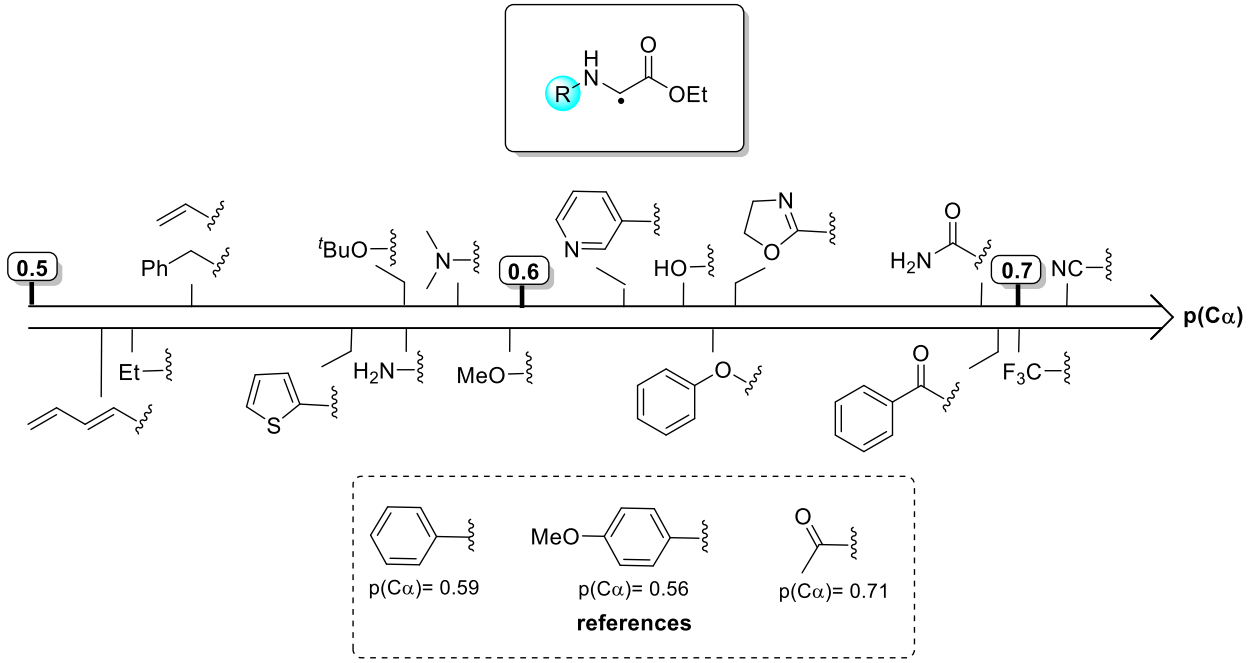

Figure 11. Different delocalization ρ(Cα) values for EDG and EWG groups.

As depicted on Figure 12, the delocalization of the *C*-centered radical tends to be smaller when EWG groups are used. For example, the spin density values for nitrile, benzoyl, trifluoromethyl and some heterocycles are very close to the value obtained with the *N*-acetyl group. In contrast, when EDG groups are used as substituents, the spin density values tend to be smaller. For alcohol, amine and alkyl derivatives as well as for conjugated structures these values are located between ρ(Cα)= 0.5-0.6. Based on the previous results, any of these functional groups should be able to promote the oxidation of the glycine derivative in an efficient manner. Nevertheless, existing experimental works previously developed in the field demonstrated that some of these groups, such as the benzyl group,[34a] are not effective to promote the desired oxidation step. With these consideration in mind, these results can not be considered as conclusive.

Nevertheless, we decided to select some of the functional groups to calculate the reaction mechanism and check if the variations on the energetic differences between the imine intermediate (**3-PC**) and the undesired adduct (**3-PC'**) depended on the previously obtained spin density values. First, we selected 3 functional groups in which the spin density values reflected a strong delocalization of the radical: *N*-Et (**47d**), *N*-OMe (**47e**) and *N*-(2-thienyl) (**47f**). For these Gly derivatives, the spin density values were 0.598, 0.528 and 0.566, respectively. As depicted in Figure 12, the corresponding imine intermediate **3-PC** was lower in energy than the undesired adduct **3-PC'**. For the *N*-(2-thienyl) group, the energetic difference between the imine and the adduct was of 16.89 kcal/mol, whereas for the *N*-Et group the difference was of 10.64 kcal/mol. For the *N*-OMe (**47e**) group, the imine intermediate was more stable by 21.79 kcal/mol.

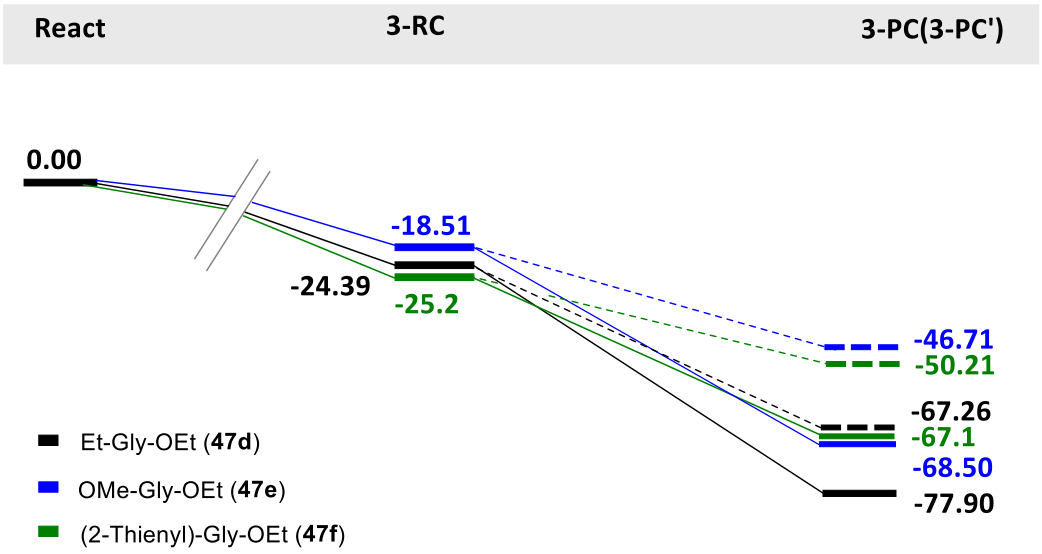

Figure 12. Comparison of the reaction energetics (in kcal/mol) for Gly containing EDG groups within route c (straight line) and route e (dashed line).

On the one hand, we also selected two EWG groups with strong spin density on the α-C atom to see if, as expected, the **3-PC'** was located lower in energy than the **3-PC** (Figure 13). For *N*-CF_3 (**47g**) and *N*-CN (**47h**) containing glycine derivatives, the spin density values were 0.700 and 0.716, respectively. As depicted on Figure 13, for the *N*-CF_3 glycine derivative the adduct **3-PC'** was located lower in energy compared with the imine intermediate **3-PC**. Nevertheless, the

energetic difference was very low (0.69 kcal/mol). Surprisingly, for the *N*-CN (**47h**) glycine derivative the imine intermediate was more stable by 2.44 kcal/mol. As a result, we can conclude that although the delocalization of the radical can affect the energetic differences between *route c* and *route e*, there should be more determining factors that have not been considered along this study.

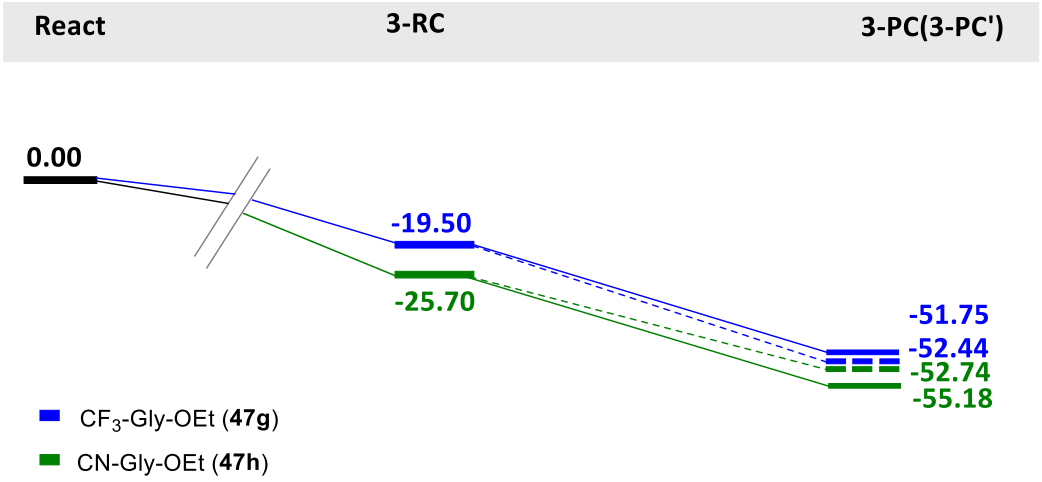

Figure 13. Comparison of the reaction energetics (in kcal/mol) for Gly containing EWG groups within route c (straight line) and route e (dashed line).

2.3.2. Further experimental studies

Considering that for the MeO-Gly-OEt (**47e**) derivative the energetic difference between **3-PC** and **3-PC'** is the highest one, we decided to synthesize this particular substrate and submit it to the standard reaction conditions. Unfortunately, the starting material was found to be quite sensitive towards the standard reaction conditions and fully decomposed, thereby delivering a complex mixture of unidentified products within the process. The use of different solvents (Table 4, entries 1-6), oxidants (Table 4, entry 8), other catalysts (Table 4, entries 9-11), and lower temperatures (Table 4, entry 7) failed to deliver the desired product.

Table 4. Screening of different reaction conditions.[a]

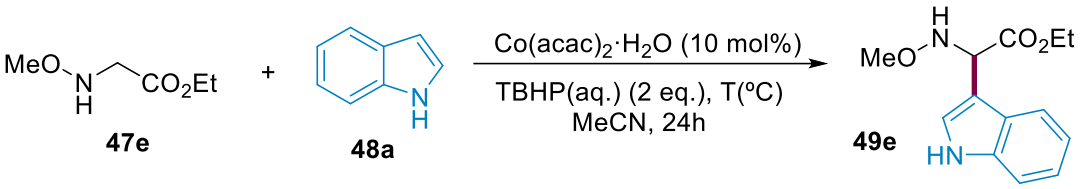

Entry	Variation from standard conditions	Yield (%)
1	-	0
2	DCE as solvent	0
3	Toluene as solvent	0
4	Acetone as solvent	0
5	$PhCF_3$ as solvent	0
6	EtOAc as solvent	0
7	T (ºC) = rt	0
8	TBHP (dec.) as oxidant	0
9	$Cu(OAc)_2$ instead of $Co(acac)_2$	0
10	$CoCl_2$ instead of $Co(acac)_2$	0
11	$CoBr_2$ instead of $Co(acac)_2$	0

[a] Reaction conditions: **47e** (1.0 mmol), **48a** (0.5 mmol), $Co(acac)_2 \cdot H_2O$ (10 mol %), TBHP (aq.) (2.0 eq.), MeCN (1.0 mL) at 40 °C for 24 h under argon.

Curiously, under the standard reaction conditions (Table 4, entry 1), the reaction afforded trace amounts of the *N*-heteroarylated glycine derivative (Figure 14). In view of the structure of the product, the imino oxonium ion **XLVI** could be formed (Scheme 32). In this case, the reaction could start with the formation of the radical cation **XLV** catalyzed by the TBHP, followed by the loss of the NH proton through a HAT process to deliver the intermediate **XLVI**. The so-formed electrophilic species could be trapped by the indole motif, delivering the corresponding product **49e.** Further studies are required to control the regioselectivity of the formation of the cationic intermediate.

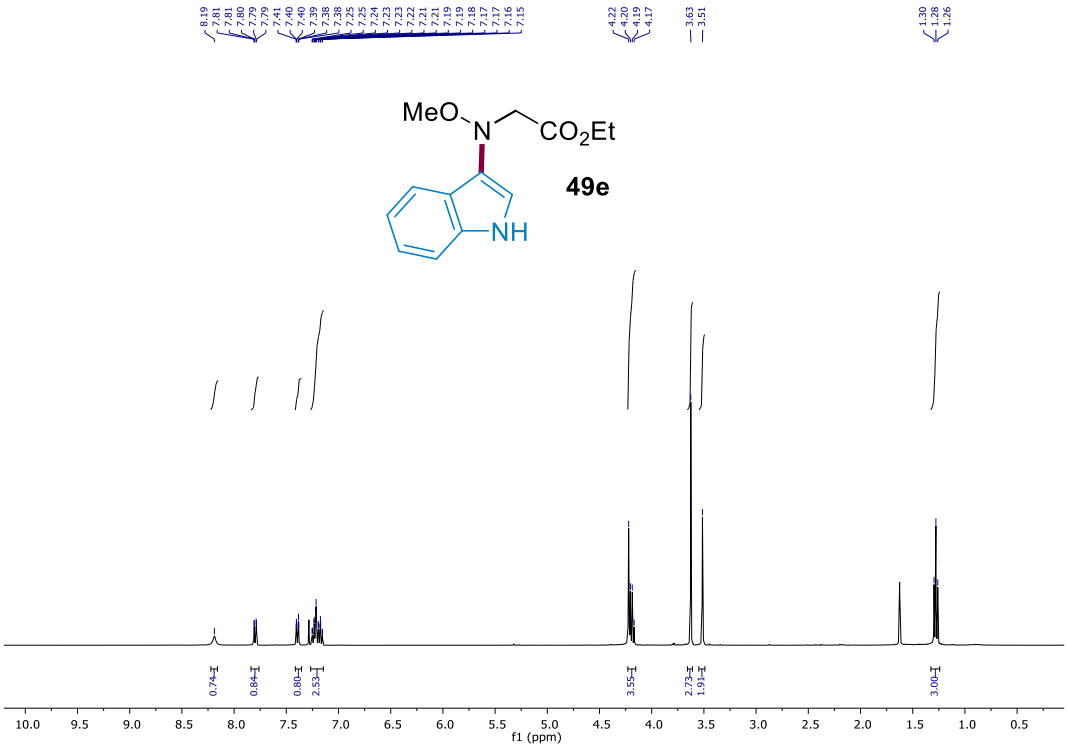

Figure 14. [1]H-NMR of the isolated product.

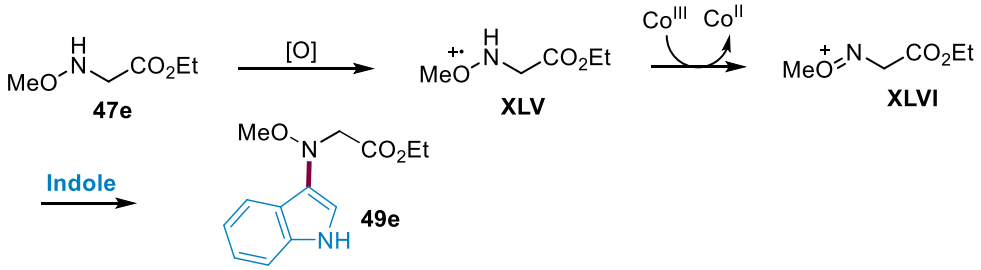

Scheme 32. Mechanistic proposal for the formation of the N-heteroarylated compound.

2.3.3. Revisiting the mechanistic proposal

Based on the DFT studies disclosed above, we revisited the originally proposed reaction mechanism featuring the intermediacy of iminium species,[54] and the most feasible reaction pathway would involve a neutral imine intermediate (Scheme 33). The reaction was proposed to start with the Co^{II}-induced cleavage of *t*BuOOH to produce the active *t*BuO$^{\bullet}$ species, which would further deliver a carbon-centered alkyl radical (**Int-A-Ph**) upon a HAT event. The latter would undergo a more energetically favored hydrogen abstraction by the Co^{III} species, thus closing the catalyst cycle and delivering the electrophilic imine intermediate **Int-E-Ph**. Eventually, the nucleophilic attack of the indole would furnish the target coupling product **49a**, which seemed to be favored by the water molecule released along the **HAT-2**.

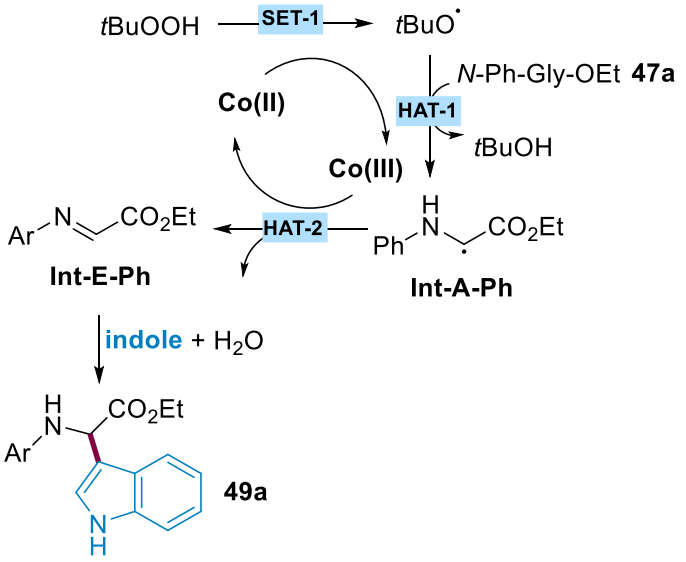

Scheme 33. Revised mechanism for the Co-catalyzed heteroarylation of N-aryl glycinates.

2.3.4. DFT Studies Performed by Other Research Groups after the Publication of This Work

After the publication of our results, Zheng and co-workers published a DFT study on the CDC reaction of *N*-aryl glycine esters and phenols catalyzed by the CuBr/TBHP system (Figure 15).[72] Interestingly, the oxidation potentials of a wide variety of substrates with different substitution patterns were also studied, explaining the SET occurring tendency from a thermodynamic point of view. They found that the presence of EDG groups in the *ortho*- and *meta*-positions of the aromatic ring significantly decreased the oxidation potential of the substrates and hence, facilitated the electron transfer processes. Regarding the mechanistic study, they proposed different reaction pathways that are depicted in Figure 15. Among those mechanisms, the most favorable ones were selected for discussion. The oxidation of the catalyst by TBHP to form the radical *t*BuO$^{\bullet}$ and $BrCu^{II}$-OH is common for all the mechanistic pathways and the Gibbs energy difference is of 3.22 kcal/mol (**XLVII**). On *route a*, the *N*-aryl glycine ester would first undergo a SET to form a *N*-centered radical cation **XLVIII** with an energy penalty of 34.88 kcal/mol. The subsequent hydrogen abstraction, which would render the iminium ion through **TS1**, has an energy barrier of 25.62 kcal/mol. Due to the higher energy profile of this pathway compared with the *route b* and *route c*, it could be reasonably discarded. On *route b*, the *t*BuO$^{\bullet}$ radical could easily abstract a proton with a small energy barrier of 4.87 kcal/mol over the reactant complex, forming the thermodynamically favored **LI** with an energy of -27.12 kcal/mol. At this point, two possible reaction pathways could happen: The first one would imply the formation of the iminium ion **LII** through a SET event with an energy penalty of 18.04 kcal/mol. The second one would be a hydrogen atom transfer towards the formation of the imine **LIV**, reducing the Cu^{II} and releasing a molecule of water at the same time. As depicted on Figure 15, the latter was the most favorable one since the imine intermediate was located 22.16 kcal/mol lower in energy than the reactant complex.

[72] Xu, X.; Zheng, W.; Ren, L.; Jiao, P. *Bull. Chem. Soc. Jpn.* **2022**, *95*, 989.

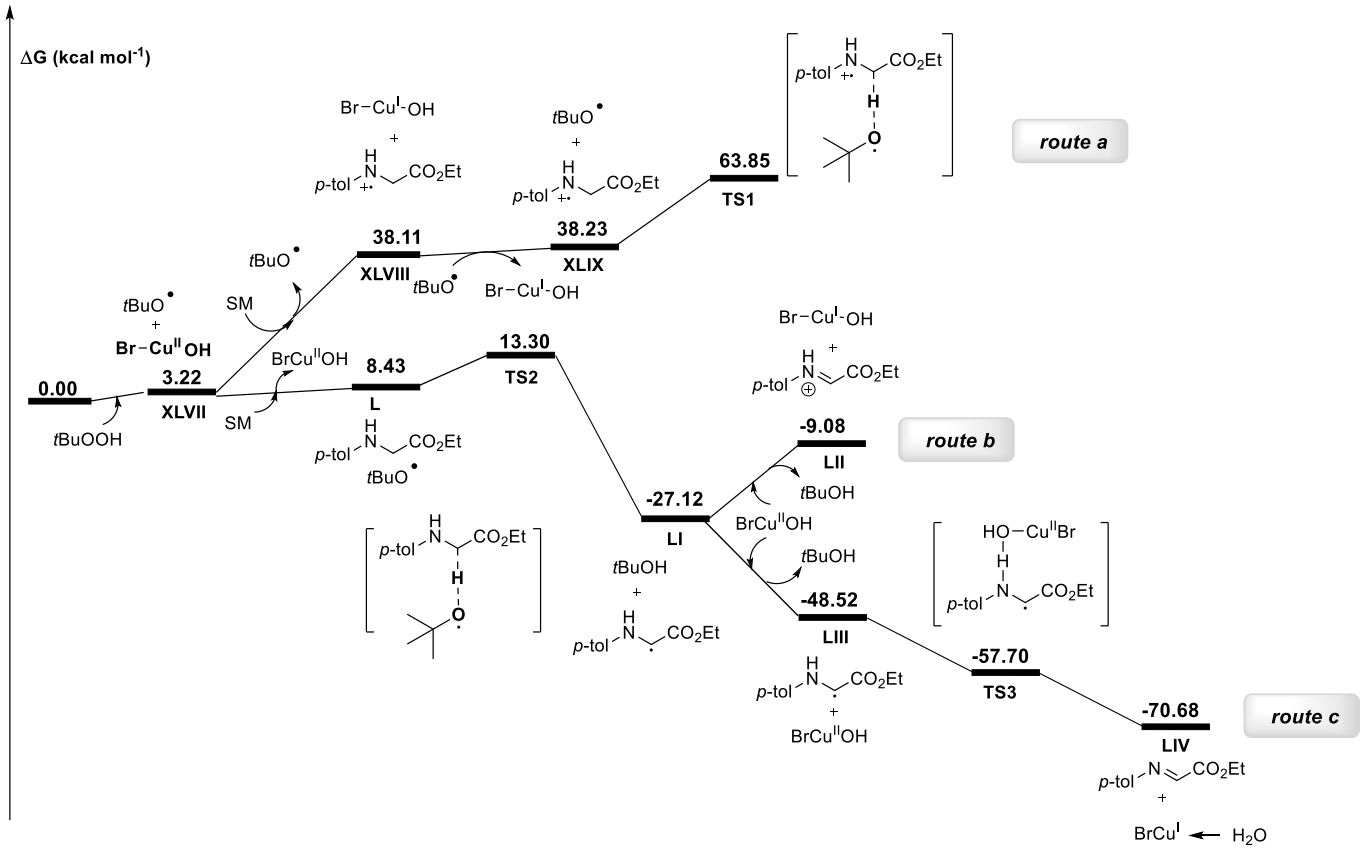

Figure 15. Mechanistic studies performed by the group of Zhen.

Although these computational studies identified the formation of the imine as the most favorable pathway, the formation of an iminium ion could not be discarded. This report was in agreement with our results obtained for Co-catalyzed functionalization of Gly derivatives.

2.4. Conclusions

In summary, we have investigated the mechanism of Co-catalyzed CDC of *N*-substituted glycinates with indoles by DFT studies.[73] Although merely speculative, existing reports commonly proposed the intermediacy of both imine and iminium-type species in these endeavors; however, the nature of the actual electrophilic intermediate remained unclear. Our computational studies supported the formation of a neutral imine species as the more favorable pathway in the Co-catalyzed heteroarylation of glycine-containing compounds. Likewise, this route seemed to be favored when using *N*-aryl substituted derivatives and secondary amines as substrates due to the strong delocalization of the α-carbon-centered radical intermediate. However, although the delocalization could favor the formation of the neutral imine species, there should be more determining factors that influence the effective oxidation of Gly derivatives. This work described herein could lay the foundation for further developments in this field of expertise.

[73] Andrade-Sampedro, P.; Matxain, J. M.; Correa, A. *J. Org. Chem.* **2020**, *85*, 13133.

2.5. Supporting information

For the electronic energies, enthalpy and Gibbs free energy corrections, total enthalpy and Gibbs free energy values as well as the enthalpy and Gibbs free energy differences of interest, please see the SI of the published article.[73]

Chapter 3.

Pd-Catalyzed C(sp^2)–H Alkoxycarbonylation of Phenethyl- and Benzylamines with Chloroformates as CO Surrogates

ABSTRACT: The site-selective functionalization of C–H bonds within a complex molecule remains a challenging task of capital synthetic importance. Herein, we report an unprecedented Pd-catalyzed C(sp^2)–H alkoxycarbonylation of phenylalanine derivatives and other amines featuring picolinamide as the directing group (DG). This oxidative coupling is distinguished by its scalability, operational simplicity and avoids the use of toxic carbon monoxide as the C1 source. Remarkably, the easy cleavage of the DG enables the efficient assembly of isoindolinone compounds. Density Functional Theory calculations support a Pd(II)/Pd(IV) catalytic cycle.

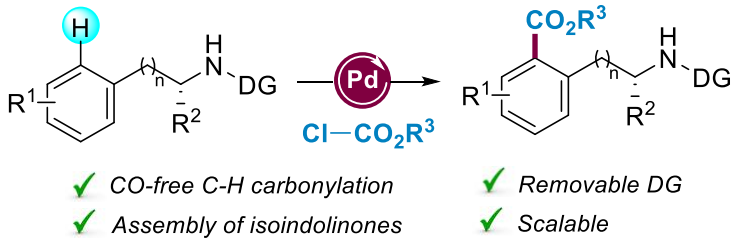

3.1. Introduction

3.1.1. C(sp^2)–H Functionalization at the Amino Acid Side-Chain

Owing to the aromatic nature of the side-chain of amino acids such as Tyrosine, Phenylalanine, Tryptophan and Histidine in combination with the large number of possibilities offered by the C(sp^2)–H activation methodologies, they are suitable substrates for the synthesis of non-proteinogenic derivatives upon transition metal catalysis (Figure 16). Although the landscape of transition metal-mediated peptide synthesis is experiencing an exponential growth and several advances are achieved every year,[74] the selective modification of aromatic amino acids and peptides still represents a challenging task. In particular, the modification of inert δ-C(sp^2)–H bonds of Phe is of primary interest since it has been less studied in comparison with Trp[75] and Tyr[76] residues, which have been widely used due to the innate nucleophilic character of their aromatic ring.[77]

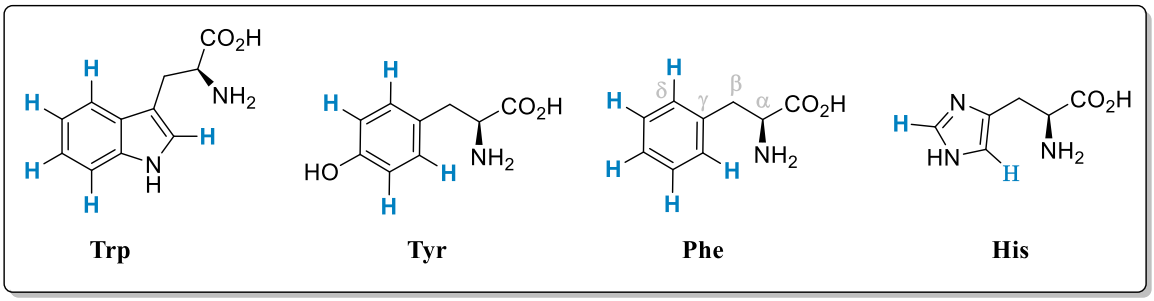

Figure 16. C(sp^2)–H functionalization sites in aromatic amino acids.

[74] a) For selected reviews, see: Guerrero, I.; Correa, A. *Asian J. Org. Chem.* **2020**, *9*, 898. b) Wang, W.; Lorion, M. M.; Shah, J.; Kapdi A. R.; Ackermann, L. *Angew. Chem. Int. Ed.* **2018**, *57*, 14700. c) Kjærsgaard, N. L.; Nielsen, T. B.; Gothelf, K. V. *ChemBioChem* **2022**, *23*, e2022002.
[75] For selected examples, see: a) Gruß, H.; Sewald. N. *Chem. Eur. J.* **2020**, *26*, 5328. b) Tolnai, G. L.; Brand, J. P. ; Waser, J. *Beilstein J. Org. Chem.* **2016**, *12*, 745. c) Zhu, Y.; Bauer, M.; Ackermann, L. *Chem. Eur. J.* **2015**, *21*, 9980. d) Liu, W.; Richter, S. C.; Mei, R.; Feldt, M.; Ackermann, L. *Chem. Eur. J.* **2016**, *22*, 17958.
[76] For selected examples of the functionalization of Tyr residues in the absence of DGs, see: a) Bedford, R. B.; Haddow, M. F.; Webster, R. C.; Mitchell, C. J. *Org. Biomol. Chem.* **2009**, *7*, 3119. b) Zorzi, A.; Deyle, K.; Heinis, C. *Curr. Opin. Chem. Biol.* **2017**, *38*, 24. c) Ichiishi, N.; Caldwell, J. P.; Liu, M.; Zhong, W.; Zhu, X.; Streckfuss, E.; Kim, H.-Y.; Parish, C. A.; Krska, S. W. *Chem. Sci.* **2018**, *9*, 4168. d) Dou, Y.; Kenry.; Liu, J.; Jiang, J.; Zhu, Q. *Chem. Eur. J.* **2019**, *25*, 6896.
[77] Correa, A. *Eur. J. Inorg. Chem.* **2021**, 2928.

The modification of the Phe side-chain has been addressed by following two general strategies: a) the installation of a directing group at the terminal amino moiety and b) using the peptide backbone as an effective *N*,*N*- or *N*,*O*-endogenous bidentate ligand (Scheme 34). In both cases, the formation of a highly reactive Pd^{IV} species within the catalytic cycle is frequently suggested. In the following section, metal-catalyzed C–H functionalization reactions for the modification at the δ-C–H bond of Phe compounds will be analyzed.

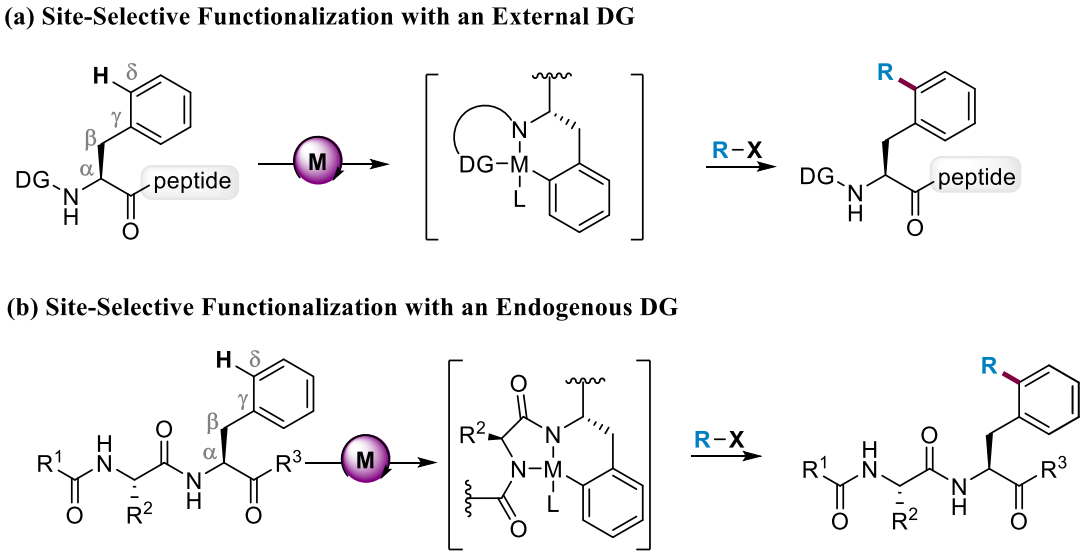

Scheme 34. Different activation modes for the δ-C(sp^2)–H functionalization of Phe derivatives.

3.1.2. C(sp^2)–H Arylation of Phe Derivatives

The C(sp^2)–H arylation with aryl halides could be considered as one of the most developed protocols for the synthesis of non-proteinogenic amino acids. Indeed, the majority of these reactions have been successfully applied at the C(sp^3)–H bonds of aliphatic side-chains[78] as well

[78] a) Zhang, M.; Zhong, S.; Peng, Y.; Jiang, J.; Zhao, Y.; Wan, C.; Zhang, R.; Zhang, A. Q. *Org. Chem. Front.* **2021**, *8*, 133. b) Zhan, B.-B.; Jiang, M.-X.; Shi, B.-F. *Chem. Commun.* **2020**, *56*, 13950.

as at the indole ring of Trp-containing peptides.[75a] However, the δ-C(sp^2)–H arylation of Phe or its derivatives has been much less studied.

The work of Jiang and co-workers set the basis in the field of δ-C(sp^2)–H arylation of Phe units when they discovered that picolinamide could be successfully applied as a DG to obtain the corresponding *ortho*-diarylated derivatives (Scheme 35).[79] In the presence of Ag_2CO_3 as the oxidant and 5.0 equivalents of aryl iodides at 130 ºC, they were able to obtain the desired products in moderate to good yields. Nevertheless, the employment of high temperatures, long reaction times and high excess of the iodide coupling partner could be due to the challenging generation of a 6-membered palladacycle.

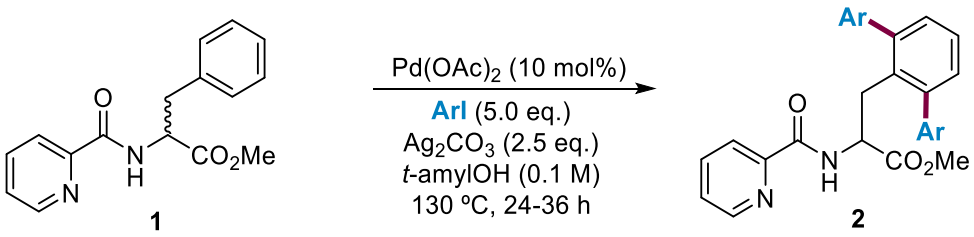

Scheme 35. Arylation of racemic PA-Phe-OMe.

Inspired by the Catellani reaction,[80] an attractive *meta*-C–H functionalization protocol was developed by Yu and co-workers in which the *ortho*-palladacycle intermediate was relayed to the adjacent *meta*-position (Scheme 36).[81] Using nosyl-protected amines as directing groups and pyridine-type ligands, they were able to introduce aryl units in the *meta* position of Phe and Phe-containing dipeptides using catalytic amounts of norbornene for the first time. The authors suggested that the acidity of the amino group was crucial for the successful formation of the Pd–N bond while enough electrophilicity of the Pd^{II} center was maintained. Moreover, the evaluation of a variety of pyridine-based ligands showed that their use was indispensable for the reaction to occur. DFT studies performed by Ehara suggested that pyridine-based ligands could profoundly

[79] Zeng, W.; Nukeyeva, M.; Wang, Q.; Jiang, C. *Org. Biomol. Chem.* **2018**, *16*, 598.
[80] For the pioneering work of the Catellani reaction, see: a) Catellani, M.; Frignani, F.; Rangoni, A. *Angew. Chem. Int. Ed. Engl.* **1997**, *36*, 119. For a selected review on the Catellani reaction, see: b) Della Ca, N.; Fontana, M.; Motti, E.; Catellani, M. *Acc. Chem. Res.* **2016**, *49*, 1389.
[81] Ding, Q; Ye, S.; Cheng, G.; Wang, P.; Farmer, M. E.; Yu, J.-Q. *J. Am. Chem. Soc.* **2017**, *139*, 417.

affect the kinetics of the norbornene-mediated *meta*-C–H functionalization processes and may change the rate-determining step as well as inhibit the formation of the undesired cyclobutene (Scheme 36).[82] In the presence of 4-Ac-Py and 3.0 equivalents of AgOAc, the arylation reaction proceeded with moderate to excellent yields and was compatible with a wide range of aryl and heteroaryl iodides. On the basis of previous reports, they proposed a plausible reaction mechanism. First, the resulting product of the *ortho*-palladation **I** could react with the NBE to generate intermediate **II**, which would react with the adjacent *meta*-C–H bond to form the 5-membered palladacycle **III**. The latter could undergo oxidative addition with the aryl halide to form a highly reactive Pd^{IV} species **IV**, which is prone to suffer a reductive elimination step affording the product, while releasing norbornene and regenerating the active catalyst.

[82] Yang, T.; Kong, C.; Yang, S.; Yang, Z.; Yang, S.; Ehara, M. *Chem. Sci.* **2020**, *11*, 113.

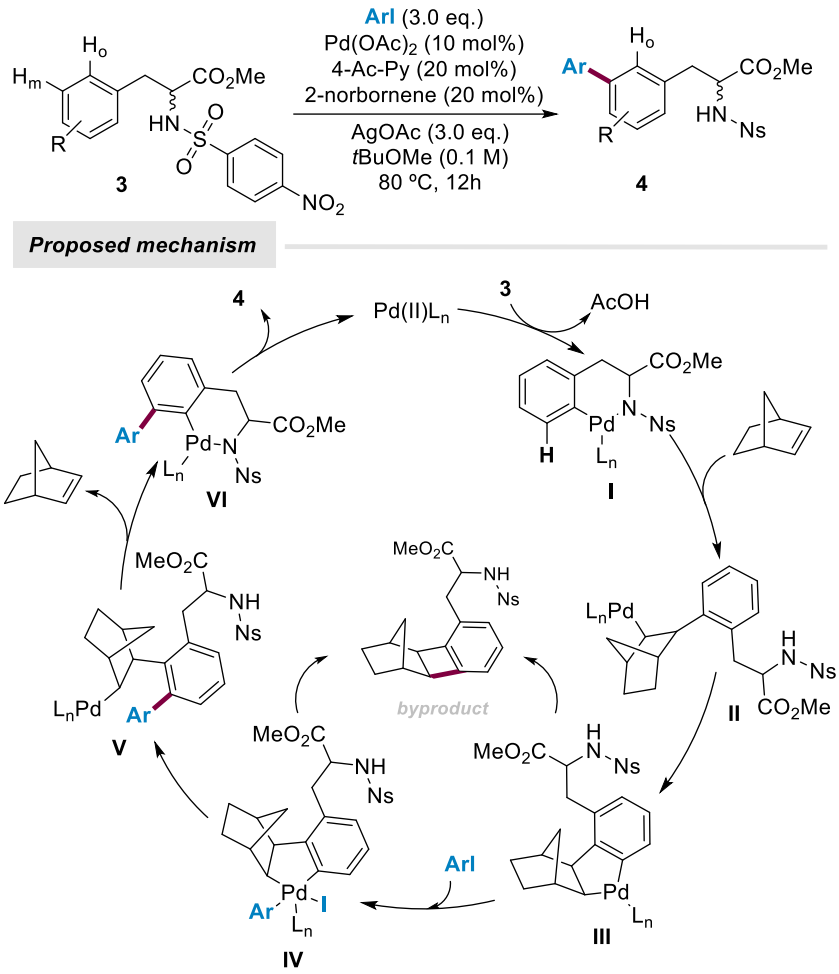

Scheme 36. meta-C(sp²)–H arylation of Phe derivatives.

Over the last decades, great efforts have been done in the synthesis of cyclopeptides since they are considered as important drug candidates in medicinal chemistry.[83] In this context, in 2015 Lavilla and co-workers presented a Pd-catalyzed new peptide stapling strategy involving Trp and *meta*-iodo substituted Phe residues without the aid of an external directing group.[84] This protocol allowed the synthesis of constrained peptides of different ring sizes and set the basis for further discoveries in the field. More recently, Albericio[85] and Wang[86] simultaneously published a highly

[83] a) Buckton, L. K.; Rahimi, M. L.; McAlpine, S. R. *Chem. Eur. J.* **2021**, *27*, 1487. b) Martí-Centelles, V.; Pandey, M. D.; Burguete, I. Luis, S. V. *Chem. Rev*. **2015**, *115*, 8736.
[84] Mendive-Tapia, L.; Preciado, S.; García, J.; Ramón, R.; Kielland, N.; Albericio, F.; Lavilla, R. *Nat. Commun.* **2015**, *6*, 7160.
[85] Noisier, A. F. M.; García, J.; Ionut, I. A.; Albericio, F. *Angew. Chem. Int. Ed.* **2017**, *56*, 314.
[86] Tang, J.; He, Y.; Chen, H. Sheng, W.; Wang, H. *Chem. Sci.* **2017**, *8*, 4565.

versatile peptide macrocyclization method through a peptide backbone directed Pd-catalyzed β-C(sp^3)–H activation of Ala residues and the aromatic side-chain of *meta*-iodinated Phe. Complementing these strategies, Chen and co-workers reported Pd-catalyzed arylation[87] and alkylation[88] reactions using the PA as a *N*-terminal bidentate DG (Scheme 37). These methods overcome the limitation of previous works on the field by being compatible with more functional groups and tolerating the less strained *para*-substituted Phe linkage. As expected, the reaction is believed to start with the C–H palladation to form a kinetically favored 5-membered palladacycle, which is followed by the oxidative addition step to render a Pd^{IV} intermediate. Reductive elimination from a Pd^{IV} intermediate would form the stapled peptide, thereby releasing the active catalyst. Owing to the reversibility of the C–H activation step, the diastereoselectivity was influenced by the conformational bias of the corresponding peptide. Intramolecular arylation of the *trans* intermediate appeared to be more thermodynamically favored than the parent *cis* structure, enhancing diastereoselectivity during the process.

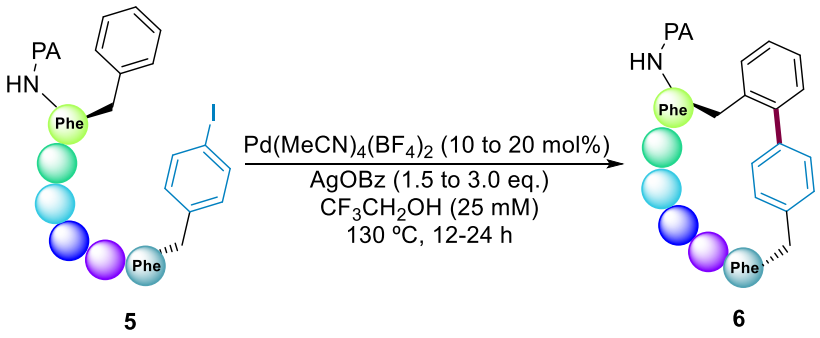

5 **6**

Scheme 37. Intramolecular C(sp^2)–H arylation developed by Chen and co-workers.

3.1.3. C(sp^2)–H Alkynylation and Olefination of Phe Derivatives

Although the Fujiwara-Moritani reaction,[89] in which aromatic and olefinic C–H bonds are coupled directly, represents an atom-economical alternative to the widely used Heck-coupling reaction, it

[87] Han, B.; Li, B.; Qi, L.; Yang, P.; He, G.; Chen, G. *Org. Lett.* **2020**, *22*, 6879.
[88] Li, B.; Li, X.; Han, B.; Che, Z.; Zhang, X.; He, G.; Chen, G. *J. Am. Chem. Soc.* **2019**, *141*, 9401.
[89] For the original report of F-M reaction, see: Moritani, I.; Fujiwara, Y. *Tetrahedron Lett.* **1967**, *12*, 1119.

has not been widely used due to the required highly oxidative and acidic reaction conditions to form a more electrophilic Pd center. In addition, poor selectivity or multiple substitutions are often observed. Even so, in the last decade several advances have been achieved by the use of DGs, different transition metals and milder protocols that are tolerant toward different functionalities.[90] Although the whole reaction mechanism is not completely understood, it generally involves a Pd^{II}/Pd^{0} regime, in which the C–H activation, 1,2-migratory insertion and β-hydride elimination are the main elemental steps.

Continuing with their studies on the design of optimal DGs for different C–H functionalization events, Yu's group demonstrated that the trifluoromethanesulfonyl (-SO_2CF_3) protecting group was a very suitable DG for promoting the C–H activation step in a wide range of palladium-catalyzed reactions, including F-M reactions.[91] A combination of AgOAc and $Pd(OAc)_2$ enabled the δ-alkenylation of Phe and Tyr compounds. Notably, a tandem C–H alkenylation and aza-Michael addition was reported when using vinyl ketones to yield isoquinolines in a diastereoselective fashion (Scheme 38).

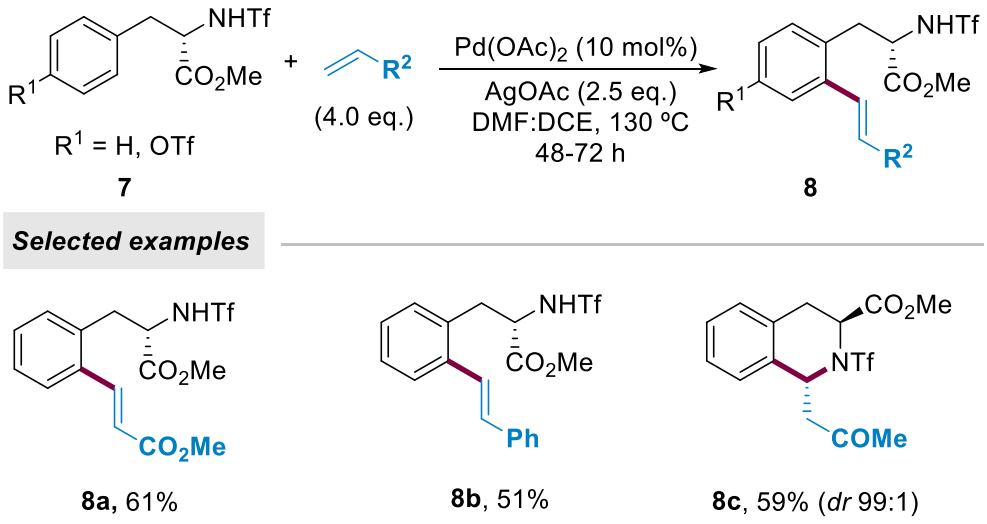

Scheme 38. C(sp^2)–H olefination of Phe derivatives.

[90] a) Nishikata, T.; Lipshutz, B. H. *Org. Lett.* **2010**, *12*, 1972. b) Liu, X. Hii, K. K. *J. Org. Chem*. **2011**, *76*, 8022. c) Manna, M. K.; Bhunia, S. K.; Jana, R. *Chem. Commun.* **2017**, *53*, 6906.
[91] Li, J.-J.; Mei, T.-S.; Yu, J.-Q. *Angew. Chem. Int. Ed.* **2008**, *47*, 6452.

Unfortunately, although long reaction times and high amounts of the olefin were used, the yields were moderate and the scope was limited to a few examples of Phe derivatives. Later on, a similar protocol was reported by Carretero featuring the use of *N*-(2-pyridyl)sulfonyl (SO_2Py) as the DG.[92] Likewise, this protocol was also limited to the use of simple Phe units and the deprotection/Aza-Michael sequence proceeded with a small degree of racemization.

To overcome these limitations, the group of Zhao proposed a complementary strategy for the olefination of phenylethylamine derivatives directed by a removable PA directing group (Scheme 39).[93]

[92] García-Rubia, A.; Laga, E.; Cativiela, C.; Urriolabeitia, E. P.; Gómez-Arrayás, R.; Carretero, J. C. *J. Org. Chem*. **2015**, *80*, 3321.
[93] Zhao, F.; Jia, X.; Zhao, J.; Fei, C.; Liu, L.; Liu, G.; Wang, D.; Chen, F. *RSC Adv*. **2017**, *7*, 25031.

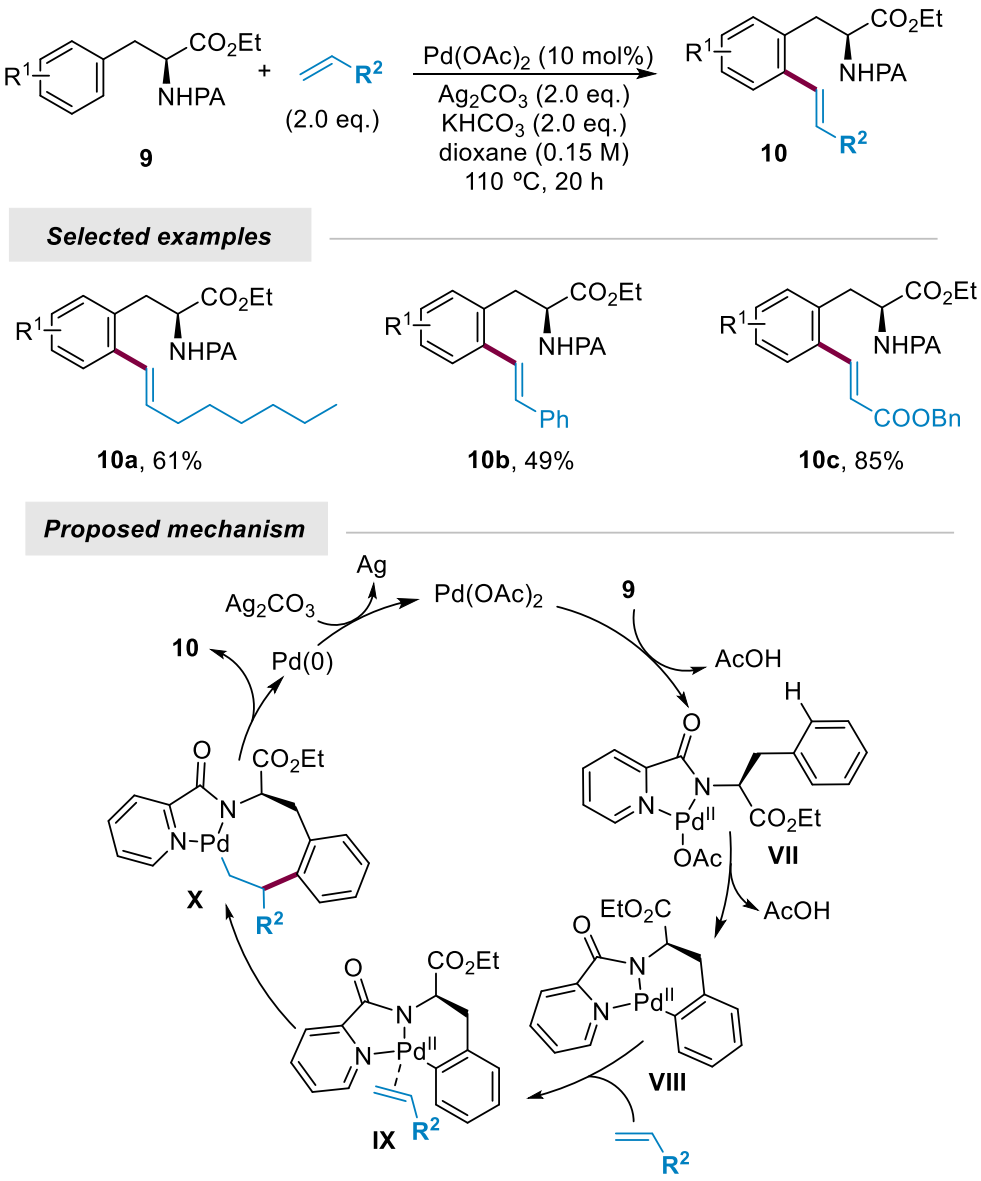

Scheme 39. C(sp^2)–H alkenylation using PA as DG.

The use of $KHCO_3$ seemed to be crucial for the acceleration of the C–H activation step. Contrary to previous works, electron-rich and deactivated alkenes afforded the corresponding products with moderate yields. Although the reaction was found to be scalable and could be used for the derivatization of more challenging phenylethylamines, high amounts of solvent were used and in some cases selectivity issues took place. The authors suggested a plausible mechanism based on previous reports. After a PA-directed *ortho*-metalation step, the resulting 6-membered metallacycle **VIII** could undergo a 1,2-migratory insertion forming the unstable intermediate **X**,

which was prone to suffer a β-H elimination step. Ag_2CO_3 could act as an oxidizing agent to regenerate the active Pd^{II} catalyst.

In 2019, Cross and co-workers developed the first catalytic olefination of Phe-containing peptides using the peptide backbone as a bidentate endogenous DG (Scheme 40).[94] The treatment of the corresponding peptides with four equivalents of styrene derivatives afforded the difunctionalized products in moderate to good yields. Surprisingly, the diolefination reaction only occurred for Phe residues located in the C-terminus or in inner positions within the peptide sequence through the formation of the intermediate **XI** (Scheme 40a). The authors proposed that when placing the Phe residue at the N-terminus, due to the square planar structure of the Pd^{II} center adopted within intermediate **XIII**, the C–H activation event would be geometrically unfeasible and could only proceed through an energetically demanding monodentate intermediate, which would be inaccessible under the standard reaction conditions (Scheme 40b).

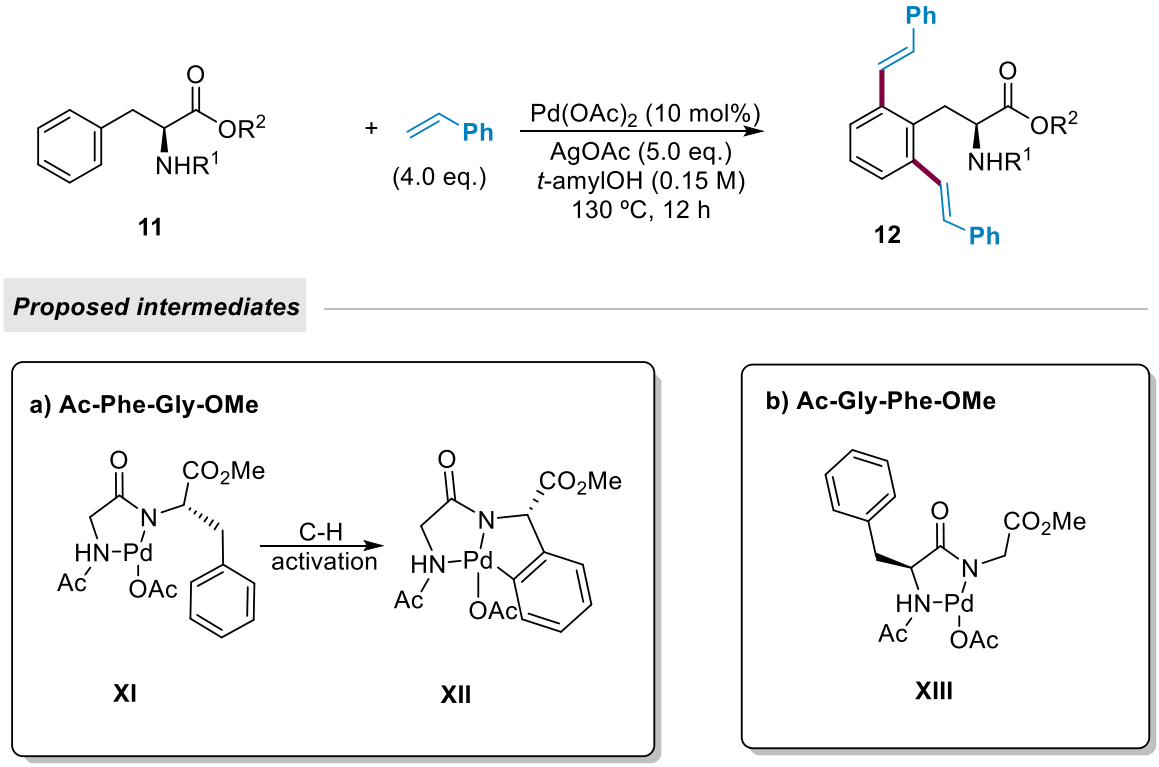

Scheme 40. Peptide backbone-enabled C(sp^2)–H olefination with styrenes.

[94] Terrey, M. J.; Perry, C. C.; Cross, W. B. *Org. Lett.* **2019**, *21*, 104.

Later on, the group of Song published a similar procedure for the olefination of Phe-containing peptides under similar reaction conditions (Scheme 41).[95] Although this work expanded the scope to electron-deficient alkenes, the corresponding products were obtained as a mixture of mono- and difunctionalized compounds. Interestingly, the slight modification of the reaction conditions allowed the use of alkynyl bromides as coupling partners. Using K_2CO_3 as a base and catalytic amount of PivOH as an additive, various di- and tripeptides were alkynylated in very good yields. In concordance with the work of Cross,[94] control experiments showed that the formation of an amide bonded bidentate intermediate was crucial for the reaction to occur. Despite its novelty, this alkynylation protocol suffered from selectivity issues and only four examples of peptides were reported. The reaction starts with the coordination of the peptide backbone in a bidentate manner and further C–H activation to deliver the palladacycle **XV**. The latter could undergo the oxidative addition of the alkynyl bromide, thereby resulting in the formation of Pd^{IV} intermediate **XVI**. A final reductive elimination step would deliver the product and regenerate the active palladium catalyst.

[95] Zheng, Y.; Song, W. *Org. Lett.* **2019**, *21*, 3257.

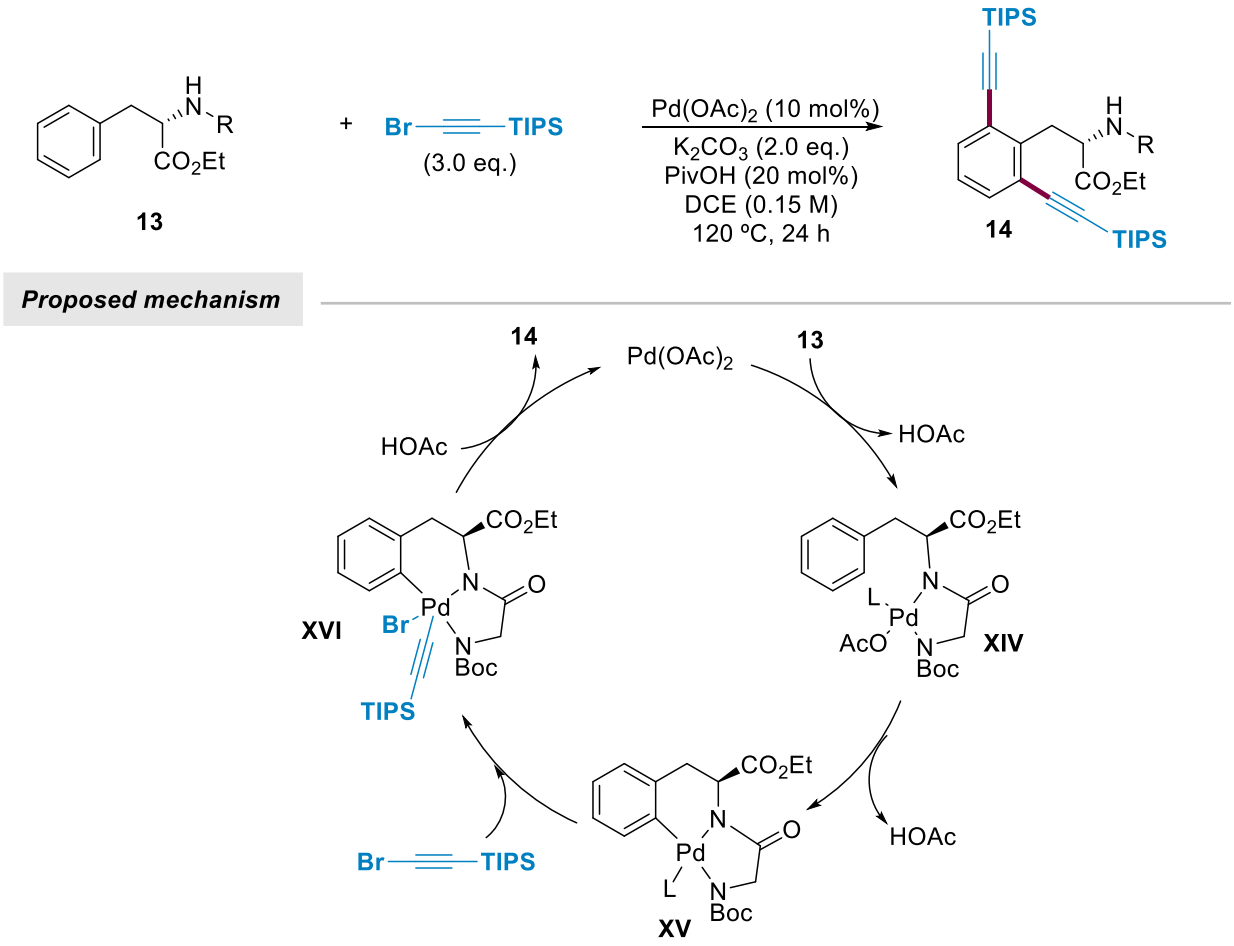

Scheme 41. Pd-catalyzed alkynylation of Phe derivatives.

In connection with their studies in peptide macrocyclizations,[96] Wang and co-workers reported the late-stage Pd-catalyzed C(sp^2)–H olefination of Phe residues directed by the peptide backbone, in which the backbone amides located *N*-terminally to a Phe residue served as internal DGs (Scheme 42a).[97] This reaction displayed broad substrate scope and could be applied for the synthesis of cyclic peptides with unique aryl-alkene cross-links. Once again, the presence of two amide bonds *N*-terminally to the Phe residue were crucial to bind with the catalyst effectively through a six-membered palladacycle. The failure of C-to-N macrocyclization was most likely because for C-terminal amides the formation of a kinetically unfavored seven-membered palladacycle would be required. Owing to the presence of azoles in bioactive molecules, the same authors have recently

[96] Tang, J.; Chen, Y.; He, Y.; Sheng, W.; Bai, Q.; Wang, H. *Nat. Commun.* **2018**, *9*, 3383.
[97] Bai, Z.; Cai, C.; Yu, Z.; Wang, H. *Angew. Chem. Int. Ed.* **2018**, *57*, 13912.

reported related macrocyclization reactions featuring thiazoles and oxazoles as internal DGs (Scheme 42b). Although high amounts of silver acetate and copper acetate were required, the reaction exhibited a broad substrate scope (protected Trp and Tyr were tolerated) and penta- or hexapeptide substrates with internal Phe units successfully underwent the olefination reaction with good yields. In the case of peptides with two N-terminal and C-terminal Phe residues, the reaction was found to be selective at the oxazole-neighboring Phe unit, indicating that the DG outcompeted potential side reactions of backbone-assisted alkenylation reaction by forming the kinetically favoured five-membered palladacycle.[98]

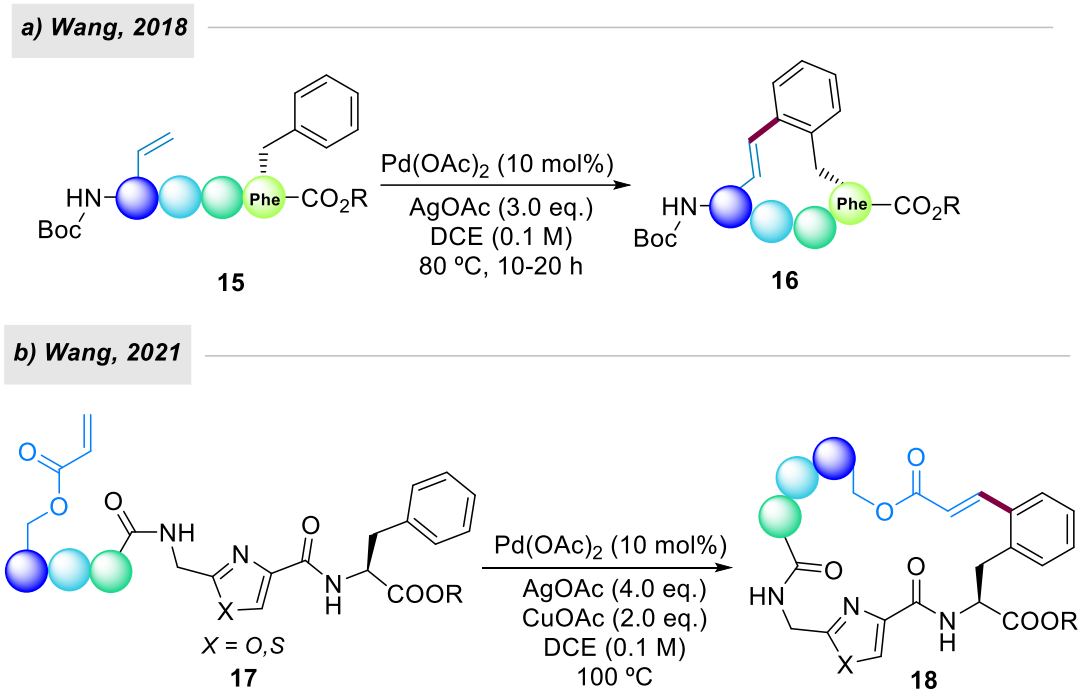

Scheme 42. Intramolecular C(sp^2)–H olefination for the synthesis of macrocycles.

[98] a) Liu, S.; Cai, C.; Bai, Z.; Sheng, W.; Tan, J.; Wang, H. *Org. Lett.* **2021**, *23*, 2933. b) Cai, C.; Wang, F.; Xiao, X.; Sheng, W.; Liu, S.; Chen, J.; Zheng, J.; Xie, R.; Bai, Z.; Wang, H. *Chem. Commun.* **2022**, *58*, 4861.

3.1.4. C(sp^2)–H Alkylation of Phe Derivatives

Unlike olefination reactions of Phe compounds, the parent alkylation processes are scarce and only a couple of examples have been reported. In general, the formation of C(sp^2)-C(sp^3) bonds by transition metal catalysis has been limited due to the preferential β-hydrogen elimination over the desired reductive elimination step. Indeed, the existing protocols only include alkyl groups lacking hydrogen atoms on the beta position relative to the palladium atom and therefore reductive elimination is favored.

In continuation with their previous work on Pd-catalyzed C(sp^2)–H functionalization of PA-protected benzylamines with alkyl halides,[99] the group of Chen expanded the protocol to simple Phe derivatives obtaining excellent yields (Scheme 43). The beneficial effect of Ag_2CO_3 was attributed to its halide scavenging ability and its tendency to facilitate the oxidative addition step. Moreover, they found that the use of catalytic amounts of phosphoric acids could improve the feasibility of the process avoiding the high concentration of free Ag^+ ions and thus preventing the induced decomposition of the electrophile through an E2 elimination pathway.[100] Although they suggested that a $Pd^{II/IV}$ manifold might be operative, a Pd^{III} catalytic pathway cannot be ruled out.[101]

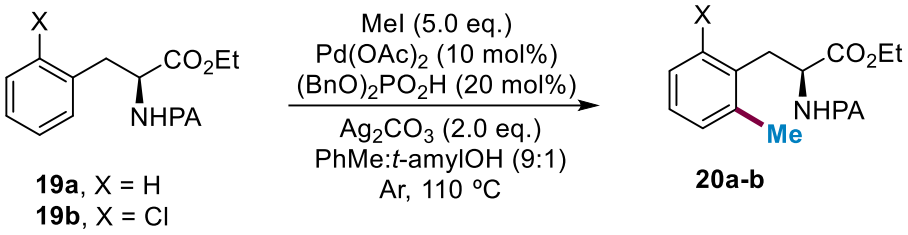

Scheme 43. C(sp^2)–H alkylation of phenethylamines reported by Chen.

In 2018, the group of Peng proposed a complementary strategy for the *meta*-alkylation of Phe derivatives using a modified norbornene as a transient mediator (Scheme 44).[102] It is noteworthy

[99] Zhao, Y.; Chen, G. *Org. Lett.* **2011**, *13*, 4850.
[100] Hamilton, G. L.; Kanai, T.; Toste, F. G. *J. Am. Chem. Soc.* **2008**, *130*, 14984.
[101] a) Powers, D. C.; Geibel, M. A. L.; Klein, J. E. M. N.; Ritter, T. *J. Am. Chem. Soc.* **2009**, *131*, 17050. b) Deprez, N. R.; Sanford, M. S. *J. Am. Chem. Soc.* **2009**, *131*, 11234.
[102] Liu, J.; Ding, Q.; Fang, W.; Wu, W.; Zhang, Y.; Peng, Y. *J. Org. Chem.* **2018**, *83*, 13211.

that the mechanism of this alkylation protocol is similar to the one depicted in Scheme 44. Due to the complexity of the reaction mechanism, many side reactions could take place: the formation of undesired benzocyclobutene, the functionalization of the NBE instead of the aromatic ring and when the β-carbon elimination is difficult to achieve, a second palladation could take place (known as *ortho*-constraint). The modification of the NBE skeleton played a crucial role in almost all the steps of the catalytic cycle. While C1- or C2-substituted norbornenes can inhibit the undesired second metalation and promote β-carbon elimination as well as the C–H palladation itself, the C5,C6-substituted norbornenes tend to accelerate the reaction rates compared with their unsubstituted analogues.[103]

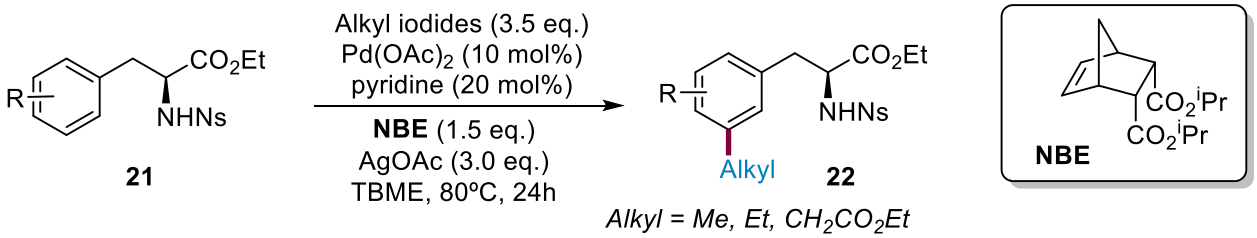

Scheme 44. Palladium-catalyzed C(sp^2)–H alkylation of Phe derivatives.

The use of other alkylating agents would clearly expand the synthetic scope of this technique. However, the multiple reaction pathways that these substrates could undergo indicate that other alternatives may be more practical. In this respect, CDC processes utilizing unsubstituted hydrocarbons could be a reliable alternative.

3.1.5. C(sp^2)–H Acylation of Phe Derivatives

Compared with the number of protocols developed for the functionalization of peptides via outer-sphere mechanisms, inner-sphere radical reactions remain much less explored.[104] Although radical

[103] Li, R.; Dong, G. *J. Am. Chem. Soc.* **2020**, *142*, 17859.
[104] a) Aguilar Troyano, F. J.; Merkens, K.; Anwar, K.; Gómez-Suárez, A. *Angew. Chem. Int. Ed.* **2021**, *60*, 1098. b) Sun, X.; Dong, X.; Liu, H.; Liu, Y. *Adv. Synth. Catal.* **2021**, *363*, 1527.

acylation has been extensively studied by numerous of research groups,[105] the translation of the method to structurally complex peptides remained elusive. In 2019 our group developed a novel acylation protocol for the late-stage modification of PA-protected Phe-containing peptides (Scheme 45).[106] Interestingly, this method features the use of a wide range of aromatic and heteroaromatic aldehydes, which in general terms tend to react with the Phe unit in a mono-selective manner. The use of DCP as oxidant was indispensable for the process to occur and the addition of silver salts was shown to increase the yield. The reaction starts with the coordination of the PA-containing Phe derivative in a bidentate manner and further C–H activation to deliver the 6-membered palladacycle **XVIII**. The latter could suffer from the addition of the acyl radical species, thereby resulting in the formation of a Pd^{III} center, which would be likely oxidized to Pd^{IV} intermediate **XIX**. The final reductive elimination step would deliver the product and regenerate the active palladium catalyst. Although the role of the silver carbonate was not clear, the authors suggested that the beneficial effect could be due to the formation of heterodimeric species as well as for promoting the regeneration of the active catalyst.[107]

[105] For selected reviews, see: a) Kumar, P.; Dutta, S.; Kumar, S.; Bahadur, V.; Van der Eycken, E. V.; Vimaleswaran, K. S.; Parmar, V. S.; Singh, B. K. *Org. Biomol. Chem.* **2020**, *18*, 7987. b) Santiago, C.; Sotomayor, N.; Lete, E. *Molecules* **2020**, *25*, 3247. c) Yang, W.-C.; Feng, J.-G.; Wu, L.; Zhang, J.-Q. *Adv. Synth. Catal.* **2019**, *361*, 1700.
[106] San Segundo, M.; Correa, A. *Chem. Sci.* **2019**, *10*, 8872.
[107] a) Bhaskararao, B.; Shing, S.; Anand, M.; Verma, P.; Prakash, P.; Malakar, S. A. C.; Schaefer, H. F.; Sunoj, R. B. *Chem. Sci.* **2020**, *11*, 208. b) Mudarra, A. L.; Martínez de Salinas S.; Perez-Temprano, M. H. *Org. Biomol. Chem.* **2019**, *17*, 1655. c) Anand, M.; Sunoj, R. B.; Schaeffer, H. F. *J. Am. Chem. Soc.* **2014**, *136*, 5535.

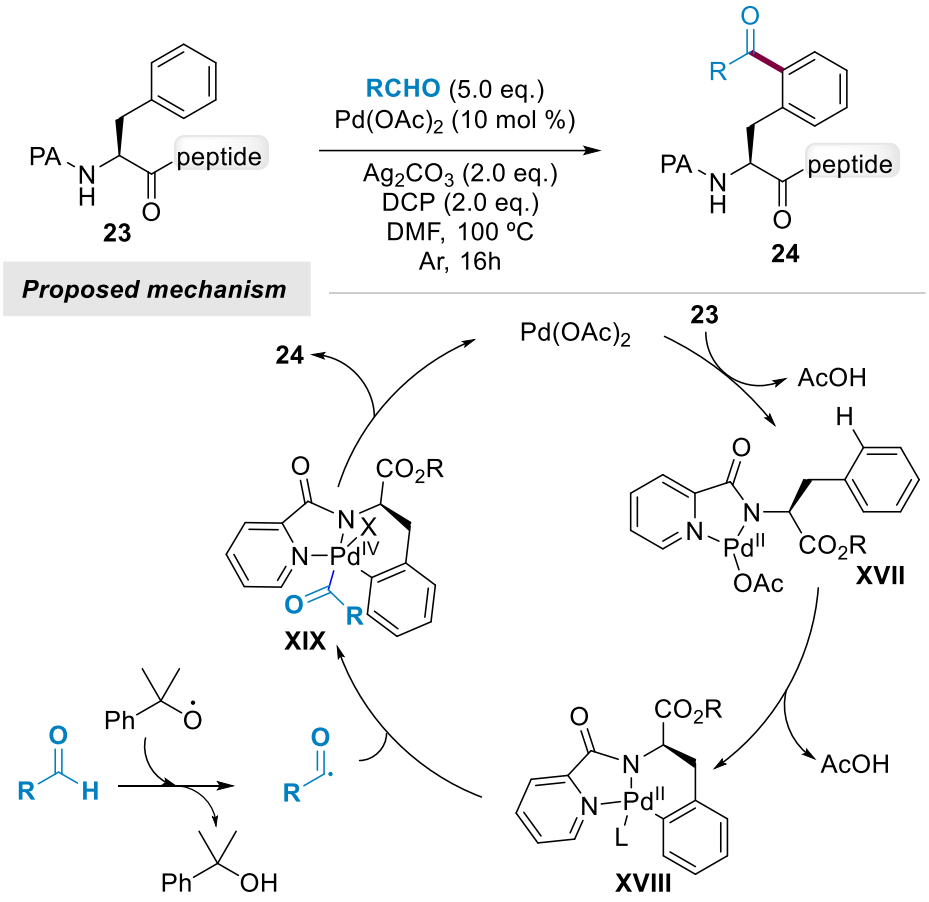

Scheme 45. Pd-catalyzed C(sp^2)–H acylation developed by our group.

3.1.6. C(sp^2)–H Amination of Phe Derivatives

Transition metal-catalyzed C–N bond formation is a fundamental process in organic chemistry due to the prevalence of these bonds in natural products as well as in compounds with interesting biological properties. Since Buchwald[108] and Hartwig[109] introduced Pd- and Cu-catalyzed amination of aryl halides, they have become indispensable tools of widespread use in synthesis and represent an area of increasing interest. In particular, C–H amination reactions have emerged

[108] Surry, D. S.; Buchwald, S. L. *Chem. Sci.* **2011**, *2*, 27.
[109] Hartwig, J. F. *Acc. Chem. Res.* **2008**, *41*, 1534.

as an attractive alternative because of their ability to construct nitrogenated compounds in an atom-economical and inexpensive manner.[110]

Over the last decade, a high number of indoline syntheses have been developed upon palladium-catalyzed C–H functionalization reactions. The pioneering work published by Yu and co-workers in 2009 demonstrated that single-electron or two-electron oxidants could be suitable reagents to selectively obtain indoline derivatives through a highly efficient C–N reductive elimination pathway (Scheme 46a).[111] On the one hand, using catalytic amounts of $Pd(OAc)_2$ as catalyst, $Ce(SO_4)_2$ as oxidant and DMF as a labile ligand, various triflamide-protected phenyletylamines selectively underwent the intramolecular C–H amination reaction. When other oxidants were used nonselective reductive elimination pathways were observed, which rendered halogenated or acyloxylated compounds preferentially. They suggested that when using $Ce(SO_4)_2$ as the oxidant a monomeric-square planar Pd^{III} complex could be formed, being the OAc group oriented in the *trans* position relative to the aryl group and hence, preventing the undesired reductive elimination event. On the other hand, they were pleased to find that F^+-based oxidants could also be suitable oxidants since the notorious strength of the Pd–F bond also prevented the undesired reductive elimination step. Although the use of a triflamide was found to be crucial for the efficient C–H bond cleavage, long reaction times as well as high temperatures were required.

[110] For selected reviews, see: a) Park, Y.; Kim, Y.; Chang, S. *Chem. Rev.* **2017**, *117*, 9247. b) Hazelard, D.; Nocquet, P.-A.; Compain, P. *Org. Chem. Front.* **2017**, *4*, 2500. c) Louillat, M.-L.; Patureau, F. W. *Chem. Soc. Rev.* **2014**, *43*, 901.
[111] Mei, T.-S.; Wang, X.; Yu, J.-Q. *J. Am. Chem. Soc.* **2009**, *131*, 10806.

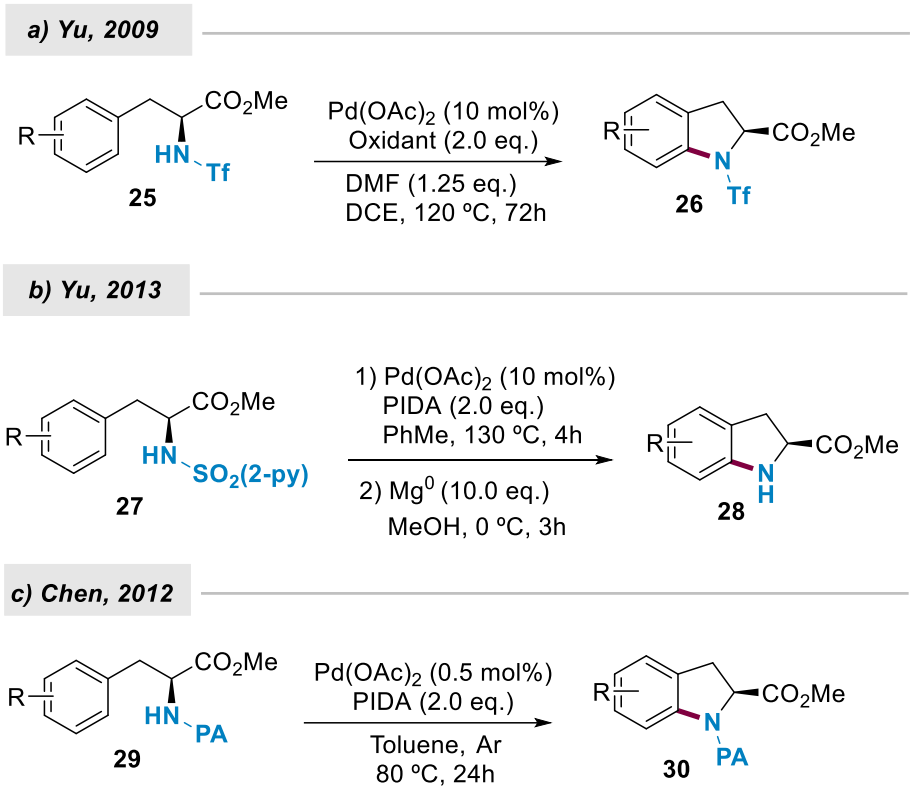

Scheme 46. C(sp^2)–H amination strategies developed by Yu and Chen.

To overcome these limitations, four years later they reported a new protocol for the synthesis of indolines utilizing the 2-pyridilsulfonyl directing group and $PhI(OAc)_2$ as oxidant (Scheme 46b).[112] This method allowed the use of cheaper oxidants, shorter reaction times and the DG could be easily removed under mild reaction conditions, thereby avoiding racemization within the process.

At the same time, the group of Chen demonstrated that picolinamide could also be a suitable DG for intramolecular C(sp^2)–H amination reactions using PIDA as oxidant (Scheme 46c).[113] Interestingly, the reaction could be carried out with very low catalyst loadings and the addition of carboxylic acid derivatives allowed the reaction to proceed under air. Although in most cases low or moderate amounts of acyloxylated products were obtained, the reaction showed an excellent tolerance for iodo-substituted arenes, which is rare in related Pd-catalyzed C–H functionalization

[112] Mei, T.-S.; Leow, D.; Xiao, H.; Laforteza, B. N.; Yu, J.-Q. *Org. Lett.* **2013**, *15*, 3058.
[113] a) He, G.; Lu, C.; Zhao, Y.; Nack, W. A.; Chen, G. *Org. Lett.* **2012**, *14*, 2944. b) He, G.; Zhao, Y.; Zhang, S.; Lu, C.; Chen, G. *J. Am. Chem. Soc.* **2012**, *134*, 3.

events due to competitive reaction pathways. Later on, the group of Shi expanded this methodology to the amination of more complex dipeptides slightly modifying the triflamide-protocol developed by Yu.[114]

In 2015, Ma and co-workers described a novel method for the synthesis of indoline-2-carboxylate-enbodied Phe-containing dipeptides under palladium catalysis and using the 2-methoxyiminoacyl (MIA) as a powerful amine auxiliary (Scheme 47).[115] After a careful examination of different F^+ sources, the pyridinium salt, which is able to oxidize Pd^{II} to Pd^{IV}, gave the best results. Curiously, as described in the pioneering work of Yu,[111] the addition of DMF as a labile ligand seemed to be crucial to achieve good conversion. Although the treatment of the products with Raney Ni afforded the corresponding peptides in good yields, the cleavage of the auxiliary afforded a mixture of diastereomers. The authors proposed the formation of the double palladium chelate **XXI** through a C–H activation event, which may undergo an oxidative process to render the Pd^{IV} complex **XXII**. The latter would deliver the product through a reductive elimination event, regenerating the active catalyst within the process. Nevertheless, the formation of a Pd^{III} intermediate along the reaction pathway could not be discarded.

[114] Yang, M.; Jiang, X.; Shi, Z.-J. *Org. Chem. Front.* **2015**, *2*, 51.
[115] He, Y.-P.; Zhang, C.; Fan, M.; Wu, Z.; Ma, D. *Org. Lett.* **2015**, *17*, 496.

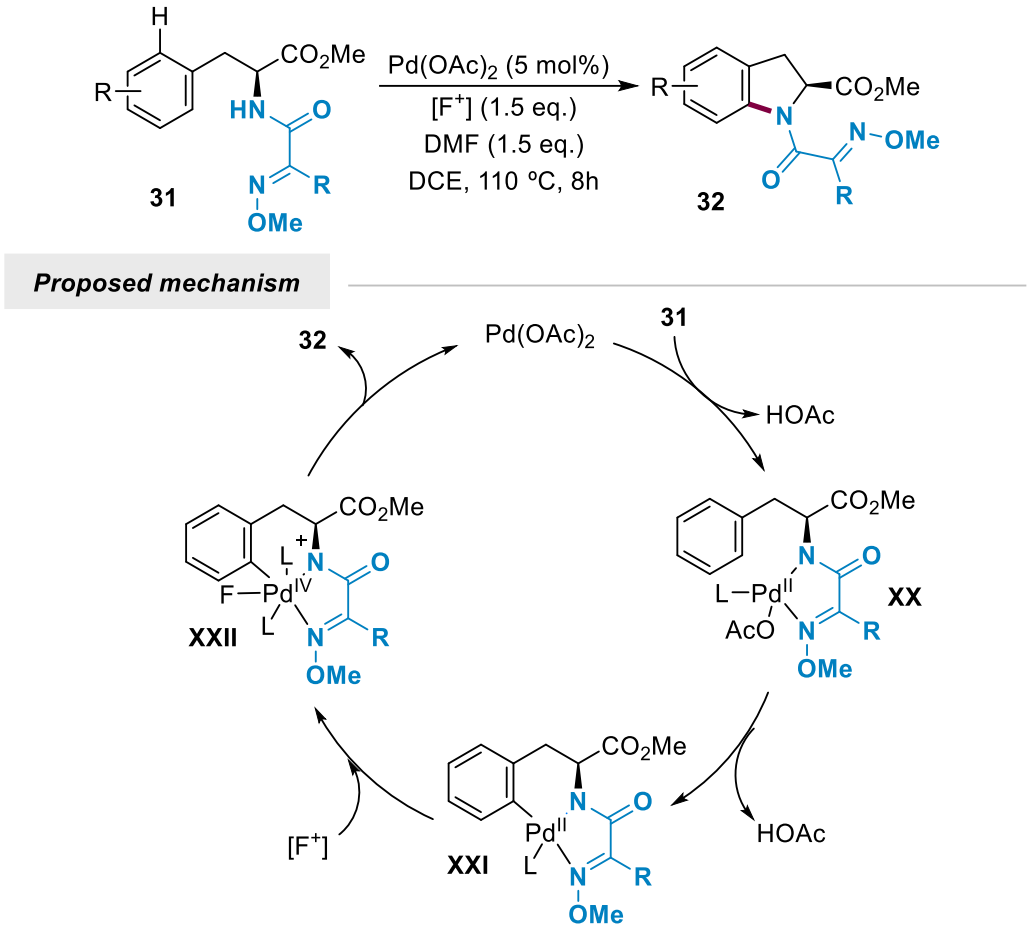

Scheme 47. C(sp^2)–H amination using MIA as an auxiliary.

More recently, the group of Xuan proposed a complementary strategy for the synthesis of indoline-2-carboxylate-dipeptides using the peptide backbone as an intrinsic bidentate DG (Scheme 48).[116] Using palladium as catalyst and $PhI(OAc)_2$ as the terminal oxidant, the corresponding Phe derivatives underwent the corresponding intramolecular amination reaction providing very good yields. Notably, although harsh oxidative conditions were used, protected serine and indole units were tolerated. Some control experiments conducted with tertiary amines at the N-terminus revealed that the bidentate coordination was crucial for the process to occur.

[116] Zheng, Y.; Song, W.; Zhu, Y.; Wei, B.; Xuan, L. *Org. Biomol. Chem.* **2018**, *16*, 2402.

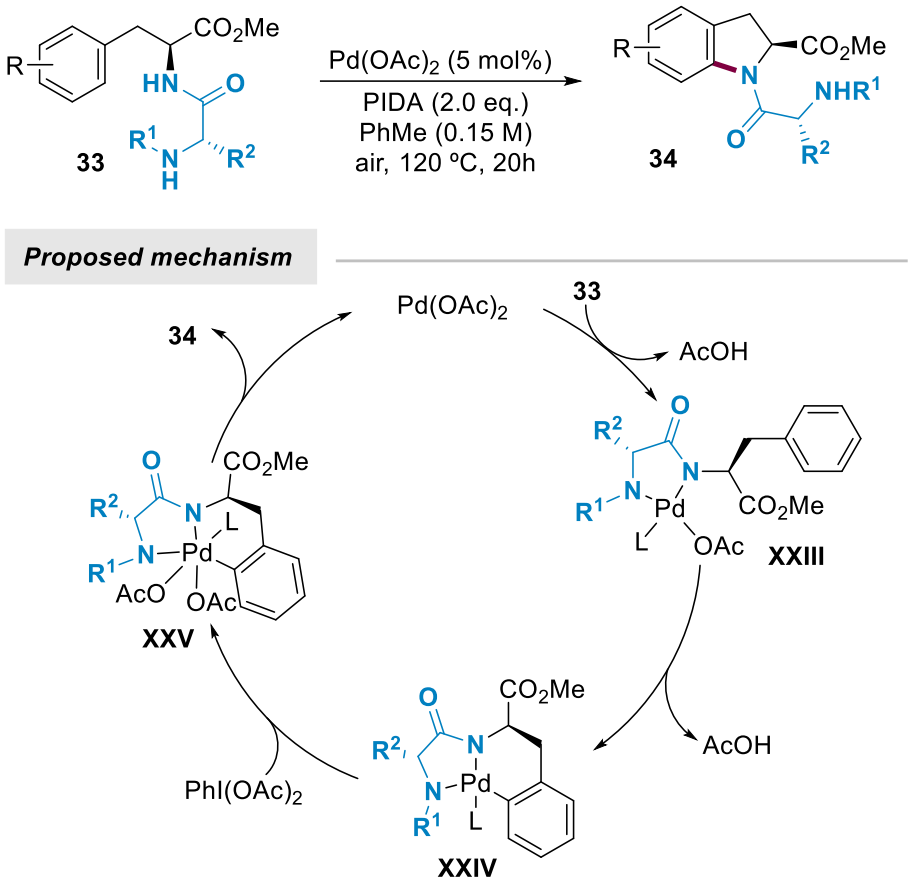

Scheme 48. C(sp^2)–H amination using the peptide backbone as the DG.

It is noteworthy that other protecting groups were also used in combination with PIDA to obtain the corresponding indoline derivatives. Specifically, Zhao[117] and Shi[118] simultaneously demonstrated that 1,2,3-triazoles and oxalyl amides were also suitable DGs to obtain these particular heterocyclic cores.

In all the amination reactions explained above, the formation of a highly reactive Pd^{IV} center seems to be necessary. In many cases, cross-coupling chemistry is controlled by the rate and the scope of the reductive elimination step.[119] In general, Pd-catalyzed C–N and C–O bond formations are challenging to develop because these complexes tend to be reluctant to undergo the reductive

[117] Wang, C.; Chen, C.; Zhang, J.; Han, J.; Wang, Q.; Guo, K.; Liu, P.; Guan, M.; Yao, Y.; Zhao, Y. *Angew. Chem. Int. Ed.* **2014**, *53*, 9884.
[118] Ye, X.; He, Z.; Ahmed, T.; Weise, K.; Akhmedov, N. G.; Petersen, J. L.; Shi, X. *Chem. Sci.* **2013**, *4*, 3712.
[119] Hartwig, J. F. *Inorg. Chem.* **2007**, *46*, 1936.

elimination step.[120] Accordingly, the formation of a highly reactive Pd^{IV} intermediate, which is prone to undergo a facile reductive elimination step, could enhance the cyclization process. Moreover, the formation of a very stable five-membered ring could also act as a driving force of the reaction.

With the aim to set the basis for further discoveries in the field, Hoarau and co-workers performed mechanistic studies on the synthesis of indoline compounds from NH_2-bound cyclopalladated natural phenylalanine (Scheme 49).[121] After careful screening of the reaction conditions, they concluded that the complex **XXVII** could undergo the reductive elimination to render the corresponding indoline in the presence of K_2CO_3 at 100 ºC. The nature of the counterion and phosphine ligand profoundly affected the kinetics of the reaction. The energetically favored carbonate-assisted N–H activation prior to the reductive elimination event was demonstrated by DFT studies.

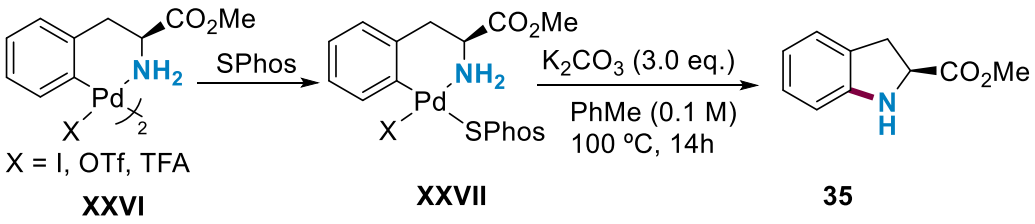

Scheme 49. Mechanistic studies carried out by Horau and co-workers.

3.1.7. C–Heteroatom Bond-Forming Processes with Phe

In continuation with their studies on triflamide-directed C–H functionalization reactions, Yu and co-workers developed a novel procedure for the acetoxylation of various arylethylamines using $MeCOOO^tBu$ as the stoichiometric oxidant and Ac_2O as the promoter (Scheme 50).[122] Interestingly, the synthetic scope includes a few examples of Phe and Tyr derivatives. In these specific cases, the use of high amounts of DMF was found to be necessary to achieve high yields

[120] Hartwig, J. F. *Acc. Chem. Res.* **1998**, *31*, 852.
[121] Jacquin-Labarre, A.; Coufourier, S.; Tamion, R.; Le Foll, A.; Levacher, V.; Afonso, C.; Gandon, V.; Journot, G.; Brière, J.-F.; Hoarau, C. *Organometallics* **2020**, *39*, 767.
[122] Vickers, C. J.; Mei, T.-S.; Yu, J.-Q. *Org. Lett.* **2010**, *12*, 2511.

presumably due to its tendency to act as a labile ligand and consequently stabilize the transient intermediates. The reaction proceeded under mild reaction conditions and was compatible with a wide range of different functional groups. Importantly, the corresponding products were converted to indoline derivatives under previously developed reaction conditions.[111] More recently, Sharma and co-workers developed a protocol for the chalcogenation of Phe derivatives using a PA auxiliary.[123]

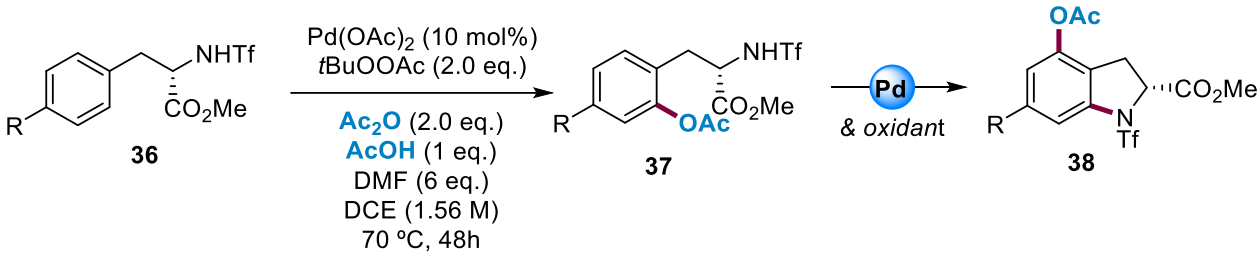

Scheme 50. Acetoxylation of arylethylamines developed by Yu.

The introduction of boronic esters into the structure of α-amino carbonyl compounds could be considered of great interest due to their synthetic versatility within the field of cross-coupling chemistry. In 2010, James and co-workers described an elegant Ir-catalyzed C–H borylation of substituted phenylalanine derivatives (Scheme 51).[124] Unfortunately, the reaction was found to be quite sensitive to the steric effects caused by the substitution pattern of the aromatic ring and only the *meta*-substituted Phe derivatives underwent the borylation process with high levels of regioselectivity. In addition, Ir complexes are known to be expensive and have high toxicity. As an alternative, a complementary strategy for *ortho*-C(sp^2)–H borylation of PA-Phe-OMe derivatives was developed by Shi and co-workers.[125] This reaction features the use of mild reaction conditions as well as the employment of palladium as catalyst, PA as DG and oxygen as terminal oxidant.

[123] Bag, R.; Sharma, N. K. *Org. Chem. Front.* **2023**, Advance article.
[124] Meyer, F.-M.; Liras, S.; Guzman-Perez, A.; Perreault, C.; Bian, J.; James, K. *Org. Lett.* **2010**, *12*, 3870.
[125] Zhang, L.-S.; Chen, G.; Wang, X.; Guo, Q.-Y.; Zhang, X.-S.; Pan, F.; Chen, K.; Shi, Z.-J. *Angew. Chem. Int. Ed.* **2014**, *53*, 3899.

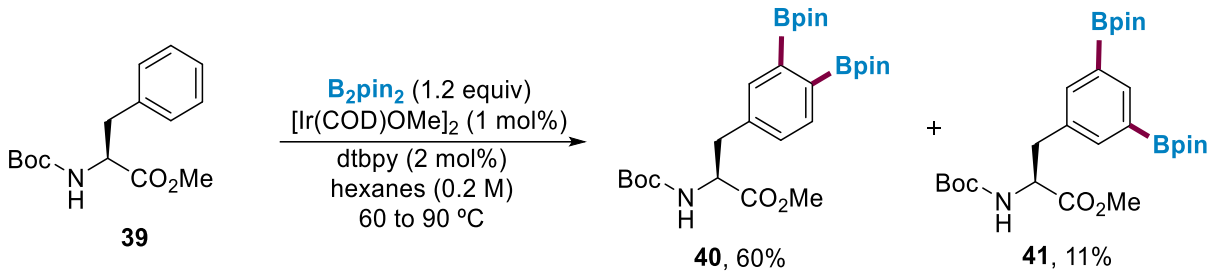

Scheme 51. Iridium-catalyzed C–H borylation of Phe.

Regarding the halogenation of Phe derivatives, the existing methodologies could be divided into two general approaches. On the one hand, the group of Yu[91] and Correa[106] demonstrated the feasibility of using palladium catalysis for the C–H iodination, chlorination and bromination of triflamide and picolinamide protected Phe derivatives, respectively (Scheme 52). A similar approach featuring the use of the native free amine as the DG has been also reported.[126] On the other hand, Barluenga[127] demonstrated that iodination reaction could be also performed under metal-free reaction conditions. Nevertheless, this approach led to mixtures of *ortho*- and *para*-iodinated compounds.

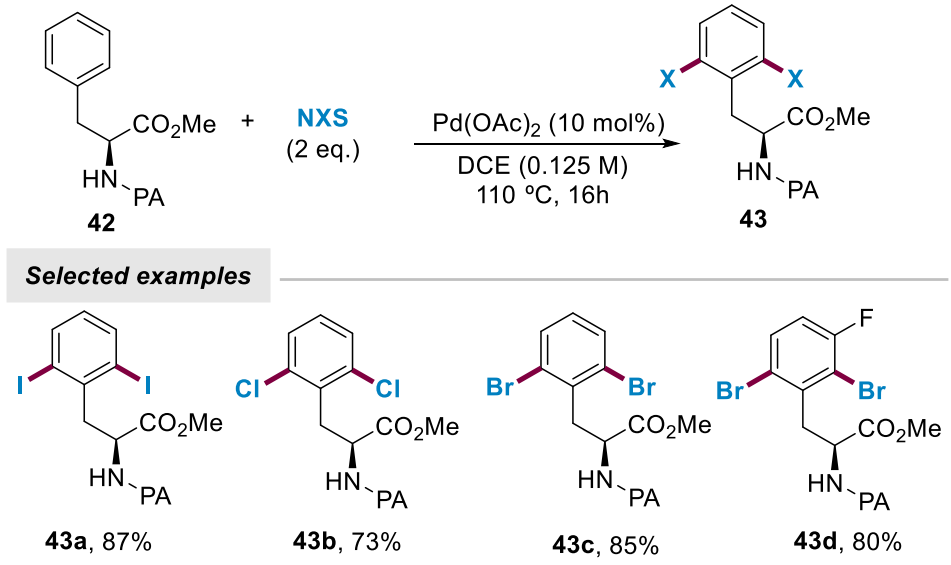

Scheme 52. C–H halogenation protocol developed by Correa and co-workers.

[126] Ville, A.; Annibaletto, J.; Coufourier, S.; Hoarau, C.; Tamion, R.; Journot, G.; Schneider, C.; Brière, J.-F. *Chem. Eur. J.* **2021**, *27*, 13961.
[127] Barluenga, J.; Álvarez-Gutierrez, J. M.; Ballesteros, A.; González, J. M. *Angew. Chem. Int. Ed.* **2007**, *46*, 1281.

3.1.8. C(sp^2)–H Carbonylation Reactions of Phe Derivatives with CO

Despite its toxicity, carbon monoxide is a cheap, abundant and very versatile feedstock in organic synthesis, being the precursor of a wide variety of functional groups such as aldehydes, ketones, esters, carbamates, ureas and carboxylic acids, among others. Although the bond dissociation energy of CO is the strongest chemical bond known, the synergistic interaction of the σ donation of the HOMO molecular orbital of CO to a suitable atomic orbital of a metal, and the π back donation from a metal atom to the LUMO orbital of CO stabilize the M-CO bond, thereby resulting in the activation of C≡O bond. Nowadays, carbonylation reactions catalyzed by heavy metals such as Pd, Ru, Rh and Ir as well as by first-row transition metals are known.[128] Among all the strategies developed in the field, the oxidative C–H carbonylation reactions can be considered as one of the most efficient synthetic methods since they allow the direct synthesis of ketone derivatives using readily available and simple starting materials (Scheme 53).[129] From a mechanistic point of view, generally these reactions start with the formation of an organometallic complex **XXVIII** through a Pd^{II}-catalyzed C–H activation step. The coordination of CO followed by the insertion to the metal center would form an acyl-Pd complex **XXX**, which could be attacked by different nucleophiles via a ligand exchange. The latter species (**XXXI**) could undergo a reductive elimination step, thereby releasing the product **45** and liberating a Pd^0 complex, which could be oxidized to Pd^{II} with the aid of a suitable oxidant.

[128]a) Peng, J.-B.; Geng, H.-Q.; Wu, X.-F. *Chem* **2019**, 5, 523. b) Wu, X.-F.; Fang, X.; Wu, L. Jackstell, R.; Neumann, H. Beller, M. *Acc. Chem. Res.* **2014**, *47*, 1041. c) Wu, X.-F.; Neumann, H. *ChemCatChem* **2012**, *4*, 447.
[129] a) Liu, Y.; Chen, Y.-H.; Yi, H.; Lei, A. *ACS Catal.* **2022**, *12*, 7470. b) Zhu, C.; Liu, J.; Li, M.-B.; Bäckvall, J.-E. *Chem. Soc. Rev.* **2020**, *49*, 341.

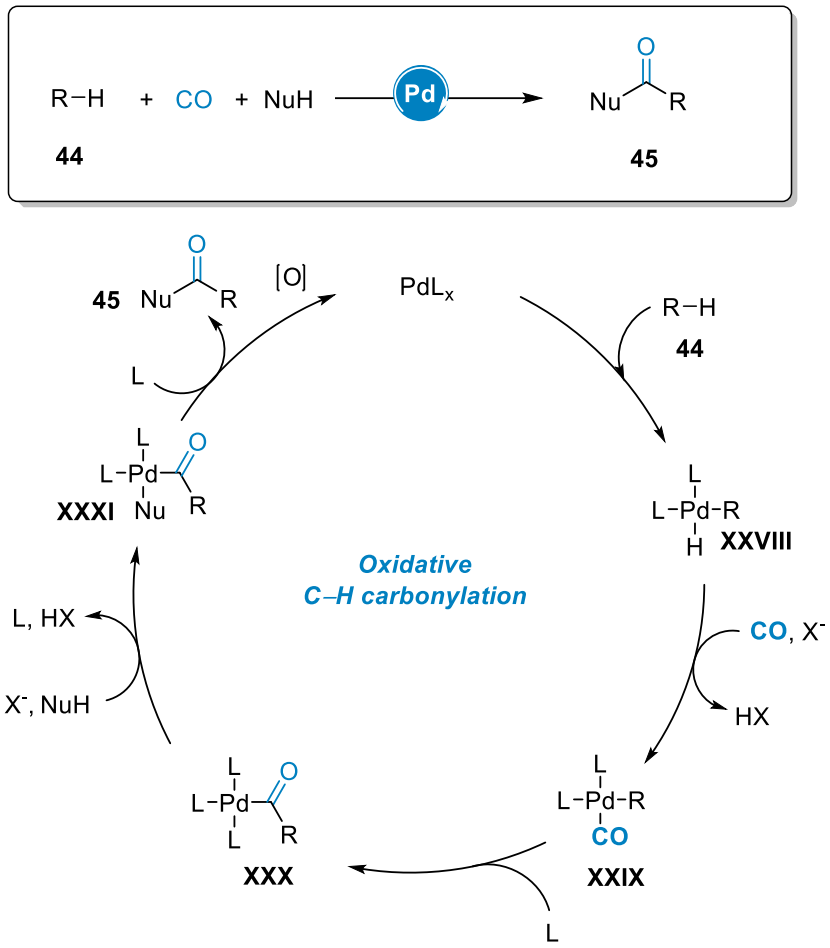

Scheme 53. A general example of an oxidative C–H carbonylation reaction.

In the particular case of amino acids and peptides, C(sp^2)–H carbonylation reactions with CO have been much less explored compared to other protocols which have been previously described along this chapter. In 2007, Vicente and co-workers reported for the first time the selective carbonylation of simple L-phenylalanine by mixing the previously prepared chloride-bridged dinuclear *ortho*-palladacycle **XXXII** with gaseous CO monoxide (Scheme 54).[130] Under the optimal reaction conditions, they were able to prepare the tetrahydroisoquinoline derivative **47** at room temperature. In addition, they also synthesized the mononuclear *ortho*-palladacycle **48** by treating the complex **XXXII** with NaBr and the corresponding pyridine ligand. NMR and X-ray diffraction analysis revealed a distorted-square-planar structure in which the amino acid ligand showed a boat

[130] Vicente, J.; Saura-Llamas, I.; García-López, J.-I.; Calmuschi-Cula, B. *Organometallics* **2007**, *26*, 2776.

conformation. Although this study does not rationalize the experimental observations of this specific type of reactions, the isolation of the complexes and the elucidation of their structure is a key finding for the better understanding of the reaction mechanisms as well as for the development of future research in the field.

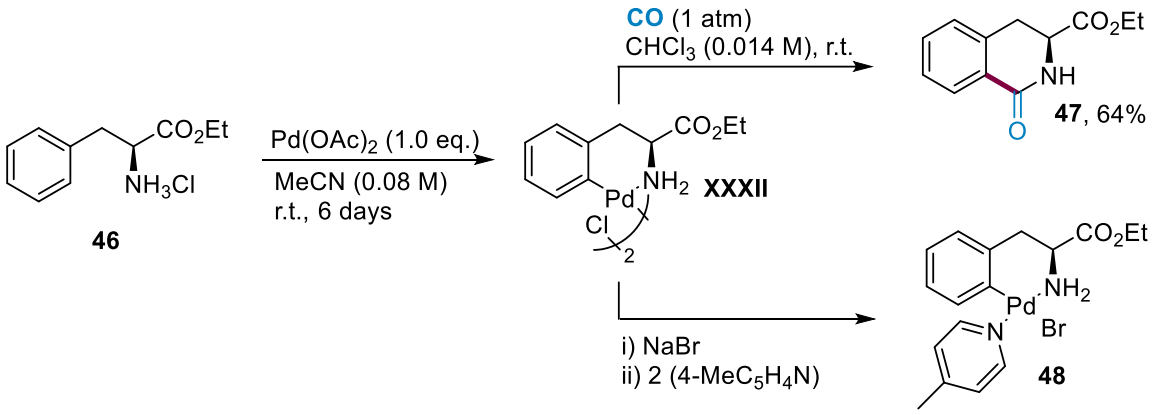

Scheme 54. Carbonylation of simple Phe units reported by Vicente and co-workers.

Later on, Granell and co-workers also published the carbonylation of arylethylamine derivatives in which the functionalization of a single phenylalanine methyl ester unit was included (Scheme 55).[131] However, the reaction seemed to be very sensitive to the steric hindrance in α-position and the best results were obtained using quaternary α-amino ester derivatives. The performance of various experiments showed that in the case of α-aryl substituted Phe units, even if 5-membered and 6-membered palladacycles were in equilibrium, the latter could react faster with CO towards the selective formation of 6-membered benzolactam. Indeed, the employment of unsubstituted Phe units rendered a mixture of the desired benzolactam and the undesired acetamide almost in a 1:1 ratio. Consequently, this protocol is not suitable for the functionalization of natural Phe units.

[131] López, B.; Rodriguez, A.; Santos, D.; Albert, J.; Ariza, X.; García, J.; Granell, J. *Chem. Commun.* **2011**, *47*, 1054.

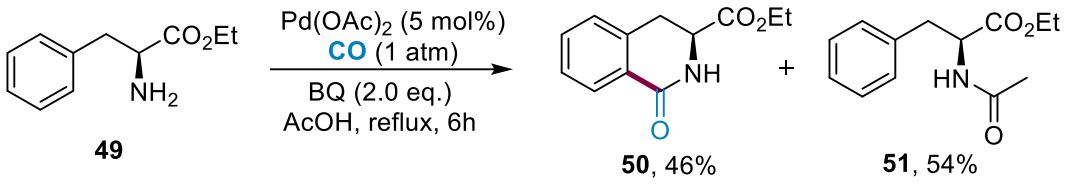

Scheme 55. Direct synthesis of benzolactams under oxidative conditions.

More recently, the group of Grigorjeva reported an efficient method for the selective carbonylation of Phe derivatives using PA as traceless directing group (Scheme 56).[132] Importantly, short peptides could be functionalized as well, albeit partial racemization occurred within the process. The reaction was found to be very sensitive towards the catalyst loading, which was attributed to the coordination of the released 2-picolinic acid to the metal center. Interestingly, they did not observe the formation of indole or indoline byproducts resulting from an intramolecular amination process. Control experiments with radical traps supported the formation of an enamine intermediate upon radical elemental steps. It is noteworthy that the formation of the enamine would be in concordance with the unexplained lack of reactivity of α-quaternary Phe derivatives. On the other hand, some of the intermediates were isolated and characterized. On the basis of these results and previous literature reports,[133] they proposed a plausible reaction mechanism. Initially, the imine intermediate **XXXIII** would be formed with the aid of the catalyst under oxidative conditions. Next, the latter could coordinate with the Co^{II} and *in situ* form Co^{III} intermediate **XXXIV**, which could undergo the C–H activation event forming the metallacycle **XXXV**. Finally, the insertion of CO followed by the reductive elimination step would deliver the desired product and release the active Co^{III} catalyst.

[132] Lukasevics, L.; Cizikovs, A.; Grigorjeva, L. *Org. Lett.* **2021**, *23*, 2748.
[133] For selected examples, see: a) Ni, J.; Li, J.; Fan, Z.; Zhang, A. *Org. Lett.* **2016**, *18*, 5960. b) Barsu, N.; Bolli, S. K.; Sundararaju, B. *Chem. Sci.* **2017**, *8*, 2431. c) Landge, V. G.; Jaiswal, G.; Balaraman, E. *Org. Lett.* **2016**, *18*, 812.

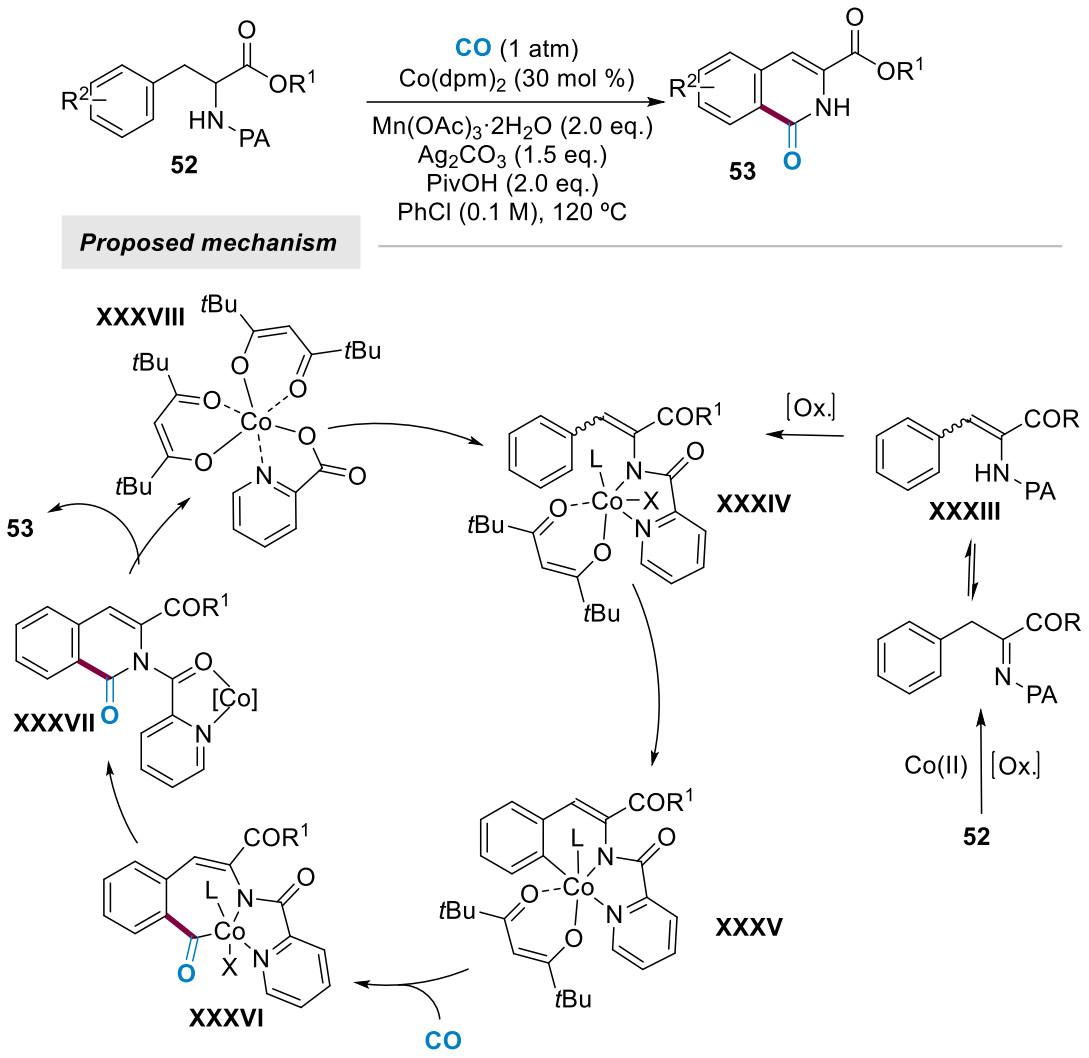

Scheme 56. Co-catalyzed C(sp^2)–H carbonylation of short peptides with gaseous CO.

In this context, the site-selective appendance of versatile ester motifs within a Phe setting still remains unexplored and hence the development of a late-stage carbonylation reaction of Phe compounds would open up new vistas in this burgeoning field.

3.1.9. Ester Synthesis via Transition Metal Catalysis

Over the last decades, transition metal-catalyzed alkoxycarbonylation reactions have gained considerable attention due to their versatility to synthesize functionalized compounds in a

straightforward manner. The continuous development of different variants of these reactions provides efficient alternatives to the conventional synthetic routes and hence expands the synthetic scope on laboratory and industrial scale. In particular, esters are widespread functional groups in natural compounds and are widely used in organic chemistry and biologic materials as well as in material science. Traditionally, esters have been generated by condensation of an alcohol and a carboxylic acid under acidic or basic conditions. Even so, the preparation of the starting materials requires multi-step protocols and could not be tolerant toward specific functionalities. Over the last decades, several complementary strategies have been developed to overcome those limitations. Although Tishchenko reaction[134] and oxidative esterification of aldehydes[135] are among these methodologies, their limited scope and generation of byproducts can limit their applications. In contrast, transition metal-catalyzed C–H alkoxycarbonylation reactions have drawn considerable attention since they enable the assembly of ester skeletons in a single-step and atom-economical manner. These methodologies could be classified in two main groups depending on the type of C–H bond and on the reactivity modes: 1) Direct alkoxycarbonylation using gaseous CO and alcohols or with other CO surrogates or via 2) aldehydic or formate C–H activation (Scheme 57).

[134] Seki, T.; Nakajo, T.; Onaka, M. *Chem. Lett.* **2006**, *35*, 824.
[135] a) Tang, S.; Yuan, J.; Liu, C.; Lei, A. *Dalton Trans.* **2014**, *43*, 13460. b) Miyamura, H.; Kobayashi, S. *Acc. Chem. Res.* **2014**, *47*, 1054.

1) Direct C–H alkoxycarbonylation with CO or their surrogates

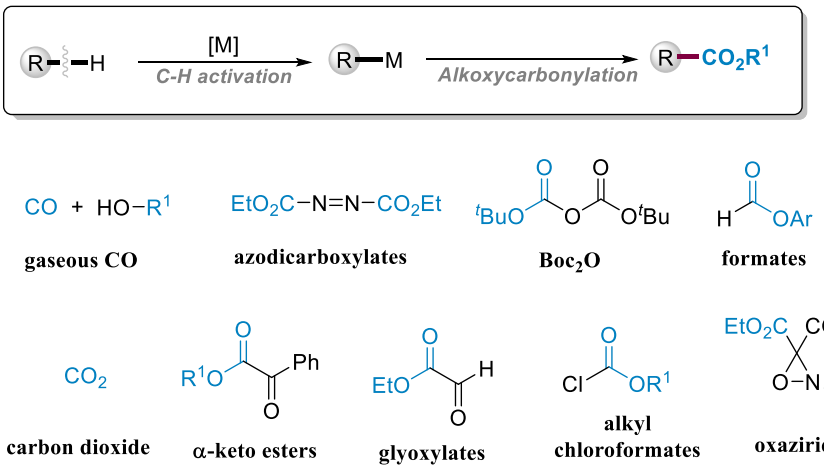

2) Aldehidic C–H activation and addition to C=C or C=O double bonds

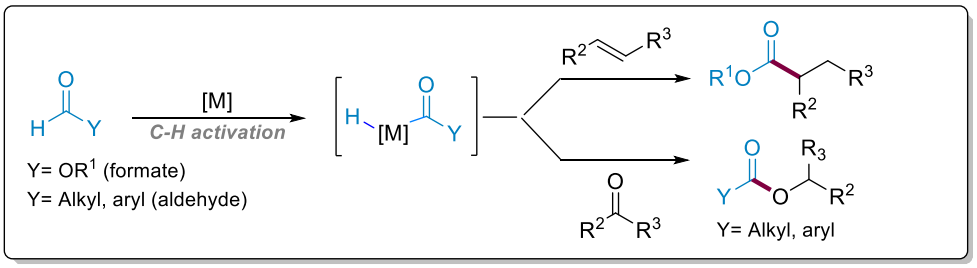

Scheme 57. Transition metal-catalyzed ester synthesis via C–H activation.

Generally, the first type of reactions imply the activation of C(sp^2)–H or C(sp^3)–H bonds through transition metal catalysis to form an organometallic species followed by the alkoxycarbonylation step. Depending on the alkoxycarbonylating reagent, the second step can also be a radical process. Conversely, the second type of reactions involve the cleavage of an aldehydic C–H bond to form a metal hydride, which is prone to react with C–C or C–O double bonds. In the following section, alkoxycarbonylation reactions will be only discussed.

3.1.9.1. C(sp^2)–H Alkoxycarbonylation Reactions with Alkyl Chloroformates

The use of alkyl chloroformates for the synthesis of aromatic esters via traditional methods such as Friedel-Crafts reaction has been limited due to the rapid decarboxylation of the required

reagents. The first study of a metal-catalyzed coupling of alkyl chloroformates via C–H bond cleavage was published in 2009 by the group of Kakiuchi (Scheme 58).[136] The authors proposed a Ru^{II}/Ru^{IV} catalytic cycle in which potassium carbonate could facilitate the initial proton abstraction. Although this seminal study opened new opportunities and expanded the landscape of transition metal catalysis, the reaction proceeded with moderate yields, the synthetic scope was limited to a few and structurally simple 2-arylpyridines and the pyridyl directing group could not be removed.

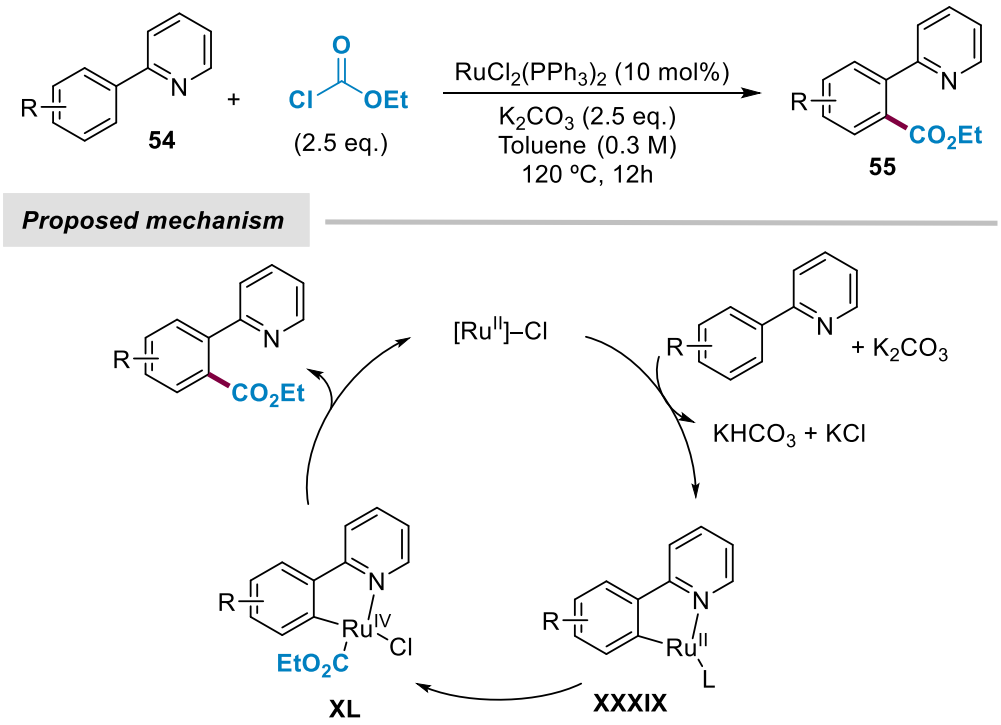

Scheme 58. First Ru-catalyzed C–H alkoxycarbonylation with alkyl chloroformates.

Inspired by the pioneering example mentioned above, Shi and co-workers developed a Pd-catalyzed method for the synthesis of phthalic acid derivatives with alkyl chloroformates as CO surrogates (Scheme 59a).[137] Whereas the reaction provided very good yields with different solvents, it was quite sensitive to the amount and the nature of the oxidant. This elegant method was found scalable and besides alkoxycarbonylation of β-C(sp^2)–H bonds, γ-C(sp^2)–H

[136] Kochi, T.; Urano, S.; Seki, H.; Mizushima, E.; Sato, M.; Kakiuchi, F. *J. Am. Chem. Soc.* **2009**, *131*, 2792.
[137] Liao, G.; Chen, H.-M.; Shi, B.-F. *Chem. Commun.* **2018**, *54*, 10859.

alkoxycarbonylation could also be achieved. Furthermore, the DG was easily removable, giving access to phthalamides, 1,2-dibenzyl alcohols and phthalic acid esters.

Two years later, a complementary and efficient method to functionalize 1-napththylamines via Pd catalysis was reported by Wu and co-workers (Scheme 59b).[138] Contrary to the above-mentioned works and based on some mechanistic experiments, they proposed the generation of a Pd^{III} intermediate within the catalytic cycle. Curiously, they suggested that radical species could be formed and the addition of the alkyl chloroformate to the Pd center seemed to proceed via a radical process.

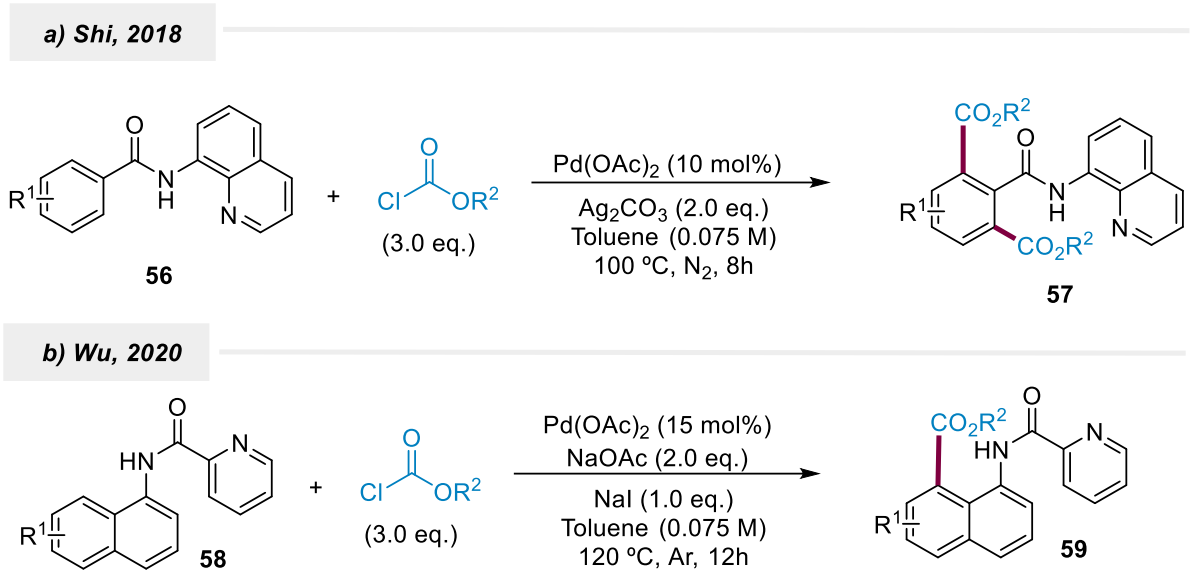

Scheme 59. C–H alkoxycarbonylation of naphthyl and phthalic acid derivatives.

Despite the synthetic versatility of these methods, all of them were applied to simple molecules, mostly *ortho*-substituted arenes to block a competitive difunctionalization event. Indeed, the application of this type of reactivity to more complex amino acid or peptide-like molecules, which have sensitive functional groups as well as multiple amide bonds within their structure is not a trivial task.

[138] Shi, Y.; Yang, F.; Wu, Y. *Org. Biomol. Chem.* **2020**, *18*, 4628.

In 2016, Shi and co-workers designed an elegant and stereoselective C(sp^3)–H alkoxycarbonylation of aliphatic carboxamides bearing 8-aminoquinoline as DG under palladium catalysis.[139] It is noteworthy that the carbonylation reactions were limited to the functionalization of methyl C(sp^3)–H bonds,[140] whereas the parent carbonylation of sterically more hindered methylene C(sp^3)–H bonds remained unexplored.[141]

As a proof of concept, they compared the carbonylation with CO via a Pd^{II}/Pd^0 regime with the alkoxycarbonylation via a Pd^{II}/Pd^{IV} catalytic cycle to find out whether the latter could offer a different platform for the reaction development (Scheme 60). They began synthesizing the previously known palladacycle **XLI** treating the phenylalanine derivative **60a** with stoichiometric amounts of $Pd(OAc)_2$ in MeCN. On the one hand, when they treated this complex with CO under various reaction conditions, the desired product was not obtained. However, the coordination of CO to yield complex **XLIII** was confirmed by its characteristic infrared absorption. In view of these results, they concluded that the carbonylation via a Pd^{II}/Pd^0 catalytic cycle was unfeasible due to the difficulty of CO migratory insertion and subsequent reductive elimination.[142] Conversely, they speculated that the formation of a high-valent Pd^{IV} intermediate (**XLII**) via oxidative addition of alkyl chloroformates could be an alternative for the formation of the suitable intermediate and hence obtain the corresponding ester derivatives.[143] When they treated the same complex with alkyl chloroformates in the presence of Ag_2CO_3, the desired products were obtained.

[139] Gang, L.; Yin, X.-S.; Chen, K.; Zhang, Q.; Zhang, S.-Q.; Shi, B.-F. *Nat. Commun.* **2016**, *7*, 12901.
[140] a) Yoo, E.; Masa, M.; Yu, J.-Q. *J. Am. Chem. Soc.* **2010**, *132*, 17378. b) McNally, A.; Haffemayer, B.; Collins, B. S. L.; Gaunt, M. J. *Nature* **2014**, *510*, 129. c) Li, S.; Chen, G.; Feng, C. J.; Gong, W.; Yu, J.-Q. *J. Am. Chem. Soc.* **2014**, *136*, 5267.
[141] a) Xie, P.; Xie, Y.; Qian B.; Zhou, H.; Xian, C.; Huang, H. *J. Am. Chem. Soc*. **2012**, *134*, 9902. b) Xie, P.; Xia, C.; Huang, H. *Org. Lett.* **2013**, *15*, 3370.
[142] a) Barnard, C. F. *Organometallics* **2008**, *27*, 5402. b) Brennfuhrer, A.; Neumann, H.; Beller, M. *Angew. Chem. Int. Ed.* **2009**, *48*, 4114.
[143] a) Topczewski, J.; Sanford, M. S. *Chem. Sci.* **2014**, *6*, 70. b) Hickman, A. J.; Sanford, M. S. *Nature* **2012**, *484*, 177.

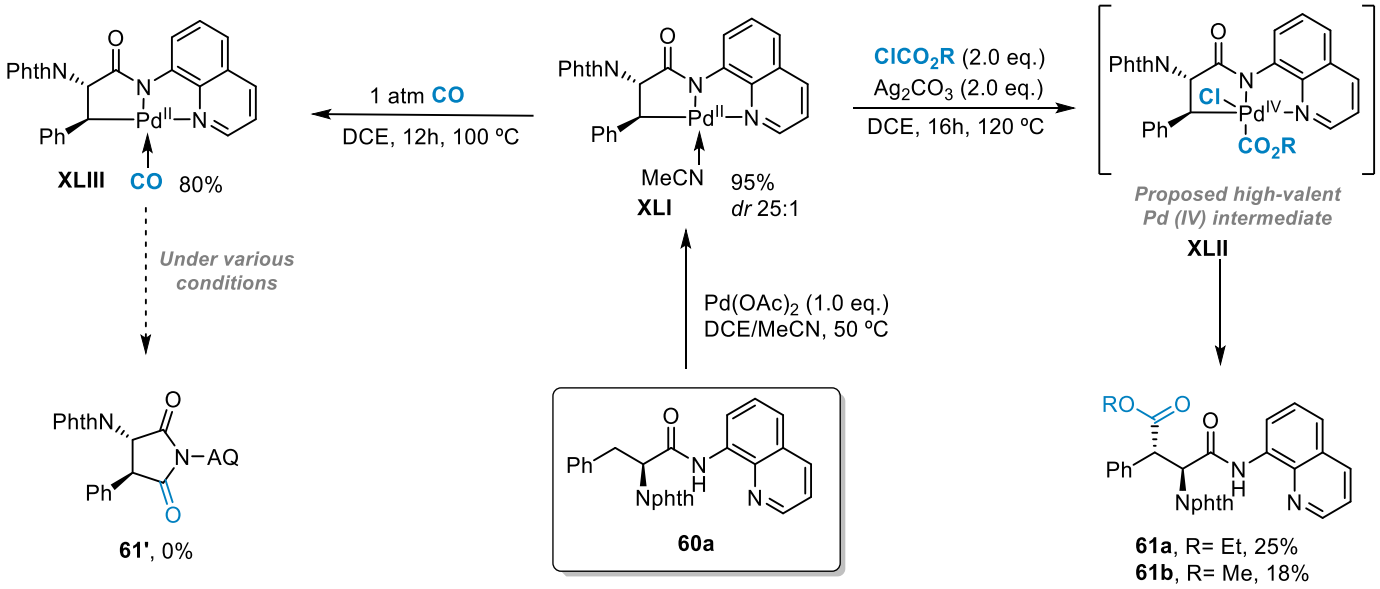

Scheme 60. Control experiments carried out with CO monoxide and various alkyl chloroformates.

After a careful examination of the reaction parameters, they found that using $Pd(OAc)_2$ as catalyst, 2.0 equivalents of Ag_2CO_3 and I_2 as additive a variety of Phe derivatives underwent the alkoxycarbonylation at the benzylic position through the formation of a five-membered metallacycle. Under these conditions, a broad range of alkyl chloroformates were also found compatible with this protocol (Scheme 61). It should be noted that the reaction was quite sensitive to the amount of silver carbonate. All attempts to reduce the Ag_2CO_3 loading resulted in the inhibition of the reaction, forming variable amounts of undesired β-lactam through a competitive C–N reductive elimination. This method was found to be scalable and the DG could be removed under mild reaction conditions avoiding racemization during the process.

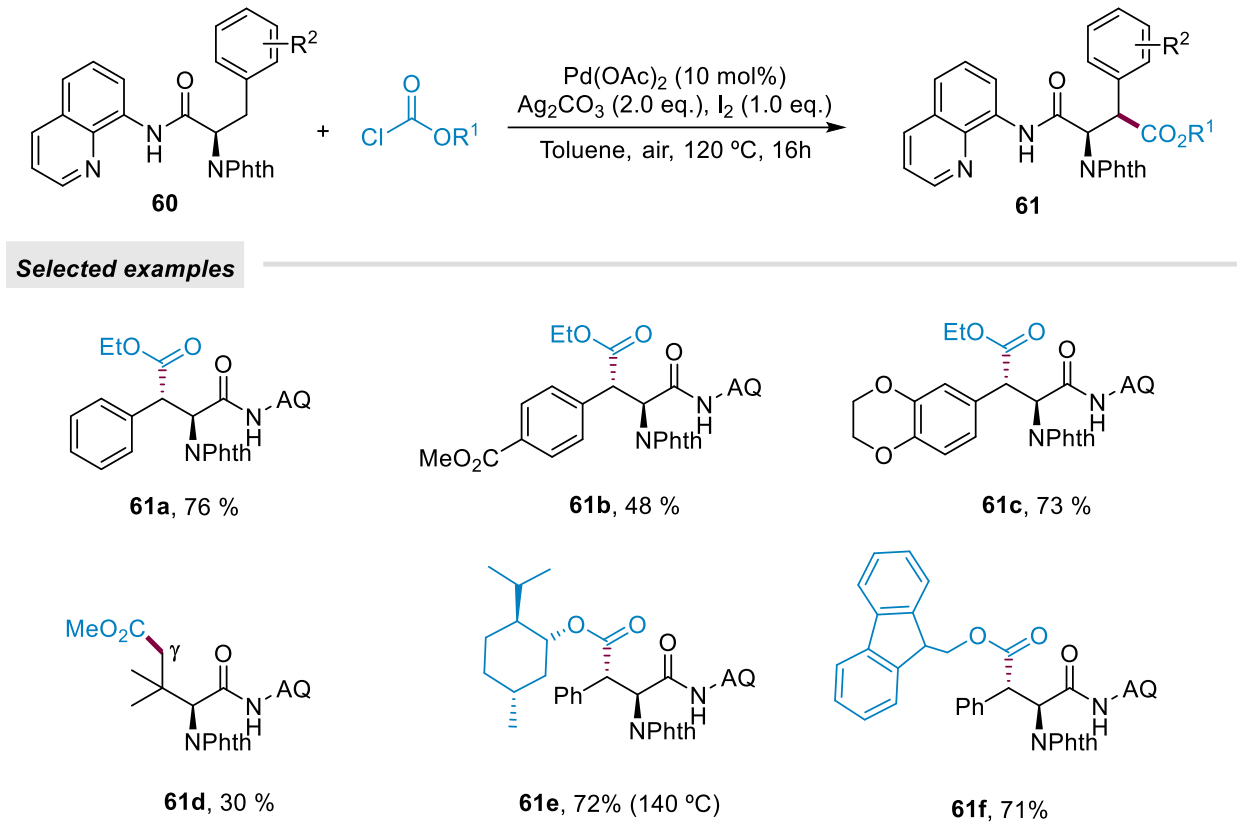

Scheme 61. Synthetic scope of alkoxycarbonylation reaction of Phe derivatives developed by Shi.

To gain more insight about the reaction mechanism, some control experiments were carried out. First, they performed KIE experiments and found a secondary kinetic isotope effect, which suggested that the cleavage of the C–H bond would not be the rate determining step of the reaction. Then, when they submitted the presynthesized complex **XLI** to the standard conditions and in the absence of Ag_2CO_3 the undesired β-lactam was formed selectively, indicating that the addition of the silver salt was crucial for the process to occur. The authors suggested that this effect could be due to its halide scavenger ability as well as to the possible formation of Pd-Ag bimetallic complexes.[144]

[144] a) Calleja, J.; Pla, D.; Gorman, T. W.; Domingo, V.; Haffemayer, D.; Gaunt, M. J. *Nat. Chem.* **2015**, *7*, 1009. b) Kozitsyna, N. Y.; Nefedov, S. E.; Klyagina, A. P.; Markov, A.; Dobrokhotova, Zh. V.; Velikodny, Y. A.; Kochubey, D.; Zyubina, T. S.; Gekhman, A. E.; Vargaftik, M.; Moiseev, I. I. *Inorg. Chim. Acta.* **2011**, *370*, 382.

3.2. Objective

Despite the abundance and low-price of carbon monoxide, its use could be inconvenient due to its flammability and toxicity, which make it difficult to handle and store, turning the carbonylation processes relatively hazardous. In contrast, the use of CO surrogates such as alkyl chloroformates could offer new vias to synthesize unprecedented ester derivatives in a safer, atom-economical and operationally simple manner since they are readily available compounds with high structural diversity. To date, only two detailed studies of the carbonylation of Phe residues were known: the synthesis of 1-oxo-1,2-dihydroisoquinolines described by Grigorjeva[132] and the above mentioned β-C(sp^3)–H functionalization developed by Shi.[139] The absence of protocols for the δ-C(sp^2)-H alkoxycarbonylation of Phe derivatives encouraged us to explore the feasibility of using alkyl chloroformates for the introduction of ester groups within the aromatic side-chain of this specific amino acid residue.

Inspired by the results of Shi,[139] we envisioned a complementary strategy for the δ-functionalization of Phe derivatives upon the formation of a more challenging six-membered palladacycle. For this purpose, we anticipated that the installation of the bidentate picolinamide directing group at the *N*-terminus would enable the formation of the suitable intermediate, which could further react with the corresponding alkyl chloroformates to form the corresponding highly reactive Pd^{IV} species (Scheme 62).

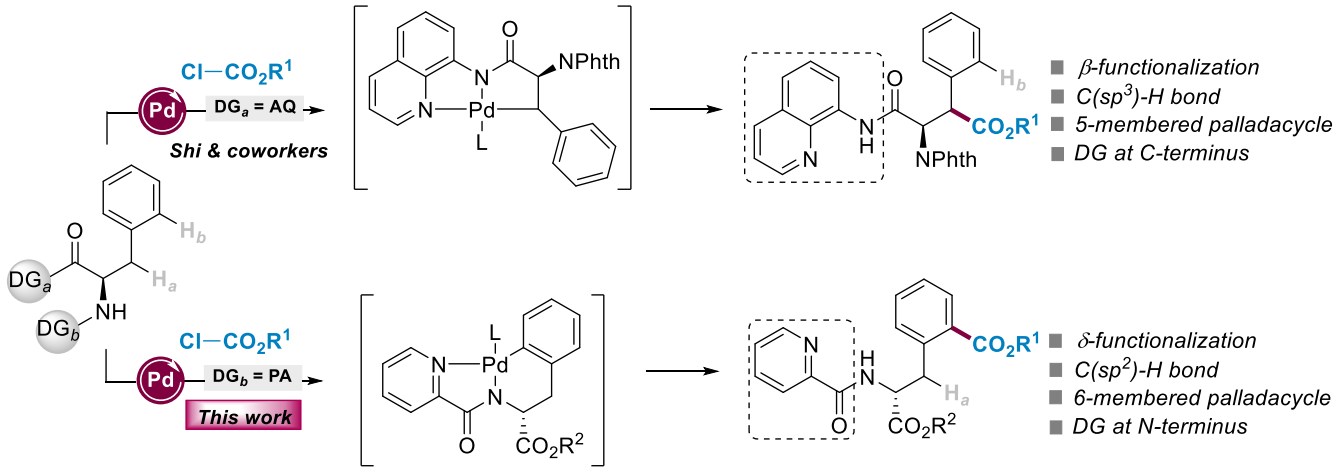

Scheme 62. Comparison between the protocol developed by Shi and our project.

With these considerations in mind, for this project we established the following objectives:

- To develop a novel and site-selective C(sp^2)–H process for the derivatization of Phe residues
- To apply the developed protocol to more complex peptide sequences
- To achieve a racemization-free and scalable transformation
- To gain more information about the reaction mechanism upon DFT studies

3.3. Pd-Catalyzed C(sp^2)–H Alkoxycarbonylation of Phenethyl and Benzylamines with Chloroformates as CO Surrogates

3.3.1. Optimization process

We began our study by using picolinamide protected derivative PA-Phe-OMe (**62a**) and $ClCO_2Et$ as counterpart. This DG has shown great abilities in palladium catalysis for the C–H diversification of α-amino carbonyl compounds[79,87,88,93,99,106,113,132,138] and consequently we envisioned that it could be a suitable DG for the development of an alkoxycarbonylation protocol. First, the most widely used $Pd(OAc)_2$ was selected as catalyst along with three equivalents of $ClCO_2Et$. This reaction involves very different type of substances: lipophilic reactants, metal complexes and inorganic additives. For the correct dissolution of organic species and most of the inorganic bases, polar aprotic solvents are usually more appropriate. In our case, dioxane was chosen as the model solvent. On the other hand, high temperatures were established assuming that the formation of the transient intermediate would be energetically demanding. Under these conditions, several bases were tested (Table 5). Inorganic bases could help to enhance the C–H activation as well as act as a neutralizing agent for the released hydrochloric acid. Unfortunately, under these reaction conditions the alkoxycarbonylation reaction did not work. Instead, except AgOAc and Li*O*t*Bu* (Table 5, entries 2 and 8), all other bases resulted in the formation of the corresponding carboxylic acid upon ester hydrolysis.

Table 5. Screening of bases[a]

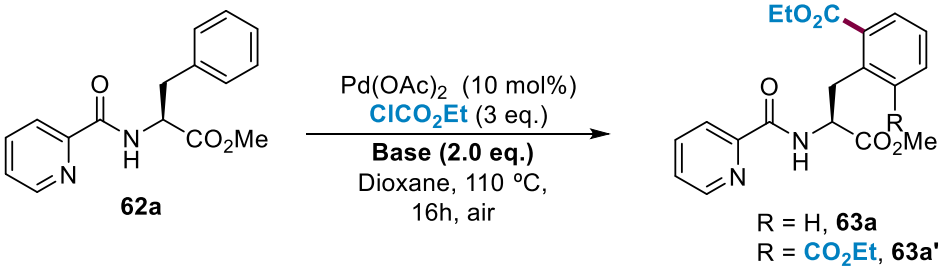

Entry	Base	Yield (%)
1	Ag_2CO_3	0
2	AgOAc	0
3	K_2CO_3	0
4	K_3PO_4	0
5	Cs_2CO_3	0
6	KH_2PO_4	0
7	$NaHCO_3$	0
8	Li*O*tBu	0

[a] Reaction conditions: **62a** (0.25 mmol), $ClCO_2Et$ (3 eq.), Base (2.0 eq.), $Pd(OAc)_2$ (10 mol%), dioxane (1 mL), 110 ºC, 16h, under air.

In order to avoid the hydrolysis of the ester group, different solvents were tested. It is well-known that solvents often allow for thermodynamic and kinetic control over a chemical reaction and hence they could inhibit or induce the generation of different side products. In this case, Ag_2CO_3 was chosen as the base due to its tendency to improve the reactivity and avoid side reactions on previously reported similar alkoxycarbonylation protocols.[139] When polar solvents such as DMF, DMSO and DMA (Table 6, entries 2,3 and 4) were used, the starting material remained unreactive. This could be due to the saturation of the coordination sphere of the metal complex, since these solvents can act as Lewis bases and donate electrons to the metal center. Other solvents delivered a complex mixture of the hydrolyzed carboxylic acid and small amounts of the *N*-alkoxycarbonylated byproduct (Table 6, entries 1, 5, 6 and 7). In striking contrast, *t*-amylOH exhibited a distinct reactivity profile and enabled the process to occur delivering alkoxycarbonylated product **63a** in a promising 24% yield (Table 6, entry 8).

Table 6. Screening of solvents[a]

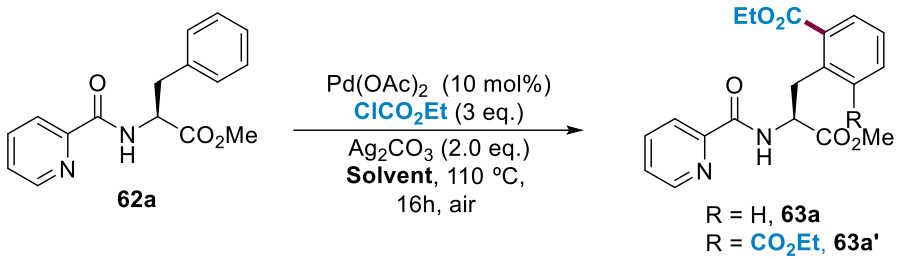

Entry	Solvent	Yield (%)[b]
1	DCE	0
2	DMF	0
3	DMA	0
4	DMSO	0
5	Toluene	0
6	PhCl	0
7	MeCN	0
8	*t*-amylOH	24

[a] Reaction conditions: **62a** (0.25 mmol), $ClCO_2Et$ (3 eq.), Ag_2CO_3 (2.0 eq.), $Pd(OAc)_2$ (10 mol%), solvent (1 mL), 110 ºC, 16h, under air. [b] Isolated yield after column chromatography.

Owing to their halide scavenger ability as well as to their tendency to form heterobimetallic complexes with palladium catalysts,[145,107a,107c] we decided to investigate if other silver salts could enhance the reactivity and improve the reaction yield. Accordingly, we decided to combine the commonly used Na_2CO_3 with different silver salts to test whether the synergistic effect of the two species could be even more beneficial. We were pleased to find that under these reaction conditions, with Ag_2CO_3 and AgOAc the yield was slightly improved (Table 7, entries 1 and 2). Although AgOAc showed the highest yield, the reaction also afforded a great number of unidentified byproducts and the starting material was almost consumed within the process. In contrast, when silver carbonate was used the reaction was cleaner and we decided to continue the

[145] Yang, Y.-F.; Cheng, G.-J.; Liu, P.; Leow, D.; Sun, T.-Y.; Chen, P.; Zhang, X.; Yu, J.-Q.; Wu, Y.-D.; Houk, K. N. *J. Am. Chem. Soc.* **2014**, *136*, 344.

optimization process with the latter species. Even so, the higher reactivity resulted in mixtures of mono- and difunctionalized products **63a** and **63a'**, respectively, which revealed that regioselectivity issues would come into play along our optimization process.

Table 7. Screening of silver salts[a]

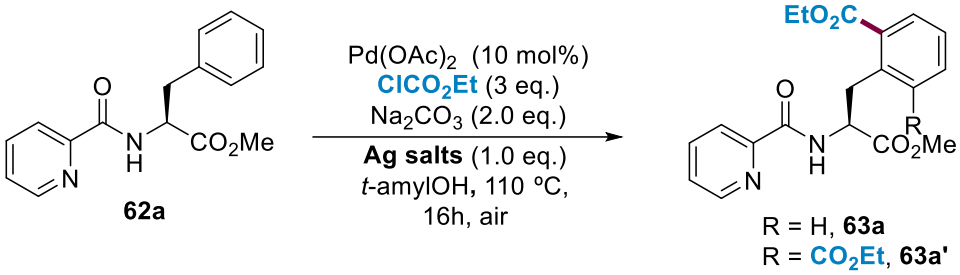

Entry	Ag salts	Yield (%)[b,c]
1	AgOAc	48 (65:35)
2	Ag_2CO_3	30 (40:60)
3	AgOTf	0
4	AgTFA	Degradation
5	AgF	Traces
6	AgCl	Traces
7	$AgNO_3$	Traces
8	AgI	Traces

[a] Reaction conditions: **62a** (0.25 mmol), $ClCO_2Et$ (3 eq.), Ag salts (1.0 eq.), Na_2CO_3 (2.0 eq.), $Pd(OAc)_2$ (10 mol%), *t*-amylOH (1 mL), 110 ºC, 16h, under air. [b] Isolated yield after column chromatography. [c] Ratio of mono- and disubstituted products **63a:63a'**

It is well-known that iodide ions could react via ligand exchange with organopalladium complexes to form $(L)_nPd$-I species, which are more prone to undergo a reductive elimination event and hence improve the reactivity of the corresponding intermediates.[146] Moreover, in order to raise the reaction temperature and after a careful examination of other co-solvents, PhCl was added to the

[146] Maitlis, P. M.; Haynes, A.; James, B. R.; Catellani, M.; Chiusoli, G. P. *Dalton Trans.* **2004**, *21*, 3409.

reaction mixture. Accordingly, we decided to investigate the influence of different I sources. To our delight, when LiI was used the yield was significantly improved (Table 8, entry 2). Other I sources such as KI, I_2 and MgI_2 gave lower yields (Table 8, entries 4, 5 and 7).

Table 8. Screening of iodide additives[a]

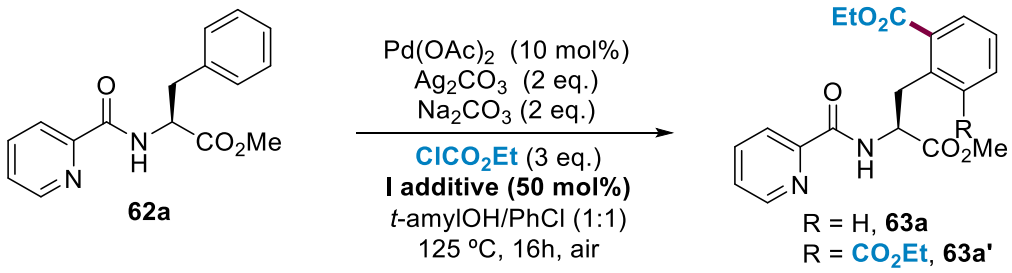

Entry	I additive	Yield (%)[b,c]
1	none	30 (40:60)
2	LiI	69 (37:63)
3	TBAI	0
4	KI	51 (44:56)
5	I_2	58 (33: 67)
6	Me_4NI	0
7	MgI_2	53 (41:59)

[a] Reaction conditions: **62a** (0.25 mmol), $ClCO_2Et$ (3 eq.), Ag_2CO_3 (2 eq.), Na_2CO_3 (2 eq.), LiI (1 eq.), $Pd(OAc)_2$ (10 mol%), *t*-amylOH/PhCl (1:1) (1.5 mL), 125 ºC, 16h, under air. [b] Isolated yield after column chromatography. [c] Ratio of mono- and disubstituted products **63a:63a'**

In order to improve the selectivity of the process toward the mono-alkoxycarbonylation, the influence of the amount of all reagents and coupling partners was evaluated. Whereas the reaction was quite sensitive towards the amount of Ag_2CO_3 and Na_2CO_3 (Table 9, entries 3 and 4), by increasing the amount of chloroformate equivalents the yield remained intact (Table 9, entries 5 and 6). However, the use of 2 mL of solvent slightly improved the yield. This could be due to the improved solubility of all the inorganic compounds that were employed (Table 9, entry 2).

Table 9. Screening of equivalents[a]

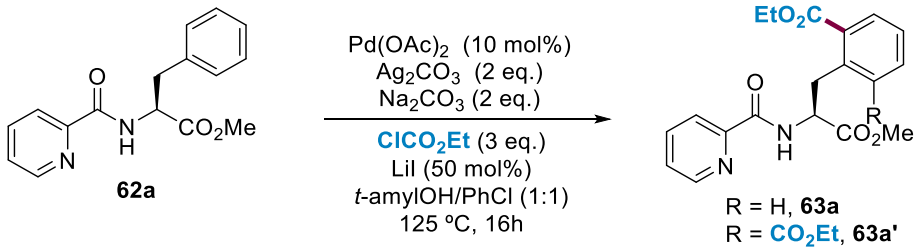

Entry	Variation from standard conditions	Yield (%)[b,c]
1	none	69 (37:63)
2	solvent (2 mL)	75 (36:64)
3	Na_2CO_3 (1 eq.)	64 (44:56)
4	Ag_2CO_3 (1 eq.)	58 (36:64)
5	$ClCO_2Et$ (4 eq.)	74 (34:66)
6	$ClCO_2Et$ (3 eq.)	75 (36:64)

[a] Reaction conditions: **62a** (0.25 mmol), $ClCO_2Et$ (3 eq.), Ag_2CO_3 (2 eq.), Na_2CO_3 (2 eq.), LiI (1 eq.), $Pd(OAc)_2$ (10 mol%), *t*-amylOH/PhCl (1:1) (2 mL), 125 ºC, 16h. [b] Isolated yield after column chromatography. [c] Ratio of mono- and disubstituted products **63a:63a'**

Further screening of the dilution effect and the ratio of solvents revealed that besides the reaction yield, the selectivity of the process was strongly affected by the solvent ratio. On the one hand, when *t*-amylOH or PhCl were individually used, the reaction proceeded with lower yields (Table 10, entries 1 and 2). On the other hand, by increasing the amount of solvent the formation of the difunctionalized derivative was favoured (Table 10, entries 3 and 4). As mentioned above, this could be due to the better solubility of all inorganic compounds in a higher amount of solvent. Finally, the use of more *t*-amylOH slightly diminished the selectivity of the process (Table 10, entry 5).

Table 10. Screening of dilution effect and solvent ratio[a]

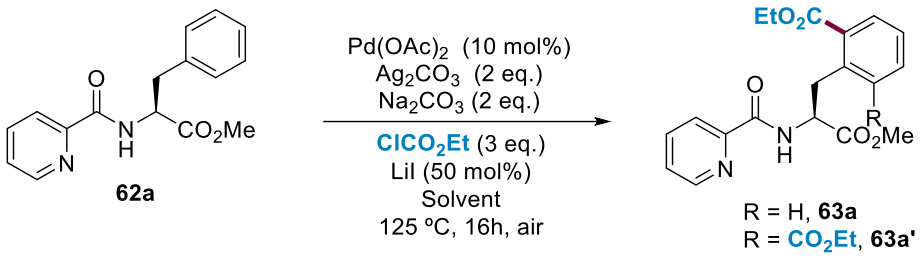

Entry	Solvent	Yield (%)[b,c]
1	PhCl	54 (61:39)[d]
2	*t*-amylOH	46 (60:40)[e]
3	*t*-amylOH/PhCl (1:1) (2 mL)	75 (36:64)
4	*t*-amylOH/PhCl (1:1) (4 mL)	72 (22:78)
5	*t*-amylOH/PhCl (3:1) (2 mL)	71 (44:56)

[a] Reaction conditions: **62a** (0.25 mmol), $ClCO_2Et$ (3 eq.), Ag_2CO_3 (2 eq.), Na_2CO_3 (2 eq.), LiI (1 eq.), $Pd(OAc)_2$ (10 mol%), *t*-amylOH/PhCl (1:1) (2 mL), 125 ºC, 16h, under air. [b] Isolated yield after column chromatography. [c] Ratio of mono- and disubstituted products **63a:63a'**. [d] AgOAc (2 equiv.) was used instead of Ag_2CO_3. [e] The reaction was performed without LiI (50 mol%)

With the optimal reaction conditions in hand, some control experiments were performed (Table 11). As expected, the role of both $Pd(OAc)_2$ as catalyst and Ag_2CO_3 as oxidant was crucial for the process to occur, as not even traces of the product were observed in their absence (Table 11, entries 2 and 4). The reaction could be carried out in the absence of Na_2CO_3 or LiI (Table 11, entries 3 and 5), but lower yields were achieved. It should be noticed that the alkoxycarbonylation reaction could be carried out under air, which represents an advantage on terms of operational simplicity.

Table 11. Control experiments[a]

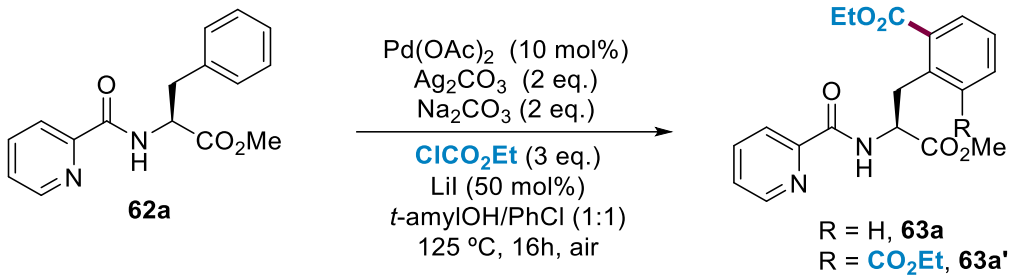

Entry	Variation from standard conditions	Yield (%)[b,c]
1	none	75 (36:64)
2	Without $Pd(OAc)_2$	0
3	Without Na_2CO_3	42 (63:37)
4	Without Ag_2CO_3	0
5	Without LiI	30 (40:60)

[a] Reaction conditions: **62a** (0.25 mmol), $ClCO_2Et$ (3 eq.), Ag_2CO_3 (2 eq.), Na_2CO_3 (2 eq.), LiI (50 mol%), $Pd(OAc)_2$ (10 mol%), *t*-amylOH/PhCl (1:1) (2 mL), 125 ºC, 16h, under air. [b] Isolated yield after column chromatography. [c] Ratio of mono- and di- substituted products **63a:63a'**

Finally, along with picolinamide other DGs were tested (Scheme 63). As expected, other *N*-containing DGs such as a versatile 1,2,3-triazole unit afforded the desired products, albeit with lower yields. Other DGs such as benzoyl and tosyl were found unreactive, demonstrating the essential role of the *N*-chelating heterocycle. Finally, the lack of reactivity of the substrate bearing a the 3-pyridine regioisomer demonstrated the importance of the bidentate coordination for the process to occur.

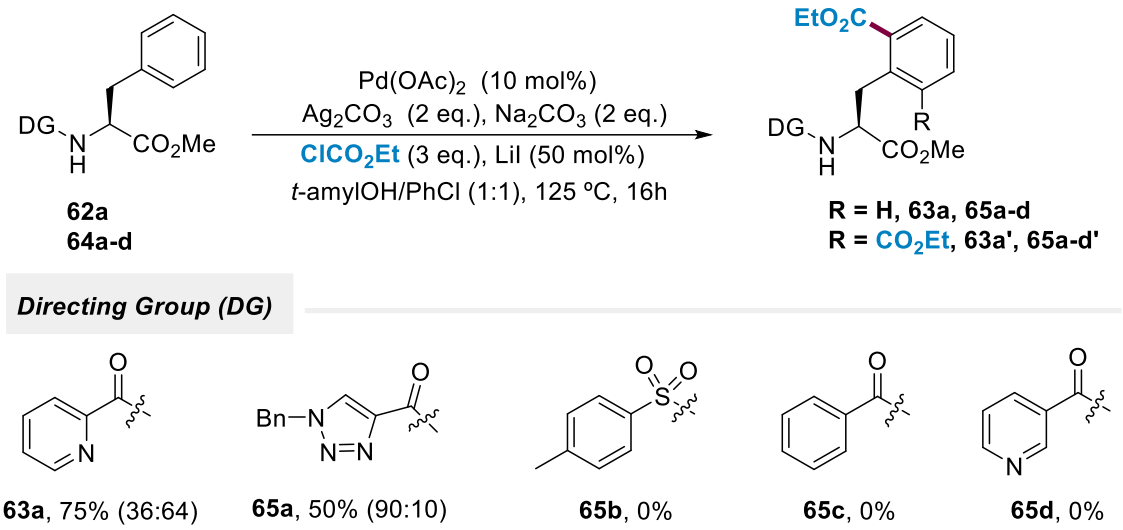

Scheme 63. Screening of different DGs. Ratio of mono- and difunctionalized compounds is depicted in parenthesis.

This optimization study validated our hypothesis and demonstrated that the challenging Pd-catalyzed δ-alkoxycarbonylation of a simple Phe derivative can take place upon chelation assistance of a N-terminal PA. We observed that there was an interplay between reactivity and regioselectivity and in general terms the higher conversion the higher amount of difunctionalized product. Further studies with other Phe derivatives as well as chloroformates would indicate whether a more selective process can happen or this observed trend remains a general issue.

3.3.2. Synthetic Scope

With the optimized reaction conditions in hand, we next investigated the scope of our reaction with different commercially available chloroformates (Scheme 64). Gratifyingly, the model substrate PA-Phe-OMe (**62a**) smoothly underwent the alkoxycarbonylation process with a wide variety of electronically and sterically diverse counterparts. Not only the simplest alkyl chloroformates such as ethyl (**63a**), benzyl (**63d**), and hexadecyl derivatives (**63f'**) but also the structurally more complex 9-fluorenylmethyl (**63h**) and menthyl chloroformates (**63g'**) furnished the corresponding products in moderate to high yields, as a separable mixture of mono- and dialkoxycarbonylated compounds. Remarkably, the reaction between **62a** and ethyl chloroformate

was also performed in 3.5 mmol scale, delivering a separable mixture of compounds **63a:63a'** in 75% yield. In contrast with the alkoxycarbonylation protocols developed by other research groups,[136-139] the challenging phenyl chloroformate (**63e**) was also tolerated, albeit with low yield. Notably, the reaction was tolerant with chloroformates bearing chloro (**63c**) and methoxy (**63b**) groups within the alkyl chain. Intriguingly, the use of menthyl (**63g'**) and hexadecyl chloroformates (**63f'**) resulted in the exclusive formation of dialkoxycarbonylated products. This could be explained by the change on the solubility caused by the large size of the newly introduced alkyl moieties. Importantly, HPLC analysis of the product **63f'** verified that no racemization occurred within the process. Unfortunately, some chloroformates did not afford the desired products. In the case of **66k** and **66j**, the lack of reactivity could be explained by the affinity of the palladium atom to coordinate and react with unsaturated bonds. Regarding chloroformate **66j**, under these highly basic conditions, the formation of an alkene through an E2 elimination should not be discarded. In this case, the cationic species could be stabilized by the ion pair of the adjacent oxygen atom as well as by the secondary nature of the functionalized carbon. This hypothesis could explain why the chloroformate housing a primary alkyl chloride could deliver the product **63c** with good yield. On the other hand, for chloroformate **66i**, although the same elimination pathway can be considered, the reactivity could be affected by the particular electronic and steric properties of such species.

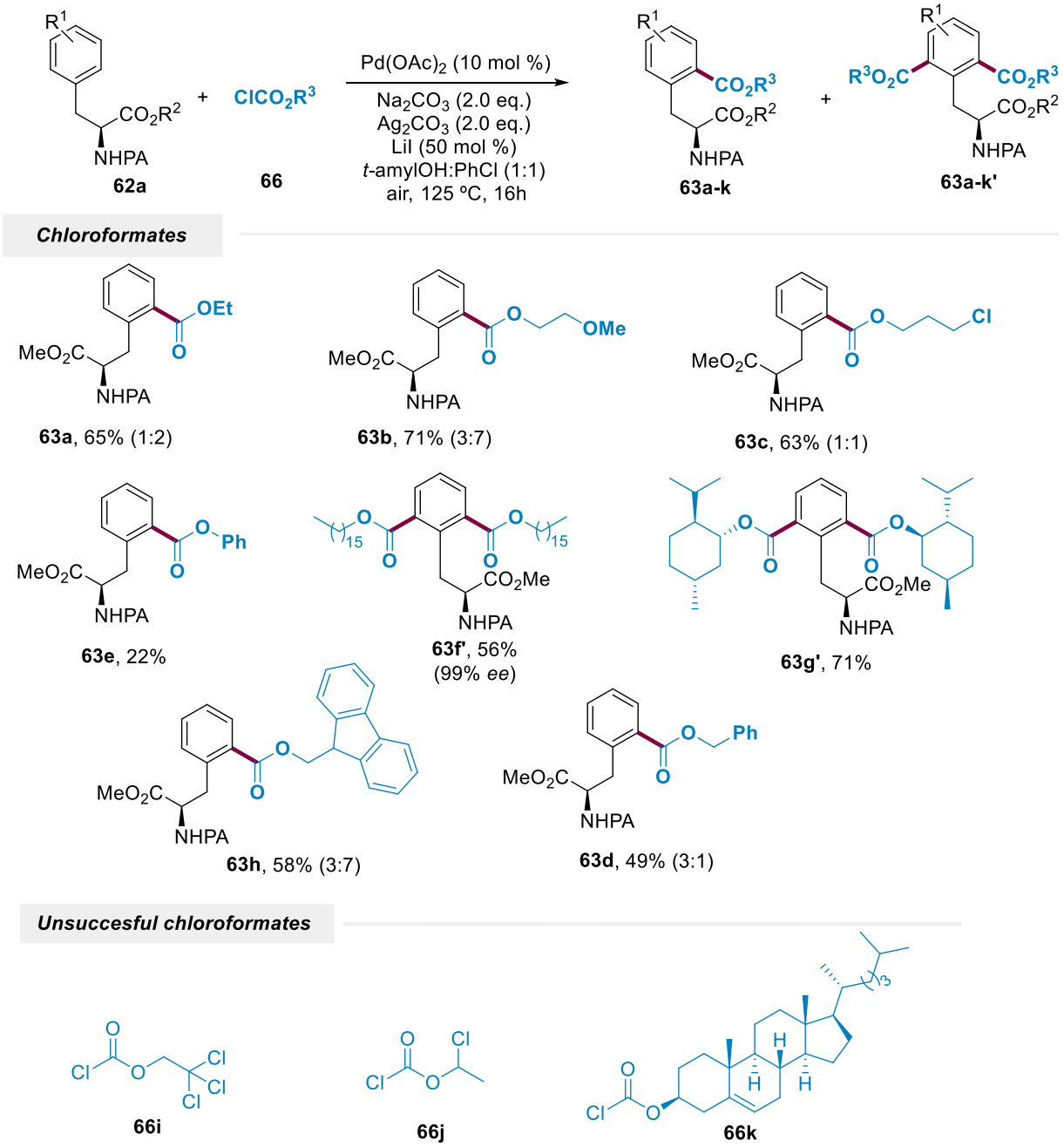

Scheme 64. Scope of alkyl chloroformates. Ratio of mono- and difunctionalized compounds is depicted in parenthesis.

Next, we prepared a collection of Phe derivatives by installation of the required 2-pyridinecarbonyl motif within commercially available Phe compounds or by conventional methods from PA-Phe-OMe. As expected, the use of Phe derivatives bearing *ortho*- or *meta*-substituents within the aromatic ring provided the monoalkoxycarbonylated products in a selective fashion (**63l-n**)

(Scheme 65). In contrast, *para*-substituted Phe derivatives were found to be sensitive towards the electronic nature of the corresponding substituents, resulting in the preferential or exclusive formation of difunctionalized products (**63r-63t**). Remarkably, the method could be also applied to Phe derivatives bearing alkyl nitriles (**63o**) and to those including biologically relevant cyclic ethers (**63p**, **63q**). Unfortunately, unprotected Tyr unit did not undergo the desired alkoxycarbonylation reaction. Instead, the reaction delivered the O-functionalized compound. In the case of *para*-NO_2-containing Phe derivative, a complex mixture of unidentified compounds was observed (**63t**). Moreover, X-ray analysis verified the structure of the product **63r'** (Figure 17).

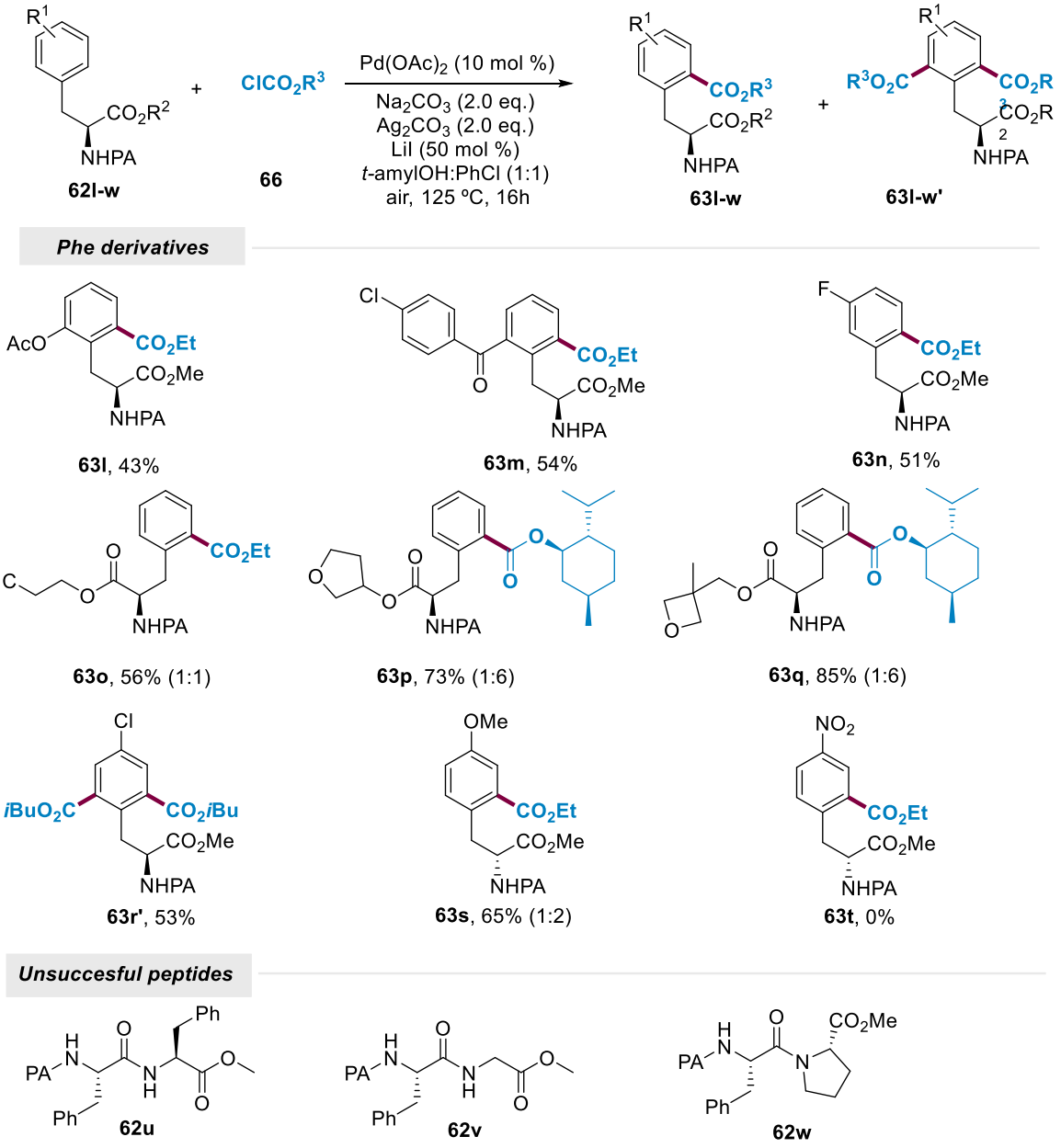

Scheme 65. Scope of Phe derivatives. Ratio of mono- and difunctionalized compounds is depicted in parenthesis.

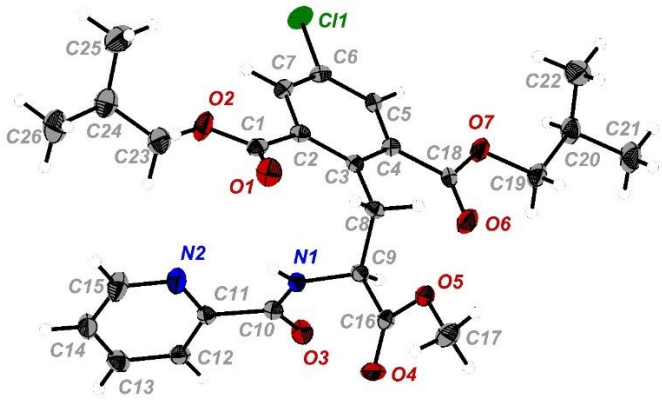

*Figure 17. X-Ray of compound **63r'**.*

Aimed by the absence of reports regarding the alkoxycarbonylation of more complex molecules, we decided to apply this protocol to challenging peptide sequences. We submitted various PA-protected Phe dipeptides to the standard reaction conditions. However, PA-Phe-Gly-OMe (**62v**), PA-Phe-Phe-OMe (**62u**) and PA-Phe-Pro-OMe (**62w**) remained unreactive (Scheme 65). We selected dipeptide **62u** for evaluating the process and conducting a careful screening. Unfortunately, although different reaction conditions were tested, only small amounts of the hydrolyzed peptide were detected (Table 12, entry 3).

Table 12. Screening of PA-Phe-Phe-OMe[a]

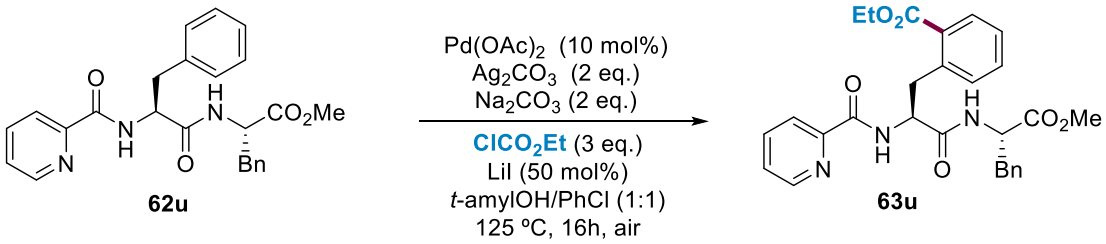

Entry	Variation from standard conditions	Yield (%)
1	none	0[b]
2	*t*-amylOH/Dioxane as solvent	0
3	Dioxane as solvent	0
4	I_2 instead of LiI	0
5	MgI_2 instead of LiI	0
6	$Pd(TFA)_2$ instead of $Pd(OAc)_2$	0

[a] Reaction conditions: **62u** (0.25 mmol), $ClCO_2Et$ (3 eq.), Ag_2CO_3 (2 eq.), Na_2CO_3 (2 eq.), LiI (50 mol%), $Pd(OAc)_2$ (10 mol%), *t*-amylOH/PhCl (1:1) (2 mL), 125 ºC, 16h, under air. [b] 23% of the *N*-alkoxycarbonylated derivative was detected.

Considering that the peptide backbone is often used as an endogenous DG within the field of C–H functionalization,[85,86,94,95,97,116] these results suggested that this lack of reactivity could be attributed to the coordination of the amide bonds to the active catalyst. The involvement of the highly electrophilic Pd^{IV} intermediate could be the origin of the irreversible complexation of the peptide backbone to the metal core. In fact, the scope of the acylation protocol previously developed by our own group,[106] which could proceed via Pd^{III} intermediates, was successfully extended to very complex peptide sequences. Nevertheless, it is noteworthy that in the latter case the reaction proceeded via radical pathway and consequently the two mechanistic scenarios are not entirely comparable. Beside the geometric differences between Pd^{III} and Pd^{IV} complexes,[147] the addition of each electrophile occurs in a different manner (OA *vs* radical addition). The formation of other unexpected intermediates as well as unproductive reaction pathways could not be discarded.

In view of these results and with the aim of expand the synthetic scope of the reaction, a collection of simple benzylamines bearing PA as the DG were tested. The application of the previously optimized reaction conditions did not provide high yields of the corresponding products and all the reaction parameters were reevaluated. For this purpose, we selected compound **67a** as the model substrate. A representative set of experiments are displayed on Table 13. In these cases, we

[147] Mirica, L. M.; Khusnutdinova, J. R. *Coord. Chem. Rev.* **2013**, *257*, 299.

found that I additives were not necessary. Moreover, when using AgOAc instead of Ag_2CO_3 reaction yields were slightly improved. Surprisingly, some control experiments revealed that this reaction can occur even without silver acetate or sodium carbonate, albeit with lower yield (Table 13, entries 3 and 4). Reducing the amount of Ag salts resulted in a significant loss of yield (Table 13, entries 5 and 6).

*Table 13. Control experiments with **67a** [a]*

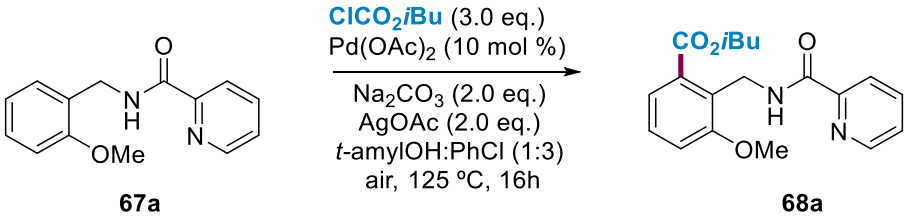

Entry	Variation from standard conditions	Yield (%)[b]
1	none	76
2	Without $Pd(OAc)_2$	0
3	Without Na_2CO_3	54
4	Without AgOAc	21
5	AgOAc (1.0 eq.)	39
6	AgOAc (0.5 eq.)	33

[a] Reaction conditions: **67a** (0.25 mmol), $ClCO_2$*i*Bu (3 eq.), $Pd(OAc)_2$ (10 mol %), AgOAc (2 eq.), Na_2CO_3 (2 eq.), *t*-amylOH/PhCl (1:3) (4 mL), 125 ºC, under air, 16h. [b] Isolated yield after column chromatography.

After modification of the reaction conditions, a wide variety of simple benzyl amines smoothly underwent the monoalkoxycarbonylated process to furnish the corresponding products in moderate to good yields (Scheme 66). In this case, the reactivity of the starting material could be enhanced by the formation of a kinetically more favored 5-membered metallacycle. This method enabled the use of simple benzyl amines with different substitution pattern and electronic properties and therefore complemented the synthetic protocols developed by Shi[139] and Wu[138] (**68a-68g**). Benzyl amines bearing *ortho*- and *meta*-substituents resulted in the exclusive formation of the monofunctionalized product. Likewise, a challenging heterocyclic amine could be selectively

alkoxycarbonylated, albeit in low yields (**68h)**. Moreover, the structure of **68f** was verified by X-ray analysis (Figure 18). Surprisingly, other β-arylethylamines devoid of the ester moiety of Phe provided the desired products (**68i-68k**) with very low yields. We hypothesized that the ester motif of the Phe unit could stabilize the transient intermediates upon a Thorp-Ingold effect. A smilar effect was observed in the carbonylation protocol developed by Grigorjeva and co-workers.[132]

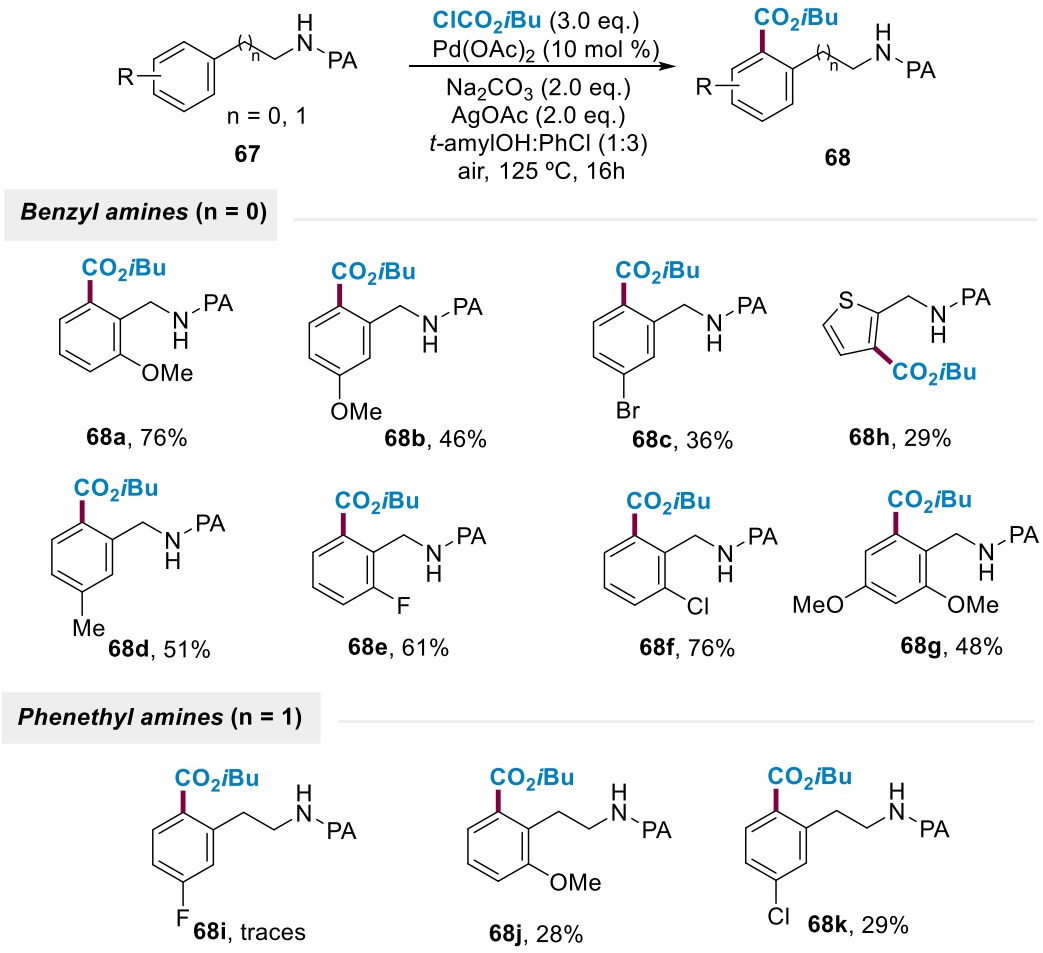

Scheme 66. Scope of benzyl- and phenethyl amines

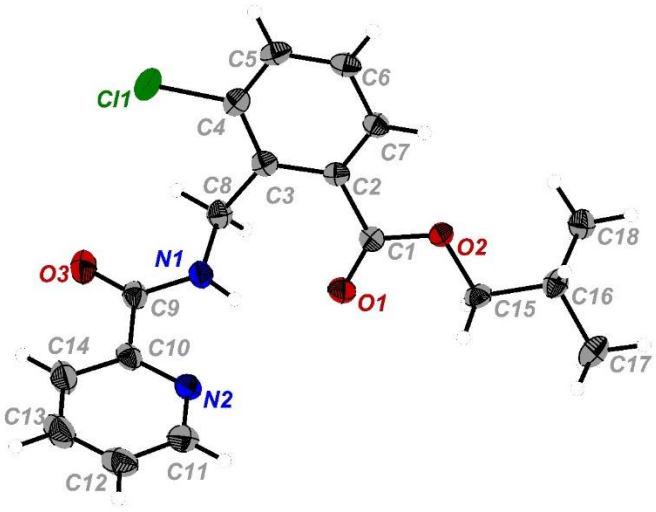

*Figure 18. X-Ray of compound **68f**.*

Unfortunately, although a careful screening of the reaction conditions was carried out with the unsubstituted benzylamine its alkoxycarbonylation did not occur. As depicted on Scheme 66, only substituted benzyl and phenethylamines can react with isobutyl chloroformate in an efficient manner.

In order to demonstrate the versatility of the process, we further explored the cleavage of the required DG. In particular, the treatment of the alkoxycarbonylated products with NaOH along with simultaneous hydrolysis of the ester motif, delivered the corresponding benzolactams upon an intramolecular condensation event in excellent yields (Scheme 67). X-Ray analysis of compound **69b** verified the formation of these heterocyclic cores. This tandem reaction sequence could be considered as an attractive alternative to the Pd-catalyzed carbonylation of alkylamines, which involves the use of toxic and flammable CO gas.[148]

[148] For example, see: a) Zhang, C.; Ding, Y.; Gao, Y.; Li, S.; Li, G. *Org. Lett.* **2018**, *20*, 2595. b) Ling, F.; Ai, C.; Lv, Y.; Zhong, W. *Adv. Synth. Catal.* **2017**, *369*, 3707. c) Haffemayer, B.; Gulias, M.; Gaunt, M. J. *Chem. Sci.* **2011**, *2*, 312.

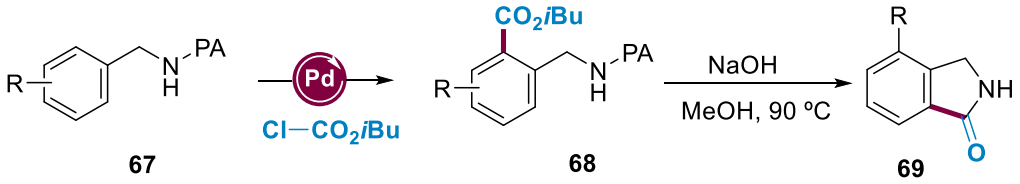

Benzolactams

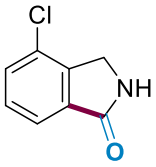

69a, 84%
(from **68f**)

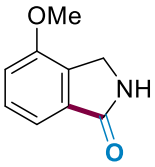

69b, 80%
(from **68a**)

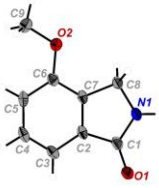

*X-ray of **69b***

Scheme 67. Synthesis of benzolactams.

3.3.3. DFT Studies

In order to understand the reaction mechanism and some of the experimental evidences, DFT studies were carried out for the C(sp^2)–H alkoxycarbonylation of PA-Phe-OMe (**62a**) with $ClCO_2Et$. These calculation were carried out following the methodology described in section 1.4 of Chapter 1. On the basis of related PA-directed Pd-catalyzed C(sp^2)–H functionalization reactions, we proposed the mechanism depicted on Scheme 68. Although the involvement of dimeric species can not be discarded, only monomeric palladium species were considered. Complexation of **62a** with $Pd(OAc)_2$ would initially afford Pd^{II} complex **Int-A**,[106] which would next undergo a directed *ortho*-selective cyclometallation to provide the six-membered palladacyle **IntB**.[95,96] The oxidative addition of the ethyl chloroformate would deliver the corresponding Pd^{IV} **IntC**, which would afford the monocarbonylated product complex **PC-1** through a C–C bond forming reductive elimination. Eventually, **PC-1** could either release product **63a**, thereby recovering the active catalyst or undergo a second functionalization event to yield dialkoxycarbonylated derivative **63a'** (Scheme 68).

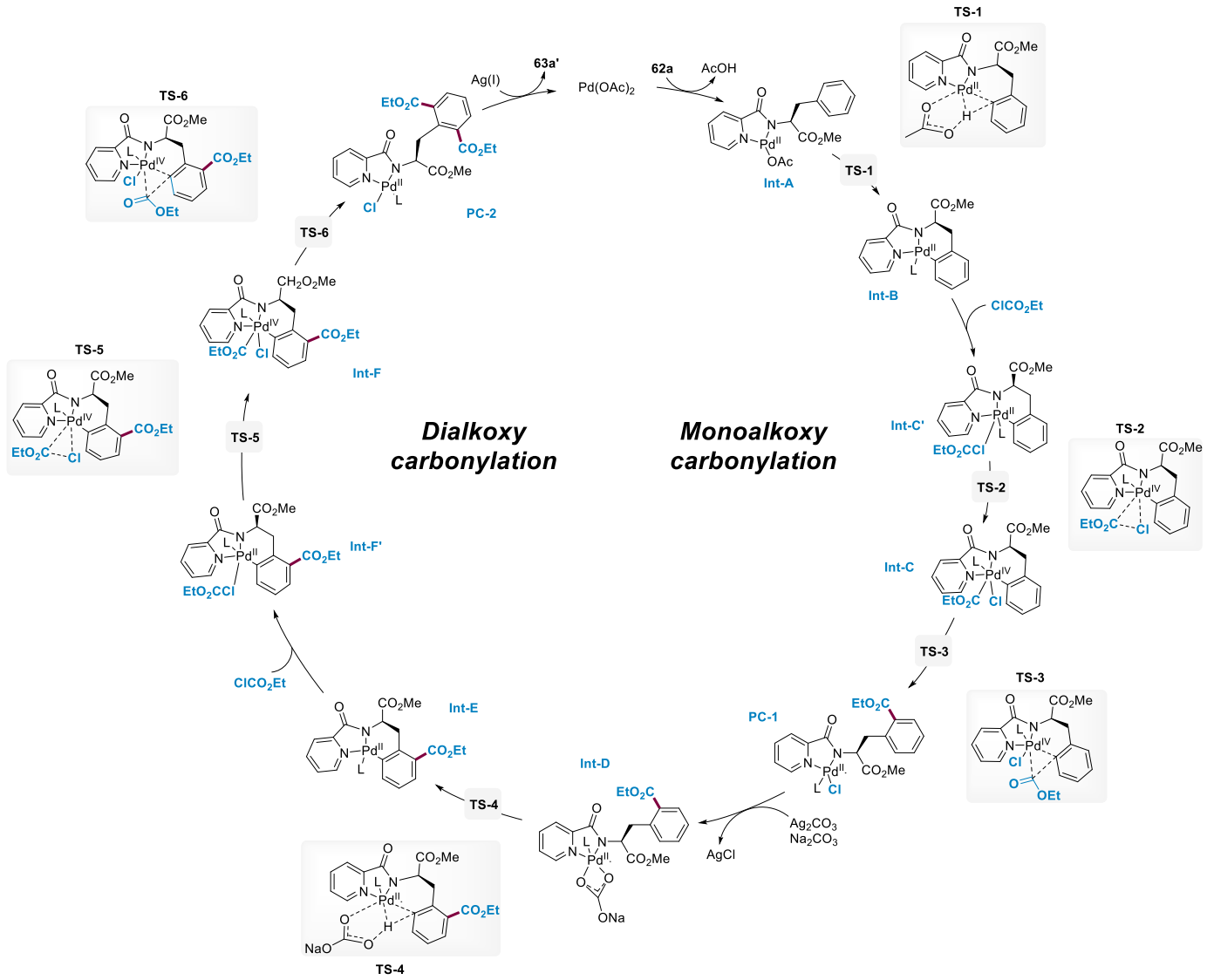

Scheme 68. Catalytic cycle for Pd-catalyzed C(sp^2)–H alkoxycarbonylation of PA-Phe-OMe.

In view of the beneficial effect of using *t*-amylOH as solvent as well as Ag_2CO_3 and LiI as additives, we anticipated that they could have a crucial role in favoring the formation of some of the putative reaction intermediates. We experimentally observed that the nature of the solvent had a profound effect in the reaction rate, yield and selectivity of the process. Indeed, competitive *N*-alkoxycarbonylation (resulting from reductive elimination from **Int-C**) and hydrolysis of the ester group under basic conditions could be inhibited when adding *t*-amylOH to the reaction medium. Accordingly, DFT calculations were undertaken both in the absence and presence of *t*-amylOH molecules in an implicit manner (Figure 19, black and blue reaction pathways, respectively). With the energy values in hand, we can conclude that the reaction pathway when considering *t*-amylOH is energetically more favored and the latter showed a high stabilizing effect through coordination of the alcohol to the metal center and the formation of hydrogen bonds with the ester group of the Phe residue.

As mentioned above, the proposed mechanism would involve three fundamental steps. The first one would consist of the formation of **Int-A** through deprotonation and coordination of substrate **62a** to the initial catalyst, leading to a reactant complex stabilized by -22.5 Kcal/mol with respect to the separated species. The latter would next undergo a C–H activation event to afford **Int-B** through **TS_1**. Although this path could proceed via different mechanisms, we have assumed a CMD pathway wherein the C–H bond activation was assisted by an auxiliary carboxylate/carbonate ion acting as a base, which is often invoked in the directed *ortho*-palladation of aromatic substrates.[149] The optimized structure of the transition state (**TS_1**) reveals an elongation of the C–H bond from 1.08 Å to 1.38 Å and the approximation of the O atom to the H atom ($d_{O–H}$ = 1.34 Å) coupled with the formation of the Pd–C bond ($d_{Pd–C}$ = 2.17 Å). In this case, the C–H activation step would be the rate-limiting step of the catalytic cycle with a barrier of 27.4 Kcal/mol. Intermediate **Int-B** would next coordinate with ethyl chloroformate to deliver **Int-C'** with an energy penalty of 5.2 Kcal/mol. The optimized structure of this intermediate reveals a Pd–C bond length of 2.63 Å. The latter would undergo oxidative addition via a concerted pathway with a barrier of 11.8 kcal/mol to afford thermodynamically favored Pd^{IV} species **Int-C** through **TS_2**. In this three-membered transition state, the Pd–Cl and Pd–C distances are shortened to 2.42 Å and 2.23 Å, respectively, whereas the C–Cl distance is lengthened to 2.02 Å. With the formation of **Int-C** and dissociation

[149] a) Lapointe, D.; Fagnou, K. *Chem. Lett.* **2010**, *39*, 1118; b) García-Cuadrado, D.; Braga, A. A. C.; Maseras, F.; Echavarren, A. M. *J. Am. Chem. Soc.* **2006**, *128*, 1066.

of the C–Cl bond, Pd–Cl and Pd–C distances are shortened and maintained over 1.96 and 2.36 Å, respectively. Although this species has been proposed to exist as both monomeric Pd^{IV} and dimeric Pd^{III} species, we have considered the monomeric form due to its relative stability. Finally, this reactant complex could undergo a reductive elimination with a barrier of 12.9 Kcal/mol via a three-membered transition state **TS_3**, in which the C–C distance is shortened to 2.03 Å and the Pd–C distance is lengthened in 0.11Å, leading to the thermodynamically favored product complex **PC-1** with an energy of -47.4 Kcal/mol. At this point, two possible scenarios could occur: the dissociation of the product complex to provide the monofunctionalized product **63a**, thereby releasing the active Pd^{II} catalyst or a series of ligand exchange reactions to deliver **Int-D**, which could undergo the second C–H functionalization process. It is worth noting that the formation of **Int-D** has been simplified and reduced to a simple one-step reaction. In this regard, despite the fact that the presence of silver carbonate was found indispensable for the process to occur, its actual role cannot be attributed as a mere halide scavenger since heterodimeric Pd–Ag intermediates could be also formed within our catalytic cycle. Some studies carried out by different groups have showed that Pd–Ag complexes are lower in energy than the mononuclear ones.[145] They concluded that the hydrogen atom of the C–H bond that is being activated becomes more protic as compared with the mononuclear species. This is presumably because of the active involvement of silver-bound ligands in the CMD step. Moreover, higher charge concentration over the aryl carbon and enhanced electronic delocalization through de Pd-Ag bridge were also observed.

The formation of the dialkoxycarbonylated product **63a'** would take place following an analogue catalytic cycle featuring C–H functionalization, oxidative addition and reductive elimination steps. The geometries of the transient species are similar to those mentioned in the catalytic cycle toward the monoalkoxycarbonylated compound **63a**. As depicted on Figure 19, the C–H activation event is also the rate-limiting step with an energy barrier of 35.3 Kcal/mol. Moreover, not only the oxidative addition (**TS_5**) and reductive elimination (**TS_6**) steps, with energy barriers of 11.4 and 13.5 Kcal/mol, respectively, but also all the intermediates described are energetically viable. Therefore, the thermodynamically favored product complex **PC-2** would be easily formed at the optimized reaction conditions involving a reaction temperature of 125 ºC. As in the first catalytic cycle, coordination of the transient species with *t*-amylOH led to a more favored reaction pathway (blue *vs* black pathway in Figure 19).

Concerning the key role of LiI within the reaction outcome, we performed some DFT calculations assuming a ligand exchange prior to the reductive elimination step but we did not obtain any significant energy values (Orange pathway in Figure 19). Accordingly, further studies are required to clarify the role of iodide additives as they could accelerate other fundamental steps and, likewise, the intermediacy of iodide bridged Pd dimers could not be entirely discarded.[150]

[150] Zhang, Y.; Chen, Z.-N.; Zhang, X.; Deng, X.; Zhuang, W.; Su, W. *Commun. Chem.* **2020**, *3*, 41.

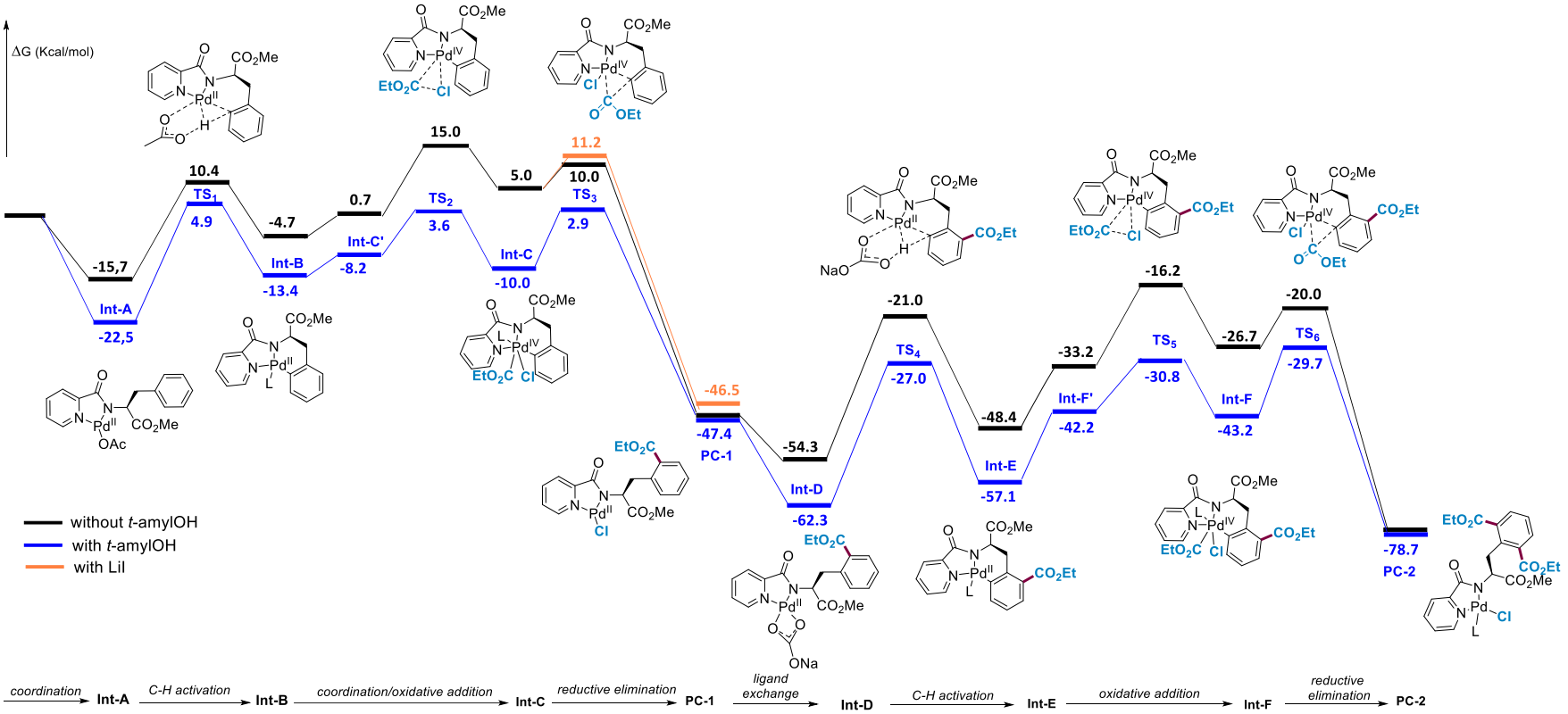

Figure 19. Energy profile for the C–H alkoxycarbonylation of ***62a*** *with* $ClCO_2Et$.

Finally, with the aim to rationalize the experimentally observed lower reactivity of aryl chloroformates and the failure of peptides devoid of the ester motif within our alkoxycarbonylation manifold, some DFT studies were carried out. Surprisingly, the kinetic barriers and the thermodynamic values when using $ClCO_2Ph$ are similar to those obtained with highly reactive $ClCO_2Et$. However, the use of $ClCO_2Ph$ led to the target product **63e** in low yields. Accordingly, we hypothesized that its lower reactivity might be derived from unproductive reaction pathways.

Despite the structural analogy between picolinamide protected phenylalanine **62a** and dipeptide PA-Phe-Gly-OMe (**62v**), all attempts to obtain the alkoxycarbonylated product were unsuccessful. With the aim to rationalize these experimental observations, computational studies with PA-Phe-Gly-OMe (**62v**) as the model substrate were undertaken. As depicted on Scheme 69, the nitrogen atom of the peptide backbone could also coordinate to the palladium center, thereby resulting in a distinct reaction intermediate that could eventually undergo oxidative addition of $ClCO_2Et$ instead of the desired C(sp^2)–H carbonylation reaction. In fact, although the C–H alkoxycarbonylation reaction is thermodynamically and kinetically viable, small amounts of *N*-alkoxycarbonylated product were often obtained instead of the desired product. Some control experiments revealed that the Pd catalyst may participate in the formation of the *N*-alkoxycarbonylated product. Therefore, an alternative reaction pathway was considered in order to rationalize the experimental results (Scheme 70).

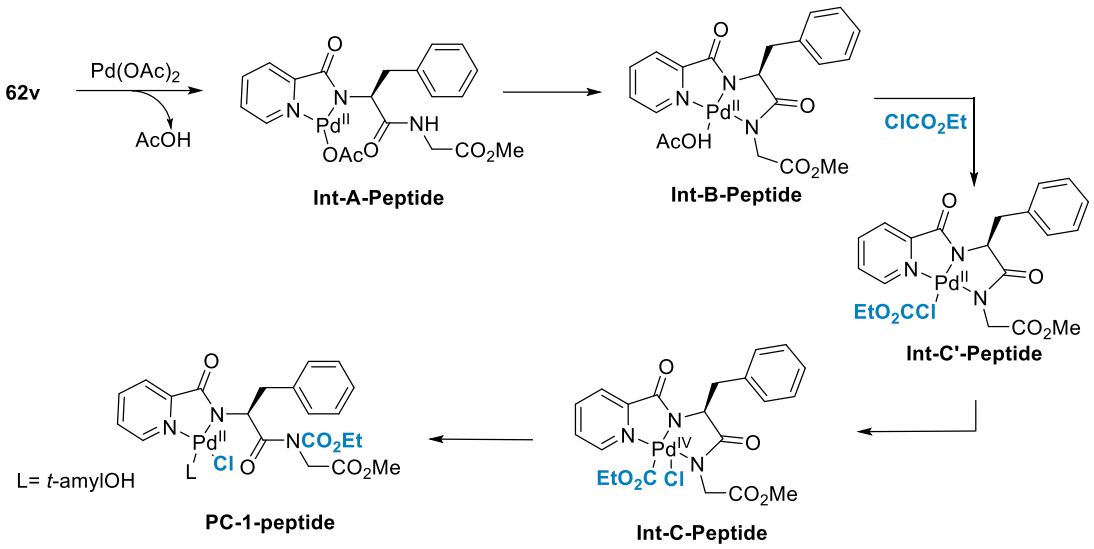

Scheme 69. Proposal of an unproductive reaction pathway for PA-Phe-Gly-OMe.

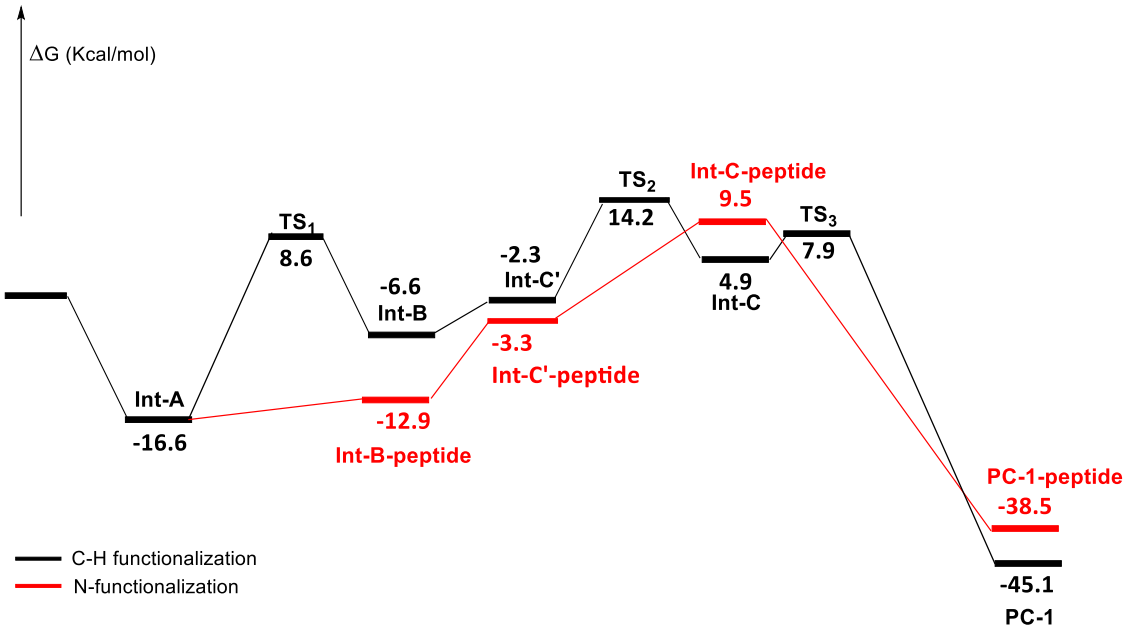

Scheme 70. Energy profiles for the C–H functionalization and N-functionalization.

The competitive N-functionalization would start by coordination of the nitrogen atom of the amide backbone of the **Int-A-peptide** with the Pd center, thereby affording the palladacycle **Int-B-peptide** with an energy value of -12.9 Kcal/mol. Conversely, the enthalpy of the δ-C(sp^2)–H

activation product **Int-B** within the previously proposed mechanism was found to be -6.6 Kcal/mol. As a result, the formation of the δ-C(sp^2)–H activation complex is unfavored since it is located higher in energy in the potential energy surface. At this point, the approach of ethyl chloroformate to the **Int-B-peptide** would lead to the formation of reactant complex **Int-C'-peptide** with an energy of -3.3 Kcal/mol. The latter would next undergo oxidative addition of $ClCO_2Et$, thus forming **Int-C-peptide** with an energy of 9.5 Kcal/mol and eventually would afford the very stable *N*-alkoxycarbonylated product **PC-1-peptide** upon C–N bond-forming reductive elimination. This step could be defined as strongly exothermic with an enthalpy difference of -48.1 Kcal/mol. Although these calculations can not explain the actual reason of this lack of reactivity, they demonstrated the feasibility of the formation of more stable intermediates than the desired ones, which may lead to unproductive but stabilized intermediates or reaction pathways.

On balance then, we have performed computational studies which support the following mechanism proposal (Scheme 71).

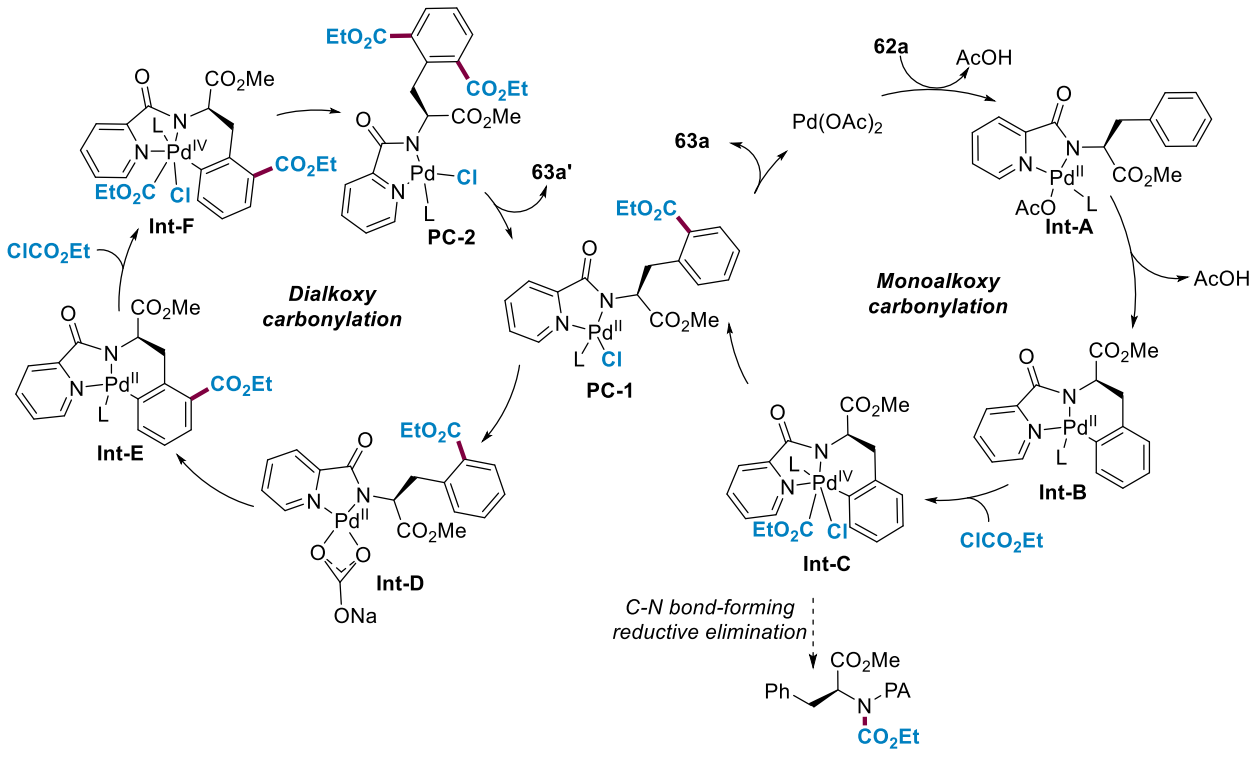

Scheme 71. Proposed reaction pathway based on performed DFT studies.

The reaction starts with the coordination of the substrate to the catalyst rendering the **Int-A**, followed by a C–H activation to deliver the **Int-B**. The latter could react with ethyl chloroformate via oxidative addition to furnish the Pd^{IV}-containing **Int-C**. At this point, two competitive pathways could take place. On the one hand, an undesired *N*-alkoxycarbonylated product could be formed through a C–N reductive elimination step. On the other hand, the C–C reductive elimination would deliver the monoalkoxycarbonylated product **PC-1**, thereby releasing the catalyst. The latter species could undergo a second catalytic cycle, delivering the difunctionalized compound.

3.4. Conclusions and Future Work

In summary, we have developed an unprecedented C(sp^2)–H alkoxycarbonylation of phenethyl and benzylamines with chloroformates as CO surrogates which occurred in a simple fashion.[151] This method avoids the use of toxic CO gas and is tolerant toward different alkyl chloroformates with high structural diversity. Under the optimized reaction conditions, the feasibility of the functionalization via 5- or 6-membered palladacycles has been demonstrated. Notably, our method enables the removal of the directing group from benzylamines to afford isoindolinone skeletons in a straightforward manner. The performance under air and the reliable scalability represent a practical bonus in terms of operational simplicity. Computational studies supported a Pd^{II}/Pd^{IV} catalytic cycle and provided insights about the key role of *t*-amylOH as co-solvent.

For future work, the application of the C(sp^2)–H alkoxycarbonylation reaction in more complex peptide settings would be highly desirable. For this purpose, the use of CO sources that can proceed via radical pathways such as azodicarboxylates, α-keto esters or glyoxolates could be the best choice. Inspired by the successful radical modification techniques for the late-stage functionalization of peptides recently developed in our group, those radical alkoxycarbonylation events may be feasible too in complex oligopeptides. The different mechanistic scenario that could take place could offer an opportunity for the late-stage functionalization of complex peptides in an efficient manner.

[151] Andrade-Sampedro, P.; Matxain, J. M.; Correa, A. *Chem. Eur. J.* **2021**, *27*, 5782.

3.5. Supporting Information

In this section, the general synthetic procedures will be detailed. For the full characterization data, please see the SI of the published article.[151]

3.5.1. General procedure for Pd-catalyzed δ-C(sp2)-H alkoxycarbonylation of Phe derivatives

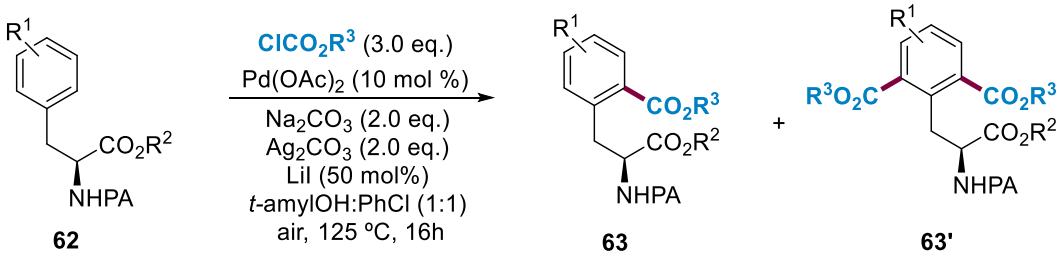

General procedure: A reaction tube containing a stirring bar was charged with **62** (0.25 mmol, 1 eq.), Ag_2CO_3 (0.50 mmol, 2 eq.), Na_2CO_3 (0.50 mmol, 2 eq.), LiI (50 mol %), the corresponding chloroformate (if solid) (0.75 mmol, 3 eq.) and $Pd(OAc)_2$ (10 mol %). Then, the corresponding chloroformate (if liquid) (0.75 mmol, 3 eq.) and a mixture of solvents (PhCl: *t*-amylOH, 1:1) (2 mL) were added by syringe under air. The reaction tube was warmed up to 125 ºC and stirred for 16 hours. The mixture was allowed to cool to room temperature, concentrated under reduced pressure and the product was purified by column chromatography.

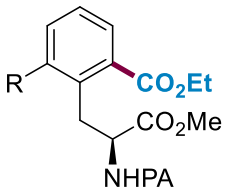

63a, R = H
63a', R = CO_2Et

Ethyl (*S*)-2-[3-methoxy-3-oxo-2-(picolinamido)propyl]benzoate (63a). Following the general procedure, using commercially available ethyl chloroformate (0.75 mmol, 72 µL) and **62a**[106] (0.25 mmol, 71 mg) provided 17.4 mg (20 % yield) and 58 mg (55% yield) of **63a** and **63a'**, respectively, as a white solid. *Both isomers were separated and independently characterized.* **Monofunctionalized 63a:** Mp 62-63 ºC. $[\alpha]_D^{14} = -69.3$ (c = 0.30, CH_2Cl_2). ^{1}H NMR (400 MHz, $CDCl_3$) δ 8.81 (d, *J* = 8.3 Hz, 1H), 8.57 (d, *J* = 4.3 Hz, 1H), 8.10 (d, *J* = 7.8 Hz, 1H), 7.95 (d, *J* = 7.9, 1.4 Hz, 1H), 7.81 (td, *J* = 7.7, 1.7 Hz, 1H), 7.49 – 7.39 (m, 2H), 7.38 – 7.27 (m, 2H), 5.08 (dd,

J = 12.0, 8.0 Hz, 1H), 4.41 (qd, *J* = 7.1, 2.2 Hz, 2H), 3.75 (s, 3H), 3.65 (d, *J* = 7.6 Hz, 2H), 1.42 (t, *J* = 7.1 Hz, 3H). ^{13}C NMR (101 MHz, $CDCl_3$) δ 172.1, 167.4, 164.2, 149.3, 148.1, 138.2, 137.0, 132.1, 131.7, 130.9, 130.2, 127.0, 126.1, 122.2, 61.2, 54.0, 52.3, 35.9, 14.2. IR (cm $^{-1}$): 3347, 2983, 1744, 1710, 1660, 1522, 1432, 1347, 1228, 1136, 1079, 996, 753, 665. HRMS *calcd*. for ($C_{19}H_{20}N_2O_5$): 356.1372, *found* 356.1371. **Difunctionalized 63a'**: Mp 104-105 ºC. $[\alpha]_D^{14} = -87.5$ (c = 1.00, CH_2Cl_2). ^{1}H NMR (400 MHz, $CDCl_3$) δ 9.02 (d, *J* = 9.0 Hz, 1H), 8.52 (d, *J* = 4.4 Hz, 1H), 8.00 (d, *J* = 7.8 Hz, 1H), 7.94 (d, *J* = 7.8 Hz, 1H), 7.74 (td, *J* = 7.7, 1.7 Hz, 1H), 7.45 – 7.25 (m, 2H), 5.31 – 5.24 (m, 1H), 4.48 – 4.36 (m, 4H), 4.10 – 3.87 (m, 2H), 3.75 (s, 3H), 1.39 (t, *J* = 7.1 Hz, 6H). ^{13}C NMR (101 MHz, $CDCl_3$) δ 172.0, 167.4, 164.2, 149.4, 147.9, 138.4, 136.9, 133.7, 132.7, 126.6, 125.9, 122.1, 61.6, 53.1, 52.3, 31.1, 14.0. IR (cm $^{-1}$): 3388, 2990. 1720, 1677, 1511, 1433, 1356, 1231, 1034, 747, 619. HRMS *calcd.* for ($C_{22}H_{24}N_2O_7$): 428.1584, *found* 428.1576. *This reaction was also performed in a higher scale: the use of* ***62a*** *(3.52 mmol, 1.00 g) and* ***66a*** *(10.56 mmol, 1.01 mL) provided 925 mg (75 % yield) of* ***63a:63a'*** *(1:2 ratio) as a white solid.*

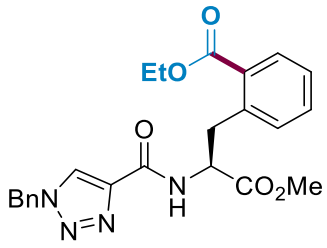

(65a)

Ethyl-(*S*)-2-[2-(1-benzyl-*1H*-1,2,3-triazole-4-carboxamido)-3-methoxy-3-oxopropyl]benzoate (65a). Following the general procedure, using commercially available ethyl chloroformate (0.75 mmol, 72 µL) and **64a**[106] (0.25 mmol, 91 mg) provided 49 mg (45 % yield) and 6 mg (5% yield) of **65a** and **65a'**, respectively, as a white solid. *Both isomers were separated and the following data correspond to the major monofunctionalized product* **65a**. Mp 89-90 ºC. $[\alpha]_D^{14} = -102.8$ (c = 0.45, CH_2Cl_2). ^{1}H NMR (400 MHz, $CDCl_3$) δ 7.67 (s, 1H), 7.42 – 7.40 (m, 3H), 7.31 – 7.23 (m, 4H), 7.19 (t, *J* = 7.4 Hz, 2H), 7.15 – 7.09 (m, 1H), 5.52 (s, 2H), 5.40 (dd, *J* = 10.5, 5.1 Hz, 1H), 4.07 - 4.01 (m, 2H), 3.78 (s, 3H), 3.56 (dd, *J* = 14.2, 5.2 Hz, 1H), 3.41 (dd, *J* = 14.2, 10.5 Hz, 1H), 0.97 (t, *J* = 7.1 Hz, 3H). ^{13}C NMR (101 MHz, $CDCl_3$) δ 170.1, 163.5, 154.2, 143.6, 137.0, 133.7, 129.5, 129.3, 129.2, 129.1, 128.3, 128.2, 126.6, 126.2, 63.4, 59.5, 54.3, 52.6, 35.8, 13.5. IR (cm $^{-1}$): 3130, 2933, 1741, 1678, 1540, 1434, 1376, 1297, 1257, 1173, 1026, 854, 752, 712, 694, 582, 387. HRMS *calcd*. for ($C_{23}H_{24}N_4O_5$): 436.1747, *found* 436.1739.

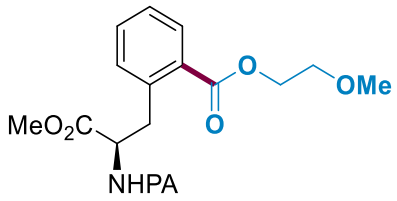

(63b)

2-Methoxyethyl (*S*)-2-[3-methoxy-3-oxo-2-(picolinamido)propyl]benzoate (63b). Following the general procedure, using commercially available 2-methoxyethyl chloroformate (0.75 mmol, 87 µL) and **62a** (0.25 mmol, 71 mg) provided 22.6 mg (23 % yield) and 58 mg (48% yield) of **63b** and **63b'**, respectively, as a colorless oil. *Both isomers were separated and independently characterized.* **Monofunctionalized 63b:** $[\alpha]_D^{14} = -46.0$ (c = 0.68, CH_2Cl_2). ^{1}H NMR (400 MHz, $CDCl_3$) δ 8.78 (d, *J* = 8.3 Hz, 1H), 8.57 (d, *J* = 5.3 Hz, 1H), 8.10 (d, *J* = 7.8 Hz, 1H), 7.97 (dd, *J* = 7.9, 1.4 Hz, 1H), 7.81 (td, *J* = 7.7, 1.7 Hz, 1H), 7.52 – 7.39 (m, 2H), 7.36 (dd, *J* = 7.8, 1.3 Hz, 1H), 7.34 – 7.25 (m, 1H), 5.09 (td, *J* = 8.5, 6.4 Hz, 1H), 4.50 (t, *J* = 4.8 Hz, 2H), 3.76 (m, 2H), 3.74 (s, 3H), 3.66 – 3.63 (m, 2H), 3.44 (s, 3H). ^{13}C NMR (101 MHz, $CDCl_3$) δ 172.1, 167.4, 164.2, 149.3, 148.1, 138.4, 137.1, 132.3, 131.7, 131.1, 129.9, 127.0, 126.2, 122.2, 70.3, 64.1, 58.9, 54.0, 52.3, 35.9. IR (cm^{-1}): 3368, 2950, 1713, 1672, 1510, 1433, 1366, 1254, 1124, 1078, 996, 866, 749, 619. HRMS *calcd.* for ($C_{20}H_{22}N_2O_6$): 386.1478, *found* 386.1474. **Difunctionalized 63b':** $[\alpha]_D^{14} = -79.8$ (c = 1.20, CH_2Cl_2). ^{1}H NMR (400 MHz, $CDCl_3$) δ 8.99 (d, *J* = 9.0 Hz, 1H), 8.55 (d, *J* = 4.8 Hz, 1H), 8.04 – 7. 99 (m, 3H), 7.77 (td, *J* = 7.7, 1.7 Hz, 1H), 7.45 – 7.29 (m, 2H), 5.35 – 5.30 (m, 1H), 4.58 – 4.47 (m, 4H), 4.05 (dd, *J* = 13.3, 5.5 Hz, 1H), 3.93 (dd, *J* = 13.4, 10.7 Hz, 1H), 3.75 (s, 3H), 3.76 – 3.69 (m, 4H), 3.43 (s, 6H). ^{13}C NMR (101 MHz, $CDCl_3$) δ 172.4, 167.7, 164.6, 149.9, 148.3, 139.2, 137.2, 134.5, 132.7, 127.0, 126.3, 122.6, 70.5, 64.8, 59.2, 53.3, 52.7, 31.6. IR (cm^{-1}): 2950, 1718, 1674, 1587, 1511, 1434, 1365, 1242, 1118, 1027, 867, 751. HRMS *calcd.* for ($C_{24}H_{28}N_2O_9$): 488.1795, *found* 488.1786.

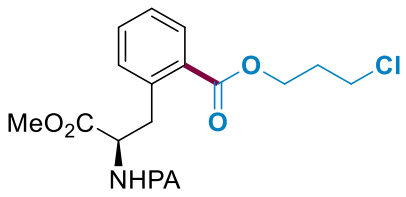

(63c)

3-Chloropropyl (*S*)-2-(3-methoxy-3-oxo-2-(picolinamido)propyl)benzoate (63c). Following the general procedure, using commercially available 3-chloropropyl chloroformate (0.75 mmol, 90 µL) and **62a** (0.25 mmol, 71 mg) provided 29.3 mg (29 % yield) and 44.6 mg (34% yield) of **63c** and **63c'**, respectively, as a colorless oil. *Both isomers were separated and independently*

characterized. **Monofunctionalized 63c:** $[\alpha]_D^{14}$ = + 54.2 (c = 0.20, CH_2Cl_2). ^{1}H NMR (400 MHz, $CDCl_3$) δ 8.76 (d, *J* = 8.4 Hz, 1H), 8.58 (d, *J* = 4.6 Hz, 1H), 8.09 (d, *J* = 7.8 Hz, 1H), 7.94 (dd, *J* = 7.9, 1.4 Hz, 1H), 7.82 (td, *J* = 7.7, 1.7 Hz, 1H), 7.51 – 7.40 (m, 2H), 7.40 – 7.24 (m, 2H), 5.10 (td, *J* = 8.5, 6.3 Hz, 1H), 4.50 (td, *J* = 6.2, 1.7 Hz, 2H), 3.75 (s, 3H), 3.72 (t, *J* = 6.4 Hz, 2H), 3.65 (dd, *J* = 7.5, 3.3 Hz, 2H), 2.27 (p, *J* = 6.3 Hz, 2H). ^{13}C NMR (101 MHz, $CDCl_3$) δ 172.4, 167.5, 164.5, 149.6, 148.5, 138.9, 137.4, 132.7, 132.2, 131.3, 130.0, 127.4, 126.5, 122.6, 62.3, 54.2, 52.7, 41.7, 36.4, 31.9. IR (cm $^{-1}$): 3372, 2953, 1713, 1674, 1513, 1433, 1359, 1255, 1078, 997, 749. HRMS *calcd.* for ($C_{20}H_{21}ClN_2O_5$): 404.1139, *found* 404.1134. **Difunctionalized 63c':** $[\alpha]_D^{13}$ = −72.1 (c = 1.35, CH_2Cl_2). ^{1}H NMR (400 MHz, $CDCl_3$) δ 8.95 (d, *J* = 9.1 Hz, 1H), 8.56 (d, *J* = 4.5 Hz, 0H), 8.01 (d, *J* = 7.7 Hz, 1H), 7.97 (d, *J* = 7.9 Hz, 2H), 7.77 (td, *J* = 7.7, 1.7 Hz, 1H), 7.44 – 7.33 (m, 2H), 5.31 – 5.25 (m, 1H), 4.67 – 4.44 (m, 4H), 4.15 – 3.90 (m, 2H), 3.78 (s, 3H), 3.70 (t, *J* = 6.4 Hz, 4H), 2.25 (td, *J* = 6.3, 2.6 Hz, 4H). ^{13}C NMR (101 MHz, $CDCl_3$) δ 172.4, 167.5, 164.5, 149.8, 148.4, 139.3, 137.4, 134.3, 132.7, 127.1, 126.4, 122.6, 62.8, 53.3, 52.8, 41.6, 31.7, 31.6. IR (cm $^{-1}$): 3377, 2957, 1719, 1674, 1586, 1510, 1433, 1358, 1227, 1144, 997, 751. HRMS *calcd.* for ($C_{24}H_{26}Cl_2N_2O_7$): 524.1117, *found* 524.1107.

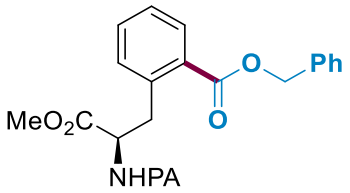

(63d)

Benzyl (*S*)-2-[3-methoxy-3-oxo-2-(picolinamido)propyl]benzoate (63d). Following the general procedure, using commercially available benzyl chloroformate (0.75 mmol, 107 µL) and **62a** (0.25 mmol, 71 mg) provided 58 mg (49 % yield) of **63d:63d'** (3:1 ratio) as a colorless oil. *The following data correspond to a mixture of mono- and difunctionalized compounds.* ^{1}H NMR (400 MHz, $CDCl_3$) δ 9.00 (d, *J* = 9.0 Hz, 1H), 8.80 (d, *J* = 8.2 Hz, 1H), 8.53 (d, *J* = 5.2 Hz, 1H), 8.47 (d, *J* = 4.6 Hz, 1H), 8.11 (d, *J* = 7.7 Hz, 1H), 8.04 – 7.94 (m, 3H), 7.81 (td, *J* = 7.7, 1.7 Hz, 1H), 7.77 – 7.73 (m, 1H), 7.51 – 7.26 (m, 15H), 5.44 – 5.27 (m, 5H), 5.10 (dd, *J* = 16.0, 8.0 Hz, 1H), 4.13 – 3.96 (m, 2H), 3.74 (s, 3H), 3.72 (s, 3H), 3.67 (d, *J* = 7.5 Hz, 2H). ^{13}C NMR (101 MHz, $CDCl_3$) δ 172.0, 167.1, 167.0, 164.2, 164.1, 149.5, 149.3, 148.1, 148.0, 139.3, 138.6, 137.1, 136.9, 135.8, 135.5, 134.12, 132.3, 131.8, 131.0, 129.7, 128.5, 128.3, 128.2, 128.2, 127.0, 126.7, 126.1, 125.9, 122.2, 77.3, 77.0, 76.7, 67.3, 66.8, 53.9, 53.1, 52.4, 52.3, 35.9, 31.2. IR (cm $^{-1}$): 3369, 2951, 1713,

1673, 1588, 1509, 1433, 1370, 1214, 1141, 1075, 747, 696. HRMS *calcd.* for ($C_{32}H_{28}N_2O_7$) (**63d'**): 552.1897, *found* 552.1885.

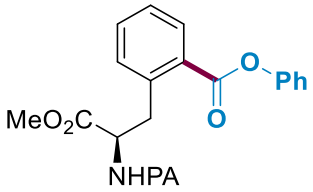

(63e)

Phenyl (*S*)-2-[3-methoxy-3-oxo-2-(picolinamido)propyl]benzoate (63e). Following the general procedure, using commercially available phenyl chloroformate (0.75 mmol, 94 µL) and **62a** (0.25 mmol, 71 mg) provided 22.3 mg (22 % yield) of **63e** as a white solid. Mp 124-125 ºC. $[\alpha]_D^{14}$ = −63.7 (c = 0.28, CH_2Cl_2). ^{1}H NMR (400 MHz, $CDCl_3$) δ 8.74 (d, *J* = 8.5 Hz, 1H), 8.54 (d, *J* = 5.1 Hz, 1H), 8.22 (dd, *J* = 7.9, 1.4 Hz, 1H), 8.09 (d, *J* = 7.8 Hz, 1H), 7.81 (td, *J* = 7.7, 1.7 Hz, 1H), 7.59 – 7.37 (m, 6H), 7.34 – 7.24 (m, 3H), 5.14 (td, *J* = 8.3, 6.8 Hz, 1H), 3.84 – 3.72 (m, 2H), 3.72 (s, 3H). ^{13}C NMR (101 MHz, $CDCl_3$) δ 171.9, 165.7, 164.1, 150.8, 149.2, 148.1, 139.6, 137.1, 132.9, 132.1, 131.5, 129.4, 128.9, 127.2, 126.2, 125.9, 122.3, 121.8, 53.8, 52.4, 36.0. IR (cm $^{-1}$): 1726, 1663, 1517, 1432, 1347, 1236, 1189, 1046, 997, 753, 612, 541. HRMS *calcd*. for ($C_{23}H_{20}N_2O_5$): 404.1372, *found* 404.1364.

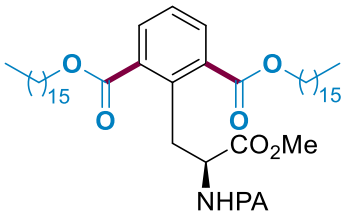

(63f')

Dihexadecyl (*S*)-2-[3-methoxy-3-oxo-2-(picolinamido)propyl]isophthalate (63f') Following the general procedure, using commercially available hexadecyl chloroformate (0.75 mmol, 247 µL) and **62a** (0.25 mmol, 71 mg) provided 112 mg (56 % yield) of **63f'** as a white solid. Mp 50-51 ºC. $[\alpha]_D^{13}$ = −51.2 (c = 1.00, CH_2Cl_2). ^{1}H NMR (400 MHz, $CDCl_3$) δ 9.03 (d, *J* = 9.0 Hz, 1H), 8.54 (d, *J* = 4.3 Hz, 1H), 8.03 (d, *J* = 7.8 Hz, 1H), 7.96 (d, *J* = 7.8 Hz, 2H), 7.76 (td, *J* = 7.7, 1.7 Hz, 1H), 7.52 – 7.24 (m, 2H), 5.32 – 5.26 (m, 1H), 4.39 – 4.32 (m, 4H), 4.05 (dd, *J*= 13.2, 5.3 Hz, 1H), 3.99 – 3.93 (m, 1H), 3.77 (s, 3H), 1.76 (p, *J* = 7.0 Hz, 4H), 1.45 – 1.25 (m, 54H), 0.90 (t, *J* = 6.7 Hz, 6H). ^{13}C NMR (101 MHz, $CDCl_3$) δ 172.1, 167.5, 164.2, 149.6, 148.0, 138.8, 136.9, 133.8, 132.7, 126.6, 125.9, 122.2, 65.9, 53.2, 52.4, 31.9, 31.2, 29.6, 29.6, 29.5, 29.5, 29.3, 29.2, 28.5, 26.0, 22.6, 14.1. IR (cm $^{-1}$): 2916, 2848, 1725, 1672, 1510, 1467, 1242, 1147, 1044, 821, 752, 620. HRMS *calcd*. for ($C_{51}H_{82}N_2O_7$): 834.6122, *found* 834.6125.

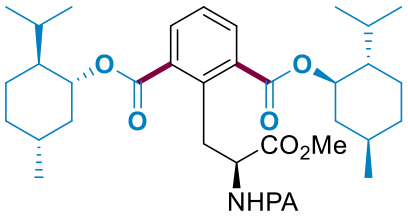

(63g')

Bis[(1*R*,2*S*,5*S*)-2-isopropyl-5-methylcyclohexyl]-2-[3-methoxy-3-oxo-2-picolinamido)propyl]isophthalate (63g'). Following the general procedure, using commercially available (1*R*)-(-)-menthyl chloroformate (0.75 mmol, 161 µL) and **62a** (0.25 mmol, 71 mg) provided 113 mg (70 % yield) of **63g'** as a white solid. Mp 142-143 ºC. $[\alpha]_D^{13} = -107.3$ (c = 1.00, CH_2Cl_2). ^{1}H NMR (400 MHz, $CDCl_3$) δ 9.23 (d, *J* = 8.7 Hz, 1H), 8.52 (d, *J* = 4.7 Hz, 1H), 8.02 (d, *J* = 7.8 Hz, 1H), 7.94 (d, *J* = 7.8 Hz, 2H), 7.74 (td, *J* = 7.7, 1.7 Hz, 1H), 7.42 – 7.30 (m, 2H), 5.31 – 5.24 (m, 1H), 5.05 (td, *J* = 10.9, 4.3 Hz, 2H), 4.06 (dd, *J* = 13.2, 5.3 Hz, 1H), 3.88 (dd, *J* = 13.2, 11.5 Hz, 1H), 3.77 (s, 3H), 2.31 – 2.19 (m, 2H), 2.03 – 1.96 (m, 2H), 1.78 – 1.73 (m, 4H), 1.64 – 1.50 (m, 4H), 1.16 (q, *J* = 11.9 Hz, 4H), 0.99 (d, *J* = 6.5 Hz, 6H), 0.93 (d, *J* = 6.9 Hz, 6H), 0.84 (d, *J* = 6.9 Hz, 6H). ^{13}C NMR (101 MHz, $CDCl_3$) δ 173.4, 168.3, 165.7, 151.1, 149.3, 140.1, 138.1, 134.8, 134.3, 127.9, 127.1, 123.6, 54.7, 53.6, 48.3, 41.9, 35.5, 32.7, 32.3, 27.6, 24.6, 23.4, 22.1, 17.4. IR (cm $^{-1}$): 2956, 1715, 1680, 1517, 1452, 1359, 1227, 1143, 1096, 965, 752, 620. HRMS *calcd.* for ($C_{38}H_{52}N_2O_7$): 648.3775, *found* 648.3764.

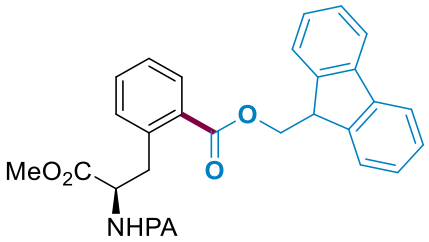

(63h)

(9*H*-fluoren-9-yl)methyl-(*S*)2-[3-methoxy-3-oxo-2-(picolinamido)propyl]isophthalate (63h). Following the general procedure, using commercially available 9-fluorenylmethyl chloroformate (0.75 mmol, 194 mg), **62a** (0.25 mmol, 71 mg) and 4 mL of solvent (PhCl/*t*-amylOH, 1:1) provided 97 mg (58 % yield) of **63h: 63h'** (3:7 ratio) as a yellow oil. *The following data correspond to a mixture of mono- and difunctionalized compounds.* ^{1}H NMR (400 MHz, $CDCl_3$) δ 8.97 (d, *J* = 9.1 Hz, 1H), 8.80 (d, *J* = 8.2 Hz, 1H), 8.43 (d, *J* = 4.5 Hz, 1H), 8.37 (d, *J* = 4.5 Hz, 1H), 8.09 (d, *J* = 7.8 Hz, 1H), 8.06 – 7.97 (m, 2H), 7.94 (d, *J* = 7.8 Hz, 2H), 7.82 (d, *J* = 7.6 Hz, 4H), 7.76 (td, *J* = 7.7, 1.7 Hz, 1H), 7.61 – 7-71 (m, 6H), 7.52 – 7.25 (m, 13H), 7.23 (ddd, *J* = 7.6, 4.8, 1.3 Hz, 1H), 5.36 (td, *J* = 9.3, 6.3 Hz, 1H), 5.12 (td, *J* = 8.5, 6.2 Hz, 1H), 4.89 – 4.53 (m, 5H), 4.43 – 4.31 (m,

2H), 4.10 – 3.96 (m, 2H) 3.75 – 3.65 (m, 6H). ^{13}C NMR (101 MHz, $CDCl_3$) δ 171.9, 167.1, 164.2, 149.3, 149.2, 148.0, 147.9, 143.7, 143.6, 143.5, 141.2, 139.6, 138.9, 137.0, 136.8, 133.8, 132.3, 132.3, 131.9, 130.7, 127.7, 127.7, 127.1, 126.9, 126.1, 125.9, 124.9, 124.9, 122.1, 120.0, 67.2, 66.9, 53.9, 53.2, 52.4, 52.3, 46.7, 46.7, 35.7, 31.1. IR (cm $^{-1}$): 3367, 2950, 1720, 1672, 1587, 1512, 1448, 1368, 1216, 1143, 906, 726, 619. HRMS *calcd.* for ($C_{46}H_{36}N_2O_7$) (**63h'**): 728.2523, *found* 728.2519.

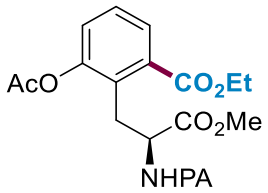

(63l)

Ethyl (*S*)-3-acetoxy-2-[3-methoxy-3-oxo-2-(picolinamido)propyl]benzoate (63l). Following the general procedure, using commercially available ethyl chloroformate (0.75 mmol, 72 µL), Phe derivative **62l** (0.25 mmol, 85.6 mg) and 4 mL of solvent (PhCl/*t*-amylOH, 1:1) provided 45 mg (43 % yield) of **63l** as a colorless oil. $[\alpha]_D^{13}$ = +78.0 (c = 0.28, CH_2Cl_2). ^{1}H NMR (400 MHz, $CDCl_3$) δ 9.00 (d, *J* = 9.0 Hz, 1H), 8. 56 (d, *J* = 4.8 Hz, 1H), 8.03 (d, *J* = 7.8 Hz, 1H), 7.92 (dd, *J* = 7.8, 1.4 Hz, 1H), 7.78 (td, *J* = 7.7, 1.7 Hz, 1H), 7.74 (d, *J* = 7.8 Hz, 1H), 7.45 – 7.33 (m, 2H), 5.23 – 5.17 (m, 1H), 4.48 – 4.39 (m, 2H), 3.96 (dd, *J* = 13.3, 5.2 Hz, 1H), 3.78 (s, 3H), 3.77 – 3.70 (m, 1H), 2.64 (s, 3H), 1.41 (t, *J* = 7.2 Hz, 3H). ^{13}C NMR (101 MHz, $CDCl_3$) δ 202.6, 172.0, 167.5, 164.3, 149.5, 148.1, 140.6, 137.0, 136.7, 133.2, 133.2, 131.6, 126.6, 126.0, 122.2, 61.7, 53.1, 52.4, 30.8, 30.5, 14.1. IR (cm $^{-1}$): 3431, 3367, 2981, 1713, 1672, 1580, 1510, 1433, 1356, 1211, 1091, 996, 750, 619. HRMS *calcd*. for ($C_{22}H_{24}N_2O_7$): 428.4410, *found* 428.4415.

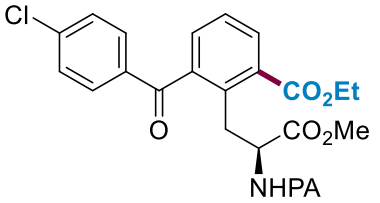

(63m)

Ethyl (*S*)-3-(4-chlorobenzoyl)-2-[3-methoxy-3-oxo-2-(picolinamido)propyl]benzoate (63m). Following the general procedure, using commercially available ethyl chloroformate (0.75 mmol, 72 µL), Phe derivative **62m**[106] (0.25 mmol, 105.7 mg) and 4 mL of solvent (PhCl/*t*-amylOH, 1:1) provided 66 mg (54 % yield) of **63m** as a colorless oil. $[\alpha]_D^{13}$ = +10.5 (c = 1.12, CH_2Cl_2). ^{1}H NMR (400 MHz, $CDCl_3$) δ 8.83 (d, *J* = 9.0 Hz, 1H), 8.46 (d, *J* = 4.6 Hz, 1H), 8.10 – 7.93 (m, 2H), 7.82

– 7.73 (m, 2H), 7.63 (d, *J* = 8.1 Hz, 1H), 7.51 – 7.48 (m, 2H), 7.44 – 7.34 (m, 3H), 7.32 – 7.23 (m, 1H), 5.18 – 5.12 (m, 1H), 4.45 (p, *J* = 7.2 Hz, 2H), 3.95 – 3.74 (m, 2H), 3.73 (s, 3H), 1.42 (t, *J* = 7.1 Hz, 3H). ^{13}C NMR (101 MHz, $CDCl_3$) δ 196.0, 171.7, 167.2, 164.3, 149.3, 148.0, 139.8, 138.8, 137.3, 136.9, 134.7, 133.3, 133.0, 132.6, 132.0, 130.2, 129.7, 128.7, 126.2, 126.0, 122.2, 61.7, 53.4, 52.5, 31.2, 14.1. IR (cm $^{-1}$): 3369, 2980, 1714, 1670, 1569, 1509, 1433, 1238, 1133, 1087, 996, 748, 690. HRMS *calcd.* for ($C_{26}H_{23}ClN_2O_6$): 494.1245, *found* 494.1235.

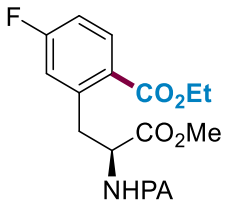

(63n)

Ethyl (*S*)-4-fluoro-2-[3-methoxy-3-oxo-2-(picolinamido)propyl]benzoate (63n). Following the general procedure, using commercially available ethyl chloroformate (0.75 mmol, 72 µL), Phe derivative **62n** (0.25 mmol, 76 mg) and 4 mL of solvent (PhCl/*t*-amylOH, 1:1) provided 47 mg (51 % yield) of **63n** as a colorless oil. $[\alpha]_D^{13} = -51.6$ (c = 2.22, CH_2Cl_2). ^{1}H NMR (400 MHz, $CDCl_3$) δ 8.78 (d, *J* = 8.5 Hz, 1H), 8.56 (dd, *J* = 4.8, 0.8 Hz, 1H), 8.09 (d, *J* = 7.8 Hz, 1H), 7.99 (dd, *J* = 8.8, 6.0 Hz, 1H), 7.82 (td, *J* = 7.7, 1.7 Hz, 1H), 7.42 (ddd, *J* = 7.6, 4.8, 1.2 Hz, 1H), 7.05 (dd, *J* = 9.5, 2.6 Hz, 1H), 7.00 – 6.94 (m, 1H), 5.09 (td, *J* = 8.8, 5.9 Hz, 1H), 4.38 (qd, *J* = 7.2, 1.8 Hz, 2H), 3.75 (s, 3H), 3.71 – 3.58 (m, 2H), 1.40 (t, *J* = 7.1 Hz, 3H). ^{13}C NMR (101 MHz, $CDCl_3$) δ 171.8, 166.4, 164.2 (d, $J_{C\text{-}F}$ = 282.0 Hz), 164.1, 149.2, 148.1, 141.8 (d, $J_{C\text{-}F}$ = 8.3 Hz), 137.1, 133.6 (d, $J_{C\text{-}F}$ = 9.2 Hz), 126.2, 122.2, 118.5 (d, $J_{C\text{-}F}$ = 21.7 Hz), 114.1 (d, $J_{C\text{-}F}$ = 21.4 Hz), 61.2, 53.0, 52.4, 36.0, 14.1. IR (cm $^{-1}$): 3373, 2954, 1711, 1672, 1587, 1511, 1433, 1365, 1235, 1078, 997, 750. HRMS *calcd*. for ($C_{19}H_{19}FN_2O_5$): 374.1278, *found* 374.1274.

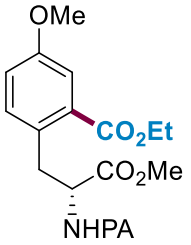

(63s)

Ethyl (*R*)-5-methoxy-2-[3-methoxy-3-oxo-2-(picolinamido)propyl]benzoate (63s). Following the general procedure, using commercially available ethyl chloroformate (0.75 mmol, 72 µL), Phe derivative **62s** (0.25 mmol, 78.6 mg) provided 20.7 mg (21 % yield) and 49.8 mg (44% yield) of **63s** and **63s'**, respectively, as a colorless oil. *Both isomers were separated and independently*

characterized. **Monofunctionalized 63s:** $[\alpha]_D^{12} = +5.4$ (c = 0.31, CH_2Cl_2). ^{1}H NMR (400 MHz, $CDCl_3$) δ 8.78 (d, *J* = 8.3 Hz, 1H), 8.57 (d, *J* = 4.6 Hz, 1H), 8.11 (d, *J* = 7.8 Hz, 1H), 7.82 (td, *J* = 7.7, 1.7 Hz, 1H), 7.46 (d, *J* = 2.9 Hz, 1H), 7.42 (ddd, *J* = 7.6, 4.8, 1.2 Hz, 1H), 7.25 (d, *J* = 8.5 Hz, 1H), 6.98 (dd, *J* = 8.5, 2.9 Hz, 1H), 5.04 (dd, *J* = 16.0, 8.0 Hz, 1H), 4.41 (qd, *J* = 7.1, 1.6 Hz, 2H), 3.82 (s, 3H), 3.75 (s, 3H), 3.57 (d, *J* = 7.4 Hz, 2H), 1.42 (t, *J* = 7.1 Hz, 3H). ^{13}C NMR (101 MHz, $CDCl_3$) δ 172.2, 167.3, 164.1, 158.1, 149.3, 148.0, 137.2, 132.9, 131.1, 130.1, 126.2, 122.3, 118.1, 115.7, 61.3, 55.4, 54.1, 52.3, 35.3, 14.2. IR (cm $^{-1}$): 1711, 1673, 1608, 1570, 1433, 1365, 1278, 1219, 1072, 1038, 750. HRMS *calcd.* for ($C_{20}H_{22}N_2O_6$): 386.1478, *found* 386.1459. **Difunctionalized 63s':** $[\alpha]_D^{13} = +54.5$ (c = 0.70, CH_2Cl_2). ^{1}H NMR (400 MHz, $CDCl_3$) δ 9.01 (d, *J* = 8.9 Hz, 1H), 8.55 (d, *J* = 5.0 Hz, 1H), 8.04 (d, *J* = 8.0 Hz, 1H), 7.77 (td, *J* = 7.7, 1.7 Hz, 1H), 7.48 (s, 2H), 7.38 (ddd, *J* = 7.6, 4.7, 1.2 Hz, 1H), 5.26 – 5.20 (m, 1H), 4.44 (qd, *J* = 7.1, 4.8 Hz, 4H), 4.00 – 3.84 (m, 2H), 3.83 (s, 3H), 3.77 (s, 3H), 1.41 (t, *J* = 7.1 Hz, 6H). ^{13}C NMR (101 MHz, $CDCl_3$) δ 172.2, 167.3, 164.3, 157.4, 149.5, 148.0, 137.0, 133.8, 130.0, 126.0, 122.3, 119.3, 61.8, 55.5, 53.3, 52.3, 30.6, 14.1. IR (cm $^{-1}$): 3376, 2980, 1717, 1675, 1601, 1510, 1464, 1433, 1366, 1217, 1093, 1046. HRMS *calcd.* for ($C_{23}H_{26}N_2O_8$): 458.1689, *found* 458.1681.

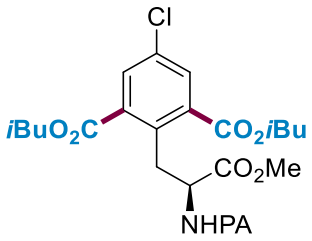

(63r')

Diisobutyl (*S*)-5-chloro-2-[3-methoxy-3-oxo-2-(picolinamido)propyl]isophthalate (63r'). Following the general procedure, using commercially available isobutyl chloroformate (0.75 mmol, 97 µL) and Phe derivative **63r**[152] (0.25 mmol, 80 mg) provided 68 mg (53 % yield) of **63r'** as a white solid. Mp 101-102 ºC. $[\alpha]_D^{14} = -64.4$ (c = 1.00, CH_2Cl_2). ^{1}H NMR (400 MHz, $CDCl_3$) δ 8.94 (d, *J* = 9.1 Hz, 1H), 8.55 (d, *J* = 4.8 Hz, 1H), 8.04 (d, *J* = 7.8 Hz, 1H), 7.93 (s, 2H), 7.78 (td, *J* = 7.7, 1.7 Hz, 1H), 7.40 (ddd, *J* = 7.5, 4.8, 1.3 Hz, 1H), 5.70 – 4.86 (m, 1H), 4.24 – 4.06 (m, 4H), 4.04 – 3.92 (m, 2H), 3.77 (s, 3H), 2.12 – 2.02 (m, 2H), 1.02 (d, *J* = 6.7 Hz, 12H). ^{13}C NMR (101 MHz, $CDCl_3$) δ 172.2, 166.5, 164.6, 149.8, 148.3, 137.9, 137.3, 134.5, 133.9, 132.9, 126.4, 122.6,

[152] Wang, X.; Niu, S.; Xu, L.; Zhang, C.; Meng, L.; Zhang, X.; Ma, D. *Org. Lett.* **2017**, *19*, 246.

72.4, 53.2, 52.8, 31.1, 28.0, 19.5. IR (cm $^{-1}$): 3359, 2957, 1734, 1669, 1578, 1510, 1431, 1153, 1095, 1051, 995, 772, 647, 547. HRMS *calcd.* for ($C_{26}H_{31}ClN_2O_7$): 518,1820, *found* 518.1809.

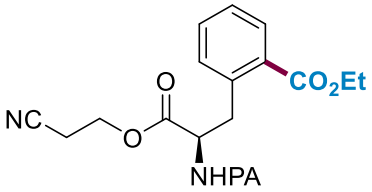

(63o)

Diethyl (*S*)-2-[3-(2-cyanoethoxy)-3-oxo-2-(picolinamido)propyl]isophthalate (63o). Following the general procedure, using commercially available ethyl chloroformate (0.75 mmol, 72 µL) and Phe derivative **62o** (0.25 mmol, 81 mg) provided 61 mg (56 % yield) of **63o:63o'** (1:1 ratio) as a colorless oil. *The following data correspond to a mixture of mono- and difunctionalized compounds.* ^{1}H NMR (400 MHz, $CDCl_3$) δ 9.10 (d, *J* = 8.5 Hz, 1H), 8.86 (d, *J* = 7.7 Hz, 1H), 8.61 – 8.53 (m, 2H), δ 8.09 (d, *J* = 7.8 Hz, 1H), 8.04 (d, *J* = 7.8 Hz, 1H), 8.01 – 7.92 (m, 2H), 7.80 (dtd, *J* = 15.1, 7.7, 1.7 Hz, 2H), 7.53 – 7.28 (m, 7H), 5.27 (ddd, *J* = 10.5, 8.5, 5.6 Hz, 1H), 5.30 – 5.24 (m, 1H), 4.67 – 4.27 (m, 10H), 4.23 – 3.89 (m, 2H), 3.88 – 3.47 (m, 2H), 2.80 – 2.61 (m, 4H), 1.44 – 1.42 (m, 10H). ^{13}C NMR (101 MHz, $CDCl_3$) δ 149.3, 149.1, 148.1, 148.1, 138.1, 137.9, 137.1, 137.0, 133.9, 133.4, 132.7, 132.2, 131.8, 130.9, 130.1, 127.2, 126.8, 126.3, 126.1, 122.2, 122.2, 116.4, 61.8, 61.5, 61.3, 59.3, 54.2, 53.3, 35.6, 31.1, 17.7, 14.2, 14.1. IR (cm $^{-1}$): 3378, 2980, 2200, 1710, 1673, 1510, 1365, 1244, 1087, 997, 750. HRMS *calcd*. for ($C_{24}H_{25}N_3O_7$) (**63o'**): 467.1693, *found* 467.1685.

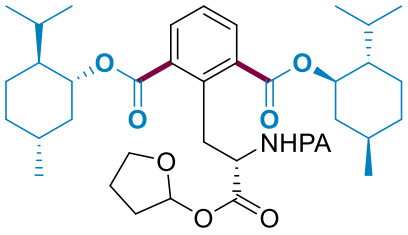

(63p')

1-[(1*R*,2*S*,5*S*)-2-isopropyl-5-methylcyclohexyl] 3-[(1*S*,2*R*,5*R*)-2-isopropyl-5-methyl cyclohexyl] 2-[3-oxo-2-(picolinamido)-3-[(tetrahydrofuran-3-yl)oxy]propyl]iso- phthalate (63p'). Following the general procedure, using commercially available (1*R*)-(-)-menthyl chloroformate (0.75 mmol, 161 µL) and Phe derivative **62p** (0.25 mmol, 85 mg) provided 34.6 mg (18 % yield) and 96.4 mg (55% yield) of **63p** and **63p'**, respectively as a yellowish oil. Diasteromeric ratio: 65:35. *Both isomers were separated and the following data correspond to the major difunctionalized **63p'**.* $[\alpha]_D^{13} = -65.7$ (c = 1.00, CH_2Cl_2). ^{1}H NMR (400 MHz, $CDCl_3$) δ 9.28 (t, *J* = 8.3, 1H), 9.12 (d, *J* = 8.5 Hz, 1H), 8.53 – 8.50 (m, 1H), 8.07 – 8.02 (m, 2H), 7.96 – 7.91 (m,

1H), 7.76 (td, *J* = 7.7, 1.7 Hz, 1H), 5.38 – 5.31 (m, 1H), 5.26 – 5.17 (m, 1H), 5.10 – 5.00 (m, 2H), 4.17 – 3.74 (m, 5H), 2.23 (d, *J* = 11.8 Hz, 2H), 2.20 – 1.89 (m, 5H), 1.76 (d, *J* = 11.0, Hz, 4H), 1.68 – 1.51 (m, 4H), 1.10 – 1. 23 (m, 4H), 1.04 – 0.92 (m, 14H), 1.01 - 0.82 (m, 6H). ^{13}C NMR (126 MHz, $CDCl_3$) δ 172.8, 172.8, 172.7, 172.7, 168.2, 168.2, 165.8, 165.6, 165.6, 151.0, 150.9, 149.3, 149.2, 139.9, 139.8, 139.7, 139.7, 138.2, 138.2, 134.7, 134.6, 134.5, 134.5, 134.4, 128.0, 128.0, 128.0, 128.0, 127.2, 123.6, 123.5, 77.0, 77.0, 77.0, 76.9, 76.8, 76.7, 74.2, 74.2, 74.1, 68.3, 68.3, 68.2, 54.8, 54.8, 54.7, 54.7, 48.4, 48.3, 42.0, 42.0, 35.5, 35.5, 34.2, 34.2, 34.1, 32.8, 32.8, 32.5, 32.5, 32.4, 32.4, 27.7, 27.6, 24.6, 24.6, 23.4, 23.3, 22.2, 22.1, 17.5, 17.4. IR (cm $^{-1}$): 3368, 2926, 2868, 1716, 1678, 1510, 1454, 1368, 1239, 1143, 1085, 960, 912, 729, 620. HRMS *calcd.* for ($C_{41}H_{56}N_2O_8$): 704.4037, *found* 704.4024.

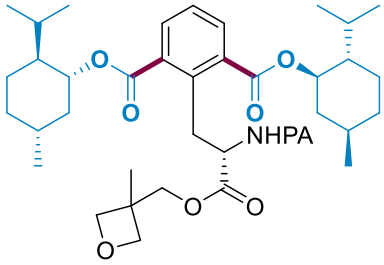

(63q')

1-[(1*R*,2*S*,5*S*)-2-isopropyl-5-methylcyclohexyl] 3-[(1*S*,2*R*,5*R*)-2-isopropyl-5-methylcyclohexyl] 2-[3-[(3-methyloxetan-3-yl)methoxy]-3-oxo-2-(picolinamido) propyl]isophthalate (63q'). Following the general procedure, using commercially available menthyl chloroformate (0.75 mmol, 161 µL) and Phe derivative **62q** (0.25 mmol, 87 mg) provided 6 mg (12 % yield) and 131 mg (73% yield) of **63q** and **63q'**, respectively as a yellowish oil. *Both isomers were separated and the following data correspond to the major difunctionalized **63q'**.* $[\alpha]_D^{14} = -89.5$ (c = 0.66, CH_2Cl_2). ^{1}H NMR (400 MHz, $CDCl_3$) δ 9.21 (d, *J* = 8.5 Hz, 1H), 8.52 (d, *J* = 4.7 Hz, 1H), 8.03 (d, *J* = 7.8 Hz, 1H), 7.94 (d, *J* = 7.8 Hz, 2H), 7.75 (td, *J* = 7.7, 1.7 Hz, 1H), 7.46 – 7.31 (m, 2H), 5.30 – 5.22 (m, 1H), 5.04 (qd, *J* = 10.9, 4.3 Hz, 2H), 4.52 (dd, *J* = 6.0, 1.8 Hz, 2H), 4.39 – 4.22 (m, 5H), 4.09 (dd, *J* = 13.1, 5.5 Hz, 1H), 3.93 – 3.77 (m, 1H), 2.24 – 2.18 (m, 2H), 2.05 – 1.94 (m, 2H), 1.80 – 1.72 (m, 4H), 1.62 – 1.50 (m, 5H), 1.33 (s, 3H), 1.23 – 1.06 (m, 5H), 1.04 – 0.77 (m, 22H). ^{13}C NMR (101 MHz, $CDCl_3$) δ 173.0, 168.2, 165.9, 149.4, 140.2, 138.2, 134.9, 134.4, 128.1, 127.2, 123.6, 80.9, 77.0, 70.7, 55.0, 48.4, 42.0, 40.5, 35.6, 32.8, 32.4, 27.7, 24.6, 23.4, 22.2, 17.5. IR (cm $^{-1}$): 3338, 2954, 2869, 1717, 1678, 1511, 1454, 1229, 1143, 1091, 980, 831, 729. HRMS *calcd.* for ($C_{42}H_{58}N_2O_8$): 718.4193, *found* 718.4179.

3.5.2. C(sp^2)-H Alkoxycarbonylation of Benzylamine and Phenylethylamines

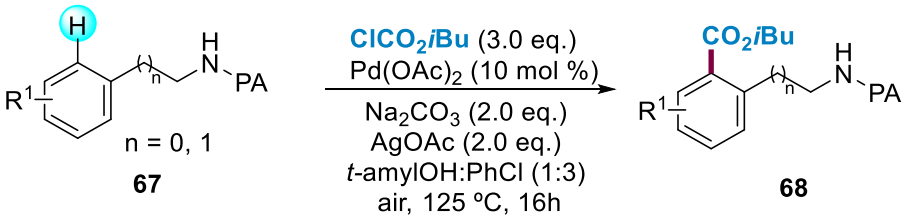

General procedure: A reaction tube containing a stirring bar was charged with **67** (0.25 mmol, 1 eq.), AgOAc (0.50 mmol, 2 eq.), Na_2CO_3 (0.50 mmol, 2 eq.) and $Pd(OAc)_2$ (10 mol %). Then, isobutyl chloroformate (0.75 mmol, 3 eq.) and a mixture of solvents (*t*-amylOH:PhCl, 1:3) (4 mL) were added by syringe under air. The reaction tube was warmed up to 125 ºC and stirred for 16 hours. The mixture was allowed to cool to room temperature, concentrated under reduced pressure and the product was purified by column chromatography.

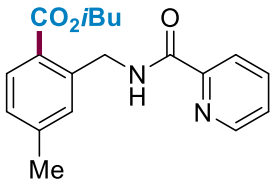

(68d)

Isobutyl 4-methyl-2-(picolinamidomethyl)benzoate (68d). Following the general procedure, using commercially available isobutyl chloroformate (0.75 mmol, 97 µL) and picolinamide **67d**[153] (0.25 mmol, 57 mg) provided 46 mg (56 % yield) of **68d** as a white solid. Mp 96-97 ºC. ^{1}H NMR (400 MHz, $CDCl_3$) δ 9.02 (brs, 1H), 8.56 (d, *J* = 5.0 Hz, 1H), 8.21 (d, *J* = 7.8 Hz, 1H), 7.93 (d, *J* = 8.0 Hz, 1H), 7.83 (td, *J* = 7.7, 1.7 Hz, 1H), 7.44 (s, 1H), 7.40 (ddd, *J* = 7.6, 4.8, 1.3 Hz, 1H), 7.18 (d, *J* = 7.0 Hz, 1H), 4.89 (d, *J* = 6.7 Hz, 2H), 4.17 (d, *J* = 6.6 Hz, 2H), 2.39 (s, 3H), 2.14 (dp, *J* = 13.4, 6.7 Hz, 1H), 1.05 (d, *J* = 6.7 Hz, 6H). ^{13}C NMR (101 MHz, $CDCl_3$) δ 167.4, 164.0, 150.1, 148.1, 143.4, 139.8, 137.1, 132.0, 131.0, 128.3, 126.5, 125.9, 122.2, 71.1, 42.4, 27.8, 21.4, 19.2. IR (cm $^{-1}$): 3412, 2947, 1701, 1671, 1504, 1429, 1263, 1232, 1152, 1079, 989, 745, 616. HRMS *calcd.* for ($C_{19}H_{22}N_2O_3$): 326.1630, *found* 326.1646.

[153] Ling, F.; Ai, C.; Lv, Y.; Zhong, W. *Adv. Synth. Catal.* **2017**, *359*, 3707.

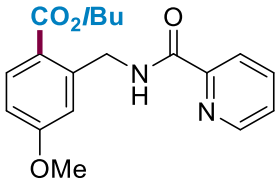

(68b)

Isobutyl 4-methoxy-2-(picolinamidomethyl)benzoate (68b). Following the general procedure, using commercially available isobutyl chloroformate (0.75 mmol, 97 µL) and picolinamide **67b**[154] (0.25 mmol, 61 mg) provided 40 mg (46 % yield) of **68b** as a white solid. Mp 78-79 ºC. ^{1}H NMR (400 MHz, $CDCl_3$) δ 9.15 – 8.90 (m, 1H), 8.56 (d, *J* = 4.0 Hz, 1H), 8.19 (d, *J* = 7.8 Hz, 1H), 8.01 (d, *J* = 8.7 Hz, 1H), 7.82 (td, *J* = 7.7, 1.7 Hz, 1H), 7.39 (ddd, *J* = 7.6, 4.8, 1.2 Hz, 1H), 7.13 (d, *J* = 2.6 Hz, 1H), 6.85 (dd, *J* = 8.8, 2.7 Hz, 1H), 4.91 (d, *J* = 6.7 Hz, 2H), 4.14 (d, *J* = 6.6 Hz, 2H), 3.85 (s, 3H), 2.28 – 1.99 (m, 1H), 1.04 (d, *J* = 6.7 Hz, 6H). ^{13}C NMR (101 MHz, $CDCl_3$) δ 166.9, 164.0, 162.7, 150.0, 148.1, 142.4, 137.1, 133.1, 125.9, 122.2, 121.3, 116.2, 112.8, 71.0, 55.4, 42.6, 27.8, 19.2. IR (cm $^{-1}$): 3460, 3391, 2957, 1695, 1663, 1514, 1430, 1253, 1145, 1084, 981, 747, 619. HRMS *calcd.* for ($C_{19}H_{22}N_2O_4$): 342.1580, *found* 342.1572.

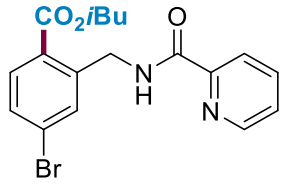

(68c)

Isobutyl 4-bromo-2-(picolinamidomethyl)benzoate (68c). Following the general procedure, using the commercially available isobutyl chloroformate (0.75 mmol, 97 µL) and picolinamide **67c**[155] (0.25 mmol, 73 mg) provided 35 mg (36 % yield) of **68c** as a white solid. Mp 84-85 ºC. ^{1}H NMR (400 MHz, $CDCl_3$) δ 8.94 (brs, 1H), 8.60 – 8.55 (m, 1H), 8.21 (d, *J* = 7.8 Hz, 1H), 7.93 – 7.83 (m, 2H), 7.80 (d, *J* = 2.0 Hz, 1H), 7.51 (dd, *J* = 8.4, 2.1 Hz, 1H), 7.43 (ddd, *J* = 7.6, 4.8, 1.2 Hz, 1H), 4.90 (d, *J* = 6.7 Hz, 2H), 4.18 (d, *J* = 6.6 Hz, 2H), 2.14 (dp, *J* = 13.4, 6.7 Hz, 1H), 1.06 (d, *J* = 6.7 Hz, 6H). ^{13}C NMR (101 MHz, $CDCl_3$) δ 166.7, 164.2, 149.8, 148.2, 141.8, 137.2, 133.9, 132.3, 130.8, 128.1, 127.5, 126.1, 122.3, 71.5, 41.9, 27.8, 19.2. IR (cm $^{-1}$): 3390, 2955, 1708, 1667, 1587, 1503, 1262, 1096, 998, 715, 661. HRMS *calcd.* for ($C_{18}H_{19}BrN_2O_3$): 390.0579, *found* 390.0572.

[154] Karmakar, U.; Samanta, R. *J. Org. Chem.* **2019**, *84*, 2850.
[155] Manu-Martínez, A.; Echavarren, J.; Alonso, I.; Rodriguez, N.; Arrayás, R. G.; Carretero, J. C. *Chem. Sci.* **2015**, *6*, 5802.

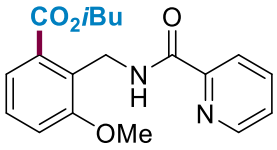

(68a)

Isobutyl 3-methoxy-2-(picolinamidomethyl)benzoate (68a). Following the general procedure, using the commercially available isobutyl chloroformate (0.75 mmol, 97 µL) and picolinamide **67a**[154] (0.25 mmol, 61 mg) provided 65 mg of **68a** (76 % yield) as an orange solid. Mp 74-75 ºC. ^{1}H NMR (400 MHz, $CDCl_3$) δ 8.67 (brs, 1H), 8.52 (d, *J* = 4.9 Hz, 1H), 8.22 (d, *J* = 7.8 Hz, 1H), 7.81 (td, *J* = 7.7, 1.7 Hz, 1H), 7.47 (d, *J* = 6.6 Hz, 1H), 7.43 – 7.25 (m, 2H), 7.09 (dd, *J* = 8.3, 1.1 Hz, 1H), 4.98 (d, *J* = 6.1 Hz, 2H), 4.16 (d, *J* = 6.7 Hz, 2H), 3.92 (s, 3H), 2.10 (dp, *J* = 13.4, 6.7 Hz, 1H), 1.01 (d, *J* = 6.7 Hz, 6H). ^{13}C NMR (101 MHz, $CDCl_3$) δ 168.2, 163.8, 158.6, 150.6, 148.2, 137.4, 133.0, 128.8, 127.3, 126.0, 122.6, 122.4, 114.7, 71.9, 56.5, 35.1, 28.0, 19.5. IR (cm $^{-1}$): 3402, 2955, 1706, 1673, 1587, 1506, 1460, 1431, 1370, 1270, 1064, 998, 759, 660. HRMS *calcd*. for ($C_{19}H_{22}N_2O_4$): 342.1580, *found* 342.1572.

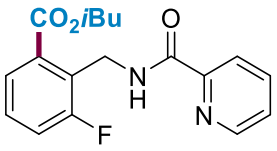

(68e)

Isobutyl 3-fluoro-2-(picolinamidomethyl)benzoate (68e). Following the general procedure, using commercially available isobutyl chloroformate (0.75 mmol, 97 µL) and picolinamide **67e**[155] (0.25 mmol, 57.6 mg) provided 50 mg (61 % yield) of **68e** as a white solid. Mp 87-88 ºC. ^{1}H NMR (400 MHz, $CDCl_3$) δ 8.85 (brs, 1H), 8.53 (d, *J* = 1.6 Hz, 1H), 8.20 (d, *J* = 7.9 Hz, 1H), 7.81 (td, *J* = 7.7, 1.7 Hz, 1H), 7.76 (d, *J* = 7.8 Hz, 1H), 7.45 – 7.22 (m, 3H), 4.98 (d, *J* = 4.7 Hz, 2H), 4.18 (d, *J* = 6.7 Hz, 2H), 2.12 (dp, *J* = 13.4, 6.8 Hz, 1H), 1.02 (d, *J* = 6.7 Hz, 6H). ^{13}C NMR (101 MHz, $CDCl_3$) δ 166.7 (d, *J* = 3.6 Hz), 163.6, 161.1 (d, *J* = 248.5 Hz), 149.9, 148.0, 137.1, 132.3 (d, *J* = 3.4 Hz), 128.9 (d, *J* = 8.8 Hz), 126.4 (d, *J* = 17.1 Hz), 126.3 (d, *J* = 3.6 Hz), 125.9, 122.2, 119.6 (d, *J* = 23.7 Hz), 71.7, 33.7 (d, *J* = 6.5 Hz), 27.7, 19.1. IR (cm $^{-1}$): 3392, 2961, 1701, 1677, 1511, 1461, 1275, 1051, 1008, 819, 751, 669. HRMS *calcd.* for ($C_{18}H_{19}FN_2O_3$): 330.1380, *found* 330.1378.

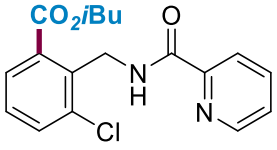

(68f)

Isobutyl 3-chloro-2-(picolinamidomethyl)benzoate (68). Following the general procedure, using commercially available isobutyl chloroformate (0.75 mmol, 97 µL) and picolinamide **67f**[154] (0.25 mmol, 61 mg) provided 65 mg (76 % yield) of **68f** as a white solid. Mp 58-59 ºC. ^{1}H NMR (400 MHz, $CDCl_3$) δ 8.69 (brs, 1H), 8.52 (d, *J* = 4.3 Hz, 1H), 8.21 (d, *J* = 7.8 Hz, 1H), 7.87 – 7.74 (m, 2H), 7.58 (d, *J* = 3.8 Hz, 1H), 7.44 – 7.35 (m, 1H), 7.32 (t, *J* = 7.9 Hz, 1H), 5.07 (d, *J* = 6.1 Hz, 2H), 4.17 (d, *J* = 6.7 Hz, 2H), 2.10 (dp, *J* = 13.4, 6.7 Hz, 1H), 1.01 (d, *J* = 6.7 Hz, 6H). ^{13}C NMR (101 MHz, $CDCl_3$) δ 167.2, 163.5, 149.8, 147.9, 137.2, 136.3, 136.0, 133.6, 133.3, 128.8, 128.6, 125.9, 122.3, 71.9, 38.5, 27.7, 19.1. IR (cm $^{-1}$): 3407, 2963, 1708, 1677, 1507, 1433, 1264, 1189, 988, 816, 621. HRMS *calcd.* for ($C_{18}H_{19}ClN_2O_3$): 346.1084, *found* 346.1076.

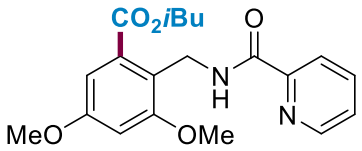

(68g)

Isobutyl 3,5-dimethoxy-2-(picolinamidomethyl)benzoate (68g). Following the general procedure, using commercially available isobutyl chloroformate (0.75 mmol, 97 µL) and picolinamide **67g**[153] (0.25 mmol, 68 mg) provided 45 mg (48 % yield) of **68g** as an orange oil. ^{1}H NMR (400 MHz, $CDCl_3$) δ 8.55 (brs, 1H), 8.50 (d, *J* = 4.1 Hz, 1H), 8.20 (d, *J* = 7.8 Hz, 1H), 7.80 (td, *J* = 7.7, 1.7 Hz, 1H), 7.36 (ddd, *J* = 7.6, 4.8, 1.3 Hz, 1H), 6.97 (d, *J* = 2.5 Hz, 1H), 6.63 (d, *J* = 2.5 Hz, 1H), 4.87 (d, *J* = 5.9 Hz, 2H), 4.15 (d, *J* = 6.7 Hz, 2H), 3.87 (s, 3H), 3.83 (s, 3H), 2.09 (dp, *J* = 13.4, 6.7 Hz, 1H), 0.99 (d, *J* = 6.8 Hz, 6H). ^{13}C NMR (101 MHz, $CDCl_3$) δ 167.8, 163.4, 159.6, 159.3, 150.3, 147.9, 137.0, 133.2, 125.6, 122.1, 119.6, 105.7, 102.0, 71.6, 56.1, 55.4, 34.5, 27.6, 19.1. IR (cm $^{-1}$): 3399, 2960, 1712, 1673, 1602, 1512, 1460, 1320, 1207, 1144, 1063, 749, 620. HRMS *calcd.* for ($C_{20}H_{24}N_2O_5$): 372.1685, *found* 372.1685.

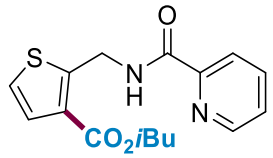

(68h)

Isobutyl 2-(picolinamidomethyl)thiophene-3-carboxylate (68h). Following the general procedure, using commercially available isobutyl chloroformate (0.75 mmol, 97 µL) and picolinamide **68h**[154] (0.25 mmol, 55 mg) provided 23 mg (29 % yield) of **68h** as a yellowish oil. ^{1}H NMR (400 MHz, $CDCl_3$) δ 8.89 (brs, 1H), 8.58 (d, *J* = 4.7 Hz, 1H), 8.23 (d, *J* = 7.9 Hz, 1H), 7.86 (td, *J* = 7.7, 1.7 Hz, 1H), 7.56 – 7.39 (m, 2H), 7.14 (d, *J* = 5.4 Hz, 1H), 5.12 (d, *J* = 6.5 Hz,

2H), 4.14 (d, *J* = 6.6 Hz, 2H), 2.12 (dp, *J* = 13.4, 6.7 Hz, 1H), 1.05 (d, *J* = 6.7 Hz, 6H). ^{13}C NMR (101 MHz, $CDCl_3$) δ 164.1, 163.4, 149.6, 149.5, 148.1, 137.2, 129.2, 126.2, 123.0, 122.4, 70.9, 36.9, 27.8, 19.2. IR (cm $^{-1}$): 3385, 2960, 1672, 1510, 1463, 1258, 1168, 1088, 1007, 703. HRMS *calcd.* for ($C_{16}H_{18}N_2O_3S$): 318.1038, *found* 318.1033.

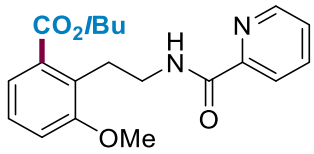

(68j)

Isobutyl 3-methoxy-2-[2-(picolinamido)ethyl]benzoate (68j). Following the general procedure, using commercially available isobutyl chloroformate (0.75 mmol, 97 µL) and picolinamide **67j**[153] (0.25 mmol, 64 mg) provided 24 mg (28 % yield) of **68j** as a yellow oil. ^{1}H NMR (400 MHz, $CDCl_3$) δ 8.60 – 8.52 (m, 2H), 8.18 (d, *J* = 7.8 Hz, 1H), 7.83 (td, *J* = 7.7, 1.7 Hz, 1H), 7.48 (d, *J* = 7.8, 1H), 7.40 (ddd, *J* = 7.6, 4.7, 1.3 Hz, 1H), 7.33 – 7.19 (m, 1H), 7.05 (d, *J* = 7.1 Hz, 1H), 4.11 (d, *J* = 6.7 Hz, 2H), 3.89 (s, 3H), 3.78 (q, *J* = 6.7, 5.5 Hz, 2H), 3.38 (t, *J* = 6.7 Hz, 2H), 2.09 (dp, *J* = 13.4, 6.7 Hz, 1H), 1.03 (d, *J* = 6.7 Hz, 6H). ^{13}C NMR (101 MHz, $CDCl_3$) δ 167.7, 164.3, 158.0, 150.2, 147.8, 137.1, 132.0, 129.3, 127.1, 125.7, 122.3, 122.1, 113.4, 71.2, 55.7, 40.1, 27.8, 25.9, 19.2. IR (cm $^{-1}$): 3358, 2959, 2873, 1712, 1671, 1587, 1568, 1522, 1460, 1268, 1245, 1069, 749. HRMS *calcd.* for ($C_{20}H_{24}N_2O_4$): 356.1736, *found* 356.1726.

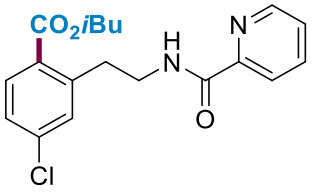

(68k)

Isobutyl 4-chloro-2-[2-(picolinamido)ethyl]benzoate (68k). Following the general procedure, using commercially available isobutyl chloroformate (0.75 mmol, 97 µL) and picolinamide **67k** (0.25 mmol, 65 mg) provided 26 mg (29 % yield) of **68k** as a colorless oil. ^{1}H NMR (400 MHz, $CDCl_3$) δ 8.60 – 8.53 (m, 1H), 8.31 (brs, 1H), 8.20 (d, *J* = 8.1 Hz, 1H), 7.92 (d, *J* = 8.4 Hz, 1H), 7.86 (td, *J* = 7.7, 1.7 Hz, 1H), 7.47 – 7.41 (m, 1H), 7.36 (d, *J* = 2.1 Hz, 1H), 7.31 – 7.23 (m, 1H), 4.11 (d, *J* = 6.7 Hz, 2H), 3.78 (q, *J* = 6.0 Hz, 2H), 3.33 (t, *J* = 7.1 Hz, 2H), 2.09 (dp, *J* = 13.4, 6.7 Hz, 1H), 1.03 (d, *J* = 6.7 Hz, 6H). ^{13}C NMR (101 MHz, $CDCl_3$) δ 166.8, 164.7, 150.1, 148.3, 143.4, 138.5, 137.6, 132.6, 131.9, 128.4, 127.1, 126.3, 122.4, 71.6, 40.8, 34.4, 28.1, 19.5. IR (cm

$^{-1}$): 3383, 29601714, 1671, 1521, 1464, 1368, 1253, 1104, 1082, 748, 620. HRMS *calcd.* for ($C_{19}H_{21}ClN_2O_3$): 360.1241, *found* 360.1238.

3.5.3. Removal of the Picolinamide Directing Group

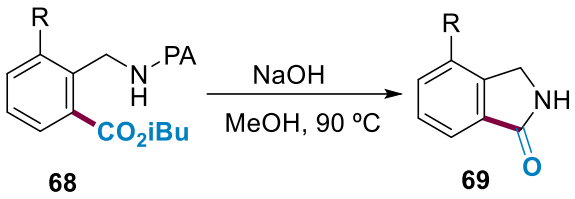

68 **69**

General procedure: A reaction tube containing a stirring bar was charged with **68** (1 eq.) and NaOH (4.0 eq.) in MeOH (15 mL/mmol). The reaction tube was warmed up to 90 ºC and stirred for 16 hours. The mixture was allowed to cool to room temperature, treated with HCl (5%) and extracted with EtOAc (three times). The resulting organic solution was concentrated under reduced pressure and the product was purified by column chromatography.

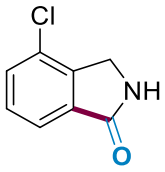

(69a)

4-Chloroisoindolin-1-one (69a). Following the general procedure, using compound **68f** (0.34 mmol, 118 mg) provided 48 mg (84 % yield) of **69a** as a white solid. The spectroscopic data correspond to those previously reported in the literature.[156] ^{1}H NMR (400 MHz, $CDCl_3$) δ 7.81 (d, *J* = 7.5, 1H), 7.58 (dd, *J* = 7.9, 1H), 7.49 (t, *J* = 7.7 Hz, 1H), 7.40 (brs, 1H), 4.48 (s, 2H). ^{13}C NMR (101 MHz, $CDCl_3$) δ 170.8, 141.6, 134.1, 131.7, 129.7, 129.4, 122.22, 44.8.

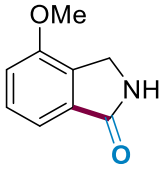

(69b)

[156] Zhang, C.; Ding, Y.; Gao, Y.; Li, S.; Li, G. *Org. Lett.* **2018**, *20*, 2595.

4-Methoxyisoindolin-1-one (69b). Following the general procedure, using compound **68a** (0.30 mmol, 103 mg) provided 39 mg (80 % yield) of **69b** as a white solid. The spectroscopic data correspond to those previously reported in the literature.[156] ^{1}H NMR (500 MHz, $CDCl_3$) δ 8.02 (s, 1H), 7.52 – 7.35 (m, 2H), 7.01 (d, *J* = 7.5 Hz, 1H), 4.39 (s, 2H), 3.89 (s, 3H) .^{13}C NMR (126 MHz, $CDCl_3$) δ 172.4, 154.9, 133.9, 132.0, 129.7, 115.7, 112.9, 55.5, 43.8.

3.5.4.-Determination of *ee* by HPLC Analysis

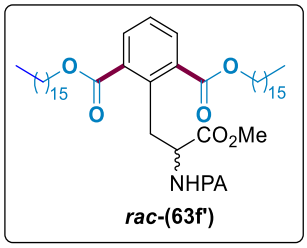

rac-(63f')

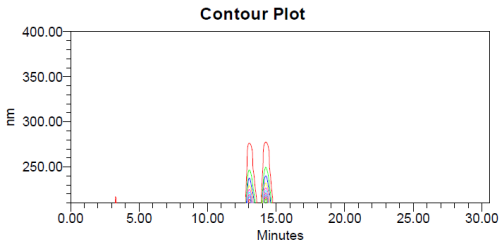

Peak Results

	Name	RT	Area	% Area
1		13.034	18067750	46.06
2		14.237	21160443	53.94

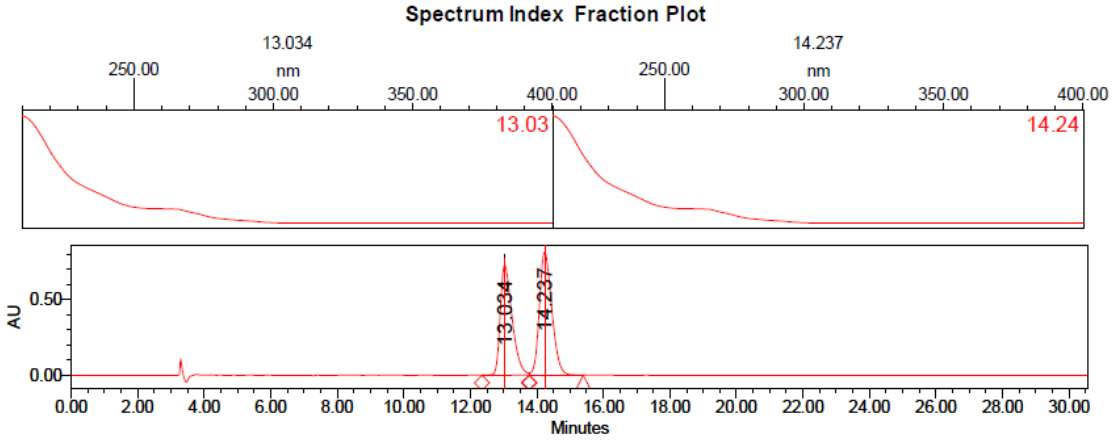

Conditions : Chiralpak IC; Hexane: isopropanol 90/10; 1 mL/min, λ = 220 nm

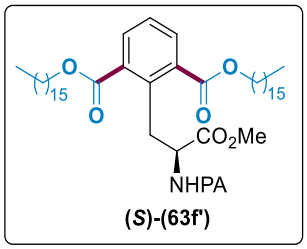

(*S*)-(63f')

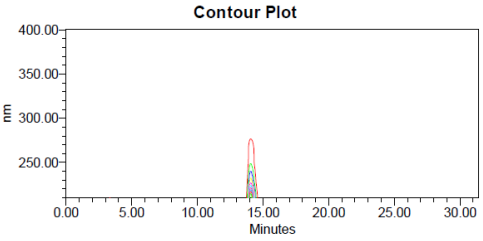

Peak Results

	Name	RT	Area	% Area
1		14.056	26635541	100.00

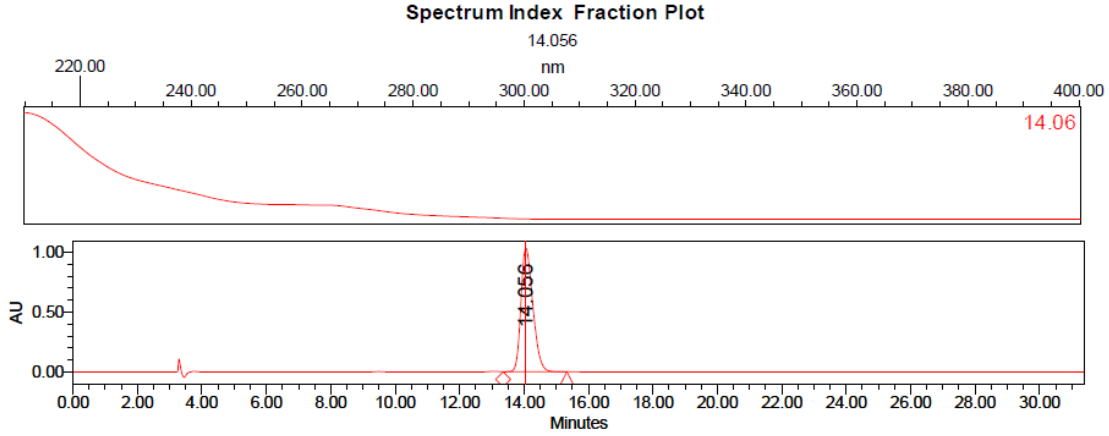

Chapter 4.

Ru-Catalyzed C–H Hydroxylation of Tyrosine-Containing Di- and Tripeptides toward the Assembly of L-DOPA derivatives

ABSTRACT: The development of catalytic tools for the late-stage modification of amino acids within a peptide framework is a challenging task of capital importance. Herein, we report a Ru-catalyzed C(sp^2)–H hydroxylation of a collection of Tyr-containing di- and tripeptides featuring the use of a carbamate as a removable directing group and $PhI(OCOCF_3)_2$ (PIFA) as oxidant. This air-compatible tagging technique is reliable, scalable and provides access to L-DOPA peptidomimetics in a racemization-free fashion. Density Functional Theory calculations support a Ru(II)/Ru(IV) catalytic cycle.

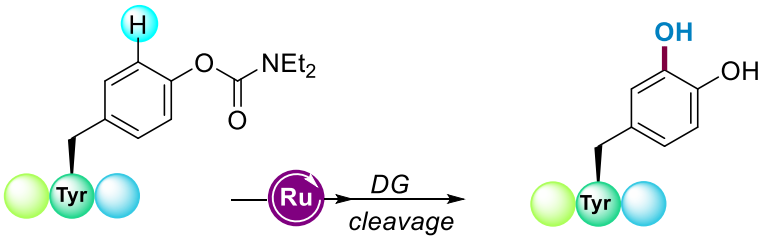

✓ *Removable directing group*
✓ *Late-stage peptide hydroxylation*
✓ *L-DOPA compounds*
✓ *DFT studies*

4.1. Introduction

As mentioned in the previous chapter, the modification of Tyr derivatives has received considerable attention owing to the innate nucleophilic character of the aromatic ring, which has a unique reactivity due to the acidic proton of the phenol. Accordingly, several diversification protocols have been published exploiting nucleophile-electrophile interactions.[157] However, the scope of these transformations is very limited. In contrast, transition-metal catalysis offers new opportunities for the modification of Tyr-containing molecules.

Regarding transition metal mediated-reactions, the existing strategies for the C–H functionalization of Tyr derivatives could be classified into two general categories: Upon chelation assistance and exploiting the innate reactivity of the phenol ring as the DG.[158] Depending on the location of the DG within the Tyr unit, the chelation strategy could be classified in two general types. On the one hand, the DG could be installed at the nitrogen atom of the *N*-terminal position of the peptide backbone and the complexation of the metal is directed toward the δ-C(sp^2)–H bond. On the other hand, if the DG is installed within the phenol ring of the amino acid side-chain the reactivity is often directed to the ε-C(sp^2)–H position (Figure 20).

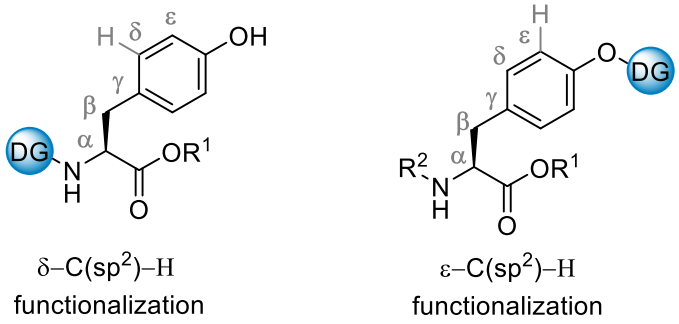

Figure 20. Site-selectivity controlled by the position of the DG.

[157] For selected examples, see: a) Joshi, N. S.; Whitaker, L. R.; Francis, M. B. *J. Am. Chem. Soc.* **2004**, *126*, 15943. b) Ban, H.; Gavrilyuk, J.; Barbas, C. F. *J. Am. Chem. Soc.* **2010**, *132*, 1523. c) Jones, M. W.; Mantovani, G.; Blindauer, C. A.; Ryan, S. M.; Wang, X.; Brayden, D. J.; Haddleton, D. M. *J. Am. Chem. Soc.* **2012**, *134*, 7406. d) Wadzinski, T. J.; Steinaver, A.; Hie, L.; Pelletier, G.; Schepartz, A.; Miller, S. J. *Nat. Chem.* **2018**, *10*, 644.

[158] For selected examples on phenol-directed C–H functionalization with transition metals, see: a) Ben-Lulu, M.; Gaster, E.; Libman, A.; Pappo, D. *Angew. Chem. Int. Ed.* **2020**, *59*, 4835. b) Ichiishi, N.; Caldwell, J. P.; Liu, M.; Zhong, W.; Zhu, X.; Streckfuss, E.; Kim, H.-Y.; Parish, C. A.; Krska, S. W. *Chem. Sci.* **2018**, *9*, 4168. c) Bedford, R. B.; Haddow, M. F.; Webster, R. C.; Mitchell, C. J. *Org. Biomol. Chem.* **2009**, 7, 3119. d) Dou, Y.; Kenry.; Liu, J.; Jiang, J.; Zhu, Q. *Chem. Eur. J.* **2019**, *25*, 6896. e) Song, C.; Liu, K.; Wang, Z.; Ding, B.; Wang, S.; Weng, Y.; Chiang, C.-W.; Lei, A. *Chem. Sci.* **2019**, *10*, 7982

Indeed, several strategies that have been applied for the δ-C(sp^2)–H functionalization of Phe derivatives bearing a DG within the nitrogen atom have also been utilized for the diversification of Tyr containing compounds. Even if only isolated examples could be found on the following works, some of the arylation,[81,84] alkenylation,[91,92,97,98b] amination,[111,113a,114,115,116] acetoxylation[122] and halogenation[104,106] protocols explained on the previous chapter have been successfully applied for the diversification of O-protected Tyr derivatives. However, these strategies are limited to the modification of molecules containing the Tyr unit within the *N*-terminal position of the peptide sequence (Figure 21).

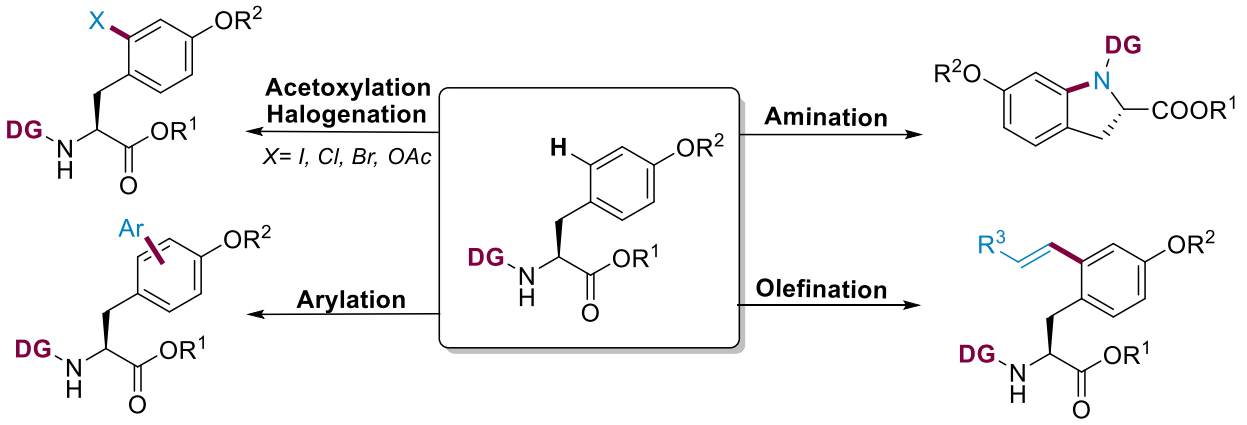

Figure 21. Summary of different strategies for the δ-C(sp^2)–H functionalization of Tyr derivatives

Besides these strategies, Ma[159] developed a general strategy for the *ortho*-alkenylation and alkylation of Tyr derivatives using a picolinamide as the DG (Scheme 72). Combining $Pd(OAc)_2$ as catalyst and K_2CO_3 as base, the alkylation protocol provided the difunctionalized Tyr derivatives **2** with excellent yields and selectivity. Nevertheless, the scope was limited to methyl iodide and the protocol was not implemented to more complex peptide sequences.

[159] Wang, X.; Niu, S.; Xu, L.; Zhang, C.; Meng, L.; Zhang, X.; Ma, D. *Org. Lett.* **2017**, *19*, 246.

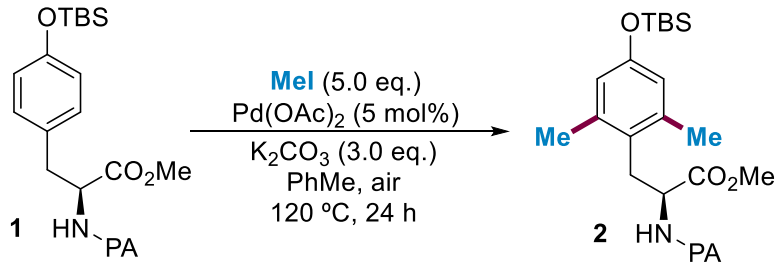

Scheme 72. Alkylation of O-protected Tyr derivatives developed by Ma and co-workers.

More recently, different strategies have been developed by introducing a chelating group into the phenol ring within the Tyr unit. This approach offers new opportunities to easily synthesize new Tyr derivatives that could not be synthesized upon the above-mentioned methodologies.

4.1.1. ε-C(sp^2)–H Functionalization Using O-Chelating DGs

4.1.1.1. C(sp^2)–H Acylation of Tyr Derivatives

Encouraged by previous results on Pd-catalyzed C(sp^2)–H acylation of Phe derivatives, our group expanded the protocol for the diversification of Tyr-containing oligopeptides by introducing the 2-pyridine unit as a chelating DG (Scheme 73).[160] Notably, this method was found to be compatible with water and the addition of silver salts was not required. Using catalytic amounts of $Pd(OAc)_2$ and an aqueous solution of TBHP as the only oxidant, a wide variety of biologically relevant oligopeptides underwent the acylation reaction in very good yields. The robustness of the method was demonstrated by synthesizing unprecedented oligopeptides bearing unique diaryl ketone cross-linking through chemical ligation (**4e**).

[160] San Segundo, M.; Correa, A. *Chem. Sci.* **2020**, *11*, 11531.

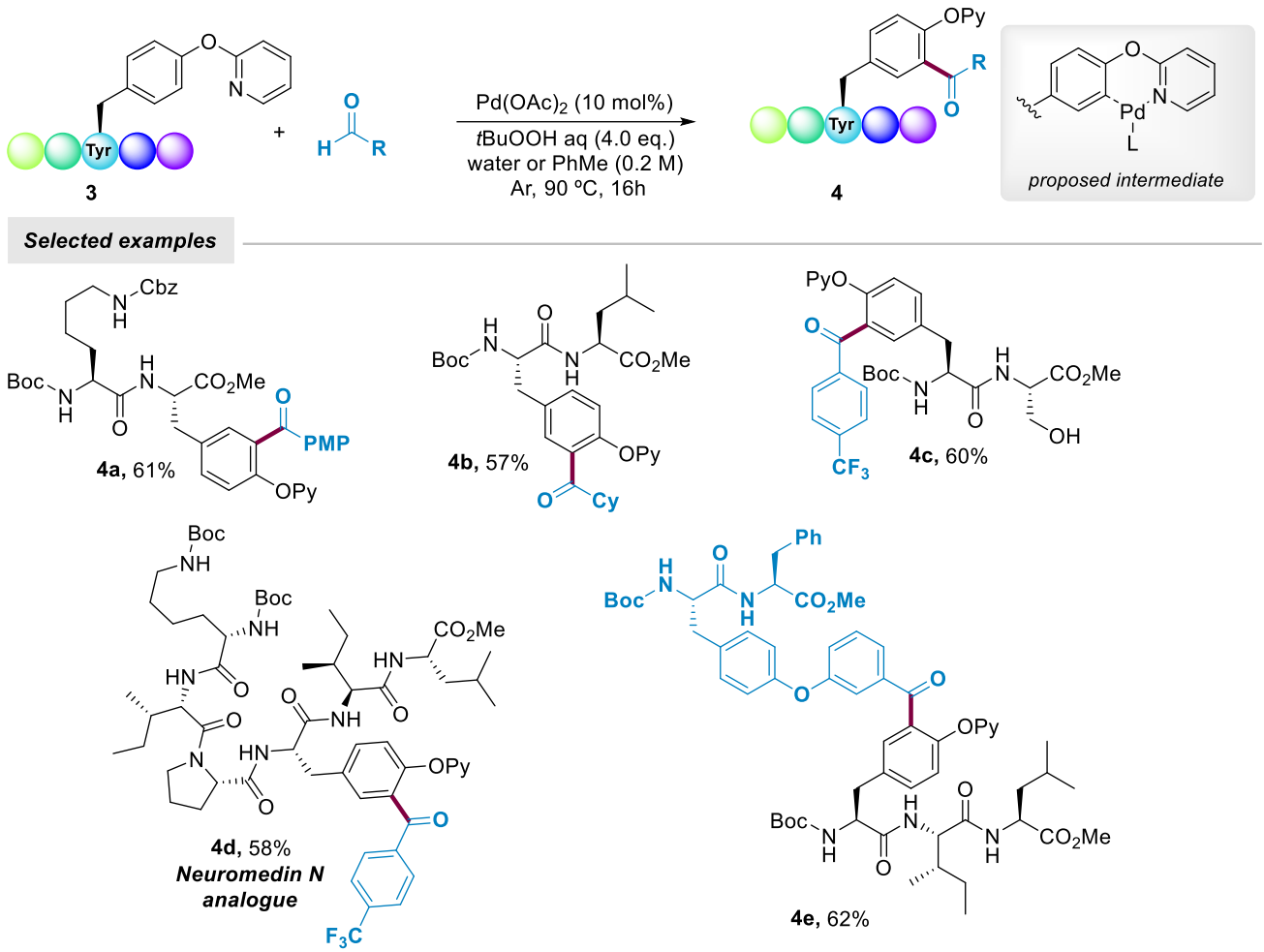

Scheme 73. C(sp^2)–H acylation protocol developed by Correa and co-workers.

More recently, our group has expanded the methodology toward the late-stage acetylation of complex peptides using simple alcohols as cheap and sustainable feedstocks (Scheme 74).[161] This protocol represents an attractive alternative to the classical Friedel-Crafts acylation reaction, which features the use of corrosive AcCl and stoichiometric amounts of $AlCl_3$. Moreover, the classical approach can not be applied to peptide sequences. Based on some mechanistic experiments, it is likely that the EtOH was *in situ* transformed into MeCHO prior to the addition to the metal center and the addition of the alcohol radical to the metal center followed by the oxidation to the carbonyl group was discarded. The high selectivity toward the monoacetylation could be due to the lower reactivity of EtOH in comparison to the parent aldehydes.

[161] Urruzuno, I.; Andrade-Sampedro, P.; Correa, A. *Org. Lett.* **2021**, *23*, 7279.

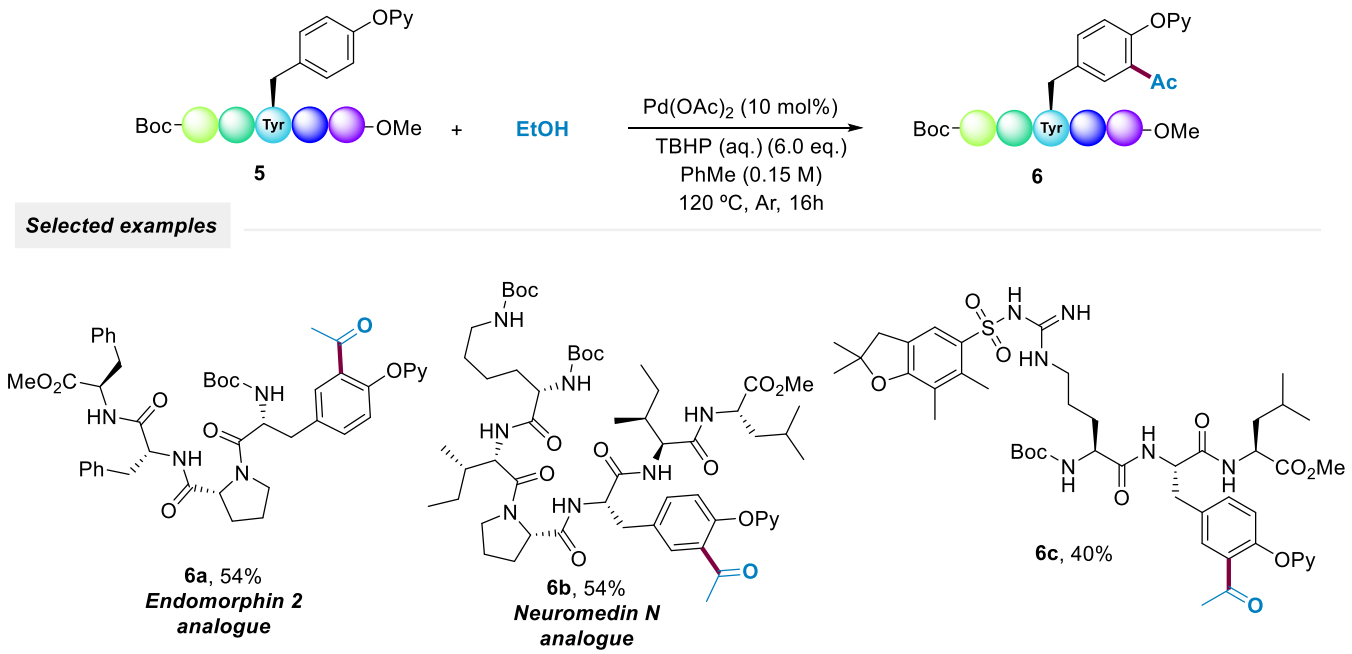

Scheme 74. Pd-catalyzed C(sp²)–H acetylation with simple EtOH.

4.1.1.2. C(sp²)–H Olefination of Tyr Derivatives

In 2020, Xiong and co-workers reported the first Pd-catalyzed olefination of Tyr derivatives by using a silanol as the DG (Scheme 75).[162] The authors suggested that the high chemo- and site-selectivity of the method relied on the bulkiness of the DG. Under the optimized reaction conditions, a wide range of activated alkenes were introduced in the *ortho* position in moderate to good yields. The method was found to be compatible with peptides bearing functional groups within the side-chain and could be applied to more complex peptide sequences, albeit with lower yields. Nevertheless, the authors did not detect any byproduct resulting from the backbone directed *meta*-olefination, which evidences the superior coordinating ability of the silanol PG. However, the significant loss of yield of peptide sequences could be attributed to the formation of a kinetically less favored six-membered metallacycle rather than the peptide backbone.

[162] Hu, Q.-L.; Hou, K.-Q.; Li, J.; Ge, Y.; Song, Z.-D.; Chan, A. S. C.; Xiong, X.-F. *Chem. Sci.* **2020**, *11*, 6070.

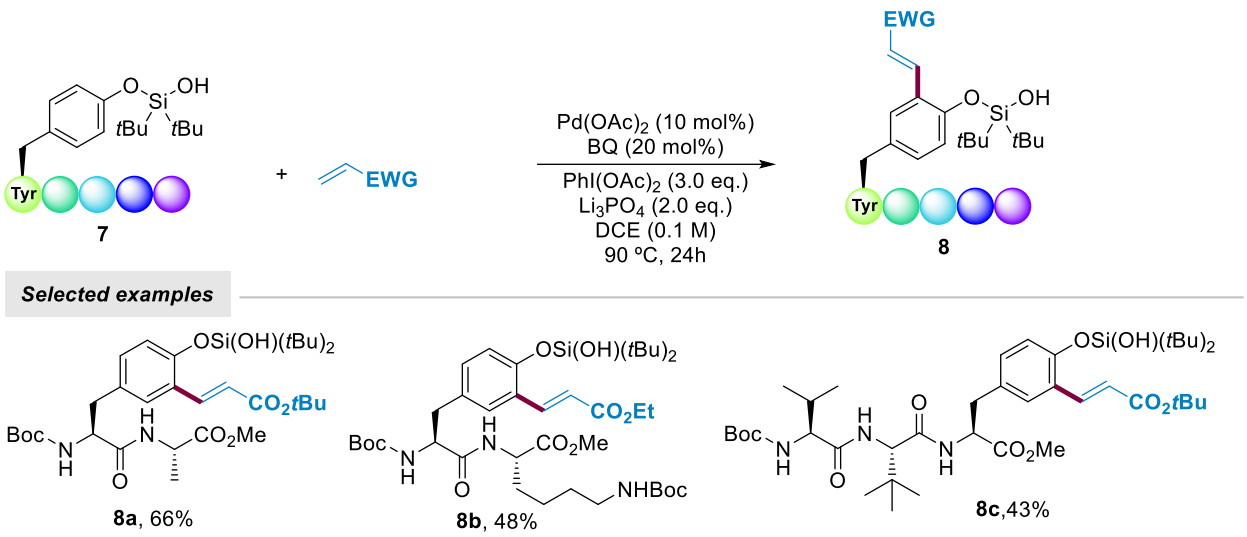

Scheme 75. Silanol-directed alkenylation of Tyr-containing oligopeptides

4.1.1.3. C(sp^2)–H Acyloxylation of Tyr Derivatives

In 2022, the group of Ackermann disclosed the first electrochemical acyloxylation of phenols for the late-stage functionalization of Tyr-containing peptides (Scheme 76).[163] Using an undivided cell setup equipped with grafite and platinum in combination with Ru catalysis, electron-rich and electron-deficient carboxylic acids were coupled with different phenols and with various di-, tri- and tetrapeptides in good yields. Notably, this method avoided the use of chemical oxidants and further studies enabled the efficient removal of the directing group. In order to gain some insights about the reaction mechanisms, some mechanistic experiments as well as DFT calculations were conducted by the authors. On the basis of their findings, the authors proposed the reaction mechanism depicted on Scheme 76. The reaction would start with two subsequent BIES C–H activation step in which two *p*-cymene ligands are dissociated, thus forming the bis-cyclometalated complex **I**. This species could undergo an anode mediated oxidation to deliver the Ru^{IV} complex **II**. Finally, a reductive elimination followed by a ligand exchange would deliver the targeted product **10** and regenerate the active catalyst.

[163] Hou, X.; Kaplaneris, N.; Yuan, B.; Frey, J.; Ohyama, T.; Messinis, A. M.; Ackermann, L. *Chem. Sci.* **2022**, *13*, 3461.

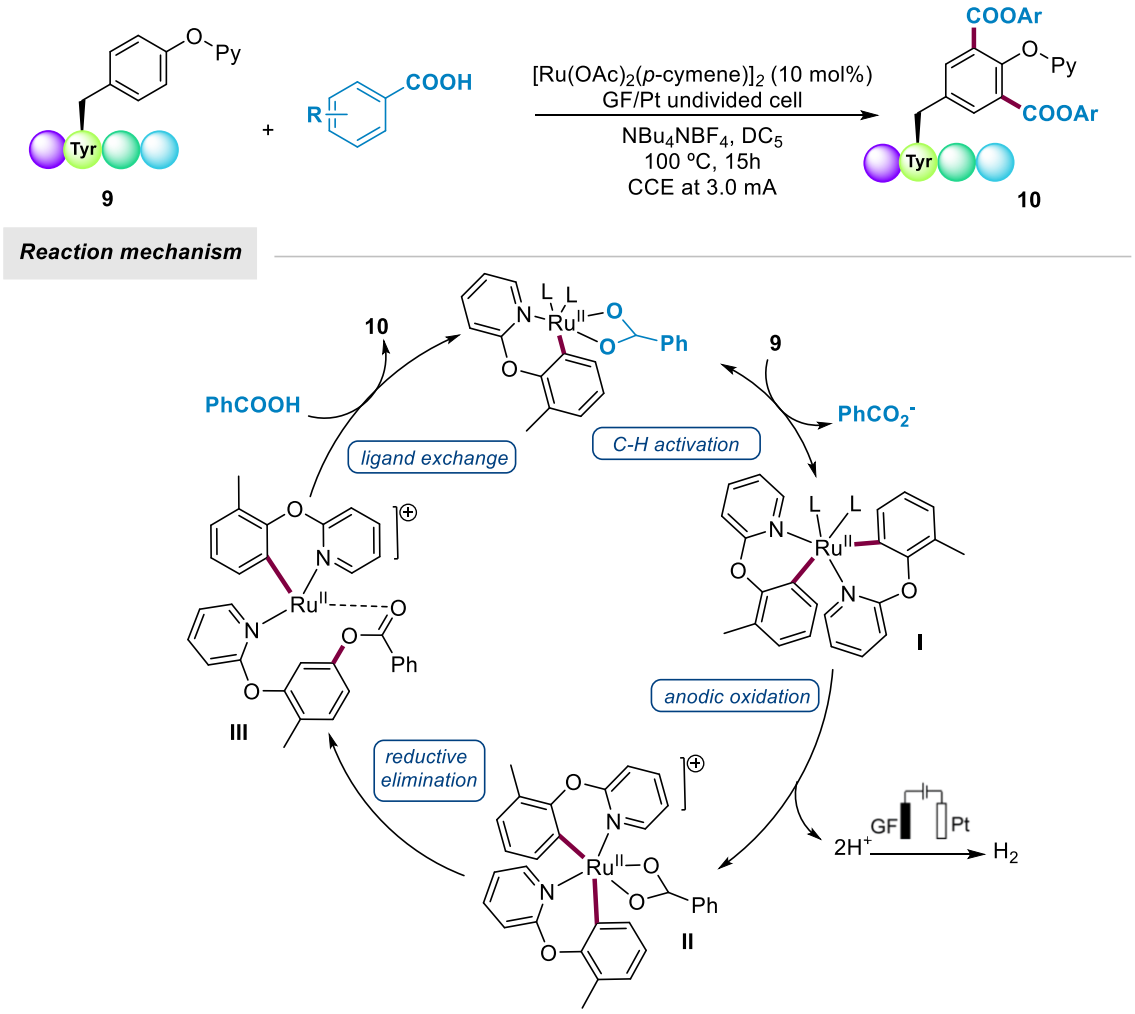

Scheme 76. Ru-catalyzed acyloxylation of Tyr-containing compounds.

4.1.1.4. C(sp^2)–H Acetoxylation of Tyr Derivatives

Despite the existence of various protocols for the C(sp^2)–H acetoxylation of aromatic compounds, they often show a limited substrate scope lacking sensitive functional groups. Regarding Tyr-containing molecules, the application of such reaction was limited to the δ-C(sp^2)–H acetoxylation of Tyr derivatives containing the trifluoromethylsulfonyl group at the nitrogen atom and hence, it was limited to the of the corresponding residue at the *N*-terminal position. Recently, our group expanded the scope of these reactions by using the 2-pyridyl unit as the DG, which resulted in the modification of the Tyr unit in both N- and C-terminal positions.[164] Notably, by slightly modifying

[164] Urruzuno, I.; Andrade-Sampedro, P.; Correa, A. *Eur. J. Org. Chem.* **2023**, e202201489.

the reaction conditions this method enabled the control of the regioselectivity toward the mono- and difunctionalization. Moreover, the reaction allowed the modification of more complex tri- and tetrapeptides with very good yields (Scheme 77).

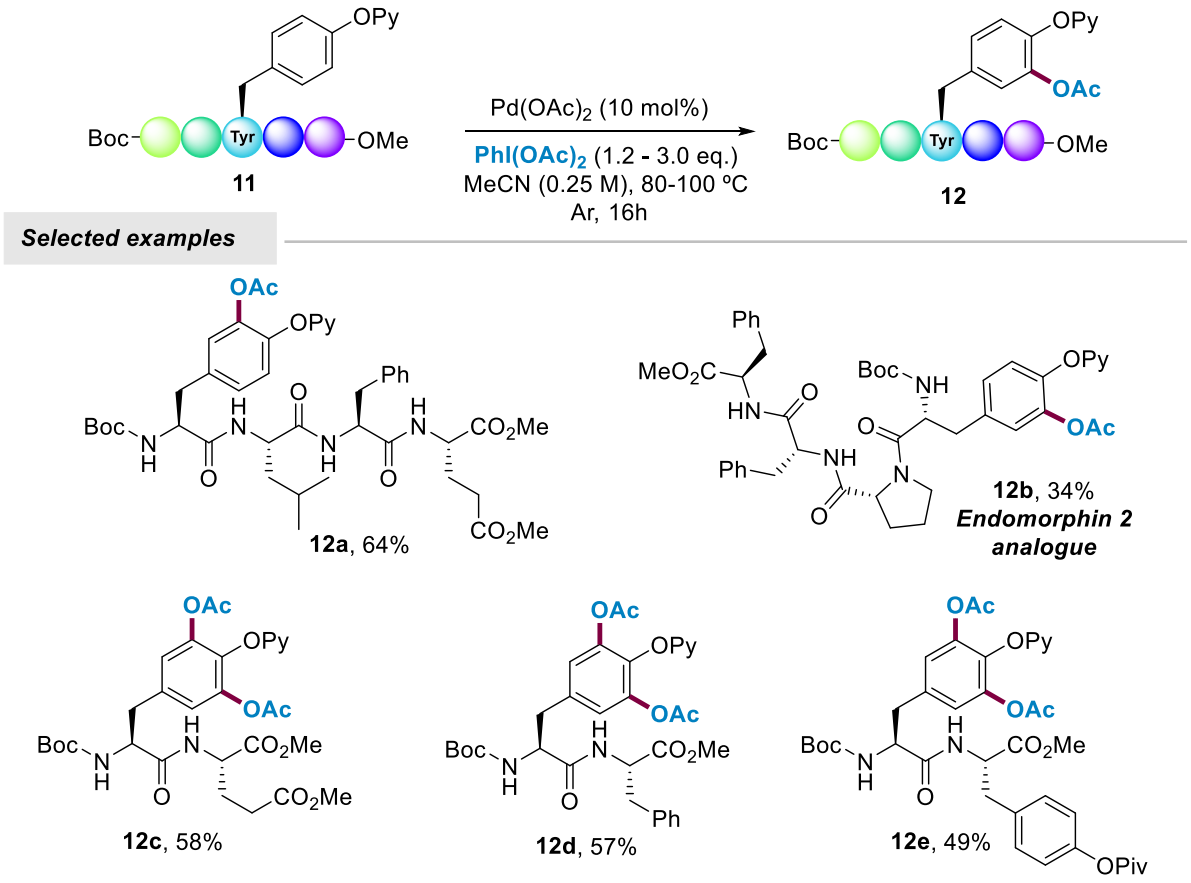

Scheme 77. Acetoxylation of Tyr-containing peptides.

Nowadays, the existing methods for the ε-C(sp^2)–H functionalization of Tyr-containing peptides are scarce. As explained in this section, only acylation, acetoxylation, acyloxylation and olefination protocols have been successfully applied for the chelation-assisted modification of Tyr-containing peptides. Importantly, the installation of small entities such as a hydroxyl groups in a given bioactive molecule often leads to compounds with higher binding affinity, different metabolism and improved pharmacokinetic properties.[165] As a result, the development of new

[165] Osberger, T. J.; Rogness, D. C.; Kohrt, J. T.; Stepan, A. F.; White, M. C. *Nature* **2016**, *537*, 214.

protocols for the introduction of this type of functional groups in a late-stage fashion could be considered of great interest within the field of drug discovery.

4.1.2. Ru-Catalyzed C(sp^2)–H Hydroxylation of Arenes by Weak Coordinating DGs

Hydroxylated aromatic compounds are ubiquitous in Nature and stand out as valuable feedstock in the chemical industry.[166] Among the existing phenol syntheses, the metal-catalyzed C(sp^2)–H hydroxylation of arenes upon chelation assistance poses the most streamlined and straightforward avenue.[167] In this respect, a variety of DGs have been reported to aid the practical oxidation of simple arenes in the presence of palladium,[168] rhodium,[169] ruthenium[170] or iron[171] catalysts, among others (Scheme 78).

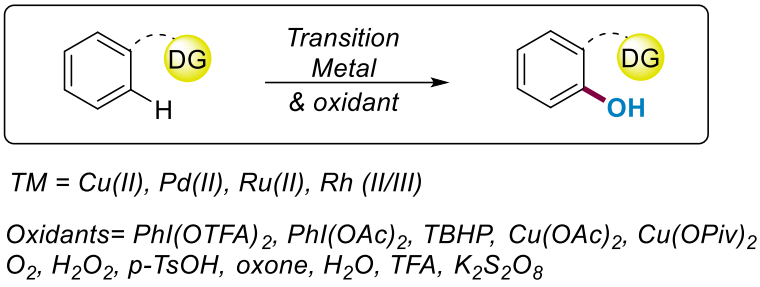

Scheme 78. General scheme of chelation-assisted hydroxylation of arenes.

In this section, we will briefly discuss the use of Ru catalysis in the hydroxylation of simple arenes upon chelation assistance. Although the use of weak chelating groups could be considered as more challenging due to formation of thermodynamically less favored metallacycles, they offer new vias to selectively modify carbonyl derivatives avoiding the installation of *N*-based strong σ-donor

[166] Quideau, S.; Deffieux, D.; Douat-Casassus, C.; Pouységu, L. *Angew. Chem. Int. Ed.* **2011**, *50*, 586.
[167] Iqbal, Z.; Joshi, A.; De, S. R. *Adv. Synth. Catal.* **2020**, *362*, 5301.
[168] Enthaler, S.; Company, A. *Chem. Soc. Rev.* **2011**, *40*, 4912.
[169] Tan, X.; Massignan, L.; Hou, X.; Frey, J.; Oliveira, J. C. A.; Hussain, M. N.; Ackermann, L. *Angew. Chem. Int. Ed.* **2021**, *60*, 13264.
[170] a) Dana, S.; Yadav, M. R.; Sahoo, A. K. *Top. Organomet. Chem.* **2016**, *55*, 189. b) Thirunavukkarasu, V. S.; Kozhushkov, S. I.; Ackermann, L. *Chem. Commun.* **2014**, *50*, 29.
[171] Cheng, L.; Wang, H.; Cai, H.; Zhang, J.; Gong, X.; Han, W. *Science* **2021**, *374*, 77.

DGs. In this regard, during the last decade, the use of weak chelating groups to selectively hydroxylate simple arenes upon Ru catalysis has attracted considerable attention. In particular, esters, amides, ketones and carbamates have been successfully used in these endeavors.[172]

Rao and co-workers developed the first protocol for the C(sp^2)–H hydroxylation of arenes using an ester as the DG. By using $K_2S_2O_8$ in combination with Ru catalysis and a mixture of TFA/TFAA, electron-rich and electron-deficient arenes selectively underwent the hydroxylation reaction in very good yields (Scheme 79a).[173] On the basis that electron-rich arenes reacted faster than the electron-poor ones and some KIE experiments, the authors identified the C–H activation step as the rate-determining step. Moreover, they suggested that the formation of a Ru^{IV} intermediate could be the most favorable pathway. At the same time, Ackermann reported a similar protocol for the hydroxylation of aryl ketones **15** using PIDA as the terminal oxidant (Scheme 79b).[174] Intramolecular competition experiments revealed that steric interactions primarily influenced the selectivity of the C–H activation step. Under similar reaction conditions, different benzamides **16** were hydroxylated with ample scope and low catalyst loadings (Scheme 79b).[175] In this case, some D/H exchange experiments revealed the reversible nature of the C–H activation step. With the aim of complementing these strategies, Ackermann expanded the scope to the oxygenation of arenes in the presence of PIFA and using a challenging aldehyde **18** as the DG, which had shown worse directing abilities compared with other carbonyl derivatives (Scheme 79c). Notably, the oxidation of the aldehyde was avoided during the process.[176] This protocol could be also applied for the oxygenation of Weinreb amides **19** by using PIDA instead of PIFA at lower temperatures featuring an irreversible C–H metalation step (Scheme 79c).[177]

[172] a) De Sarkar, S.; Liu, W.; Kozhushkov, S. I.; Ackermann, L. *Adv. Synth. Catal.* **2014**, *356*, 1461. b) Dana, S.; Yadav, M.R.; Sahoo, A.K. *Top. Organomet. Chem.* **2015**, *55*, 189.
[173] Yang, Y.; Lin, Y. Rao, Y. *Org. Lett.* **2012**, *14*, 2874.
[174] Thirunavukkarasu, V. S.; Hubrich, J.; Ackermann, L. *Org. Lett.* **2012**, *14*, 4210.
[175] Yang, F.; Ackermann, L. *Org. Lett.* **2012**, *14*, 718.
[176] Yang, F.; Rauch, K.; Kettelhoit, K.; Ackermann, L. *Angew. Chem. Int. Ed*. **2014**, *53*, 11285.
[177] Yang, F.; Ackermann, L. Org. Lett. **2013**, *15*, 718.

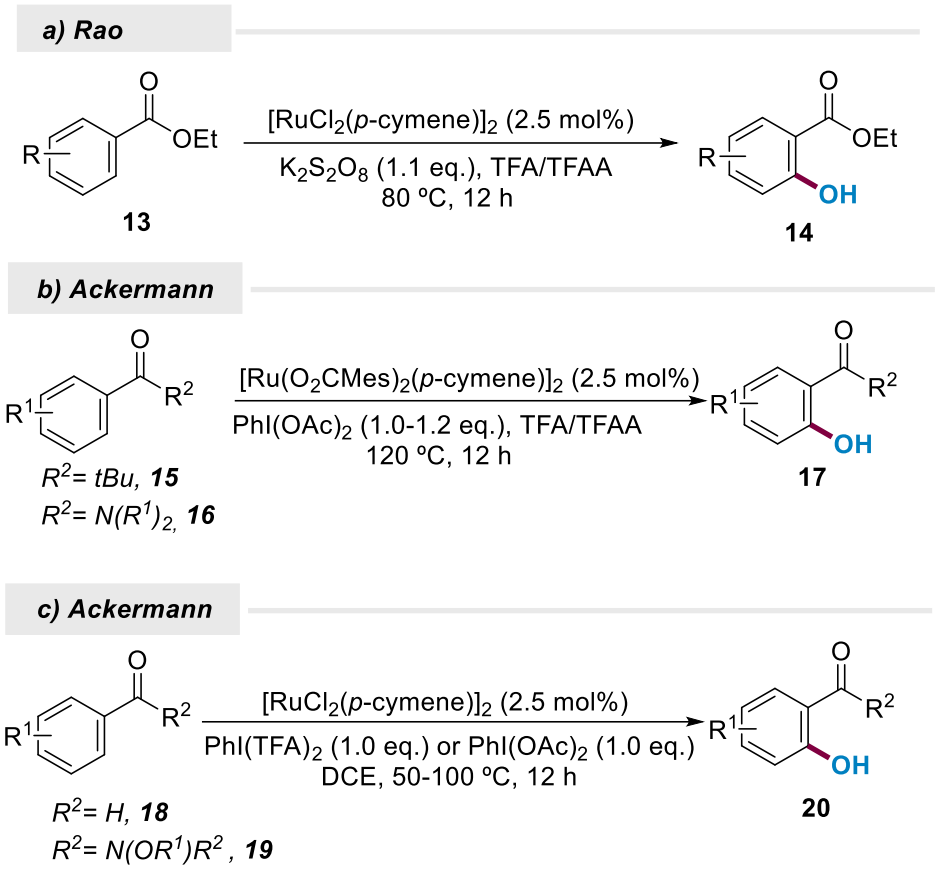

Scheme 79. Ru-catalyzed hydroxylation by carbonyl-based DGs.

Besides carbonyl derivatives, these hydroxylation protocols have also been successfully applied for the modification of *O*- and *N*-protected phenol and aniline derivatives, respectively (Scheme 80). In 2013, Rao described the Ru-catalyzed hydroxylation of anisole derivatives using $K_2S_2O_8$ as the terminal oxidant (Scheme 80a).[178] This reaction features the use of a modifiable DG, which could be easily removed within 3-4 hours by using stoichiometric amounts of hydrazine. Notably, the use of higher amount of oxidant enabled the selective synthesis of the difunctionalized products with very good yields. At the same time, Ackermann demonstrated the feasibility of using O-carbamates as DGs to selectively hydroxylate phenol derivatives under Ru catalysis and using PIFA as oxidant (Scheme 80b).[179] Under the optimized reaction conditions, electron-rich and electron-deficient phenol derivatives smoothly underwent the hydroxylation reaction to furnish the

[178] Yang, X.; Shan, G.; Rao, Y. *Org. Lett.* **2013**, *15*, 2334.
[179] Liu, W.; Ackermann, L.; *Org. Lett.* **2013**, *15*, 3484.

mono-functionalized derivatives. Some inter- and intramolecular experiments showed that the carbamate had superior directing ability over the ester motif. Further DFT studies on the field supported a Ru^{II}/Ru^{IV} catalytic cycle governed by cationic Ru intermediates, in which the C–H activation, oxidation and reductive elimination are the main fundamental steps.[180]

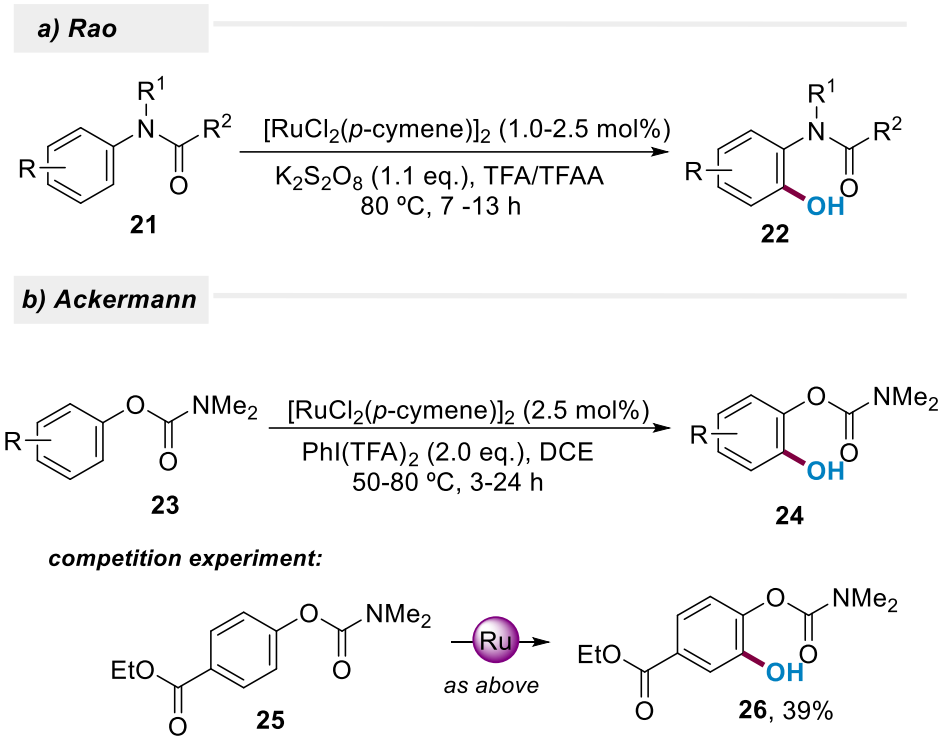

Scheme 80. Oxygenation of aniline and phenol derivatives.

To date, a wide variety of protocols have been developed for the modification of simple arenes using Ru catalysis in combination with weak coordinating groups. Although these methods enabled the synthesis of phenols in a simple fashion, the scope was limited to simple arenes substituted by inert functional groups such as halogens, methoxy or alkyl groups. Accordingly, the application of the hydroxylation platform to more complex structures bearing sensitive functional groups would be highly desirable. Due to the numerous sensitive functional groups which are

[180] Bu, Q.; Kuniyil, R.; Shen, Z.; Gonka, E.; Ackermann, L. *Chem. Eur. J.* **2020**, *26*, 16450.

present within peptide settings, the application of oxidative hydroxylation protocols in these molecules could be considered as a challenging task of prime synthetic interest.

4.1.3. C(sp^2)–H Hydroxylation of Amino Acids

Despite the enormous advances on the field, the introduction of the hydroxyl group on the structure of challenging amino acids and peptides remains virtually unexplored. In 2016, the White group accomplished the site-selective C(sp^3)–H hydroxylation of aliphatic amino acids such as proline, leucine or valine in the presence of a strategically designed iron catalyst which resembled to an enzyme-type reactivity (Scheme 81).[165] This strategy features the use of structurally complex Fe-based catalysts, which could selectively oxidize different C(sp^3)–H bonds depending on their dissociation energy as well as steric and electronic properties. For example, by combining the **Cat I** with H_2O_2 as the hydroxylating agent, they were able to selectively oxidize Pro units within complex peptide sequences. Accordingly, this catalyst was prone to react with hyperconjugatively activated C–H bonds, which would effectively avoid the oxidation of other aliphatic amino acid residues.

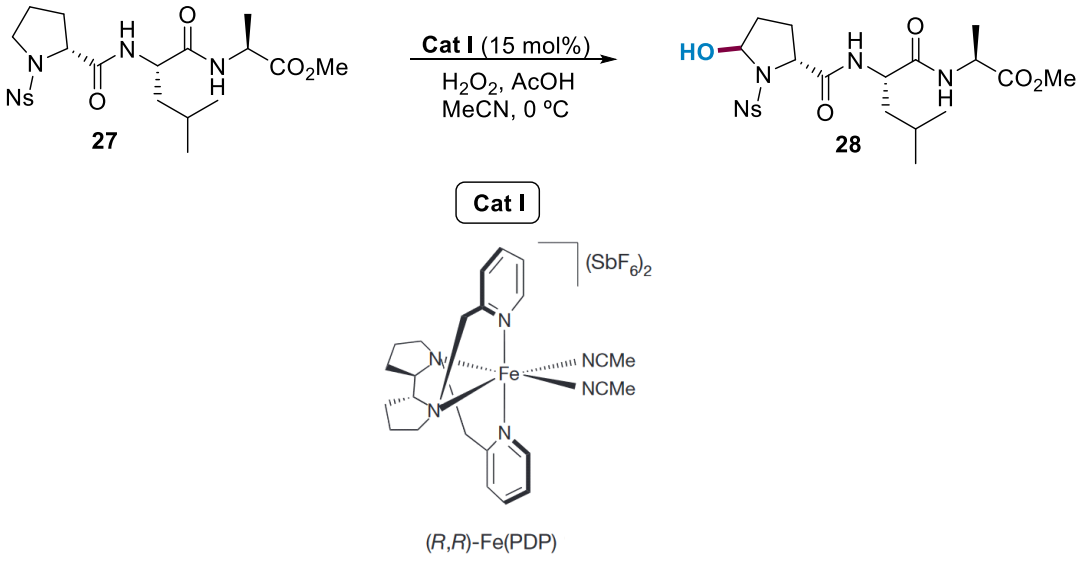

Scheme 81. Selective hydroxylation of Pro residues using Fe-based catalysts.

More recently, as part of their studies on the Pd-catalyzed *ortho*-hydroxylation of benzoic acids, Yu and co-workers disclosed the hydroxylation of a Tyr derivative in a remote position featuring the use of a tautomeric ligand and a carboxylic acid as a weak DG (Scheme 82).[181] Although the feasibility of O_2 activation by Pd catalysis had been demonstrated by different research groups,[182] the design of a viable catalytic system to promote all the elemental steps of the catalytic process was still a challenge. The success of this strategy relied on the use of the bifunctional ligand **L1**, which could tautomerize between pyridine and pyridone coordination modes, promoting the C–H activation step (pyridone) or the O_2 activation step (pyridine) depending on the tautomeric form. By combining ligand **L1**, $Pd(OAc)_2$ as catalyst and BQ as oxidant, they were able to successfully activate molecular oxygen towards the hydroxylation of the bentiromide derivative **29**.

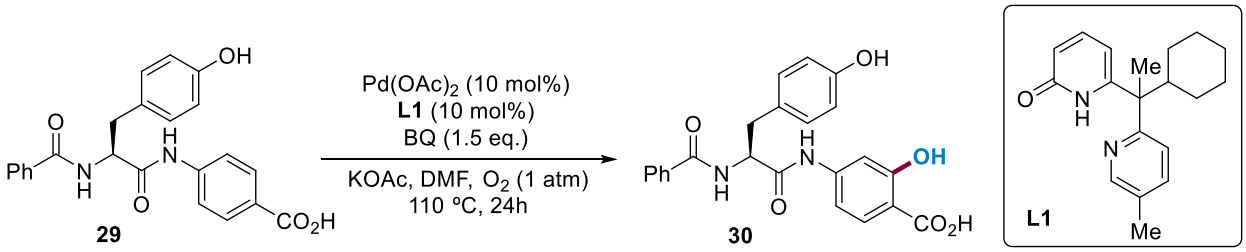

Scheme 82. Hydroxylation of Bentiromide disclosed by Yu.

To date, the challenging site-selective C–H hydroxylation of Tyr-containing peptides upon metal catalysis remains elusive. The development of a new methodology for the hydroxylation of Tyr-containing compounds would be highly desirable since it would be a valuable tool to assemble L-DOPA derivatives, which is a potent drug for the clinical treatment of Parkinson's disease and can be transformed into a wide range of neurotransmitters through biosynthetic pathways.[183] Although the hydroxylation of nonfunctionalized arenes has been extensively studied, their translation to the field of bioconjugation is not a trivial task and poses several challenges: utilize a DG with superior

[181] Li, Z.; Wang, Z.; Chekshin, N.; Qian, S.; Qiao, J. X.; Cheng, P. T.; Yeung, K.-S.; Ewing, W. R.; Yu, Y.-Q. *Science* **2021**, *372*, 1452.
[182]a) Zhang, Y. H.; Yu, J.-Q. *J. Am. Chem. Soc*. **2009**, *131*, 14654. b) Wang, D.; Zavalij, P. Y.; Vedernikov, A. N. *Organometallics* **2013**, *32*, 4882.
[183] Banerjee, A.; Chatterjee, I.; Panda, G. *Chemistry Select* **2022**, *7*, e20220275.

coordinating ability to that of the peptide backbone and select a catalyst with high tolerance for amides within peptide settings.

4.2. Objective

Despite its tremendous medicinal relevance, there is currently no general method available to directly assemble L-DOPA from the corresponding amino acid in a practical fashion. Indeed, the most well-known protocols include Rh-catalyzed asymmetric hydrogenation reactions of enamides developed by Knowles[184] or lengthy routes from L-Tyr involving a classical Friedel-Crafts acetylation entailing corrosive acetyl chloride followed by subsequent reduction steps.[185] Likewise, those methods have not been tested in peptides to produce L-DOPA peptidomimetics. Moreover, despite the commercial availability of L-DOPA or its *N*-protected derivatives, they are rather expensive and often result in low yields of the corresponding peptide derivatives.[186] Accordingly, targeting a metal-catalyzed C–H hydroxylation of Tyr-containing compounds would arguably provide an excellent straightforward approach to forge L-DOPA derivatives.

With these considerations in mind, for this project we established the following objectives:

- To develop a novel and site-selective hydroxylation process for the synthesis of L-DOPA derivatives by using a removable DG
- To achieve a racemization-free and scalable transformation
- To gain more information about the reaction mechanism upon DFT studies

Inspired by the attractive features of cost-effective ruthenium catalysis in the hydroxylation of simple arenes,[172-180] we envisaged that the phenol ring within Tyr could be easily transformed into a weak coordinating group to further assist the corresponding hydroxylation upon the formation of a 6-membered ruthenacycle (Scheme 83).

[184] a) Knowles, W. S. *Angew. Chem. Int. Ed.* **2002**, *41*, 1998; b) Knowles, W. S. *Acc. Chem. Res.* **1983**, *16*, 106.
[185] For example, see: Schneider, T.; Martin, J.; Durkin, P. M.; Kubyshkin, V.; Budisa, N. *Synthesis* **2017**, *49*, 2691.
[186] For selected peptide couplings involving Boc-DOPA-OH, see: a) Solecka, J.; Rajnisz-Mateusiak, A.; Guspiel, A.; Jakubiec-Krzesniak, K.; Ziemska, J.; Kawęcki, R.; Kaczorek, D.; Gudanis, D.; Jarosz, D.; Wietrzyk, J. *J. Antibiot.* **2018**, *71*, 757. b) Larsson, R.; Blanco, N.; Johansson, M.; Sterner, O. *Tetrahedron Lett.* **2012**, *53*, 4966.

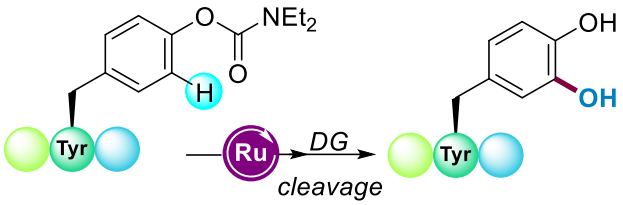

Scheme 83. Synthetic approach to obtain L-DOPA derivatives.

4.3. Ru-Catalyzed C–H Hydroxylation of Tyrosine-Containing Di- and Tripeptides toward the Assembly of L-DOPA Derivatives

4.3.1 Optimization Process

We began our study by selecting the simple Tyr derivative **31a** as the model substrate and PIFA as the terminal oxidant. Since the carbamate or its derivatives have shown great coordinating abilities in Ru-catalyzed hydroxylation reactions, we decided to start the optimization process by using the *O*-diethylcarbamate as the DG. Upon using catalytic amounts of $[RuCl_2(p\text{-cymene})]_2$ and two equivalents of PIFA under air, different solvents were tested. Among all the solvents tested, only 4-*tert*-butyltoluene and dichloroethane rendered the desired product with 10% and 39% yield, respectively (Table 14, entries 2 and 7). When other solvents were used, the substrate remained unreactive (Table 14, entries 3, 4, 5 and 6). In order to promote the hydrolysis of the trifluoroacetate group towards the hydroxylated product, we decided to use trifluoroacetic acid as additive (Table 14, entry 1). Under these conditions, the monohydroxylated product was obtained in 73% yield with excellent site-selectivity.

Table 14. Screening of solvents[a]

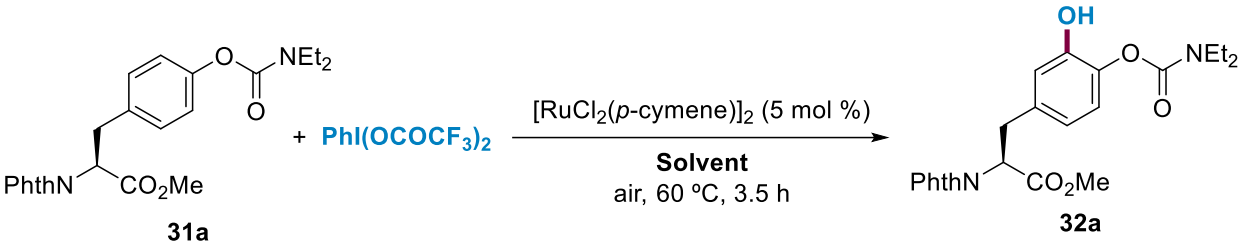

Entry	Solvent	Yield (%)[b]
1	DCE/TFA (1:1)	73
2	DCE as solvent	39[c]
3	PhCl as solvent	Traces[c]
4	Toluene as solvent	Traces[c]
5	MeCN as solvent	0[c]
6	$PhCF_3$ as solvent	Traces[c]
7	4-*tert*-Butyltoluene as solvent	10[c]

[a] Reaction conditions: **31a** (0.15 mmol), PIFA (0.30 mmol), DCE/TFA (1:1, 2.0 mL) 3.5 h at 60 °C under air. [b] Yield of isolated product after column chromatography. [c] Reaction performed without TFA at 80 °C.

In order to prove whether other catalysts could enhance the reactivity and improve the reaction yield, different Ru-based complexes were tested. Unfortunately, by using other Ru-based catalysts the yield slightly decreased (Table 15, entries 2 and 3) or the Tyr derivative **31a** did not react (Table 15, entries 4 and 5). Moreover, attempts to reduce the catalyst loading from 5 mol% to 2.5 mol%, the reaction afforded the product in 61% yield (Table 15, entry 1).

Table 15. Screening of catalysts[a]

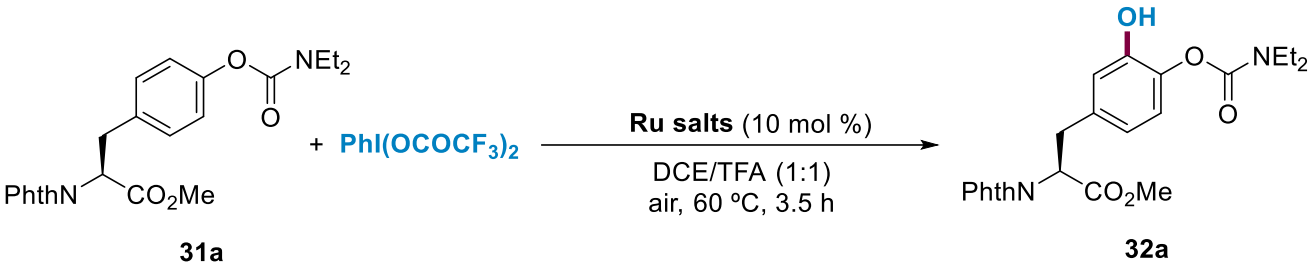

Entry	Ru salts	Yield (%)[b]
1	$[RuCl_2(p\text{-cymene})]_2$ (2.5 mol%)	61
2	$Ru(OAc)_2(PPh_3)_2$	54
3	$RuCl_2(PPh_3)_2$	21
4	$RuCl_3$	0
5	$Ru_3(CO)_{12}$	0

[a] Reaction conditions: **31a** (0.15 mmol), PIFA (0.30 mmol), DCE/TFA (1:1, 2.0 mL) 3.5 h at 60 °C under air. [b] Yield of isolated product after column chromatography.

Next, we decided to investigate the influence of other oxidizing agents. On the one hand, the screening of oxidants revealed the higher activity of PIFA in comparison with PIDA (Table 16, entry 3). On the other hand, other oxidants commonly used in oxygenation reactions were not suitable for this hydroxylation protocol (Table 16, entry 2 and 6). Likewise, when *m*-CPBA and selectfluor were used the substrate remained unreactive (Table 16, entries 4 and 5).

Table 16. Screening of oxidants[a]

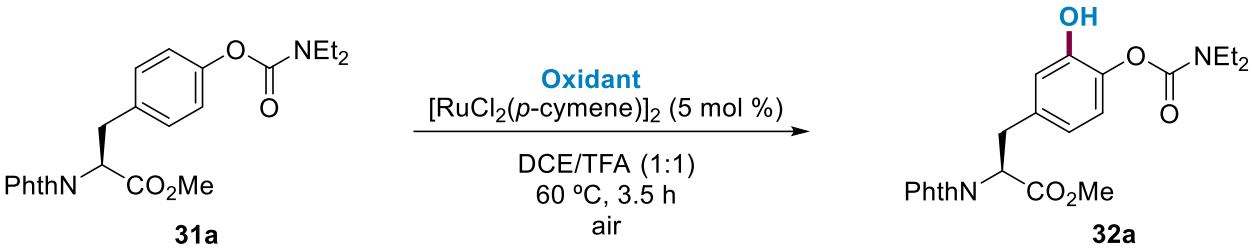

Entry	Oxidant	Yield (%)[b]
1	PIFA	73
2	$K_2S_2O_8$	Traces
3	PIDA	45
4	Selectfluor	0
5	*m*-CPBA	0
6	Oxone	Traces

[a] Reaction conditions: **31a** (0.25 mmol), oxidant (0.50 mmol), DCE/TFA (1:1, 2.0 mL) 3.5 h at 60 °C under air. [b] Yield of isolated product after column chromatography.

Further screening revealed that the overall yield was slightly affected by the dilution effect and the solvent ratio. The use of lower amount of TFA (Table 17, entries 2 and 3) and performing the process in a more concentrated system resulted in comparatively lower yields (Table 17, entry 4). The latter may be the result of the slower hydrolysis of the trifluoroacetate group.

Table 17. Screening of solvent ratio[a]

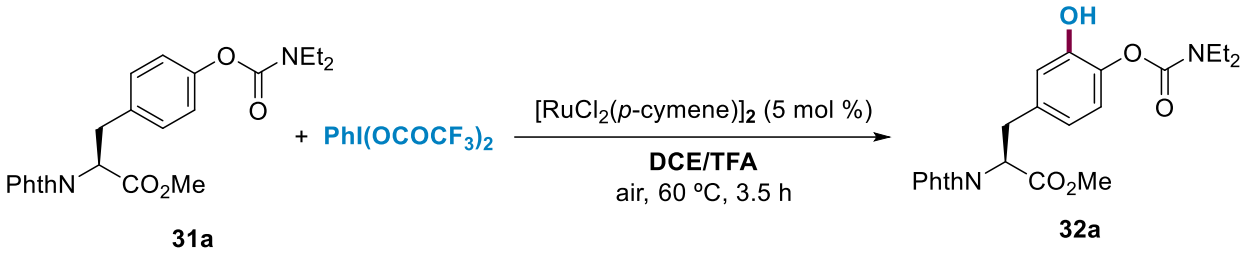

31a **32a**

Entry	Solvent ratio	Yield (%)[b]
1	DCE/TFA (1:1)	73
2	DCE/TFA (9:1)	58
3	DCE/TFA (8:2)	65
4	DCE/TFA (1:1)	62[c]

[a] Reaction conditions: **31a** (0.15 mmol), PIFA (0.30 mmol), DCE/TFA (1:1, 2.0 mL) 3.5 h at 60 °C under air. [b] Yield of isolated product after column chromatography. [c] Reaction carried out using DCE (0.5 mL) and TFA (0.5 mL)

Finally, some control experiments revealed that the reaction was quite sensitive towards the temperature. While lower temperatures decreased the yield (Table 18, entry 2), higher temperatures resulted in substrate degradation (Table 18, entry 3). By reducing the amount of PIFA, the product **32a** was obtained in 53% yield (Table 18, entry 4). Importantly, the reaction could be carried out under air atmosphere without loss of yield, which constitutes an additional bonus in terms of operational simplicity (Table 18, entry 5). Finally, the use of the catalyst was found to be crucial for the process to occur (Table 18, entry 6).

Table 18. Variations from standard conditions[a]

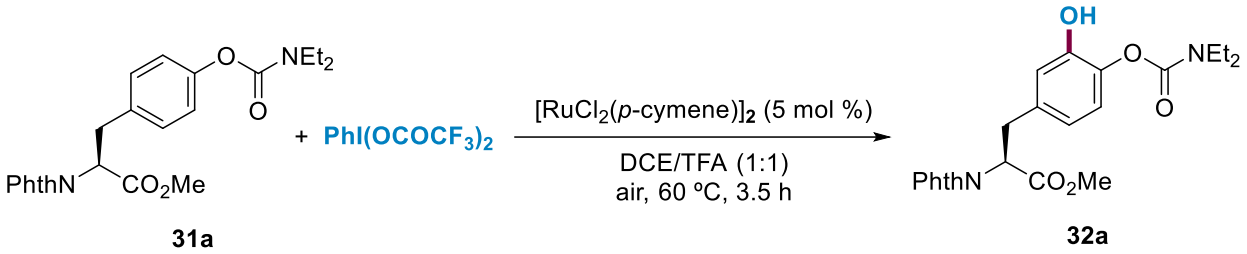

Entry	Variations from standard conditions	Yield (%)[b]
1	none	73
2	50 ºC	53
3	100 ºC	Traces
4	PIFA (1.2 eq.)	53
5	Under Ar	73
6	Without catalyst	0

[a] Reaction conditions: **31a** (0.15 mmol), PIFA (0.30 mmol), DCE/TFA (1:1, 2.0 mL) 3.5 h at 60 °C under air. [b] Yield of isolated product after column chromatography.

Further analysis of the influence of the protecting group demonstrated the feasibility to perform the reaction with Tyr derivatives housing secondary amines, albeit with lower yields (Scheme 84). For example, benzyloxycarbonyl (**32c**) and nosyl (**32d**) groups afforded the corresponding products with 43% and 37% yields, respectively. Conversely, Boc-containing Tyr compound (**32b**) decomposed under the optimized standard reaction conditions involving TFA, which is commonly used to deprotect Boc-containing amine derivatives.

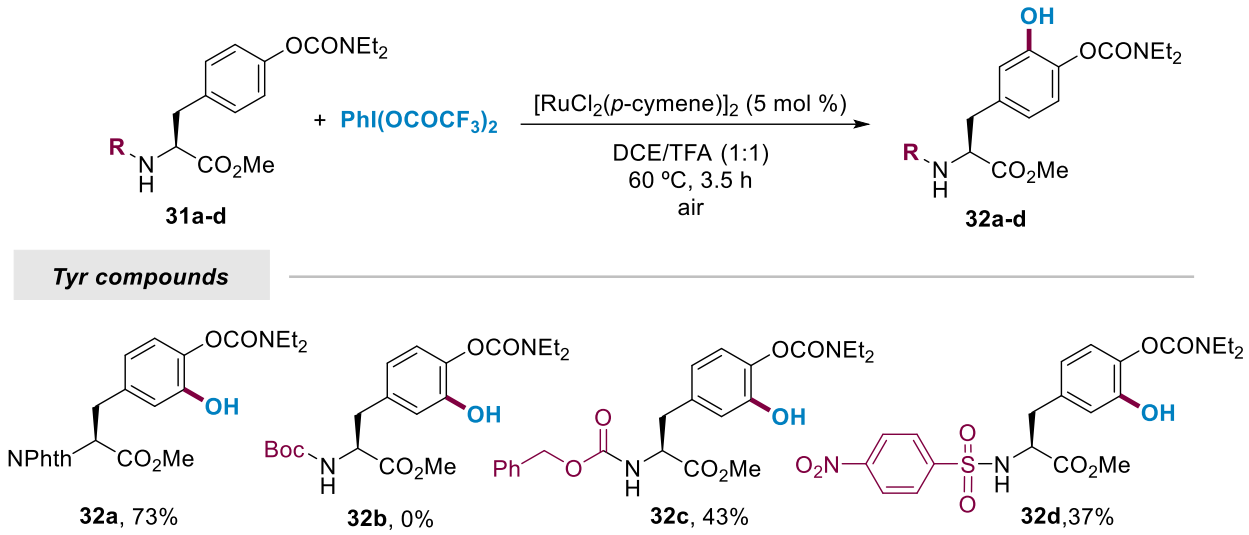

Scheme 84. Investigation of the influence of N-protecting groups

Although we tried to perform the reaction with other DGs besides the *O*-diethylcarbamate, all of our attempts failed (Scheme 85). As expected, the substrate was degraded when the reaction was carried out with a native Tyr residue (**33a**).[187] Moreover, the employment of the strong coordinating pyridine unit (**33b**) as well as the weak coordinating acetyl group (**33c**) resulted in the inhibition of the reaction.

[187] Wang, P.; Cheng, Y.; Wu, C.; Zhou, Y.; Cheng, Z.; Li, H.; Wang, R.; Su, W.; Fang, L. *Org. Lett.* **2021**, *23*, 4137.

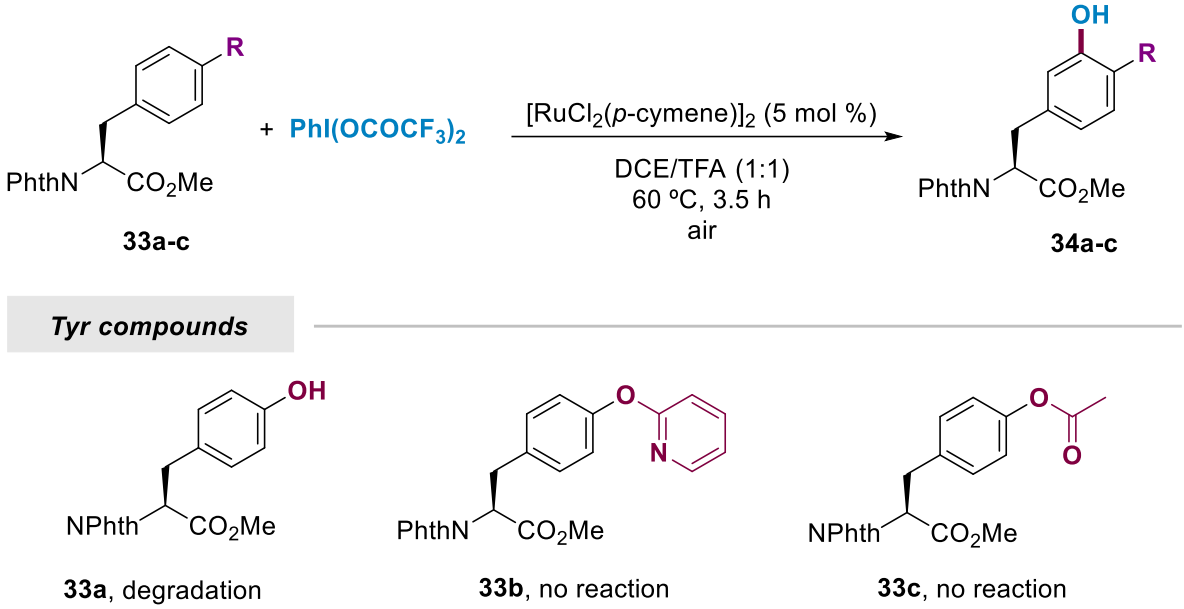

Scheme 85. Screening of DGs.

With these results in hand, we next addressed the hydroxylation reaction in more complex peptide settings to illustrate the generality of this method to deliver L-DOPA derivatives in a simple fashion. However, the direct application of the optimized conditions for simple Tyr unit resulted in lower yields. Accordingly, the reactions conditions were optimized for dipeptide **35a**. On Table 19 a collection of illustrative experiments is disclosed. It is noteworthy that longer reaction time (3.5h *vs* 16h) as well as reducing the amount of TFA resulted in the formation of **36a** in a remarkable 63% yield.

Table 19. Screening of dipeptides[a]

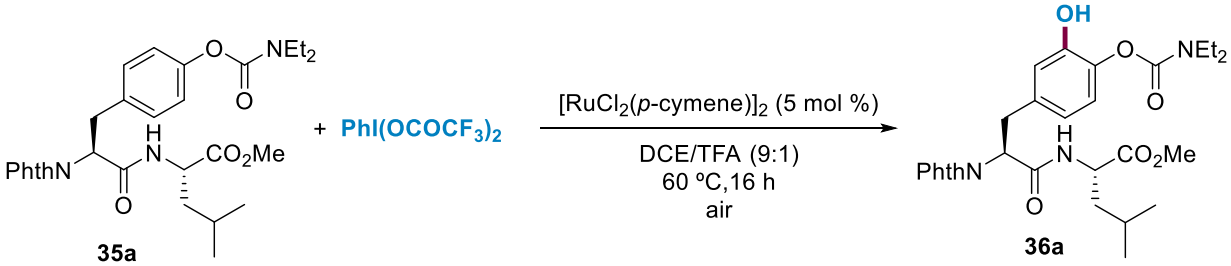

Entry	Variation from the standard conditions	Yield (%)[b]
1	none	63
2	DCE/TFA (1:1), 60 ºC, 5h, 0.075M	Traces
3	DCE/TFA (1:1), 80 ºC, 5h, 0.075M	9
4	DCE/TFA (1:3), 80 ºC, 5h, 0.075M	7
5	DCE/TFA (1:1), 100 ºC, 5h, 0.075M	27
6	DCE/TFA (1:1), 60 ºC, 24h, 0.075M	35
7	DCE/TFA (1:1), 80 ºC, 24h, 0.075M	40
8	DCE/TFA (1:1), 100 ºC, 24h, 0.075M	28
9	DCE/TFA (3:1), 80 ºC, 24h, 0.075M	51
10	DCE/TFA (8:2), 80 ºC, 24h, 0.25M	60
11	DCE/TFA (9:1), 80 ºC, 24h, 0.25M	58
12	PIFA (1.2 eq.)	27
13	PIFA (2.5 eq.)	56

[a] Reaction conditions: **35a** (0.15 mmol), PIFA (0.30 mmol), DCE/TFA (9:1, 1.0 mL) 16 h at 60 °C under air. [b] Yield of isolated product after column chromatography.

4.3.2 Synthetic Scope

In order to evaluate the synthetic utility of our technique, a family of Tyr-containing dipeptides was synthesized following classical peptide couplings as well as protection/deprotection sequences. Next, they were submitted to the optimized reaction conditions. As shown in Scheme 86, a wide number of previously inaccessible hydroxylated dipeptides could be assembled in moderate to excellent yields (up to 74%). A family of Tyr-containing dipeptides incorporating Val (**36b**), Leu (**36a**), Ile (**36c**), Pro (**36e**), Phe (**36f**), Glu (**36g**), Tyr (**36h**) and Ala (**36i**) residues underwent the *ortho*-hydroxylation reaction in a site-selective manner under slightly modified conditions featuring the use of lower amount of TFA and longer reaction times than those used with the single Tyr compound **31a**. These results clearly indicated that the *ortho*-hydroxylation of

a Tyr residue can be efficiently directed by the weak coordination of the carbamate group in the presence of other competing *O*-chelating sites such as those amides of the peptide backbone. Encouraged by these promising results with dipeptide derivatives, we synthesized a variety of tripeptide compounds to evaluate the robustness our C(sp^2)–H hydroxylation manifold. Notably, the desired chemical modification of the Tyr unit could be achieved regardless of the position of the Tyr residue within the peptide sequence. Although the hydroxylated products were obtained in low to moderate yields in certain cases (up to 56%), it is worth noting that full conversion was not always achieved and unreactive starting material was sometimes observed. Owing to the use of a highly oxidizing system, residues bearing potentially oxidizable groups such as Tyr (**36h**), Thr (**36l**) and Ser (**36m**) as well as amino groups in Lys (**36j**) were protected to chemoselectively perform the corresponding hydroxylation reaction. Importantly, biologically relevant depsipeptides **36d** and **36n** as well as a tripeptide containing a quaternary center (**36o**) could be also hydroxylated in good yields. The structure of **36q** was unambiguously assigned by X-ray diffraction and supported the appendance of the hydroxyl group at the *ortho* position of the Tyr unit (Figure 22).

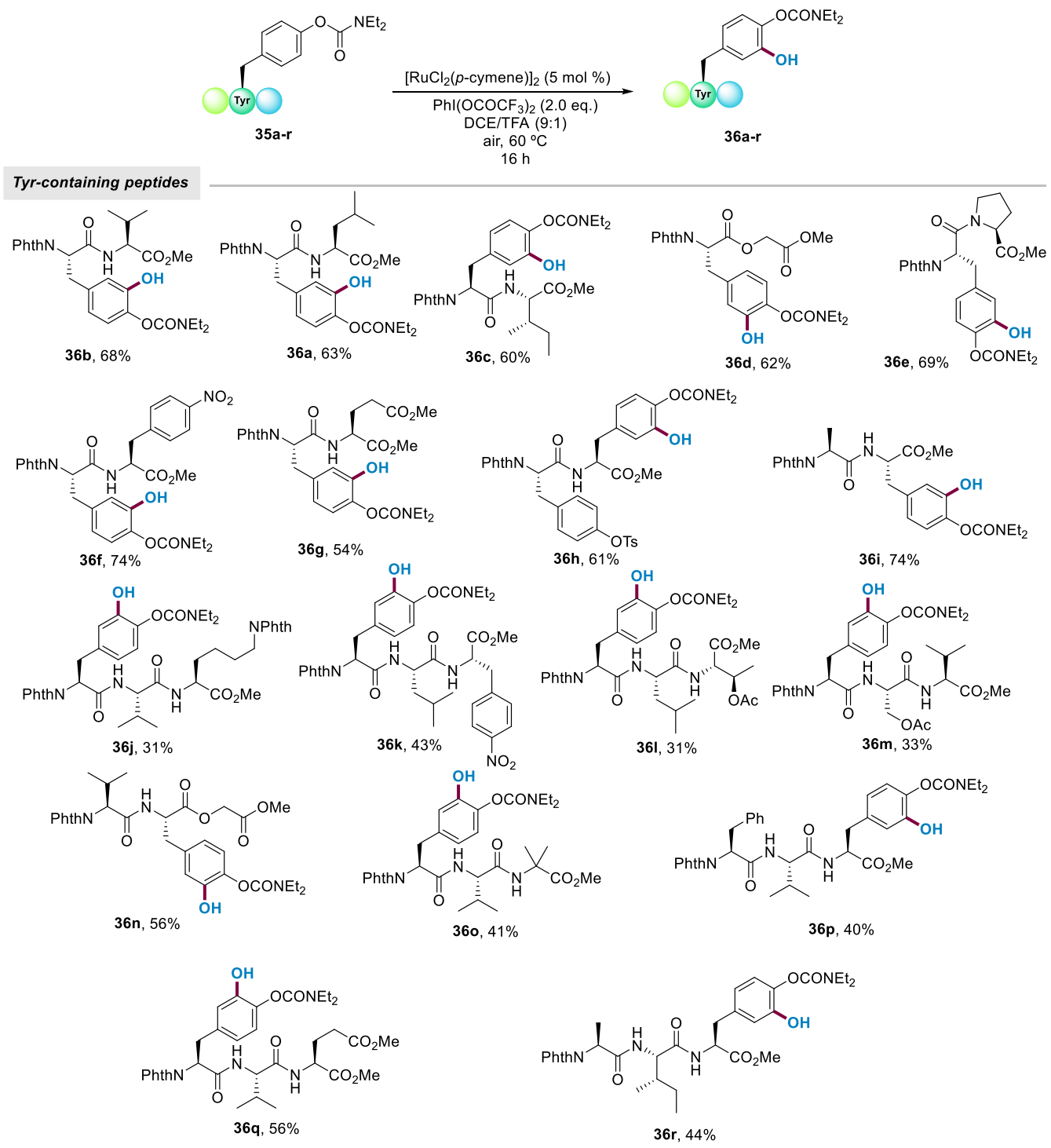

Scheme 86. Scope of the hydroxylation of di- and tripeptides.

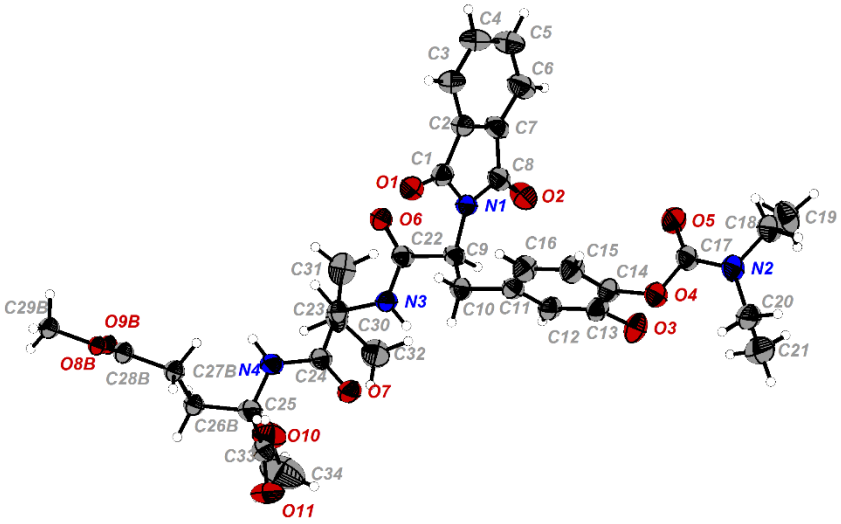

*Figure 22. X-ray of compound **36q**.*

Conversely, a dipeptide housing a methionine residue with a thioether motif (**35s**) resulted in the preferential oxidation of the sulfur atom. Moreover, the employment of unprotected Ser (**35u**) afforded a complex mixture of unidentified compounds, probably due to the oxidation of the alcohol towards the aldehyde/carboxylic acid. Likewise, even protecting the sensitive functional groups, the use of peptides bearing heterocyclic-containing amino acids such as His (**35v**) and Trp (**35t**, **35x**, **35y**) resulted in the entire inhibition of the process (Figure 23).

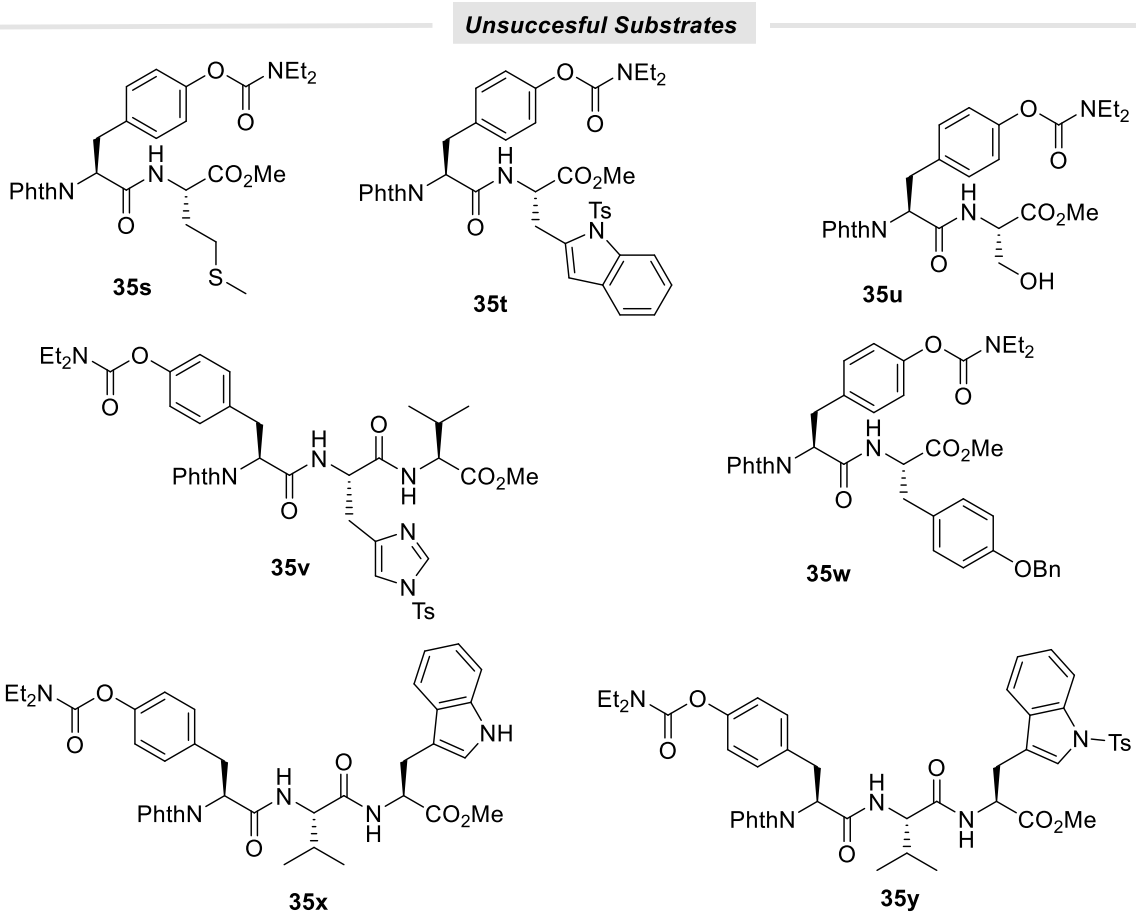

Figure 23. Failed scope.

The robustness and synthetic utility was demonstrated by the performance of the hydroxylation of amino ester **31a** and dipeptide **35a** in higher scale (Scheme 87). Although the yield slightly decreased when the hydroxylation of the simple amino acid was performed at 1.18 mmol scale, the synthesis of the hydroxylated dipeptide could be performed at 0.98 mmol scale without any loss of yield.

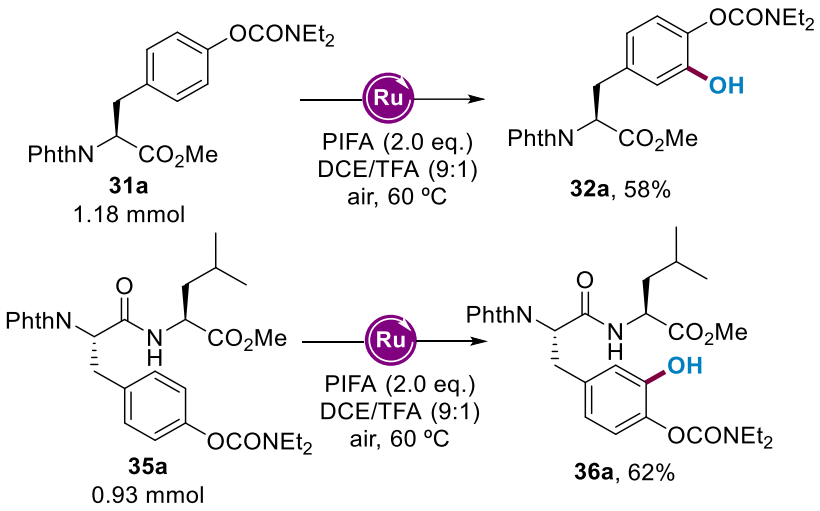

Scheme 87. High-scale synthesis.

Unfortunately, despite of our numerous attempts, the protocol could not be applied in tetra- or hexapeptides. We hypothesized that the high number of amide bonds in tetrapeptides could deeply compromise the required coordination of the Ru catalyst with the carbamate, thus outcompeting with the carbamate as weak O-coordinating groups. In fact, peptides have been used in Ru-catalyzed transformations as effective endogenous and exogenous ligands.[188] With the aim to expand the protocol to more complex tetrapeptide sequences, we revisited the optimized reaction conditions. For this purpose, we started synthesizing the peptide **37a** and submitting it to a screening of co-solvents. Given that coordinating solvents could act as labile ligands, thus partially avoiding the complexation of the peptide backbone, we started by performing the reaction with 0.1 mL of the selected solvents (Table 20, entries 2, 3 and 4). In view of the lack of reactivity of the starting material, we decided to prove whether HIFP could enhance the process and render the coupling product.[189] This solvent has emerged as a powerful tool to promote the C–H activation step on distal and proximal C–H functionalization reactions. Accordingly, on proximal C(sp^2)–H activation reactions it has been reported to stimulate weak DGs by its high H-bonding capability.

[188] For selected examples, see: a) Song, L.; Ojeda-Carralero, G.; Parmar, M. D.; González-Martínez, D. A.; Meervelt, L. V.; Van der Eycken, J.; Goeman, J.; Rivera, D. G.; Van der Eycken, E. V. *Adv. Synth. Catal.* **2021**, *363*, 3297. b) Pelagatti, P.; Carcelli, M.; Calbiani, F.; Cassi, C.; Elviri, L.; Pelizzi, C.; Rizzotti, U.; Rogolino, D. *Organometallics* **2005**, *25*, 5836. c) Bøgevig, A.; Pastor, I. M.; Adolfsson, H. *Chem. Eur. J.* **2004**, *10*, 29.
[189] Bhattacharya, T.; Ghosh, A.; Maiti, D. *Chem. Sci.* **2021**, *12*, 3857.

Moreover, by exploiting this ability, HIFP can also activate oxidizing agents in different oxidation reactions. Unfortunately, all of our attempts failed and the substrate remained unreactive.

Table 20. Screening of co-solvents[a]

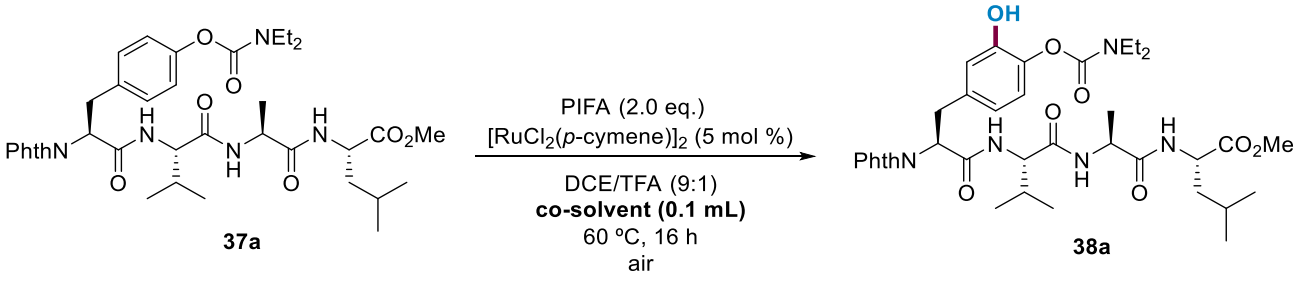

Entry	Co-solvent	Yield (%)
1	None	0
2	NMP	0
3	DMF	0
4	DMA	0
5	HFIP	0
6	DCM	0

[a] Reaction conditions: **37a** (0.15 mmol), PIFA (0.30 mmol), DCE/TFA (9:1, 1.0 mL), 16 h at 60 °C under air.

Next, we decided to investigate the influence of various supporting ligands. As explained before, we hypothesized that the complexation of these ligands could avoid the coordination of the peptide backbone to the metal center. Despite the use of a number of phosphine-based ligands, all of our efforts to obtain the coupling product failed (Table 21). In fact, it is noteworthy that it may be very difficult to avoid the complexation of the peptide backbone without affecting the coordination capability of the carbamate. Given that the coordination of the carbamate is weaker than that of the backbone itself, blocking the coordination of the peptide backbone toward the catalyst would avoid complexation of the carbamate.

Table 21. Screening of ligands[a]

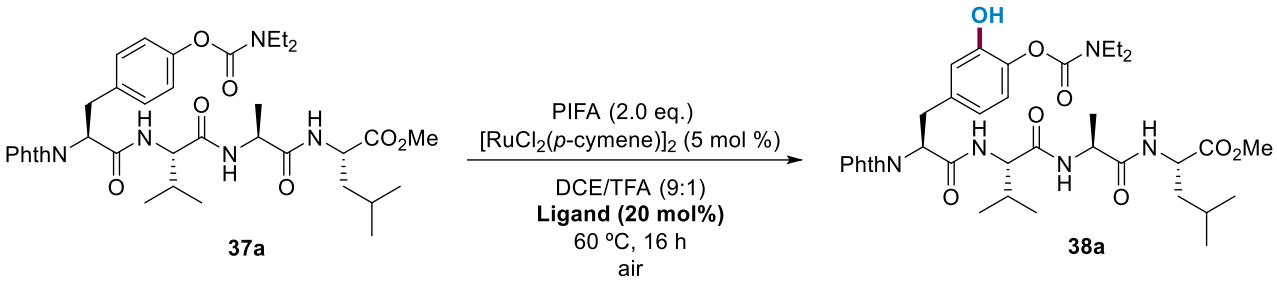

Entry	Ligand	Yield (%)
1	dppf (10 mol%)	0
2	JohnPhos	0
3	XPhos	0
4	^{t}BuXPhos	0
5	Xantphos (10 mol%)	0
6	$PCy_3 \cdot HBF_4$ + K_2CO_3 (30 mol%)	0
7	PPh_3 (10 mol%)	0

[a] Reaction conditions: **37a** (0.15 mmol), PIFA (0.30 mmol), DCE/TFA (9:1, 1.0 mL), 16 h at 60 °C under air.

Owing to the excellent performance of hypervalent iodine reagents in halogenated solvents, their influence in the reaction was analyzed. However, the target product was only detected in trace amounts in certain cases (Table 22).

Table 22. Screening of solvents[a]

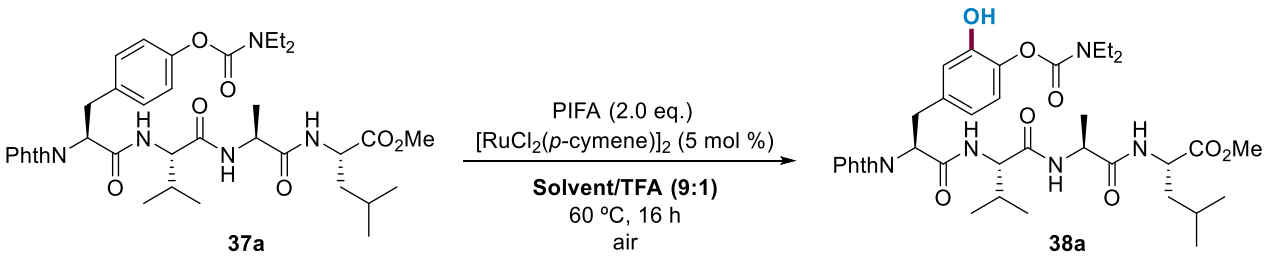

Entry	Solvents	Yield (%)
1	DCE	0
2	PhCl	Traces
3	$PhCF_3$	Traces
4	Toluene	0
5	$CHCl_3$	0
6	4-*tert*-Butyltoluene	0
7	HFIP	Traces
8	TFE	0

[a] Reaction conditions: **37a** (0.15 mmol), PIFA (0.30 mmol), Solvent/TFA (9:1, 1.0 mL), 16 h at 60 °C under air.

In view of these results, we strategically prepared a number of peptides incorporating tertiary amides devoid of NH bonds to avoid coordination of the catalyst with the peptide backbone (Scheme 88). However, the introduction of Pro or *N*-methyl Ala residues into the peptide sequence did not ushered in the formation of the product. On the one hand, we prepared the tetrapeptide **37b**, which contains a Pro unit within the C-terminal position. We hypothesized that the presence of a less coordinating tertiary amine could favor the coupling process. Likewise, we decided to incorporate a *N*-methylated Ala unit next to the Pro residue (**37c**), but this strategy did not afford the desired product either. Unfortunately, all of our attempts to hydroxylate these compounds failed.

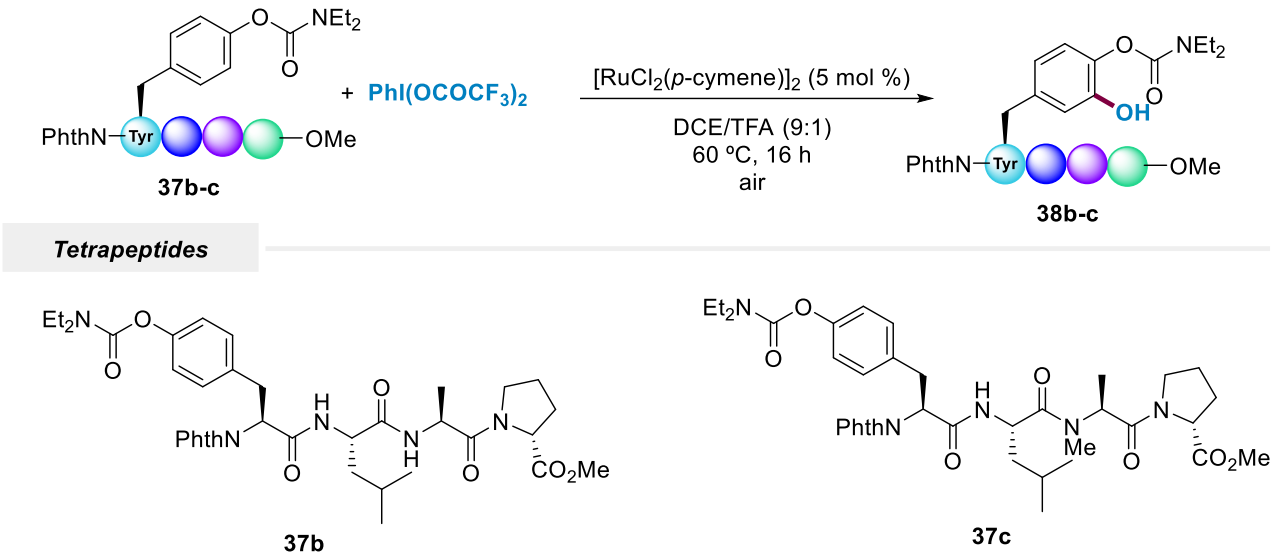

Scheme 88. Unsuccessful tetrapeptides.

In this respect, we performed further studies to determine whether other DGs could be used in these endeavours to overcome this apparent synthetic limitation. As depicted on Scheme 89, a simple Tyr unit housing other DGs with carbonyl motifs as *O*-coordinating groups such as carbonates (**34h**, **34i**) or carbamates (**34d**, **34g** and **34j**) either inhibited the reaction or afforded hydroxylated compounds in much lower yields. Conversely, among the tested strong chelating heteroarene groups pyrimidine afforded a remarkable 50% yield of the corresponding *ortho*-hydroxylated product **34e** under the standard conditions.

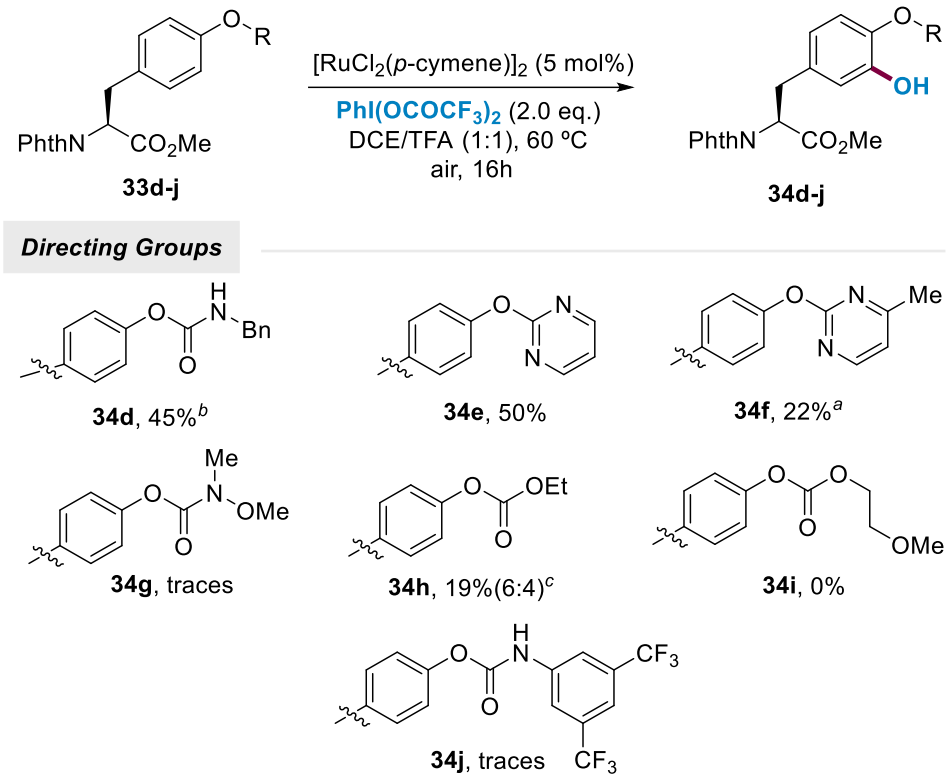

Scheme 89. Analysis of other directing groups. [a] Reaction carried out with $Pd(OAc)_2$ (10 mol%), PIFA (0.30 mmol) and DCE (2 mL) at 80°C under air. [b] Reaction carried out with DCE (0.9 mL) and TFA (0.1 mL). [c] Ratio of mono- and dihydroxylated product.

Accordingly, we decided to analyze the hydroxylation reaction on tetrapeptides by using the pyrimidine as the DG. First, we submitted the tetrapeptide **37d** to the standard reaction conditions but the substrate remained unreactive. Taking into account that palladium catalysis has been extensively used for C–O bond forming reactions, we decided to perform the hydroxylation reaction under the standard reaction conditions but using $Pd(OAc)_2$ as catalyst. To our surprise, trace amounts of the product were detected. Next, we investigated the effect of different solvents in the reaction outcome under palladium catalysis (Table 23). Although in most of the cases the substrate did not react or suffered from degradation, when DCE was used in the absence of TFA the product was obtained in 15% yield (Table 23, entry 1).

Table 23. Screening of solvents[a]

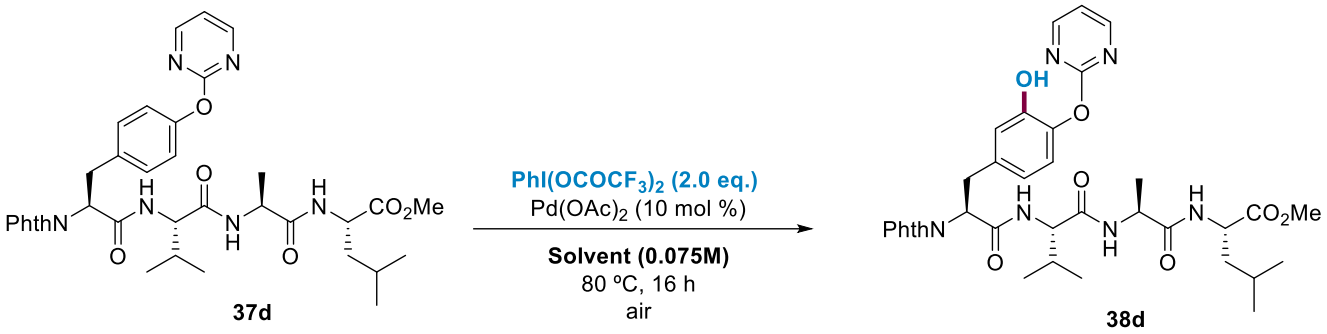

Entry	Solvents	Yield (%)[b]
1	DCE	15
2	PhCl	traces
3	Toluene	traces
4	MeCN	0
5	$CHCl_3$	0
6	HFIP	degradation
7	1,2-DME	0
8	DCE/TFA (9:1)	0
9	*o*-xylene	degradation[c]

[a] Reaction conditions: **37d** (0.15 mmol), PIFA (0.30 mmol), Solvent (0.075M) 16h at 80 °C under air. [b] Yield of isolated product after column chromatography. [c] Reaction performed at 120 ºC.

With the aim to improve the reaction yield, we decided to investigate whether higher amounts of the oxidant as well as other oxidizing agents could provide better results. After a careful examination of the reaction conditions, we found that employing toluene as the solvent, more equivalents of the oxidants and higher temperatures were tolerated. On the one hand, the reaction provided lower yields when $K_2S_2O_8$ was used as additive and was completely inhibited in the presence of BQ (Table 24, entries 2 and 3). On the other hand, by increasing the equivalents of PIFA the targeted product could be obtained in 18% yield, which did not represent a significant improvement.

Table 24. Screening of additives

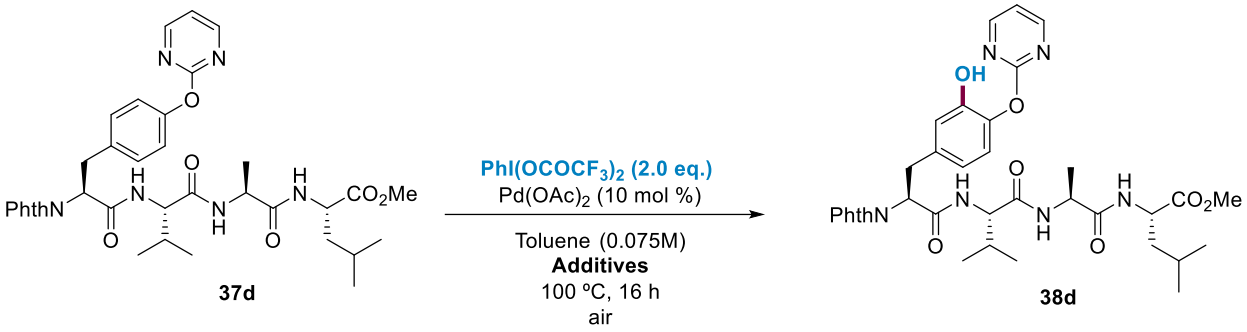

Entry	Additives	Yield (%)[b]
1	*t*BuOOH (5.0 eq.) instead of PIFA	0
2	$K_2S_2O_8$ as additive (1.0 eq.)	12
3	BQ as additive (1.0 eq.)	0
4	PIFA (4.0 eq.)	18

[a] Reaction conditions: **37d** (0.15 mmol), PIFA (0.30 mmol), toluene (0.075M) 16 h at 80 °C under air. [b] Yield of isolated product after column chromatography.

Finally, we decided to study whether other Pd catalysts could provide the hydroxylated tetrapeptide in higher yields (Table 25). Unfortunately, all of our attempts failed. While some of the Pd catalysts afforded trace amounts of the product, others were not active for this hydroxylation protocol. Therefore, the hydroxylation of peptides with more than three amino acid residues still poses a daunting challenge and represents a task which deserves further analysis.

Table 25. Screening of Pd salts.[a]

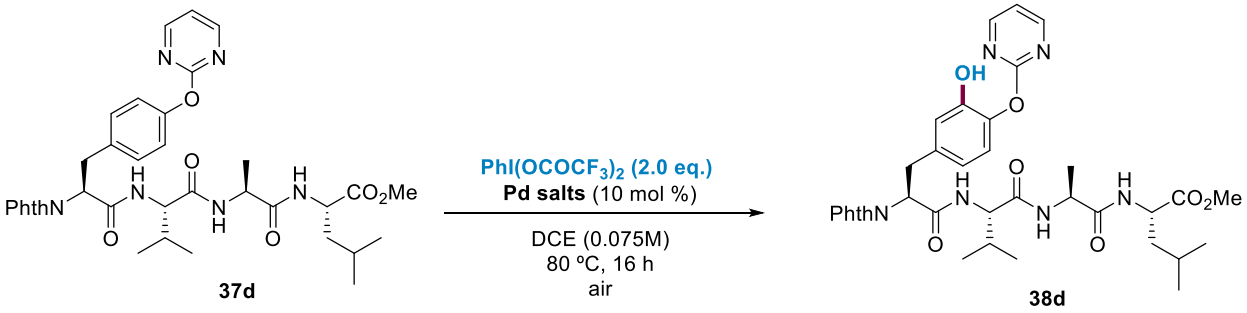

Entry	Pd salt	Yield (%)[b]
1	$Pd(OAc)_2$	15
2	PdI_2	0
3	$Pd(TFA)_2$	0
4	$PdCl_2$	12
5	$Pd(MeCN)(BF_4)_2$	0
6	$PdCl_2(PPh_3)_2$	18

[a] Reaction conditions: **37d** (0.15 mmol), PIFA (0.30 mmol), DCE (0.075M) 16 h at 80 °C under air. [b] Yield of isolated product after column chromatography.

Next, we evaluated the utility of this method by removing the DG (Scheme 90). The removal of these auxiliaries could be very challenging, especially in compounds of high structural complexity housing a variety of sensitive functional groups. Although the carbamate cleavage can be performed under a variety of conditions in simple phenols,[190] its removal within a peptide framework is not a trivial task. Certain reagents such as $LiAlH_4$ or NaOH can not be used without affecting the chiral integrity. Other reagents such as hydrazine or the Schwartz reagent did not work, presumably because of the coordination of the amides to the catalysts. After a number of attempts, the cleavage of the carbamate in product **32a** was achieved upon treatment with sulfuric acid in MeOH, which furnished the corresponding L-DOPA analogue **39a** in 81% yield. Remarkably, HPLC analysis of compound **39a** verified that no racemization occurred neither along the hydroxylation nor the cleavage step. Unfortunately, when dipeptide **36a** was submitted to those conditions a deprotected Tyr was formed, which resulted from a deprotection and amidolysis sequence. Although it seems a limitation at first sight, the access to fully decorated peptides housing a carbamate unit could offer interesting possibilities within drug discovery.[191]

[190] a) Sun, X.; Sun, Y.; Zhang, C.; Rao, Y.; *Chem. Commun.* **2014**, *50*, 1262. b) Morin, J.; Zhao, Y.; Snieckus, V. *Org. Lett.* **2013**, *15*, 4102. c) Li, B.; Ma, J.; Liang, Y.; Wang, N.; Xu, S.; Song, H.; Wang, B. *Eur. J. Org. Chem.* **2013**, 1950.
[191] Ghosh, A. K.; Brindisi, M. *J. Med. Chem.* **2015**, *58*, 2895.

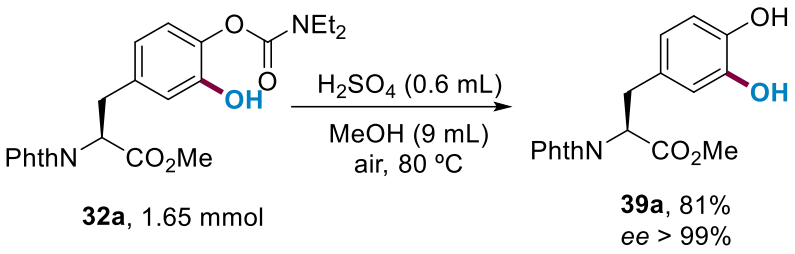

Scheme 90. Cleavage of the DG.

4.3.3 DFT Studies

In order to understand the reaction pathway as well as some of the observed experimental evidences, we further performed DFT studies. The following calculations were carried out using the computational methods described in section 1.4 of Chapter 1. In particular, we focused our studies on the C–H hydroxylation of Tyr derivative **31a** and **33b** bearing a carbamate and a pyridine as DG, respectively, which experimentally exhibited an entirely distinct reactivity profile. Assuming a similar reaction pathway to that described for the Ru-catalyzed C(sp^2)–H hydroxylation of arenes upon weak chelation assistance of secondary amides,[180] we proposed the plausible mechanism depicted in Scheme 91. The reaction would start by complexation of the Ru catalyst and the Tyr compound assisted by TFA to deliver **Int-A**. The latter would likely undergo the *ortho*-C–H metalation aided by the trifluoroacetate anion to provide the 6-membered ruthenacycle **Int-B**. Then, oxidative addition of PIFA would result in the formation of highly reactive Ru^{IV} **Int-C,** prone to undergo a subsequent reductive elimination to deliver **Int-D**, which would eventually lead to the hydroxylated product **32a**.

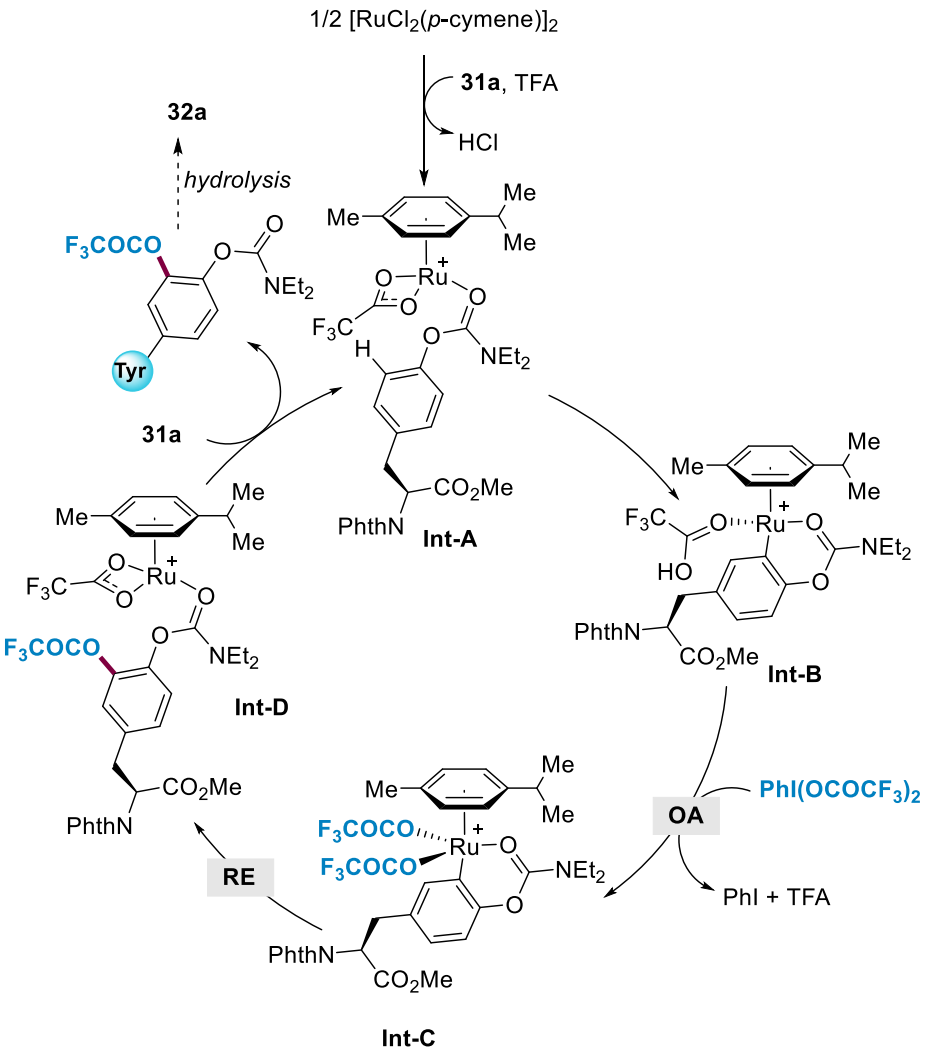

Scheme 91. Proposed reaction mechanism.

With the energy values in hand, we can conclude that whereas both the C–H activation and the oxidative addition are endergonic events, the reductive elimination is exergonic for both substrates. As depicted in Figure 24, the higher stability of the ensuing *ortho*-hydroxylated compound **32a** suggested that its formation may be the driving force to render the proposed mechanistic scenario thermodynamically favored. Indeed, all fundamental steps are thermodynamically and kinetically feasible under the optimized reaction conditions. The first step would consist of a C–H activation event of the tyrosine derivative, leading to the formation of **Int-B** through a CMD pathway with an energy penalty of 14.74 Kcal/mol. The optimized structure of **TS1** reveals an elongation of the C–H bond of 0.3 Å and the approximation of the C atom to the metal center is verified by the value of the distance of the C–Ru bond, which decreased from 2.68 Å to 2.23 Å. The oxidative addition

of PIFA to **Int-B** thereby delivering Ru(IV) species **Int-C** would not occur in a straightforward manner. As shown in Figure 24, the initial coordination of PIFA to **Int-B** upon a ligand exchange would deliver **Int-B'**, which would next undergo a formal oxidative addition through a concerted pathway leading to **Int-C'** with an energy barrier of 13.62 kcal/mol. This step could easily occur through a transition state (**TS2**) wherein a I–O bond is cleaved with the simultaneous formation of a new Ru–I bond. In fact, the I–O distance is lengthened from 2.28 Å to 3.03 Å, whereas the Ru–I distance is shortened from 3.76 Å to 2.98 Å. The so-formed **Int-C'** would furnish **Int-C** upon release of PhI and TFA. The latter could undergo a reductive elimination step with an energy barrier of 27.10 kcal/mol through a concerted transition state (**TS3**), in which the Ru–O distance is lengthened from 2.03 Å to 3.61 Å and the C–O distance is shortened from 2.64 Å to 1.38 Å. To our surprise, in sharp contrast with our experimental studies, the reaction pathway for substrate **33b** was shown also energetically feasible; whereas the C–H activation and the reductive elimination steps were slightly more favored than for substrate **31a**, the oxidative addition of PIFA was shown more likely to happen with a substrate housing a weak coordinating group. Although merely speculative, we hypothesized that the transient ruthenacycle species with a strong pyridine unit as supporting ligand may be much more stable than the parent species featuring a considerably weak coordination mode, thereby resulting in the entire inhibition of the process and likely evolving into dimers or unproductive reaction pathways. Indeed, the enthalpy value of the dimerization of compound **33b** was calculated to be 2.6 Kcal/mol, which indicated that its formation was thermodynamically more feasible than the formation of the *ortho*-hydroxylated product.

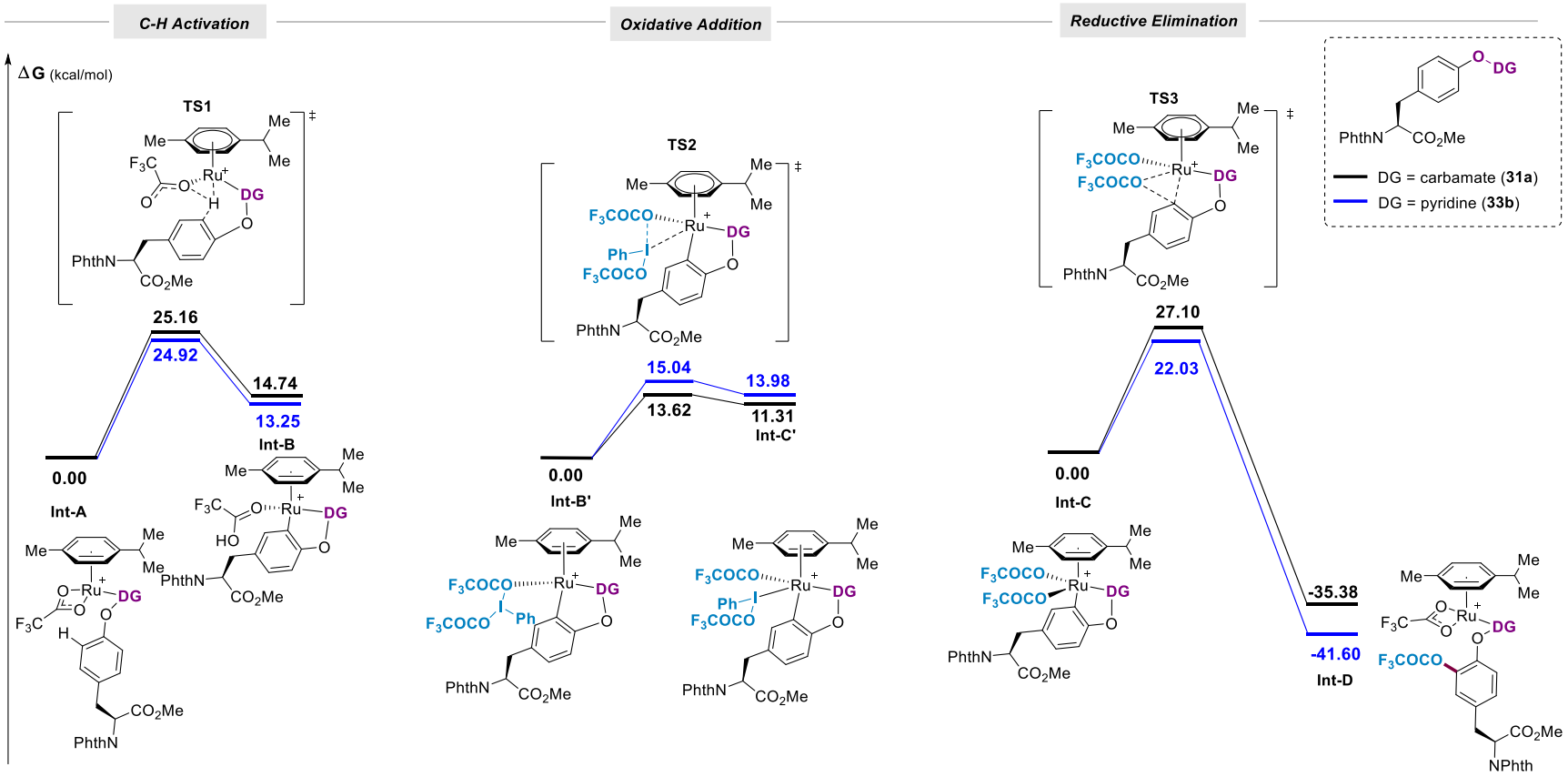

Figure 24. Energetics for the elemental steps of Ru-catalyzed hydroxylation reaction.

Finally, a control experiment with an equimolecular mixture of **31a** and **33b** under the standard conditions exclusively delivered **32a** in 41% yield, thus evidencing a partial inhibition of the process in the presence of a pyridine unit. Further studies are definitely required to conclude why tetrapeptides do not undergo the developed hydroxylation reaction.

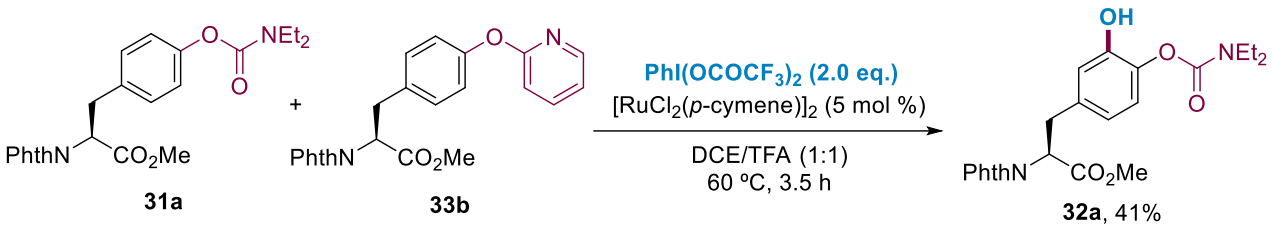

*Scheme 92. Equimolecular experiment with **31a** and **33b**.*

4.4. Conclusions

In summary, we have developed a hydroxylation reaction for the modification of privileged Tyr-containing peptides featuring the use of cost-effective and air-insensitive ruthenium catalysis.[192] Unlike the methods available for the assembly of L-DOPA, this protocol enables the rapid installation of hydroxyl groups within existing peptides in a late-stage fashion. As a result, this labelling platform represents a reliable, yet scalable, means for the diversification of Tyr-containing compounds, thereby providing access to unprecedented L-DOPA peptidomimetics. Salient features of this unique strategy are the facile introduction and removal of the required carbamate as a weak O-coordinating group, mild reaction conditions, operational simplicity and retention of the chiral integrity of the existing stereocenters within the peptide framework. Computational studies supported a Ru(II)/Ru(IV) regime occurring upon the intermediacy of a challenging 6-membered ruthenacycle.

For future work, the development of other protocols for the late-stage hydroxylation of tetra-, penta- or hexapeptides would be highly desirable. Likewise, along to the chemical waste produced by PIFA, the use of other sustainable oxygen sources would definitely represent a practical bonus in terms of green chemistry.

[192] Andrade-Sampedro, P.; Matxain, J. M.; Correa, A. *Adv. Synth. Catal*. **2022**, *364*, 2072.

4.1. Supporting Information

In this section, the general synthetic procedures will be detailed. For the full characterization data, please see the SI of the published article.[192]

4.1.1. Ru-Catalyzed C(sp^2)-H Hydroxylation of Tyr-Containing Peptides

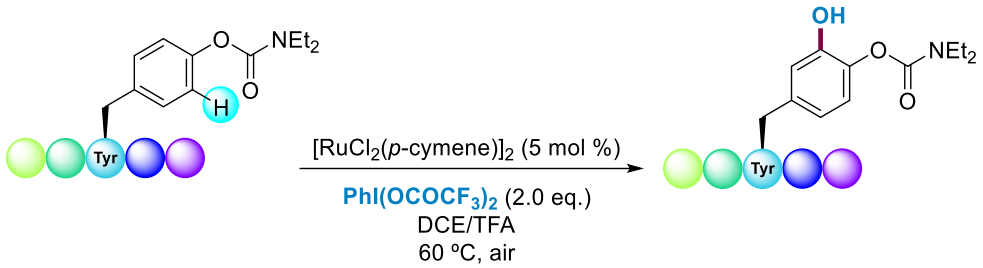

General procedure A: A reaction tube containing a stirring bar was charged with the corresponding tyrosine derivative (0.25 mmol), PIFA (0.50 mmol) and $[RuCl_2(p\text{-cymene})]_2$ (5 mol %). Then, anhydrous DCE (1.0 mL) and TFA (1.0 mL) were added by syringe. The reaction tube was next warmed up to 60 ºC in a heating block and stirred for 3.5 hours. The mixture was then allowed to warm to room temperature, the solvent was evaporated and the resulting crude was washed up with an aqueous solution of $NaHCO_3$ (20 mL). The aqueous layer was extracted with EtOAc (3 x 20 mL), dried over $MgSO_4$ and evaporated under vacuum. The resulting crude was then purified by column chromatography to afford the corresponding product.

General procedure B: A reaction tube containing a stirring bar was charged with the corresponding peptide (0.25 mmol), PIFA (0.50 mmol) and $[RuCl_2(p\text{-cymene})]_2$ (5 mol %). Then, DCE (0.9 mL) and TFA (0.1 mL) were added by syringe. The reaction tube was next warmed up to 60 ºC in a heating block and stirred for 16 hours. The mixture was then allowed to warm to room temperature, the solvent was evaporated and the resulting crude was washed up with an aqueous solution of $NaHCO_3$ (20 mL). The aqueous layer was extracted with EtOAc (3 x 20 mL), dried over $MgSO_4$ and evaporated under vacuum. The resulting crude was then purified by column chromatography to afford the corresponding product.

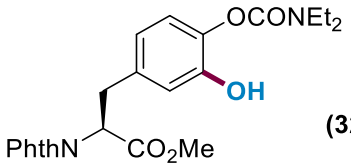

(32a)

Methyl (*S*)-3-[4-((diethylcarbamoyl)oxy)-3-hydroxyphenyl]-2-(1,3-dioxoisoindolin-2-yl)propanoate (32a). Following the general procedure A, using **31a** (0.25 mmol, 106 mg) provided 80 mg (73% yield) of **32a** as a white solid. Mp 70-71 ºC. ^{1}H NMR (400 MHz, $CDCl_3$) δ 7.82 (dd, *J* = 5.5, 3.1 Hz, 2H), 7.72 (dd, *J* = 5.5, 3.1 Hz, 2H), 7.04 – 6.80 (m, 2H), 6.74 (dd, *J* = 8.2, 2.1 Hz, 1H), 5.16 (dd, *J* = 10.7, 5.7 Hz, 1H), 3.80 (s, 3H), 3.73 – 3.49 (m, 2H), 3.46 – 3.31 (m, 4H), 1.23 (dt, *J* = 21.9, 7.1 Hz, 6H). ^{13}C NMR (101 MHz, $CDCl_3$) δ 169.2, 167.4, 154.5, 147.6, 139.0, 135.3, 134.1, 131.5, 123.5, 122.0, 120.9, 119.8, 53.0, 52.8, 42.5, 42.2, 33.9, 14.0, 13.1. IR (cm^{-1}): 3373, 2968, 1995, 1709, 1427, 1386, 1236, 1113, 716, 439. HRMS *calcd.* for ($C_{23}H_{24}N_2O_7$): 440.1584, *found* 440.1595. <u>This reaction was also performed in a higher scale:</u> the use of **31a** (1.18 mmol, 500 mg), PIFA (2.36 mmol, 1.01 g) in a mixture of DCE (8 mL) and TFA (1 mL) provided 305 mg (58% yield) of **32a** as a white solid.

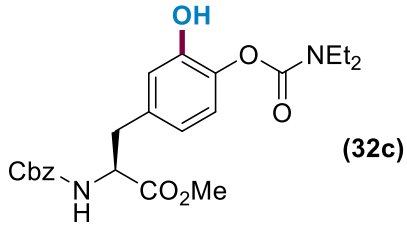

(32c)

Methyl (*S*)-2-[((benzyloxy)carbonyl)amino]-3-[4-((diethylcarbamoyl)oxy)-3-hydroxyphenyl]propanoate (32c). Following the general procedure A, using **31c** (0.25 mmol, 73 mg) provided 72 mg (65% yield) of **32c** as a brown oil. Column chromatography (Hex/EtOAc 7/3). ^{1}H NMR (400 MHz, $CDCl_3$) δ 7.52 (s, 1H), 7.39 – 7.22 (m, 5H), 6.91 (d, *J* = 8.2 Hz, 1H), 6.74 (d, *J* = 1.8 Hz, 1H), 6.59 (dd, *J* = 8.2, 1.7 Hz, 1H), 5.33 (d, *J* = 8.2 Hz, 1H), 5.14 – 5.00 (m, 2H), 4.60 (dd, *J* = 5.9 Hz, 1H), 3.70 (s, 3H), 3.45 (q, *J* = 7.1 Hz, 2H), 3.38 (q, *J* = 7.1 Hz, 2H), 3.09 – 2.90 (m, 2H), 1.26 (t, *J* = 7.0 Hz, 3H), 1.19 (t, *J* = 7.1 Hz, 3H). ^{13}C NMR (126 MHz, $CDCl_3$) δ 171.9, 155.7, 154.6, 147.9, 139.2, 136.2, 134.2, 128.4, 128.0, 128.0, 122.2, 121.3, 119.8, 66.9, 54.7, 52.3, 42.6, 42.3, 37.4, 14.0, 13.2. IR (cm^{-1}): 3314, 2953, 1691, 1429, 1200, 1154, 1057, 697. HRMS (ESI) m/z: (M^+) *calcd* for ($C_{23}H_{28}N_2O_7$): 444.1897, *found* 444.1915.

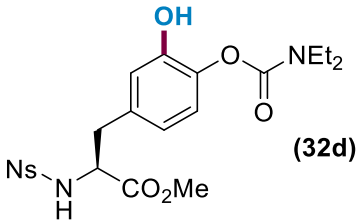

(32d)

Methyl (*S*)-3-[4-((diethylcarbamoyl)oxy)-3-hydroxyphenyl]-2-[(4-nitrophenyl)amino]propanoate (32d). Following the general procedure B, using **31d** (0.15 mmol, 72 mg) provided 28 mg (37 % yield) of **32d** as a white solid. Mp 127-128 ºC. ^{1}H NMR (500 MHz, $CDCl_3$) δ 8.20 (d, *J* = 8.8 Hz, 2H), 7.76 (d, *J* = 8.8 Hz, 2H), 7.35 (bs, 1H), 6.79 (d, *J* = 8.2 Hz, 1H), 6.62 (d, *J* = 2.1 Hz, 1H), 6.52 (dd, *J* = 8.2, 2.1 Hz, 1H), 5.77 (d, *J* = 9.6 Hz, 1H), 4.18 (td, *J* = 9.1, 4.5 Hz, 1H), 3.70 (s, 3H), 3.46 (dq, *J* = 27.3, 7.1 Hz, 4H), 3.03 (dd, *J* = 13.9, 4.5 Hz, 1H), 2.76 (dd, *J* = 13.9, 9.0 Hz, 1H), 1.28 (dt, *J* = 29.3, 7.1 Hz, 6H). ^{13}C NMR (126 MHz, $CDCl_3$) δ 171.6, 154.7, 150.0, 148.0, 145.6, 139.5, 133.9, 128.2, 124.2, 122.5, 121.5, 120.0, 57.5, 53.1, 42.9, 42.5, 38.4, 14.3, 13.3. IR (cm^{-1}): 3426, 3135, 2970, 1752, 1682, 1530, 1433, 1348, 1216, 1158, 1115, 853,735, 530, 464. HRMS *calcd.* for ($C_{21}H_{27}N_3O_{10}S$): 495.1300, *found* 495.1410.

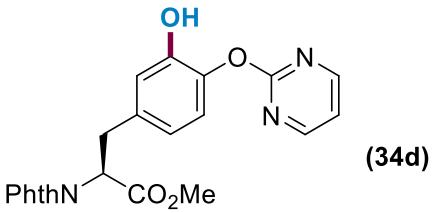

(34d)

Methyl (*S*)-2-(1,3-dioxoisoindolin-2-yl)-3-[3-hydroxy-4-(pyrimidin-2-yloxy)phenyl] propanoate (34d). Following the general procedure A, using **33d** (0.25 mmol, 100 mg), and stirring the reaction overnight provided 51.6 mg (50% yield) of **34d** as a yellowish oil. ^{1}H NMR (400 MHz, $CDCl_3$) 8.49 (d, *J* = 4.8 Hz, 1H), 8.40 (d, *J* = 4.8 Hz, 1H), 7.81 (ddd, *J* = 9.8, 5.4, 3.1 Hz, 2H), 7.71 (ddd, *J* = 9.8, 5.4, 3.0 Hz, 2H), 7.07 – 6.97 (m, 2H), 6.95 – 6.89 (m, 1H), 6.76 (dd, *J* = 8.3, 2.1 Hz, 1H), 5.19 (dd, *J* = 10.9, 5.5 Hz, 0.5H), 5.12 (dd, *J* = 10.9, 5.6 Hz, 0.5H), 3.80 (s, 1.5H), 3.78 (s, 1.5H), 3.63 – 3.48 (m, 2H). ^{13}C NMR (126 MHz, $CDCl_3$) δ 169.5, 169.5, 167.7, 167.7, 164.7, 164.6, 159.9, 159.8, 148.2, 147.1, 140.4, 139.5, 135.9, 134.3, 134.2, 131.8, 129.2, 127.4, 123.7, 123.7, 123.3, 122.8, 121.1, 118.6, 118.2, 116.6, 53.5, 53.2, 53.1, 53.1, 34.4, 34.0. IR (cm^{-1}): 2253, 1738, 1574, 1410, 1388, 1229, 902, 722, 649. HRMS *calcd.* for ($C_{22}H_{17}N_3O_6$): 419.1117, *found* 419.1117.

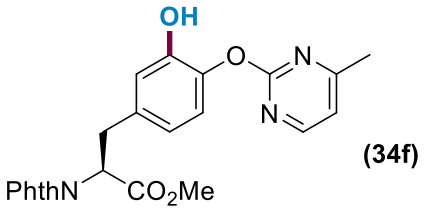

(34f)

Methyl (*S*)-2-(1,3-dioxoisoindolin-2-yl)-3-[3-hydroxy-4-((4-methylpyrimidin-2-yl)oxy)phenyl]propanoate (34f). A reaction tube was charged with **33f** (0.25 mmol, 104 mg), PIFA (0.37 mmol, 161 mg) and $Pd(OAc)_2$ (5 mol%). Then, DCE (1 mL) was added and the reaction tube was stirred at 80 ºC overnight. The mixture was then allowed to warm to room temperature, the solvent was evaporated and the resulting crude was washed up with an aqueous solution of $NaHCO_3$ (20 mL). The aqueous layer was extracted with EtOAc (3 x 20 mL), dried over $MgSO_4$ and evaporated under vacuum. The resulting crude was then purified by column chromatography to afford 23 mg (22% yield) of **34f** as a yellow oil.^{1}H NMR (400 MHz, $CDCl_3$) δ 8.26 (d, *J* = 5.0 Hz, 0.5H), 8.17 (d, *J* = 5.0 Hz, 0.5H), 7.80 (ddd, *J* = 10.7, 5.5, 3.1 Hz, 2H), 7.69 (ddd, *J* = 7.7, 5.5, 3.1 Hz, 2H), 7.04 – 6.96 (m, 1H), 6.94 – 6.90 (m, 1H), 6.81 (dd, *J* = 5.1, 1.8 Hz, 1H), 6.73 (dd, *J* = 8.3, 2.1 Hz, 1H), 5.18 (dd, *J* = 10.8, 5.6 Hz, 0.5H), 5.12 (dd, *J* = 10.9, 5.6 Hz, 0.5H), 3.79 (s, 1.5H), 3.77 (s, 1.5H), 2.38 (s, 1.5H), 2.37 (s, 1.5H). ^{13}C NMR (126 MHz, $CDCl_3$) δ 170.8, 170.8, 169.3, 169.2, 167.4, 167.4, 164.2, 164.2, 158.7, 158.6, 148.1, 147.0, 140.4, 139.5, 135.5, 134.0, 134.0, 131.6, 131.5, 128.8, 127.0, 123.4, 123.4, 123.1, 122.6, 120.6, 118.6, 118.2, 115.9, 53.2, 53.0, 52.8, 52.8, 34.1, 33.7, 23.7, 23.6. IR (cm^{-1}): 3053, 2987, 1980, 1717, 1588, 1264, 908, 731, 704. HRMS *calcd*. for ($C_{23}H_{19}N_3O_6$): 433.1274, *found* 433.1256.

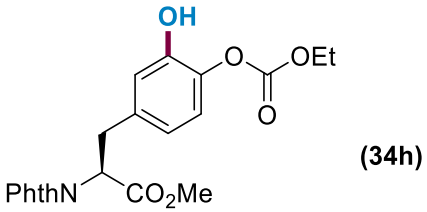

(34h)

Methyl (*S*)-2-(1,3-dioxoisoindolin-2-yl)-3-[4-((ethoxycarbonyl)oxy)-3-hydroxyphenyl]propanoate (34h). Following the general procedure A, using **33h** (0.25 mmol, 99 mg), and stirring overnight provided 19 mg (19 % yield) of **34h** as a colorless oil. The following data correspond to a mixture of mono- and difunctionalized compounds. Mp 70-71 ºC. ^{1}H NMR (500 MHz, $CDCl_3$) δ 7.80 (dd, *J* = 5.5, 3.1 Hz, 4H), 7.70 (ddd, *J* = 5.1, 3.0, 1.8 Hz, 4H), 7.06 – 6.97 (m, 2H), 6.94 (dd, *J* = 8.3, 2.1 Hz, 1H), 6.83 (d, *J* = 2.0 Hz, 1H), 6.81 (d, *J* = 8.3 Hz, 1H), 6.71 (dd,

J = 8.3, 2.1 Hz, 1H), 5.16 (dd, *J* = 11.1, 5.3 Hz, 1H), 5.11 (dd, *J* = 11.3, 5.3 Hz, 1H), 4.28 (dt, *J* = 13.6, 7.0 Hz, 4H), 3.78 (s, 6H), 3.65 – 3.41 (m, 4H), 1.53 – 1.24 (m, 6H). ^{13}C NMR (126 MHz, $CDCl_3$) δ 169.2, 169.1, 167.5, 167.5, 153.0, 152.9, 147.0, 145.8, 138.4, 137.6, 135.8, 134.1, 134.0, 131.4, 131.4, 129.2, 127.3, 123.5, 123.5, 122.5, 121.9, 120.9, 117.7, 117.5, 65.2, 65.2, 53.1, 52.9, 52.8, 34.0, 33.7, 14.0. IR (cm^{-1}): 2986, 2254, 1741, 1718, 1370, 1264, 907, 727, 703, 650. HRMS *calcd.* for ($C_{21}H_{19}NO_8$): 413.1111, *found* 413.1126.

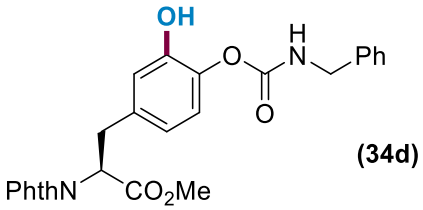

(34d)

Methyl (*S*)-3-[4-((benzylcarbamoyl)oxy)-3-hydroxyphenyl]-2-(1,3-dioxoisoindolin-2-yl)propanoate (34d). Following the general procedure B, using **33d** (0.25 mmol, 114 mg) provided 53 mg (45% yield) of **34d** as a brown oil. ^{1}H NMR (400 MHz, $CDCl_3$) δ 7.76 (dd, *J* = 5.5, 3.1 Hz, 1H), 7.66 (dd, *J* = 5.5, 3.1 Hz, 1H), 7.29 (q, *J* = 7.4, 6.6 Hz, 2H), 7.04 (s, 0H), 6.91 (d, *J* = 8.2 Hz, 0H), 6.80 (d, *J* = 2.2 Hz, 1H), 6.67 (dd, *J* = 8.3, 2.1 Hz, 1H), 5.80 (t, *J* = 6.0 Hz, 1H), 5.14 (dd, *J* = 10.9, 5.4 Hz, 1H), 4.35 (d, *J* = 6.0 Hz, 1H), 3.77 (s, 2H), 3.56 – 3.39 (m, 1H). ^{13}C NMR (126 MHz, $CDCl_3$) δ 169.2, 167.5, 154.6, 147.5, 137.9, 137.5, 135.1, 134.1, 131.3, 128.6, 127.5, 127.5, 123.4, 122.3, 120.8, 118.2, 53.0, 52.8, 45.2, 33.9. IR (cm^{-1}): 3367, 3030, 2952, 1703, 1501, 1433, 1386, 1192, 1102, 1019, 908, 717, 619, 529. HRMS *calcd.* for ($C_{26}H_{22}N_2O_7$): 474.1427, *found* 474.1434.

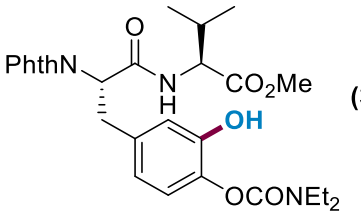

(36b)

Methyl [(*S*)-3-(4-((diethylcarbamoyl)oxy)-3-hydroxyphenyl)-2-(1,3-dioxoisoindolin-2-yl)propanoyl]-*L*-valinate (36b). Following the general procedure B, using **35b** (0.25 mmol, 131 mg) provided 89 mg (68% yield) of **36b** as a white solid. Mp 72-73 ºC. ^{1}H NMR (400 MHz, $CDCl_3$) δ 7.81 (dd, *J* = 5.4, 3.0 Hz, 2H), 7.71 (dd, *J* = 5.5, 3.1 Hz, 2H), 7.56 (s, 1H), 6.89 (d, *J* = 2.1 Hz, 1H), 6.84 (dd, *J* = 11.9, 8.4 Hz, 2H), 6.70 (dd, *J* = 8.2, 2.1 Hz, 1H), 5.22 (dd, *J* = 10.1, 6.3 Hz, 1H), 4.61 (dd, *J* = 8.7, 4.7 Hz, 1H), 3.61 (s, 3H), 3.57 – 3.50 (m, 2H), 3.40 (dq, *J* = 23.9, 7.1 Hz, 4H), 2.16 (hd, *J* = 7.0, 4.8 Hz, 1H), 1.21 (dt, *J* = 24.0, 7.1 Hz, 6H), 0.94 (d, *J* = 6.9 Hz, 3H), 0.84 (d, *J* = 6.9 Hz, 3H). ^{13}C NMR (75 MHz, $CDCl_3$) δ 173.1, 169.5, 169.0, 155.6, 149.0, 140.1, 136.3, 135.3, 132.5,

124.6, 123.4, 122.0, 120.6, 58.4, 56.8, 53.1, 43.6, 43.3, 35.4, 32.3, 19.9, 18.7, 15.1, 14.2. IR (cm^{-1}): 3312, 2970, 1715, 1525, 1429, 1378, 1216, 719, 529. HRMS *calcd.* for ($C_{28}H_{33}N_3O_8$): 539.2268, *found* 539.2285.

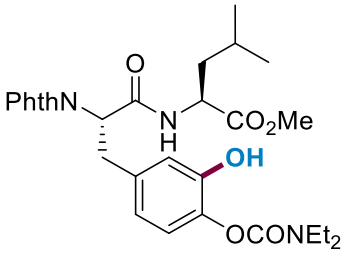

(36a)

Methyl [(*S*)-3-(4-((diethylcarbamoyl)oxy)-3-hydroxyphenyl)-2-(1,3-dioxoisoindolin-2-yl)propanoyl]-*L*-leucinate (36a). Following the general procedure B, using **35a** (0.25 mmol, 134 mg) provided 88 mg (63% yield) of **36a** as a yellow solid. Mp 147-148 ºC. ^{1}H NMR (400 MHz, $CDCl_3$) δ 7.83 (dd, *J* = 5.4, 3.1 Hz, 2H), 7.72 (dd, *J* = 5.5, 3.1 Hz, 2H), 7.43 (s, 1H), 6.90 (d, *J* = 2.1 Hz, 1H), 6.88 (d, *J* = 8.2 Hz, 1H), 6.74 (dd, *J* = 8.3, 2.1 Hz, 1H), 6.65 (d, *J* = 8.2 Hz, 1H), 5.19 (dd, *J* = 9.0, 7.5 Hz, 1H), 4.67 (td, *J* = 8.6, 4.8 Hz, 1H), 3.66 (s, 3H), 3.57 – 3.50 (m, 2H), 3.41 (dq, *J* = 21.9, 7.1 Hz, 4H), 1.66 – 1.45 (m, 3H), 1.23 (dt, *J* = 22.5, 7.1 Hz, 6H), 0.93 (dd, *J* = 8.5, 6.0 Hz, 6H). ^{13}C NMR (75 MHz, $CDCl_3$) δ 174.0, 168.9, 168.5, 155.2, 148.5, 139.7, 136.0, 134.8, 132.1, 124.1, 122.9, 121.6, 120.1, 56.1, 52.8, 51.5, 43.1, 42.9, 41.9, 34.8, 25.3, 23.4, 22.4, 14.7, 13.8. IR (cm^{-1}): 3421, 2957, 1687, 1520, 1381, 1200, 1154, 1086, 874, 722, 530. HRMS *calcd.* for ($C_{29}H_{35}N_3O_8$): 553.2424, *found* 553.2451. This reaction was also performed in a higher scale: the use of **35a** (0.93 mmol, 500 mg), PIFA (1.86 mmol, 800 mg) in a mixture of DCE (3.6 mL) and TFA (0.4 mL) provided 321 mg (62% yield) of **36a** as a yellow solid.

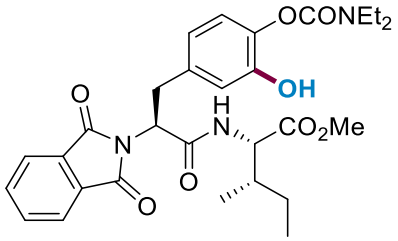

(36c)

Methyl [(*S*)-3-(4-((diethylcarbamoyl)oxy)-3-hydroxyphenyl)-2-(1,3-dioxoisoindolin-2-yl)propanoyl]-*L*-isoleucinate (36c). Following the general procedure B, using **35c** (0.25 mmol, 134 mg) provided 83.8 mg (60% yield) of **36c** as a brownish solid. Mp 66-67 ºC. Column chromatography (Hex/EtOAc 4:6). ^{1}H NMR (500 MHz, $CDCl_3$) δ 7.78 (dd, *J* = 5.5, 3.0 Hz, 2H), 7.68 (dd, *J* = 5.5, 3.1 Hz, 2H), 7.50 (s, 1H), 6.87 – 6.81 (m, 2H), 6.78 (d, *J* = 8.5 Hz, 1H), 6.69 (dd,

J = 8.2, 2.1 Hz, 1H), 5.16 (dd, *J* = 9.0, 7.4 Hz, 1H), 4.60 (dd, *J* = 8.4, 4.7 Hz, 1H), 3.62 (s, 3H), 3.54 – 3.45 (m, 2H), 3.37 (dq, *J* = 30.0, 7.1 Hz, 4H), 1.91 – 1.87 (m, 1H), 1.36 – 1.29 (m, 1H), 1.29 – 0.98 (m, 7H), 0.86 (dt, *J* = 7.4, 3.9 Hz, 6H). ^{13}C NMR (126 MHz, $CDCl_3$) δ 172.2, 168.4, 168.0, 154.7, 148.1, 139.2, 135.3, 134.4, 131.5, 123.7, 122.4, 121.0, 119.6, 56.8, 55.8, 52.2, 42.7, 42.4, 38.0, 34.4, 25.2, 15.5, 14.2, 13.3, 11.6. IR (cm^{-1}): 3323, 1773, 1712, 1380, 719. HRMS (ESI) m/z: (M^+) *calcd.* for ($C_{29}H_{35}N_3O_8$): 553.2324, *found* 553.2425.

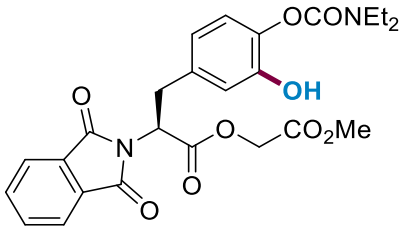

(36d)

2-Methoxy-2-oxoethyl (*S*)-3-[4-((diethylcarbamoyl)oxy)-3-hydroxyphenyl]-2-(1,3-dioxoisoindolin-2-yl)propanoate (36d). Following the general procedure B, using **35d** (0.25 mmol, 120.6 mg) provided 77.8 mg (62% yield) of **36d** as a brownish solid. Mp 120-121 ºC. Column chromatography (Hex/EtOAc 4:6). ^{1}H NMR (400 MHz, $CDCl_3$) δ 7.78 (dd, *J* = 5.5, 3.1 Hz, 2H), 7.67 (dd, *J* = 5.5, 3.1 Hz, 2H), 6.89 – 6.77 (m, 2H), 6.71 (dd, *J* = 8.3, 2.1 Hz, 1H), 5.26 (t, *J* = 8.3 Hz, 1H), 4.80 – 4.54 (m, 2H), 3.74 (s, 3H), 3.54 (d, *J* = 8.2 Hz, 2H), 3.36 (dt, *J* = 22.0, 7.1 Hz, 4H), 1.18 (dt, *J* = 22.8, 7.0 Hz, 6H). ^{13}C NMR (126 MHz, $CDCl_3$) δ 168.5, 167.6, 167.5, 154.7, 147.8, 139.2, 135.2, 134.3, 131.2, 123.7, 122.3, 121.2, 119.9, 61.7, 53.0, 52.5, 42.7, 42.4, 33.9, 14.2, 13.3. IR (cm^{-1}): 3528, 1747, 1711, 1672, 1474, 725. HRMS (ESI) m/z: (M^+) *calcd.* for ($C_{25}H_{26}N_2O_9$): 498.1638, *found* 498.1637.

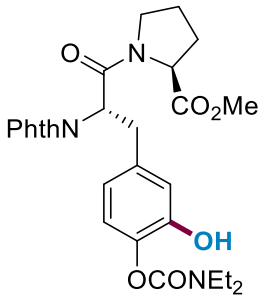

(36e)

Methyl [(*S*)-3-(4-((diethylcarbamoyl)oxy)-3-hydroxyphenyl]-2-(1,3-dioxoisoindolin-2-yl)propanoyl)-*L*-prolinate (36e). Following the general procedure B, using **35e** (0.25 mmol, 130 mg) provided 93 mg (69% yield) of **36e** as a white solid. Mp 100-101 ºC. ^{1}H NMR (400 MHz, $CDCl_3$) δ 7.80 (dd, *J* = 5.4, 3.0 Hz, 2H), 7.70 (dd, *J* = 5.5, 3.1 Hz, 2H), 7.36 (s, 1H), 6.98 – 6.86 (m,

2H), 6.76 (dd, *J* = 8.2, 2.2 Hz, 1H), 5.21 (dd, *J* = 9.9, 5.9 Hz, 1H), 4.50 (dd, *J* = 8.3, 3.5 Hz, 1H), 3.75 (s, 3H), 3.71 – 3.28 (m, 8H), 2.25 – 1.73 (m, 4H), 1.22 (dt, *J* = 25.6, 6.8 Hz, 6H). ^{13}C NMR (126 MHz, $CDCl_3$) δ 172.5, 167.6, 167.4, 154.4, 147.7, 138.9, 135.4, 134.0, 131.3, 123.4, 122.1, 121.2, 119.7, 59.4, 54.1, 52.2, 46.9, 42.4, 42.2, 33.7, 28.7, 24.9, 14.0, 13.1. IR (cm^{-1}): 3379, 2970, 2217, 1649, 1374, 1206, 990, 825, 611. HRMS *calcd.* for ($C_{28}H_{31}N_3O_8$): 537.2111, *found* 537.2135.

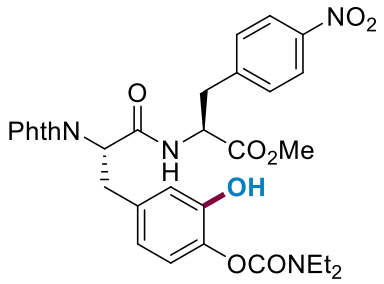

(36f)

Methyl (*S*)-2-[(*S*)-3-(4-((diethylcarbamoyl)oxy)-3-hydroxyphenyl)-2-(1,3-dioxoiso-indolin-2-yl)propanamido]-3-(4-nitrophenyl)propanoate (36f). Following the general procedure B, using **35f** (0.25 mmol, 154 mg) provided 116 mg (74% yield) of **36f** as a white solid. Mp 162-163 ºC. ^{1}H NMR (400 MHz, $CDCl_3$) δ 8.00 (d, *J* = 8.7 Hz, 2H), 7.84 – 7.78 (m, 2H), 7.76 – 7.70 (m, 2H), 7.40 (s, 1H), 7.21 (d, *J* = 8.7 Hz, 2H), 6.90 – 6.84 (m, 2H), 6.71 (dd, *J* = 8.2, 2.1 Hz, 1H), 6.57 (d, *J* = 7.4 Hz, 1H), 5.08 (dd, *J* = 9.6, 6.7 Hz, 1H), 4.93 (dd, *J* = 7.4, 6.0 Hz, 1H), 3.74 (s, 3H), 3.58 – 3.36 (m, 6H), 3.23 (ddd, *J* = 63.1, 13.9, 6.0 Hz, 2H), 1.23 (dt, *J* = 23.2, 7.1 Hz, 6H). ^{13}C NMR (75 MHz, $CDCl_3$) δ 171.6, 168.7, 168.3, 155.1, 148.5, 147.6, 144.1, 139.9, 135.7, 135.1, 131.9, 130.8, 130.7, 124.2, 124.2, 123.0, 121.7, 120.4, 55.7, 53.7, 53.3, 43.2, 43.0, 38.0, 34.5, 14.7, 13.8. IR (cm^{-1}): 3338, 2964, 1703, 1518, 1344, 1247, 1100, 873, 719, 529. HRMS *calcd.* for ($C_{32}H_{32}N_4O_{10}$): 632.2118, *found* 632.2139.

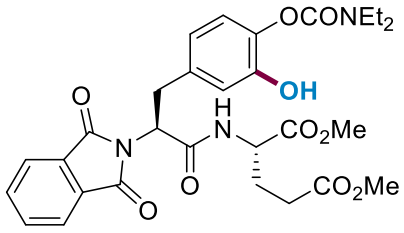

(36g)

Dimethyl [(*S*)-3-(4-((diethylcarbamoyl)oxy)-3-hydroxyphenyl)-2-(1,3-dioxo-isoindolin-2-yl)propanoyl)-*L*-glutamate (36g). Following the general procedure B, using **35g** (0.25 mmol, 142 mg) provided 77.9 mg (54% yield) of **36g** as a brownish solid. Mp 70-71 ºC. Column chromatography (Hex/EtOAc 3:7). ^{1}H NMR (500 MHz, $CDCl_3$) δ 7.77 (dd, *J* = 5.4, 3.0 Hz, 2H),

7.67 (dd, *J* = 5.5, 3.0 Hz, 2H), 7.45 (s, 1H), 7.18 (d, *J* = 7.5 Hz, 1H), 6.89 – 6.75 (m, 2H), 6.65 (dd, *J* = 8.2, 2.1 Hz, 1H), 5.17 (dd, *J* = 11.1, 5.3 Hz, 1H), 4.60 (td, *J* = 7.9, 4.8 Hz, 1H), 3.60 (s, 3H), 3.53 (s, 3H), 3.56– 3.45 (m, 2H), 3.44 – 3.25 (m, 4H), 2.44 – 2.28 (m, 2H), 2.18 – 2.11 (m, 1H), 1.92 (tt, *J* = 14.6, 7.0 Hz, 2H), 1.18 (dt, *J* = 29.6, 7.1 Hz, 6H). ^{13}C NMR (126 MHz, $CDCl_3$) δ 173.8, 172.1, 168.6, 167.9, 154.7, 147.9, 139.2, 135.5, 134.2, 131.7, 123.6, 122.4, 121.1, 119.7, 55.3, 52.6, 52.2, 51.9, 42.6, 42.4, 34.0, 30.0, 26.9, 14.2, 13.3. IR (cm^{-1}): 3326, 1773, 1713, 1274, 739. HRMS (ESI) m/z: (M^+) *calcd.* for ($C_{29}H_{33}N_3O_{10}$): 583.2166, *found* 583.2179.

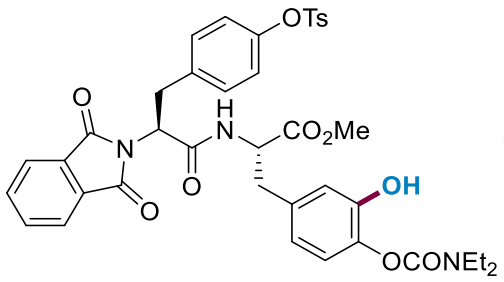

(36h)

Methyl (*S*)-3-[4-((diethylcarbamoyl)oxy)-3-hydroxyphenyl]-2-[(*S*)-2-(1,3-dioxoiso-indolin-2-yl)-3-(4-(tosyloxy)phenyl)propanamido]propanoate (36h). Following the general procedure B, using **35h** (0.25 mmol, 185 mg) provided 115 mg (61% yield) of **36h** as a brownish solid. Mp 78-79 ºC. Column chromatography (Hex/EtOAc 3:7). ^{1}H NMR (500 MHz, $CDCl_3$) δ 7.76 (dd, *J* = 5.5, 3.1 Hz, 2H), 7.69 (dd, *J* = 5.5, 3.1 Hz, 3H), 7.52 (d, *J* = 5.5 Hz, 2H), 7.21 (d, *J* = 8.1 Hz, 2H), 7.02 (d, *J* = 5.5 Hz, 2H), 6.78 – 6.68 (m, 4H), 6.64 (d, *J* = 2.1 Hz, 1H), 6.51 (dd, *J* = 8.2, 2.1 Hz, 1H), 5.03 (dd, *J* = 9.8, 6.9 Hz, 1H), 4.78 (dt, *J* = 7.7, 5.8 Hz, 1H), 3.58 (s, 3H), 3.53 – 3.29 (m, 6H), 3.08 – 2.87 (m, 2H), 2.39 (s, 3H), 1.21 (dt, *J* = 34.9, 7.1 Hz, 6H). ^{13}C NMR (126 MHz, $CDCl_3$) δ 171.5, 167.9, 167.8, 154.6, 148.5, 147.9, 145.4, 139.2, 135.9, 134.4, 134.1, 132.1, 131.3, 130.1, 129.7, 128.5, 123.7, 122.6, 122.3, 121.3, 119.9, 55.3, 53.5, 52.5, 42.6, 42.4, 36.9, 33.9, 21.8, 14.2, 13.3. IR (cm^{-1}): 3351, 3307, 1774, 1714, 1373, 720, 548. HRMS (ESI) m/z: (M^+) *calcd.* for ($C_{39}H_{39}N_3O_{11}S$): 757.2305, *found* 757.2265.

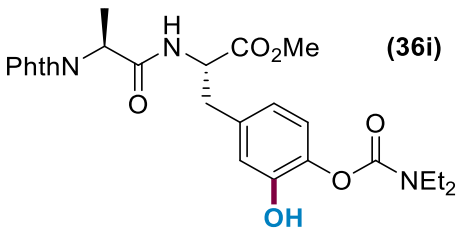

(36i)

Methyl (*S*)-3-[4-((diethylcarbamoyl)oxy)-3-hydroxyphenyl]-2-[(*S*)-2-(1,3-dioxoisoi-ndolin-2-yl)propanamido]propanoate (36i). Following the general procedure B, using **35i** (0.25 mmol, 124 mg) provided 83 mg (74% yield) of **36i** as a white solid. Mp 68-69 ºC. ^{1}H NMR (400 MHz, $CDCl_3$) δ 7.88 (dd, *J* = 5.5, 3.1 Hz, 2H), 7.74 (dd, *J* = 5.5, 3.0 Hz, 2H), 7.41 (s, 1H), 6.83 (d, *J* = 8.1 Hz, 1H), 6.70 (d, *J* = 2.1 Hz, 1H), 6.62 – 6.53 (m, 2H), 4.95 (q, *J* = 7.3 Hz, 1H), 4.83 (dt, *J* = 7.5, 5.6 Hz, 1H), 3.69 (s, 3H), 3.44 (dq, *J* = 25.2, 7.2 Hz, 4H), 3.18 – 2.98 (m, 2H), 1.71 (d, *J* = 7.4 Hz, 3H), 1.25 (dt, *J* = 27.2, 7.1 Hz, 6H). ^{13}C NMR (75 MHz, $CDCl_3$) δ 172.1, 169.4, 168.4, 155.1, 148.5, 139.8, 134.8, 134.7, 132.4, 124.2, 122.8, 121.9, 120.5, 54.0, 53.0, 49.9, 43.2, 42.9, 37.4, 15.7, 14.7, 13.9. IR (cm^{-1}): 3342, 2976, 1705, 1525, 1430, 1382, 1154, 880, 719, 529. HRMS *calcd*. for ($C_{26}H_{29}N_3O_8$): 511.1955, *found* 511.1981.

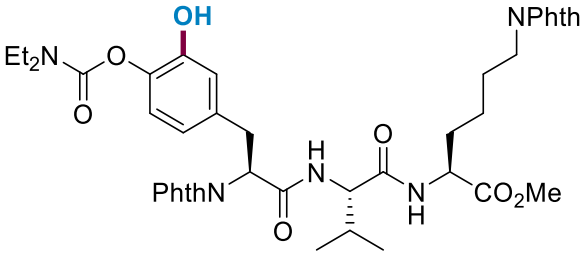

(36j)

Methyl (*S*)-2-[(*S*)-2-((*S*)-3-(4-((diethylcarbamoyl)oxy)-3-hydroxyphenyl)-2-(1,3-dioxoisoindolin-2-yl)propanamido)-3-methylbutanamido]-6-(1,3-dioxoisoindolin-2-yl) hexanoate (36j). Following the general procedure B, using **35j** (0.25 mmol, 195 mg) provided 62 mg (31% yield) of **36j** as a white solid. Mp 88-89 ºC. ^{1}H NMR (500 MHz, $CDCl_3$) δ 7.85 (dd, *J* = 5.4, 3.1 Hz, 2H), 7.77 (dd, *J* = 5.5, 3.1 Hz, 2H), 7.72 (dd, *J* = 5.5, 3.0 Hz, 2H), 7.67 (dd, *J* = 5.5, 3.1 Hz, 2H), 6.94 (d, *J* = 8.4 Hz, 1H), 6.88 (d, *J* = 2.1 Hz, 1H), 6.85 (d, *J* = 8.2 Hz, 1H), 6.82 (d, *J* = 7.3 Hz, 1H), 6.70 (dd, *J* = 8.2, 2.1 Hz, 1H), 5.19 (dd, *J* = 9.4, 7.0 Hz, 1H), 4.59 – 4.40 (m, 2H), 3.69 (s, 3H), 3.68 – 3.64 (m, 2H), 3.56 – 3.50 (m, 2H), 3.38 (dq, *J* = 32.1, 7.1 Hz, 4H), 2.27 – 2.13 (m, 1H), 1.94 – 1.74 (m, 2H), 1.67 (dq, *J* = 31.5, 7.0 Hz, 2H), 1.42 – 1.29 (m, 2H), 1.20 (dt, *J* = 31.6, 7.1 Hz, 6H), 0.94 (dd, *J* = 24.7, 6.8 Hz, 6H). ^{13}C NMR (126 MHz, $CDCl_3$) δ 172.4, 171.0, 168.9, 168.7, 168.0, 154.6, 148.2, 139.1, 135.4, 134.3, 134.2, 132.1, 131.6, 123.7, 123.5, 122.6, 121.0, 119.4, 58.7, 55.5, 52.5, 52.4, 42.6, 42.4, 37.0, 34.4, 31.5, 30.8, 28.1, 22.5, 19.2, 18.0, 14.2, 13.4. IR (cm^{-1}): 3430, 2970, 1715, 1507, 1366, 1216, 720, 529. HRMS *calcd.* for ($C_{41}H_{45}N_5O_{11}$): 798.3100, *found* 798.3353.

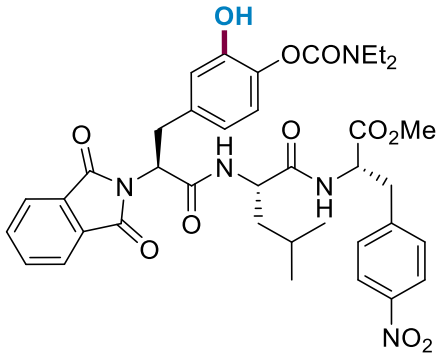

(36k)

Methyl (*S*)-2-[(*S*)-2-((*S*)-3-(4-((diethylcarbamoyl)oxy)-3-hydroxyphenyl)-2-(1,3-dioxoisoindolin-2-yl)propanamido)-4-methylpentanamido]-3-(4-nitrophenyl) propanoate (36k). Following the general procedure B, using **35k** (0.25 mmol, 182 mg) provided 80 mg (43% yield) of **36k** as a yellowish solid. Mp 108-109 ºC. Column chromatography (Hex/EtOAc 3:7). ^{1}H NMR (300 MHz, $CDCl_3$) δ 8.16 – 7.87 (m, 3H), 7.82 – 7.54 (m, 4H), 7.27 (dd, *J* = 8.8, 6.7 Hz, 3H), 7.03 (d, *J* = 7.8 Hz, 1H), 6.82 (dd, *J* = 5.1, 3.1 Hz, 2H), 6.64 (dd, *J* = 8.2, 2.0 Hz, 1H), 5.16 (dd, *J* = 10.2, 6.0 Hz, 1H), 4.86 – 4.68 (m, 1H), 4.60 – 4.35 (m, 1H), 3.63 (s, 3H), 3.59 – 2.87 (m, 8H), 2.67 – 2.39 (m, 1H), 1.65 – 1.36 (m, 3H), 1.19 (tt, *J* = 17.0, 7.0 Hz, 7H), 0.82 (d, *J* = 5.5 Hz, 6H). ^{13}C NMR (75 MHz, $CDCl_3$) δ 172.1, 171.1, 169.0, 168.0, 154.5, 148.4, 147.0, 144.0, 138.8, 135.0, 134.3, 131.4, 130.4, 123.6, 123.5, 122.7, 120.5, 118.6, 55.0, 53.2, 52.5, 52.4, 42.4, 42.1, 40.5, 37.3, 34.2, 24.6, 22.7, 22.0, 14.0, 13.3. IR (cm^{-1}): 3281, 1711, 1656, 1605, 1519, 1344, 719. HRMS (ESI) m/z: (M^+) *calcd.* for ($C_{38}H_{43}N_5O_{11}$): 745.2959, *found* 745.2973.

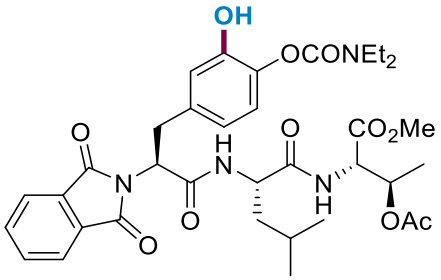

(36l)

Methyl *O*-acetyl-*N*-[(*S*)-3-(4-((diethylcarbamoyl)oxy)-3-hydroxyphenyl)-2-(1,3-dioxoisoindolin-2-yl)propanoyl)-*L*-leucyl]-*L*-threoninate (36l). Following the general procedure B, using **35l** (0.25 mmol, 170 mg) provided 54 mg (31% yield) of **36l** as a white solid. Mp 163-165 ºC. Column chromatography (Hex/EtOAc 3:7). ^{1}H NMR (300 MHz, $CDCl_3$) δ 7.77 – 7.54 (m, 5H), 7.05 – 6.94 (m, 1H), 6.92 – 6.82 (m, 1H), 6.82 – 6.72 (m, 2H), 6.61 (dd, *J* = 8.2, 2.1 Hz, 1H), 5.41 – 5.34 (m, 1H), 5.11 (dd, *J* = 10.4, 6.0 Hz, 1H), 4.67 (dd, *J* = 9.1, 2.8 Hz, 1H), 4.61 – 4.39 (m, 1H),

3.68 (s, 3H), 3.55 – 3.17 (m, 6H), 2.23 (s, 1H), 1.98 (s, 3H), 1.79 – 1.45 (m, 3H), 1.31 – 1.07 (m, 10H), 0.88 (d, *J* = 3.4 Hz, 6H). ^{13}C NMR (75 MHz, $CDCl_3$) δ 172.5, 170.0, 169.9, 168.9, 168.0, 154.5, 148.2, 139.0, 135.0, 134.4, 134.3, 131.5, 123.6, 122.6, 120.8, 119.1, 70.2, 55.6, 55.4, 52.7, 52.4, 42.5, 42.2, 40.5, 34.3, 24.7, 22.8, 22.1, 21.0, 17.0, 14.1, 13.3. IR (cm^{-1}): 3294, 1744, 1710, 1655, 1608, 1380, 719. HRMS (ESI) m/z: (M^+) *calcd.* for ($C_{35}H_{44}N_4O_{11}$): 696.3007, *found* 696.3001.

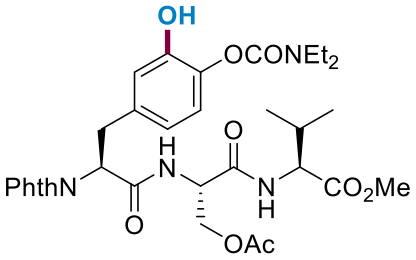

(36m)

Methyl *O*-acetyl-*N*-[(*S*)-3-(4-((diethylcarbamoyl)oxy)-3-hydroxyphenyl)-2-(1,3-dioxoisoindolin-2-yl)propanoyl]-*L*-seryl-*L*-valinate (36m). Following the general procedure B, using **35m** (0.25 mmol,163 mg) provided 56 mg (33% yield) of **36m** as a white solid. Mp 198-200 ºC. ^{1}H NMR (400 MHz, $CDCl_3$) δ 7.81 (dd, *J* = 5.5, 3.1 Hz, 2H), 7.72 (dd, *J* = 5.5, 3.1 Hz, 2H), 7.49 (s, 1H), 7.20 (d, *J* = 7.2 Hz, 1H), 6.94 (d, *J* = 8.6 Hz, 1H), 6.87 (d, *J* = 8.2 Hz, 2H), 6.72 (dd, *J* = 8.2, 2.1 Hz, 1H), 5.18 (dd, *J* = 10.0, 6.4 Hz, 1H), 4.75 (q, *J* = 6.0 Hz, 1H), 4.50 – 4.39 (m, 2H), 4.29 (dd, *J* = 11.5, 5.2 Hz, 1H), 3.71 (s, 3H), 3.68 – 3.22 (m, 6H), 2.18 (pd, *J* = 6.9, 5.0 Hz, 1H), 2.06 (s, 3H), 1.22 (dt, *J* = 23.7, 7.1 Hz, 6H), 0.91 (t, *J* = 7.2 Hz, 6H). ^{13}C NMR (126 MHz, $CDCl_3$) δ 171.6, 171.2, 168.7, 168.3, 167.7, 154.4, 147.8, 139.1, 134.9, 134.2, 131.4, 123.6, 122.3, 120.9, 119.6, 63.3, 57.4, 55.0, 52.9, 52.1, 42.5, 42.2, 34.0, 30.9, 20.6, 18.8, 17.6, 14.0, 13.1. IR (cm^{-1}): 3388, 3350, 2969, 1705, 1644, 1519, 1389, 1247, 1164, 876, 721, 562. HRMS *calcd.* for ($C_{33}H_{40}N_4O_{11}$): 668.2694, *found* 668.2706.

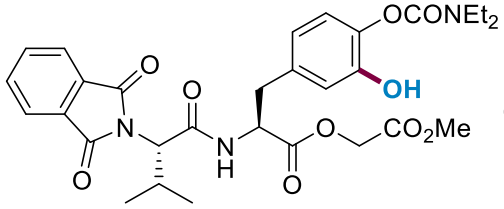

(36n)

2-Methoxy-2-oxoethyl (*S*)-3-[4-((diethylcarbamoyl)oxy)-3-hydroxyphenyl]-2-((*S*)-2-(1,3-dioxoisoindolin-2-yl)-3-methylbutanamido]propanoate (36n). Following the general procedure B, using **35n** (0.25 mmol, 145 mg) provided 84 mg (56% yield) of **36n** as a brownish solid. Mp 62-63 ºC. Column chromatography (Hex/EtOAc 3:7). ^{1}H NMR (500 MHz, $CDCl_3$) δ 7.85 (dd, *J* = 5.5,

3.1 Hz, 2H), 7.73 (dd, *J* = 5.5, 3.0 Hz, 2H), 7.37 (d, *J* = 8.1 Hz, 1H), 6.90 – 6.81 (m, 2H), 6.72 (dd, *J* = 8.2, 2.1 Hz, 1H), 4.88 (td, *J* = 8.1, 5.2 Hz, 1H), 4.67 (d, *J* = 15.9 Hz, 1H), 4.53 (d, *J* = 15.8 Hz, 1H), 4.35 (d, *J* = 11.3 Hz, 1H), 3.68 (s, 3H), 3.42 (dq, *J* = 29.9, 7.1 Hz, 4H), 3.21 (dd, *J* = 14.2, 5.2 Hz, 1H), 3.01 (dd, *J* = 14.2, 8.1 Hz, 1H), 2.81 – 2.67 (m, 1H), 1.83 (s, 1H), 1.34 – 1.15 (m, 6H), 0.91 (d, *J* = 6.6 Hz, 3H), 0.80 (d, *J* = 6.6 Hz, 3H). ^{13}C NMR (126 MHz, $CDCl_3$) δ 170.7, 168.8, 168.5, 167.8, 154.7, 147.9, 139.5, 134.6, 134.4, 131.5, 123.8, 122.3, 121.5, 120.4, 63.0, 61.2, 53.1, 52.4, 42.7, 42.5, 36.9, 27.6, 19.7, 19.6, 14.3, 13.4. IR (cm^{-1}): 3355, 1750, 1707, 1333, 718. HRMS (ESI) m/z: (M^+) *calcd.* for ($C_{30}H_{35}N_3O_{10}$): 597.2322, *found* 597.2323.

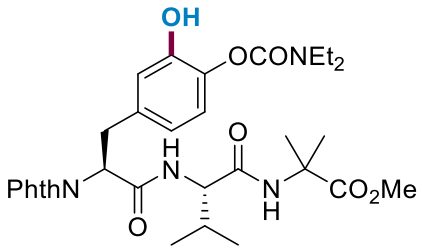

(36o)

Methyl 2-[(*S*)-2-((*S*)-3-(4-((diethylcarbamoyl)oxy)-3-hydroxyphenyl)-2-(1,3-dioxoisoindolin-2-yl)propanamido)-3-methylbutanamido]-2-methylpropanoate (36o). Following the general procedure B, using **35o** (0.25 mmol, 152 mg) provided 64 mg (41% yield) of **36o** as a white solid. Mp 120-122 ºC. ^{1}H NMR (500 MHz, $CDCl_3$) δ 7.88 – 7.72 (m, 2H), 7.71 – 7.62 (m, 2H), 7.18 (d, *J* = 8.4 Hz, 1H), 7.03 (d, *J* = 20.9 Hz, 1H), 6.97 (d, *J* = 8.5 Hz, 1H), 6.84 (ddd, *J* = 22.2, 13.9, 2.1 Hz, 2H), 6.68 (ddd, *J* = 8.2, 3.8, 2.1 Hz, 1H), 5.25 – 5.13 (m, 1H), 4.26 (ddd, *J* = 36.0, 8.5, 6.9 Hz, 1H), 3.68 (d, *J* = 2.5 Hz, 3H), 3.62 – 3.49 (m, 2H), 3.38 (dq, *J* = 30.9, 7.2 Hz, 4H), 2.29 – 2.07 (m, 1H), 1.47 (dd, *J* = 20.7, 5.2 Hz, 6H), 1.20 (dt, *J* = 31.6, 7.4 Hz, 6H), 1.06 – 0.62 (m, 6H). ^{13}C NMR (126 MHz, $CDCl_3$) δ 174.8, 174.7, 170.3, 170.2, 169.0, 169.0, 168.2, 168.1, 154.6, 154.6, 148.4, 148.4, 139.1, 139.0, 135.2, 135.1, 134.4, 134.4, 131.6, 131.6, 123.7, 122.7, 121.0, 120.8, 119.2, 119.0, 59.1, 58.8, 56.5, 56.4, 55.6, 55.3, 52.6, 52.6, 42.6, 42.6, 42.4, 34.3, 34.3, 31.1, 30.9, 25.1, 25.0, 24.8, 24.7, 19.2, 19.2, 18.3, 18.1, 14.2, 13.4. IR (cm^{-1}): 3325, 2970, 2254, 1716, 1676, 1366, 1264, 906, 727. HRMS *calcd.* for ($C_{32}H_{40}N_4O_9$): 624.2795, *found* 624.2802.

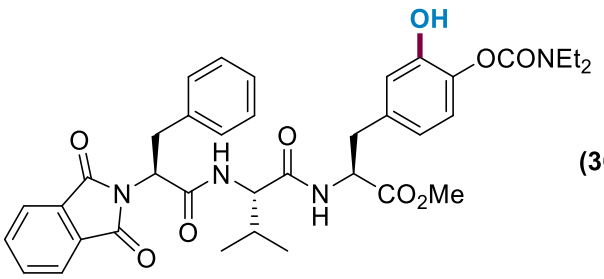

(36p)

Methyl (*S*)-3-[4-((diethylcarbamoyl)oxy)-3-hydroxyphenyl]-2-[(*S*)-2-((*S*)-2-(1,3-dioxoisoindolin-2-yl)-3-phenylpropanamido)-3-methylbutanamido]propanoate (36p). Following the general procedure B, using **35p** (0.25 mmol, 167 mg) provided 67 mg (40% yield) of **36p** as a white solid. Mp 106-107 ºC. Column chromatography (Hex/EtOAc 4:6). ^{1}H NMR (300 MHz, $CDCl_3$) δ 7.86 (s, 1H), 7.77 – 7.69 (m, 2H), 7.69 – 7.59 (m, 2H), 7.20 – 7.04 (m, 5H), 7.00 – 6.83 (m, 3H), 6.70 (d, *J* = 2.1 Hz, 1H), 6.55 (dd, *J* = 8.1, 2.0 Hz, 1H), 5.18 (dd, *J* = 9.5, 7.2 Hz, 1H), 4.76 – 4.70 (m, 1H), 4.35 – 4.30 (m, 1H), 3.65 (s, 3H), 3.57 – 3.24 (m, 6H), 3.11 – 2.88 (m, 2H), 2.39 (s, 1H), 2.12 – 1.86 (m, 1H), 1.20 (dt, *J* = 23.5, 7.3 Hz, 6H), 0.85 (dd, *J* = 15.5, 6.7 Hz, 6H). ^{13}C NMR (75 MHz, $CDCl_3$) δ 171.6, 170.8, 168.9, 168.0, 154.5, 148.4, 139.0, 136.6, 134.3, 134.0, 131.5, 129.0, 128.7, 127.0, 123.6, 123.0, 120.9, 119.3, 59.0, 55.4, 53.4, 52.4, 42.5, 42.2, 36.9, 34.9, 30.9, 19.2, 18.1, 14.1, 13.4. IR (cm^{-1}): 3281, 1777, 1712, 1646, 1380, 752. HRMS (ESI) m/z: (M^+) *calcd.* for ($C_{37}H_{42}N_4O_9$): 686.2952, *found* 686.2986.

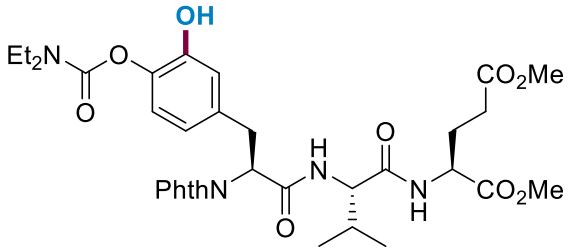

(36q)

Dimethyl [(*S*)-3-(4-((diethylcarbamoyl)oxy)-3-hydroxyphenyl)-2-(1,3-dioxoiso-indolin-2-yl)propanoyl)-*L*-valyl-*L*-glutamate (36q). Following the general procedure B, using **35q** (0.25 mmol, 167 mg) provided 95 mg (56% yield) of **36q** as a white solid. Mp 166-167 ºC. ^{1}H NMR (400 MHz, $CDCl_3$) δ 7.80 (dd, *J* = 5.5, 3.1 Hz, 2H), 7.70 (dd, *J* = 5.5, 3.1 Hz, 2H), 7.66 (s, 1H), 7.00 (d, *J* = 7.6 Hz, 1H), 6.93 (d, *J* = 8.3 Hz, 1H), 6.89 (d, *J* = 2.1 Hz, 1H), 6.86 (d, *J* = 8.2 Hz, 1H), 6.72 (dd, *J* = 8.2, 2.1 Hz, 1H), 5.21 (t, *J* = 8.2 Hz, 1H), 4.50 (td, *J* = 8.0, 5.0 Hz, 1H), 4.33 (dd, *J* = 8.3, 6.3 Hz, 1H), 3.72 (s, 3H), 3.66 (s, 3H), 3.54 (d, *J* = 8.2 Hz, 2H), 3.40 (dq, *J* = 25.5, 7.1 Hz, 4H), 2.35 (td, *J* = 7.2, 1.8 Hz, 2H), 2.24 – 2.10 (m, 1H), 2.01 (ddd, *J* = 14.5, 8.2, 6.8 Hz, 1H), 1.22 (dt, *J* = 25.0, 7.1 Hz, 6H), 0.94 (dd, *J* = 15.1, 6.8 Hz, 6H). ^{13}C NMR (75 MHz, $CDCl_3$) δ 174.0, 172.4, 171.5, 169.3, 168.5, 155.1, 148.7, 139.6, 135.8, 134.8, 132.1, 124.2, 123.1, 121.4, 119.8, 59.4, 56.0, 53.0, 52.5, 43.1, 42.8, 34.9, 31.7, 30.6, 27.1, 19.6, 18.5, 14.7, 13.8. IR (cm^{-1}): 3311, 2970, 1737, 1707, 1518, 1427, 1384, 1203, 888, 720. HRMS *calcd*. for ($C_{34}H_{42}N_4O_{11}$): 682.2850, *found* 682.2856.

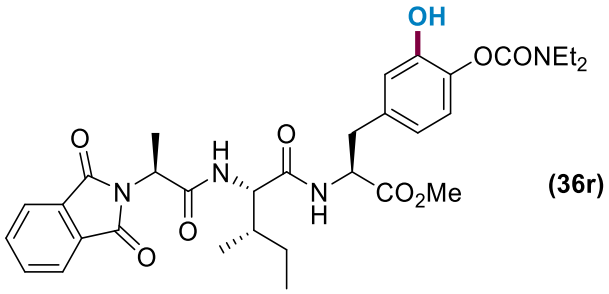

(36r)

Methyl (*S*)-3-[4-((diethylcarbamoyl)oxy)-3-hydroxyphenyl]-2-[(2*S*,3*S*)-2-((*S*)-2-(1,3-dioxoisoindolin-2-yl)propanamido)-3-methylpentanamido]propanoate (36r). Following the general procedure B, using **35r** (0.25 mmol, 152 mg) provided 69 mg (44% yield) of **36r** as a brownish solid. Mp 97-98 ºC. Column chromatography (Hex/EtOAc 3:7). ^{1}H NMR (500 MHz, $CDCl_3$) δ 7.82 (dd, *J* = 5.4, 3.2 Hz, 2H), 7.70 (dd, *J* = 5.5, 3.1 Hz, 2H), 6.91 (d, *J* = 8.1 Hz, 1H), 6.82 (dd, *J* = 12.4, 8.1 Hz, 2H), 6.69 (d, *J* = 2.1 Hz, 1H), 6.55 (dd, *J* = 8.1, 2.1 Hz, 1H), 4.94 – 4.90 (m, 1H), 4.77 – 4.73 (m, 1H), 4.35 – 4.32 (m, 1H), 3.66 (s, 3H), 3.52 – 3.23 (m, 5H), 3.17 – 2.84 (m, 2H), 2.34 (s, 1H), 1.81 (ddt, *J* = 13.3, 6.9, 3.3 Hz, 1H), 1.67 (d, *J* = 7.4 Hz, 3H), 1.38 (ddd, *J* = 13.5, 7.5, 3.5 Hz, 1H), 1.32 – 1.12 (m, 8H), 1.12 – 0.97 (m, 1H), 0.91 – 0.78 (m, 6H). ^{13}C NMR (126 MHz, $CDCl_3$) δ 171.5, 170.8, 169.5, 167.9, 154.5, 148.4, 139.0, 134.3, 134.0, 131.9, 123.6, 123.6, 123.0, 120.8, 119.3, 58.1, 53.4, 52.4, 49.2, 42.5, 42.2, 37.1, 36.8, 24.8, 15.4, 15.3, 14.1, 13.4, 11.1. IR (cm^{-1}): 3295, 1777, 1714, 1645, 756. HRMS (ESI) m/z: (M^+) *calcd.* for ($C_{32}H_{40}N_4O_9$): 624.2795, *found* 624.2814.

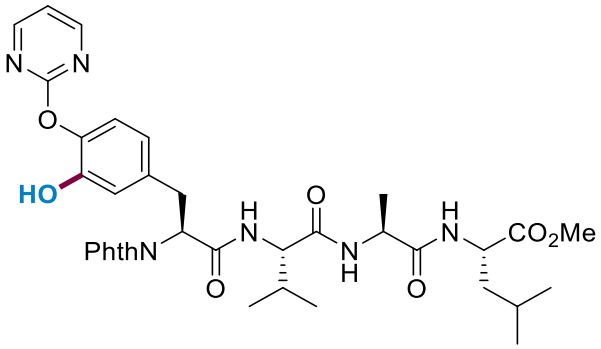

(38d)

Methyl [(*S*)-2-(1,3-dioxoisoindolin-2-yl)-3-(3-hydroxy-4-(pyrimidin-2-yloxy)phenyl) propanoyl)-*L*-valyl-*L*-alanyl-*L*-leucinate (38d) A reaction tube was charged with **37d** (0.15 mmol, 103 mg), PIFA (0.30 mmol, 129 mg) and $Pd(OAc)_2$ (10 mol%). Then, DCE (2 mL) was added and the reaction tube was stirred at 80 ºC overnight. The mixture was then allowed to warm to room temperature, the solvent was evaporated and the resulting crude was washed up with an aqueous

solution of $NaHCO_3$ (10 mL). The aqueous layer was extracted with EtOAc (3 x 10 mL), dried over $MgSO_4$ and evaporated under vacuum. The resulting crude was then purified by column chromatography to afford 16 mg (15% yield) of **38d** as a colorless oil. ^{1}H NMR (400 MHz, $CDCl_3$) δ 8.51 (d, *J* = 4.8 Hz, 1H), 8.46 (d, *J* = 4.8 Hz, 1H), 7.81 (ddd, *J* = 10.2, 5.5, 3.1 Hz, 2H), 7.72 (ddd, *J* = 6.8, 5.4, 3.0 Hz, 2H), 7.07 – 6.99 (m, 3H), 6.98 – 6.85 (m, 2H), 6.84 – 6.75 (m, 1H), 5.32 – 5.14 (m, 1H), 4.51 (tdd, *J* = 11.5, 7.8, 4.9 Hz, 2H), 4.29 (dt, *J* = 8.0, 6.0 Hz, 1H), 3.70 (d, *J* = 1.9 Hz, 3H), 3.69 – 3.39 (m, 3H), 2.15 (dtq, *J* = 13.5, 6.8, 3.4 Hz, 1H), 1.67 – 1.47 (m, 2H), 1.40 (d, *J* = 7.1 Hz, 3H), 1.04 – 0.73 (m, 12H). ^{13}C NMR (126 MHz, $CDCl_3$) δ 173.3, 172.2, 170.8, 170.7, 169.2, 168.1, 168.1, 164.9, 164.70, 159.9, 159.9, 148.8, 147.4, 140.8, 139.9, 135.4, 134.5, 134.5, 131.7, 131.7, 130.3, 128.7, 127.3, 123.8, 123.8, 123.2, 123.2, 122.0, 120.9, 118.4, 118.4, 116.8, 116.6, 116.4, 59.4, 59.3, 55.4, 55.3, 52.4, 52.4, 51.1, 51.0, 49.2, 49.2, 41.3, 41.3, 34.9, 34.4, 30.8, 30.8, 24.9, 24.9, 23.0, 22.8, 21.9, 21.9, 19.4, 19.3, 18.0, 17.9, 17.9, 17.8. IR (cm-1): 2963, 2225, 2051, 1717, 1670, 1572, 1409, 903, 725, 649. HRMS *calcd. for* ($C_{36}H_{42}N_6O_9$): 702.3013, *found* 702.2994.

4.1.2.-Removal of the DG and Determination of *ee* by HPLC Analysis

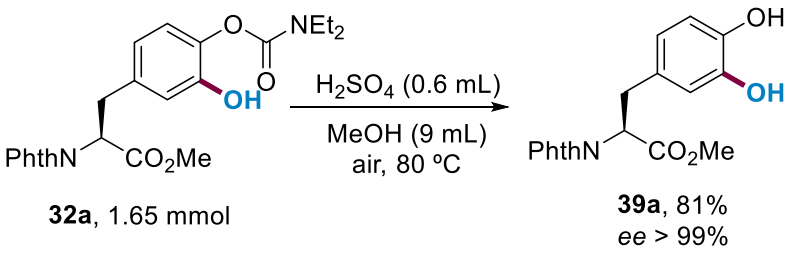

32a, 1.65 mmol

39a, 81%
ee > 99%

Methyl (*S*)-3-(3,4-dihydroxyphenyl)-2-(1,3-dioxoisoindolin-2-yl)propanoate (39a). Compound **32a** (1.65 mmol, 728 mg) was dissolved in MeOH (9 mL) and sulfuric acid (0.6 mL) was added dropwise. The resulting crude was refluxed overnight. After cooling down to room temperature, the resulting solution was carefully washed with a saturated aqueous solution of $NaHCO_3$, and extracted with EtOAc. The organic layers were combined and evaporated under vacuum. The resulting product was then purified through column chromatography (Hex/EtOAc 1:1) to provide 451 mg (81% yield) of **39a** as a yellowish solid. Mp 57-58 ºC. ^{1}H NMR (400 MHz, $CDCl_3$) δ 7.73 (dd, *J* = 5.4, 3.0 Hz, 2H), 7.64 (dd, *J* = 5.5, 3.0 Hz, 2H), 6.67 (d, *J* = 2.0 Hz, 1H), 6.61 (d, *J* = 8.0 Hz, 1H), 6.51 (dd, *J* = 8.1, 2.0 Hz, 1H), 6.18 (br s, 2H), 5.10 (dd, *J* = 11.4, 5.2 Hz, 1H), 3.75 (s, 3H), 3.52 – 3.26 (m, 2H). ^{13}C NMR (75 MHz, $CDCl_3$) δ 169.8, 168.0, 143.8, 142.9, 134.4, 131.3, 129.0, 123.7, 121.2, 115.9, 115.4, 53.5, 53.1, 34.0. IR (cm^{-1}): 3400, 1772, 1739, 1699, 1386, 716. HRMS (ESI) m/z: (M^+) *calcd.* for ($C_{18}H_{15}NO_6$): 341.0899, *found* 341.0904.

Chiralpack IA hexane:isopropanol 9:1, 1 mL/min, 210 nm.

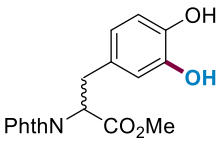

(*rac*)-39a

Retention Time	% Area
35.616	48.41
40.574	51.59

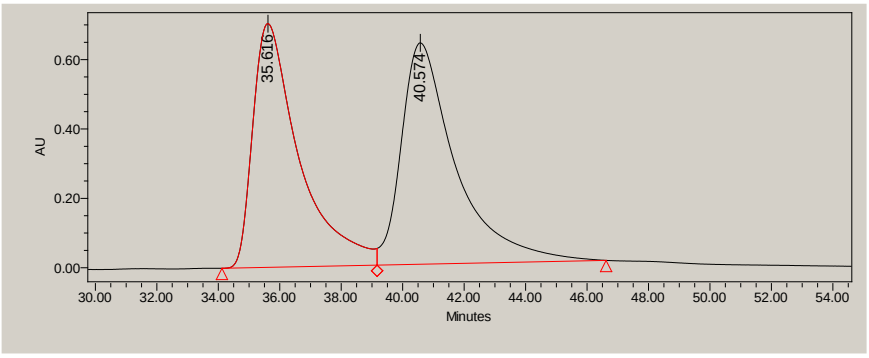

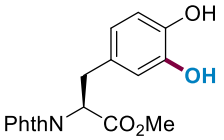

(*S*)-39a

Retention Time	% Area
42.383	100.00